

Average Circulation Conditions that Precede River Flooding in Eastern Catchments of New Zealand

Amy Bridges

A thesis submitted to
Victoria University of Wellington
In partial fulfilment of the requirements for the degree of

Master of Science
in
Physical Geography

School of Geography, Environment, and Earth Sciences
2023

Acknowledgements

This thesis has been a wild ride and would not have been possible without constant support and encouragement from my primary supervisor, Kyle Clem. I am immensely grateful to Kyle for his mentoring, for teaching me so much of his climate knowledge and coding expertise, for putting up with my many emails and frustrations, for reading through my draft's multiple times, and for providing constructive feedback that has helped improve my research and writing skills. I could not have had a more supportive and helpful supervisor. I also thank my secondary supervisor, Bethanna Jackson, for guiding me through the early stages of my hydrology research, and Andrew Rees for helping me with my RStudio codes when I got stuck.

I also acknowledge all the hydrologists and data analysts at the district and regional councils of New Zealand who took time out of their busy days to talk to me about flooding in their regions, often while flooding was occurring, and for suggesting the use of the catchments used in this research. In particular, I thank John Balingen and Robert Tasker from Northland Regional Council; Renee Prescott and Glenn Ellery from Environment Bay of Plenty; Bridget Bosworth and Peter Hancock from the Gisborne District Council; Amanda Death and Mike Gordon from Greater Wellington Regional Council; Duc Nguyen from Marlborough District Council, and Amy-Grace McIlraith, Tony Gray and Carey Lintott from Environment Canterbury. I hope my research has provided some insight into meteorological hazards in your regions.

Lastly, I would like to thank my friends and family for all their support and encouragement. A big thank you goes out to Theo for supporting me emotionally when my masters got tough, for listening to me talk about my thesis almost nonstop, and for being excited when I got excited about my results. Thank you to my parents, Dianna and Andrew, and my sister Emma, for supporting me throughout my whole university career and encouraging me to take every opportunity to learn and grow in my interests. A big thank you to my Mum especially, for spending hours proofreading my thesis.

I look forward to where this research takes me in the future, and I hope my research can make a difference to those at-risk communities who are constantly battling flooding.

Abstract

Flooding is a frequent and costly hazard in New Zealand (NZ). With two-thirds of NZ's population residing on the flood plains of large rivers, recent and significant rainfall events have resulted in many NZ cities being subjected to severe river flooding. Therefore, NZ is continuously (and increasingly) facing the challenge of how to best manage flood risks to minimise their distress and costs. Existing research has largely focused on understanding the meteorological drivers of flooding in NZ's West Coast regions, despite the higher proportion of population residing on the flood plains, and the frequency of damaging and costly floods, in NZ's eastern regions. To better understand NZ's current and future flood risk, this research aims to determine the anomalous large-scale and regional atmospheric circulation patterns associated with river flooding in 17 catchments in four of NZ eastern regions. By developing an event database of historical high flows through flood frequency analysis and employing composite analysis techniques, the key regional weather patterns and their association with large-scale modes of climate variability that cause river flows exceeding a 1-in-5-year threshold for each of the 17 catchments were identified. The primary features were an anomalous low pressure to the west or north of NZ coupled with high pressure to the east or south, which together draw deep tropical moisture down from the low latitudes, with locally enhanced low-level convergence where the flow intercepts the catchments. Overall, relationships with large-scale climate modes were generally weak. However, a key feature for the Upper North Island and Lower North Island catchments was positive sea surface temperature anomalies (SSTs) to the north of NZ over the region of moisture transport, generally associated with La Niña conditions. Additionally, an asymmetric Zonal Wave 4 atmospheric circulation pattern was a key feature for the Upper North Island and South Island catchments. The findings of this research provide a foundation for the best methods to use for flood frequency analysis for eastern NZ catchments and shed light on the meteorological drivers of NZ's ever increasing flood risk. This knowledge, alongside projections of how NZ weather systems and regional SST changes will change with climate change, can be used to aid in preparation and risk management associated with river flooding in eastern NZ regions.

Table of Contents

Acknowledgements.....	2
Abstract.....	3
List of Figures	6
List of Tables	12
1. Introduction	13
1.1 Motivation.....	13
1.2 Research Question	15
1.3 Objectives.....	15
2. Background	16
2.1. Flooding.....	16
2.1.1 Flooding in New Zealand	16
2.1.2 Flood Definition	17
2.1.3 Causes of Flooding.....	18
2.1.4 Flood Mitigation	19
2.1.5 Recent Impacts	19
2.2 Flood Frequency Analysis.....	21
2.2.1 International Regulations	22
2.2.2 New Zealand Regulations	23
2.2.3 Flood Frequency Analysis Methods.....	24
2.3 New Zealand's Climate	27
2.3.1 Geography	27
2.3.2 Large-scale Precipitation variability	33
2.3.3 Synoptic Precipitation Drivers	41
2.3.4 Extreme Events	47
3. Data and Methods	53
3.1 Catchment Information.....	53
3.1.1 Catchment Selection.....	53
3.1.2 Upper North Island	56
3.1.3 East Coast North Island.....	61
3.1.4 Lower North Island	71
3.1.5 South Island	79
3.2 Data and Methods.....	85

3.2.1 Data Collection	85
3.2.2 Data Processing	85
3.2.3 Generation of Flood Frequency Analysis and Threshold Identification.....	86
3.2.4 Selection of Flood Events for Compositing	89
3.2.5 Selection of Timesteps.....	89
3.3 Climate Analysis Methods.....	89
3.3.1 Data Collection and Composite Development	89
3.3.2 ENSO and SAM Conditions	92
4. Flood Frequency Analysis Results	94
4.1 Upper North Island.....	96
4.2 East Coast North Island	98
4.3 Lower North Island.....	100
4.4 South Island	102
5. Climate Results.....	105
5.1 Upper North Island.....	105
5.2 East Coast North Island	111
5.3 Lower North Island.....	118
5.4 South Island	125
5.5 Seasonality	131
6. Discussion and Conclusion	132
6.1 Flood Frequency Analysis	132
6.2 Climate Analysis	136
7. References	144
8. Appendix	168

List of Figures

Figure 1.1: Aerial views of the magnitude flooding during the (a) Westport July 2021 floods (Heard, 2021; Leask & Heard, 2021), and the (b) Gisborne November 2021 floods (Cave, 2021).....	13
Figure 2.1: Pictures of the environmental impacts from the August 2022 Nelson floods; (a) Whangamoa River flooding in the Whangamoa River Valley (Cuff, 2022); (b) floodwater scouring on Devenish Place, Atawhai (Hunter, 2022); and, (c) damage to a section of State Highway 6 between Nelson and Blenheim (Waka Kotahi, 2022).	21
Figure 2.2: Average (a) annual and (b-e) seasonal climatological (1979-2020) precipitation (mm day ⁻¹) and 10m wind (ms ⁻¹) for the NZ region (source: ERA5). Seasons include (b) Summer (December, January, and February), (c) Autumn (March, April, and May), (d) Winter (June, July, and August), and (e) Spring (September, October, and November).....	29
Figure 2.3: New Zealand climate zones (National Institute of Water and Atmospheric Research, 2022a).	32
Figure 2.4: New Zealand's climate regions. Shaded areas depict mountainous features and lines with letters and numbers refer to that area's climate region description located in the below table. (From Fig. 1 of Mosley (2000)).	33
Figure 2.5: Observed composites of annual (a-b) precipitation (mm/yr) and (e-f) wind anomalies (black vectors in 2m/s) in New Zealand during (a,e) El Niño and (b,f) La Niña between 1960 and 2004. (Modified from Fig. 13 of Ummenhofer & England (2007)).....	36
Figure 2.6: Same as Fig. 2.5 but for (a,e) positive SAM and (b,f) negative SAM. (Modified from Fig. 14 of Ummenhofer & England (2007)).	39
Figure 2.7: The 12 Kidson types and their associated regimes. Names of each synoptic type are denoted on the top right-hand corner, i.e. 'T' is Trough, 'SW' is Southwesterly flow, 'TNW' is Trough Northwesterly flow, and 'TSW' is Trough Southwestery; for Zonal, 'H' is High over the country, 'HNW' is High to the Northwest, and 'W' is High to the North with Westerly flow; and for Blocking, 'HSE' is High to the Southeast, 'HE' is High to the East, 'NE' is Northeasterly flow, 'HW' is High to the West, and 'R' is Ridge. (From Fig. 1 of Griffiths (2011a), modified from Fig. 2 of Kidson (2000)).	42
Figure 2.8: The 12 Kidson (2000) types and the associated daily precipitation anomalies in NZ between 1979 and 2019. The colour bar depicts precipitation anomalies in mm based on a 95% significance level, with blue indicating increased precipitation and orange indicating reduced precipitation. (From Fig. 10 of Pohl et al. (2022)).	43

Figure 2.9: Dominant Kidson types that commonly lead to extreme precipitation (extreme precipitation is defined as daily anomalies above the 95% percentile by Pohl et al. (2022)). Colour shading relates to one of the 12 Kidson (2000) types. (From Fig. 15(b) of Pohl et al. (2022)).	45
Figure 2.10: Dominant Kidson types with the highest percentage of occurrence during extreme (a) annual and (b-e) seasonal precipitation regionally within NZ. Seasons include (b) Autumn (March, April, and May), (c) Winter (June, July, and August), (d) Spring (September, October, and November), and (e) Summer (December, January, and February). (Modified from Fig. 3 of Griffiths (2011a)).	46
Figure 2.11: Atmospheric River (AR) originating in the subtropical regions north of Queensland, Australia on the 27 th of December 2010 and making landfall around the Marlborough region. The yellow boundary depicts the shape of the AR, the white dot shows the approximate landfall location (174°E, 40.625°S) and the colour shading and vectors relate to measured integrated water vapour transport ($\text{kg m}^{-1} \text{s}^{-5}$) and direction of moisture flow respectfully. (From Fig. 6 of Shu et al. (2021)).	49
Figure 2.12: Ex-tropical cyclone storm tracks across the middle latitudes. The lines indicate the cyclone track, and the line colour refers to the intensity of the cyclone (From Rhode (2006)).	51
Figure 3.1: Locations of the selected 13 eastern North Island catchments examined in this thesis.	54
Figure 3.2: Locations of the selected four eastern South Island catchments examined in this thesis.	55
Figure 3.3: The Waitangi catchment (a) location and (b) elevation.	57
Figure 3.4: Waitangi River flow (m^3/s) timeseries (22/02/1979 – 14/11/2020).	57
Figure 3.5: The Waioeka catchment (a) location and (b) elevation.	58
Figure 3.6: Waioeka River flow (m^3/s) data timeseries (01/01/70 – 24/03/2022).	59
Figure 3.7: The Otara catchment (a) location and (b) elevation.	60
Figure 3.8: Otara River flow (m^3/s) timeseries (01/03/1979 – 14/01/2022).	60
Figure 3.9: The Hikuwai catchment (a) location and (b) elevation.	62
Figure 3.10: Hikuwai River flow (m^3/s) timeseries (01/01/1975 – 15/04/2022).	62
Figure 3.11: The Waimatā catchment (a) location and (b) elevation.	64
Figure 3.12: Waimatā River flow (m^3/s) timeseries (21/04/1978 – 15/04/2022).	64
Figure 3.13: The Te Arai catchment (a) location and (b) elevation.	65

Figure 3.14: Te Arai River flow (m^3/s) timeseries (01/01/1984 – 14/04/2022).	66
Figure 3.15: The Waikohu catchment (a) location and (b) elevation.	67
Figure 3.16: Waikohu River flow (m^3/s) timeseries (05/10/1979 – 14/04/2021).	67
Figure 3.17: The Waihora catchment (a) location and (b) elevation.	68
Figure 3.18: Waihora River flow (m^3/s) timeseries (04/12/1986 – 14/04/2022).	69
Figure 3.19: The Waiapu catchment (a) location and (b) elevation.	70
Figure 3.20 Waiapu River flow (m^3/s) timeseries (01/01/1975 – 15/04/22).	70
Figure 3.21: The Ruamāhangā catchment (a) location and (b) elevation.	72
Figure 3.22: Ruamāhangā River flow (m^3/s) timeseries (31/12/1956 – 31/12/2021).	72
Figure 3.23: The Waipoua catchment (a) location and (b) elevation.	74
Figure 3.24: Waipoua River flow (m^3/s) timeseries (05/02/1979 – 20/07/2021).	74
Figure 3.25: The Waingawa catchment (a) location and (b) elevation.	76
Figure 3.26: Waingawa River flow (m^3/s) timeseries (14/03/1976 – 01/01/2022).	76
Figure 3.27: The Waiōhine catchment (a) location and (b) elevation.	78
Figure 3.28: Waiōhine River flow (m^3/s) timeseries (27/12/1954 – 01/01/2022).	78
Figure 3.29: The Wairau catchment (a) location and (b) elevation.	80
Figure 3.30: Wairau River flow (m^3/s) timeseries (05/07/1960- 23/05/2022).	80
Figure 3.31: The Hurunui catchment (a) location and (b) elevation.	81
Figure 3.32: Hurunui River flow (m^3/s) timeseries (13/12/1974 – 31/03/2022).	82
Figure 3.33: The Selwyn catchment (a) location and (b) elevation.	83
Figure 3.34: Selwyn River flow (m^3/s) timeseries (29/02/1984 – 22/02/2022).	83
Figure 3.35: The Maerewhenua catchment (a) location and (b) elevation.	84
Figure 3.36: Maerewhenua River flow (m^3/s) timeseries (04/03/1970 – 23/03/2022).	85
Figure 4.1: Flood frequency analysis results for the Upper North Island catchments: (a) Waitangi, (b) Waioeka, and (c) Otara catchment. Flow (m^3/s) is on the y axis and the return period (years) and reduced variate are on the x axis, with the Gumbel distribution in blue, LP3 in pink and GEV in purple.	97

Figure 4.2: Same as Fig. 4.1 but for the ECNI catchments: (a) Hikuwai, (b) Waimatā, (c) Te Arai, (d) Waikohu, (e) Waiapu, and (f) Waihora.	100
Figure 4.3: Same as Fig. 4.1 but for the LNI catchments: (a) Waipoua, (b) Waingawa, (c) Waiōhine, and (d) Ruamāhangā.	102
Figure 4.4: Same as Fig. 4.1 but for the SI catchments: (a) Wairau, (b) Hurunui, (c) Selwyn, and (d) Maerewhenua.	104
Figure 5.1: Local circulation features that occurred during high flow events in the UNI catchments. The left column shows composite anomalies of mean sea level pressure (MSLP) (shaded) and MSLP variance (contours) for (a) Waitangi, (c) Otara, and (e) Waioeka catchments. The right column shows composite of total column water vapour (TCWV) anomalies (shaded) and 10-m wind (vectors) for (b) Waitangi, (d) Otara, and (f) Waioeka catchments.	107
Figure 5.2: Large-scale Southern Hemispheric circulation features occurring during high flow events in the UNI catchments. The left column shows 500 hPa geopotential height (z500) anomalies (shaded) for the (a) Waitangi, (c) Otara, and (e) Waioeka catchments. The right column shows outgoing longwave radiation (OLR) anomalies (shaded) and 200 hPa streamfunction (sf200) anomalies for the (b) Waitangi, (d) Otara, and (f) Waioeka catchments.	109
Figure 5.3: Large-scale Southern Hemispheric variability occurring during high flow events in the UNI catchments. The left column shows skin temperature (SKT/SST) anomalies (shaded) for the (a) Waitangi, (c) Otara, and (e) Waioeka catchments. The right column shows outgoing longwave radiation (OLR) anomalies (shaded) for the (b) Waitangi, (d) Otara, and (f) Waioeka catchments.	110
Figure 5.4: Pie charts showing the percentage of ENSO and SAM phases for the high flow events in the UNI catchments used for compositing based on the monthly-mean phases of ENSO (left column) and SAM (right column) in the UNI. (a-b) Waitangi, (c-d) Otara, and (e-f) Waioeka catchments.	111
Figure 5.5: Local circulation features that occurred during high flow events in the ECNI catchments. The left column shows composite anomalies of mean sea level pressure (MSLP) (shaded) and MSLP variance (contours) for (a) Hikuwai, (c) Waimatā, (e) Te Arai, and (g) Waikohu catchments. The right column shows composites of total column water vapour (TCWV) anomalies (shaded) and wind (vectors) for (b) Hikuwai, (d) Waimatā, (f) Te Arai, and (h) Waikohu catchments.	113
Figure 5.6: Large-scale Southern Hemispheric circulation features occurring during high flow events in the ECNI catchments. The left column shows 500 hPa geopotential heights (z500) anomalies (shaded) for (a) Hikuwai, (c) Waimatā, (e) Te Arai, and (g) Waikohu catchments. The right column shows outgoing longwave radiation (OLR) anomalies (shaded) and 200 hPa streamfunction (sf200) anomalies for the (b) Hikuwai, (d) Waimatā, (f) Te Arai, and (h) Waikohu catchments.	115

Figure 5.7: Large-scale Southern Hemispheric variability occurring during high flow events in the ECNI catchments. The left column shows skin temperature (SKT/SST) anomalies (shaded) for the (a) Hikuwai, (c) Waimatā, (e) Te Arai, and (g) Waikohu catchments. The right column shows OLR (shaded) anomalies for the (b) Hikuwai, (d) Waimatā, (f) Te Arai, and (h) Waikohu catchments.116

Figure 5.8: Pie charts showing the percentage of ENSO and SAM phases for the high flow events in the ECNI catchments used for compositing based on the monthly-mean phase of ENSO (left column) and SAM (right column). (a-b) Hikuwai, (c-d) Waimatā, (e-f) Te Arai, and (g-h) Waikohu catchments.117

Figure 5.9: Local circulation features that occurred during high flow events in the LNI catchments. The left column shows composite anomalies of mean sea level pressure (MSLP) (shaded) and MSLP variance (contours) for (a) Waipoua, (c) Waingawa, (e) Waiōhine, and (g) Ruamāhangā catchments. The right column shows composites of total column water vapour (TCWV) anomalies (shaded) and wind (vectors) for (b) Waipoua, (d) Waingawa, (f) Waiōhine, and (h) Ruamāhangā catchments.120

Figure 5.10: Large-scale Southern Hemispheric circulation features occurring during high flow events in the LNI catchments. The left column shows 500 hPa geopotential heights (z500) anomalies (shaded) for (a) Waipoua, (c) Waingawa, (e) Waiōhine, and (g) Ruamāhangā catchments. The right column shows outgoing longwave radiation (OLR) anomalies (shaded) and sf200 anomalies for the (b) Waipoua, (d) Waingawa, (f) Waiōhine, and (h) Ruamāhangā catchments.122

Figure 5.11: Large-scale Southern Hemispheric variability occurring during high flow events in the LNI catchments. The left column shows skin temperature (SKT/SST) anomalies (shaded) for the (a) Waipoua, (c) Waingawa, (e) Waiōhine, and (g) Ruamāhangā catchments. The right column shows OLR (shaded) anomalies for the (b) Waipoua, (d) Waingawa, (f) Waiōhine, and (h) Ruamāhangā catchments.123

Figure 5.12: Pie charts showing the percentage of ENSO and SAM phases for the high flow events in the LNI used for compositing based on the monthly-mean phase of ENSO (left column) and SAM (right column). (a-b) Waipoua, (c-d) Waingawa, (e-f) Waiōhine, and (g-h) Ruamāhangā catchments.124

Figure 5.13: Local circulation features that occurred during high flow events in the SI catchments. The left column shows composite anomalies of mean sea level pressure (MSLP) (shaded) and MSLP variance (contours) for (a) Wairau, (c) Hurunui, (e) Selwyn, and (g) Maerewhenua catchments. The right column shows composite of total column water vapour (TCWV) anomalies (shaded) and wind (vectors) for (b) Wairau, (d) Hurunui, (f) Selwyn and (h) Maerewhenua catchments.126

Figure 5.14: Large-scale Southern Hemispheric circulation features occurring during high flow events in the SI catchments. The left column shows 500 hPa geopotential heights (z500) anomalies (shaded) for the (a) Wairau, (c) Hurunui, (e) Selwyn, and (g) Maerewhenua catchments. The right column shows outgoing longwave radiation (OLR) anomalies

(shaded) and sf200 anomalies for the (b) Wairau, (d) Hurunui, (f) Selwyn, and (h) Maerewhenua catchments.	128
Figure 5.15: Large-scale Southern Hemispheric variability occurring during high flow events in the SI catchments. The right left shows skin temperature (SKT/SST) anomalies (shaded) for the ((a) Wairau, (c) Hurunui, (e) Selwyn, and (g) Maerewhenua catchments. The right column shows outgoing longwave radiation (OLR) anomalies (shaded) for the (b) Wairau, (d) Hurunui, (f) Selwyn, and (h) Maerewhenua catchments.	129
Figure 5.16: Pie charts showing the percentage of ENSO and SAM phases for the high flow events in the SI catchments used for compositing based on the monthly-mean phase of ENSO (left column) and SAM (right column). (a-b) Wairau, (c-d) Hurunui, (e-f) Selwyn, and (g-h) Maerewhenua catchments.	130
Figure 5.17: Percentage bar chart showing the percentage of high flow events (identified to equal or exceed a catchment-specific 1-in-5-year threshold) that occurred in spring, summer, winter, and autumn.	131
Figure 6.1: The percentage of Log Pearson Type III, Gumbel and Generalised Extreme Value flood frequency methods selected as the best fit model for the 17 eastern catchments in this research.	133
Figure 6.2: Mean sea level pressure (contours), precipitation (shaded), and wind (arrows) map of the atmospheric conditions preceding post tropical Cyclone Hale on the 10 th of January 2023 at 3pm (Weather Watch, 2023)).	141

List of Tables

Table 3.1: Quantiles used for generating flow magnitudes for return periods.	86
Table 3.2: Data variables and their use in this research (with respect to the 3-day running mean anomaly).	91
Table 4.1: Goodness-of-fit testing results.	94
Table 4.2: Selected flood frequency method and threshold development results.	95

1. Introduction

1.1 Motivation

This research was motivated by the growing number of flooding events in recent years, such as in Westport and Gisborne, as well as in other areas of NZ. On the 15th of July 2021, over 150mm of rain deluged the Westport and Buller District within 36 hours as a westerly orientated atmospheric river (AR) approached NZ (National Institute of Water and Atmospheric Research, 2021; Stuff, 2022). The Buller River flooded, resulting in inundation and severe damage across most of Westport as shown in Fig. 1.1a, and the evacuation of nearly half the population. The flooding damaged 826 properties, 450 of which were determined unsuitable to live in, and the damages cost \$56 million (Ministry for the Environment, 2022). On the 4th of November 2021, over 200mm of rain fell within 24 hours in the Gisborne region (MacManus, 2021). Multiple rivers in the region flooded along with significant landslides, leading to the closure of main roads, the isolation of communities, and up to \$3.37 million in damages (Fig. 1.1b; Insurance Council of New Zealand, 2022). While extreme rainfall was forecast in both events, resulting in MetService issuing its most severe ‘red warning’ for Westport (Radio New Zealand, 2022), it remains poorly understood how specific catchments will respond to such a weather event, especially for the areas around Gisborne. These events therefore illustrate the need for better understanding of what influences catchment-specific river flooding in order to better prepare for hazards at a local level.



Figure 1.1: Aerial views of the magnitude flooding during the (a) Westport July 2021 floods (Heard, 2021; Leask & Heard, 2021), and the (b) Gisborne November 2021 floods (Cave, 2021).

Existing research has identified NZ's location in the Southern Hemisphere middle latitudes, along with its extremes in topography, results in an abundance of local and large-scale weather patterns that can lead to flooding (Smart & McKerchar, 2010). The West Coast of the South Island has been widely studied, with floods mainly a result of moist westerly airstreams intersecting the Southern Alps and “Trough regimes”, which can trigger intense moisture transport in the form of ARs (Kingston et al., 2022). However, it is unknown if these features impact catchments on the eastern side of NZ due to lower elevations, more varied local climates, and smaller catchments. Some interannual fluctuations in large-scale circulation, such as those associated with La Niña, have also been found to increase flooding in some eastern catchments, but the precise synoptic circulation at a catchment level remains largely unknown (Freeman, 2008).

More recently, research has recognised the value of understanding extreme precipitation and flooding in other areas of NZ, especially in the eastern regions. Pohl et al. (2022) identified weather types that drive extreme precipitation in NZ varies between the North and South Island while Kingston et al. (2022) identified the large-scale atmospheric drivers of river flooding in the Waiau Toa, a northeastern river in Kaikōura with headwaters in the Kaikoura Ranges in the South Island, were different compared to the four other South Island rivers located east of the Main Divide. This suggests the climatic conditions that drive river flooding may vary in the northern regions of NZ. To add to these two recent studies, this research will focus primarily on river flooding in North Island eastern regions and four eastern South Island rivers, three of the latter which do not have headwaters residing in the Southern Alps.

Thus, the motivation of this study is to understand the preceding circulation conditions that have caused historical high river flows in eastern regions of NZ, focusing on NZ North Island, in order to improve awareness of the various local hydrometeorological hazards in NZ and help aid in preparation and reduce the societal impact floods have on NZ's at-risk communities.

1.2 Research Question

This thesis aims to answer the question: *what are the anomalous circulation conditions that preceded historical river flooding in eastern catchments of NZ?* To answer this research question, this thesis will first complete an analysis of international and national flood frequency analysis (FFA) methods to determine the most accurate method to identify high flow events in our selected catchments. Secondly, catchment-specific event datasets are generated using the selected FFA methods, and finally, the average anomalous circulation conditions for river flows greater than 1-in-5-year flow magnitude are investigated using composite analysis of several key meteorological parameters commonly associated with heavy rainfall (described in Section 3.3.1).

1.3 Objectives

The aim of this study can be broken down into five objectives:

1. To complete an analysis of current flood frequency methods in NZ and identify their ability to determine flood magnitudes in 17 catchments in four eastern regions of NZ.
2. To develop a set of flooding thresholds using catchment-specific and robust flood frequency methods and flood magnitudes.
3. To develop an events dataset of historical high flow events that had the potential to do damage in their respective catchments.
4. To use composite techniques to examine average anomalous synoptic circulation conditions that preceded high flow events.
5. To determine their connection to large-scale modes of climate variability.

This thesis is split into six chapters: (1) Introduction; (2) Background; (3) Data and Methods; (4) Flood Frequency Analysis Results; (5) Climate Results, and (5) Discussion and Conclusion.

2. Background

2.1. Flooding

2.1.1 Flooding in New Zealand

Flood plain environments have been favoured by humans since the early days of human settlement because they provide communities with access to drinking water, fertile land, navigable corridors, and protection barriers (Alfieri et al., 2017; Merz et al., 2021). Since European settlement in NZ, populations have continuously been vulnerable to flooding during extreme weather events and as a result, there is an extensive history of flooding in all major rivers in NZ (McDowall, 2019; Paulik et al., 2019).

Changing land use and increased human activity on active flood plains of NZ's large rivers has led to flooding being a costly natural hazard in NZ (Crawford-Flett et al., 2022). Within the last 40 years a major flood has occurred on-average every four months and has resulted in an average damage cost of \$2 million dollars per flood event (Crawford-Flett et al., 2022). Insurance claims for flooding exceeded \$321.6 million dollars in 2021 and increased to \$488.5 in 2022 (Cardwell, 2022). This amount however does not include the costs of flood mitigation, risk assessments, and planning (Morton, 2020; Cardwell, 2022; Galuszka, 2022). Furthermore, modelling completed by the Ministry for the Environment (2010, 2022) identified that many regions in NZ are at an increasing risk of flooding as the severity of heavy rainfall is expected to increase with climate change. Therefore, it is likely the cost of flooding will also increase.

Flooding occurs in both the South Island and the North Island of NZ, however as discussed in Chapter 1, existing research has focused largely on the flood risk in the South Island (McKerchar et al., 1996; Kingston, et al., 2016). Yet, between 1999 and 2007, 12 of 14 flood events in NZ that caused over \$1 million worth of damage occurred in the North Island (Smart & McKerchar, 2010). It has also been estimated that 675,000 people are at risk of river flooding in NZ, 420,000 of whom reside on NZ's eastern regions (Paulik et al., 2019). Smart and McKercher (2010) identified floods in the South Island tend to be larger due to the bigger catchment sizes and higher amounts of rainfall the South Island receives on average, but

flooding in the North Island tends to occur more frequently and be more costly due to the proportion of the population and types of infrastructure exposed. More people are also settling in the North Island compared to the South Island and increased urban development is occurring on flood plains as a result, exposing more of NZ's population to frequent flood damages (Smart & McKerchar, 2010; McDowall, 2019; Paulik et al., 2019).

Despite the growing evidence of impacts from climate change, the growing costs, and growing proportion of the population and key infrastructure at risk of severe damages, there has been no in-depth analysis focused on the climatic drivers of eastern NZ flooding (McDowall, 2019; Morton, 2020).

2.1.2 Flood Definition

River flooding in NZ is primarily defined as a body of “water that spills from a river channel onto land that is normally dry” (National Institute of Water and Atmospheric Research [NIWA], 2011).

Flash flooding, river flooding, and urban flooding are the most common types of floods that occur in NZ. Flash floods occur when there is short high-intensity rainfall which exceeds the infiltration capacity of the environment, leading to a sudden flood (NIWA, 2011). River flooding is specific to areas near rivers and is common during long duration or high intensity precipitation over a large region causing flow to exceed the river’s storage capacity and no longer be maintained within the river channel (Stein et al., 2021). Urban flooding occurs in areas with impervious surfaces where precipitation cannot infiltrate the soil causing surface runoff that overwhelms the stormwater network leading to surface flooding (Zhou et al., 2017).

Floods can also be defined in relation to specific rivers using flow statistics derived from FFA methods, which is the primary focus of this research. For example, Environment Canterbury (ECAN) defines a river flood in Te Ngawai River as any flow that exceeds 1300m³/s (Environment Canterbury [ECAN], 2022). More generally, floods can be defined as a probability of occurrence. For example, in NZ there is a 50% chance of a 0.67% annual exceedance probability event (similar to a 1-in-150 year event) in a given year (NIWA, 2011).

2.1.3 Causes of Flooding

As previously mentioned, flooding in NZ is predominantly caused by extreme or prolonged precipitation, but rain-on-snow events and geomorphic and land use changes along river channels have also been identified as factors that influence flooding (Merz & Blöschl, 2003; Zhou et al., 2017; Forestieri et al., 2018). The severity of flooding is also driven by several different atmospheric and environmental factors, which vary depending on the region (McKerchar & Henderson, 2003; Smart & McKerchar, 2010).

Existing research has identified that the likelihood, location, and severity of a flood is determined by large-scale climate controls on precipitation (McKerchar & Pearson, 2001; McKerchar & Henderson, 2003). Strong interannual and interdecadal variability can influence the amount of precipitation a region receives. For example, during a La Niña, warm and wet conditions on NZ's East Coast leads to greater-than-average precipitation and an enhanced flood risk, whereas flooding on the West Coast occurs more commonly during an El Niño (McKerchar & Henderson, 2003; Smart & McKerchar, 2010; Kundzewicz et al., 2019). Extra-tropical and post-tropical cyclones, ARs, and thunderstorms are also known to cause extreme precipitation events that can lead to flooding (Trotter, 1988; Prince et al., 2021). Smart and McKercher (2010) determined that the different climatic conditions the North and South Island are exposed to have significant influence on flooding in each island. This will be discussed in more detail in Section 2.3.

Antecedent conditions, such as land use, soil moisture content, vegetation, and water storage can also predispose a catchment to a higher risk of flooding during precipitation (Ministry for the Environment, 2010). Blöschl et al., (2015) and Patel et al. (2021) identified changing patterns in precipitation and temperature can lead to dry ground conditions or oversaturated soils that can change the rate at which water enters the river system. For example, the 30th May 2021 Canterbury floods were exacerbated after months of drought conditions which caused dry hydrophobic soils, whereas the 27th March 2019 West Coast floods were more severe due to previous long periods of heavy rainfall that created oversaturated soils (Naish, 2021; NIWA, 2019).

Similar impacts to overland flow and flooding can occur due to different land use (i.e. urban or rural), vegetation, and geology characteristics of the catchment (Ettrick et al., 1987).

Forested areas are more likely to absorb and intercept rainwater, reducing the amount and speed at which water enters the river channel and lowering the risk of severe flooding from extreme weather events compared to paved impervious surfaces in urban areas (Blöschl et al., 2015). On the other hand, when looking at the effect of water storage, areas with large groundwater storage networks, such as Canterbury, have an increased risk of flooding during extreme precipitation events because such regions have a higher water table that can result in soils becoming saturated more quickly (Ettrick et al., 1987).

2.1.4 Flood Mitigation

Flood protection and mitigation in NZ is primarily comprised of hard engineering structures such as stopbanks (Crawford-Flett et al., 2022). Stopbanks are manmade embankments that are designed to withstand and protect regions from a 1-in-100-year flood event in urban areas and a 1-in-20-year flood in rural areas (Boothway, 2014). NZ's stopbank network is 5284km long with the largest networks located around the large rivers in Canterbury, Southland, Waikato, Manawatū-Whanganui, and the Bay of Plenty (Crawford-Flett et al., 2022). Stopbanks are usually part of a larger flood management scheme that can also involve culverts, pump stations, floodgates, and natural river management such as park buffers (Basheer et al., 2013). The types of flood mitigation used varies significantly by region because a region's flood mitigation efforts are maintained by the councils (Crawford-Flett et al., 2022).

Frequent maintenance is required to ensure mitigation structures continue protecting at-risk areas, which can be a significant financial burden for councils (Basheer et al., 2013; Boothway, 2014). Flood protection maintenance and renewal currently costs NZ councils an additional \$200 million dollars annually on top of flood damage expenses (Galuszka, 2022). This cost is expected to rise by \$150 million dollars annually because many stopbanks will need to be updated to align with climate change projections (Galuszka, 2022).

2.1.5 Recent Impacts

Despite significant financial investment into flood protection, many regions of NZ are still at risk of severe damage from flood events, which can have significant negative economic, social, and environmental impacts (Davies & Mcsaveney, 2011; King et al., 2014; Alfieri et al.,

2017; Crawford-Flett et al., 2022). Impacts from flooding in NZ are predominantly a result of the floodwater's hydrodynamic forces and erosive powers, deposition of large amounts of sediment and debris onto roads and around houses, and the transport of pollutants (NIWA, 2011). Flooding is however also a natural process that can be beneficial for the environment by increasing the amount of nutrients found on flood plains, redistributing sediment, improving ecosystem health, and replenishing reservoirs (Berghuijs et al., 2016). Recent negative impacts of flooding in NZ will be discussed in this section.

Agriculture is important to the economy of NZ, contributing 8% to the national GDP and accounting for 74% of total export earnings (Paulik et al., 2021). However, most agricultural industry is located on active flood plains, resulting in a high risk of severe economic impacts from flooding. The Bay of Plenty suffered severe economic impacts as a result of Ex-tropical Cyclone Debbie on the 3rd of April 2017 (Paulik et al., 2021). Three-hundred millimetres of rain fell within 48 hours, and floodwaters inundated over 3500 ha of farmland in the region, damaging weather-sensitive crops, such as kiwifruit, and resource dependent industries, such as dairy farming, resulting in an estimated \$4 million dollars' worth of damage per farm (New Zealand Media and Entertainment, 2017; Paulik et al., 2021). Flooding can also cause property damage, income losses, damage to essential infrastructure, and have flow-on effects on businesses who source items from areas within the flood risk zones (Moser, 1994; Radio New Zealand [RNZ], 2021). For example, in the 30th May 2021 Canterbury floods, the Ashburton Bridge was closed due to severe flooding in the Ashburton-Hakatere River, leading to key delivery route disruptions and a shortage of produce in Christchurch supermarkets (RNZ, 2021).

Many communities in NZ are at risk of significant negative social impacts from flooding. Major flooding events can lead to fatalities as well as disruptions to society, while frequent small floods can cause significant harm to mental wellbeing (Merz et.al, 2021). Frequent small floods are common in Christchurch and many residents near the Avon River are feeling defeated and discouraged by the constant damage and disruptions from floodwaters (Mathewson et al., 2014). Floodwaters can also impact locations of cultural significance. On the 23rd of March 2022, Gisborne received three months' worth of rainfall in 24 hours, which caused flooding that damaged many sites of significance for Māori, isolated some communities, and led to mass evacuations in Tairāwhiti (1News, 2022). 1News (2022)

described seeing residents heartbroken as they watched floodwaters of the Uawa and Hikuwai Rivers damage an Urupā (Māori burial site) and Marae.

Environmental impacts of flooding, such as increased sedimentation and erosion, are frequently observed in NZ after extreme weather events. Nelson suffered significant environmental impacts from an "atmopsheric river" on the 17th of August 2022 which brought 1006mm of rain in 72 hours (NIWA, 2022c). The rain caused major flooding that inundated farmland in sediment and water (Fig. 2.1a), and the erosive power of the floodwaters caused landslides along multiple segments of SH6 between Marlborough and Blenheim, a main lifeline between the two regions (Fig. 2.1b; RNZ, 2022). Floodwaters also scoured residential roads down to the water infrastructure shown in Fig. 2.1c.



Figure 2.1: Pictures of the environmental impacts from the August 2022 Nelson floods; (a) Whangamoa River flooding in the Whangamoa River Valley (Cuff, 2022); (b) floodwater scouring on Devenish Place, Atawhai (Hunter, 2022); and, (c) damage to a section of State Highway 6 between Nelson and Blenheim (Waka Kotahi, 2022).

2.2 Flood Frequency Analysis

FFA is a common hydrological technique used to understand the magnitude and likelihood/return period of a flood occurring in a specific catchment (Pearson, 1991; Gulap &

Gitika, 2019). Accurate and reliable FFA methods are important for understanding the associated risk of an extreme hydrological event and developing effective flood risk management (England et al., 2019). In this research, FFA will be used to develop catchment-specific event datasets which will then be used to develop the climate composites. The following section analyses the FFA methods undertaken in international and national environments to help determine the best methods for identifying high flow events in the 17 catchments in this research.

2.2.1 International Regulations

The United States (US) Water Resources Council developed a set of guidelines in 1967 that recommended the use of Log Pearson Type III (LP3) as a uniform FFA technique for all catchments within the US (England et al., 2019). LP3 was chosen due to its flexibility with different skew ranges, its ability to be used on a range of data including historical flows and paleo floods, its ability to be representative of a range of different catchments and their climatic regions, and it is not affected by outliers (Stedinger & Griffis, 2011; Bhagat, 2017; England et al., 2019). The US Water Resources Council's recommendation has led to many countries adopting the method, including NZ (Ministry for the Environment, 2010; Kumar, 2019).

In the United Kingdom (UK), the Generalized Logistic Distribution is the recommended FFA method for all catchments because of the UK's long flow records, taking a similar uniform approach to the US (Robson & Reed, 2008). In Australia, there is no universal FFA recommendation for Australian catchments, as the Australian Rainfall and Runoff's guide states there is no proof that a single FFA method is the correct theoretical procedure and instead suggests the most appropriate method depends on the probability distribution fit to the observed historical flows (Ball et al., 2019). Generalized Extreme Values (GEV) and LP3 are however commonly used in Australia with the GEV method being the option preferred by most councils because it generates an asymptotic distribution of modelled extreme values that most similarly represents the observed distribution (Ball et al., 2019). However, this method has been found to be affected by climatic variations, suggesting it is a more suitable method for arid environments where the observed flow can remain independent (Ball et al., 2019). Canada takes a similar approach to Australia, stating there is no defined standard for

FFA but the best method to use depends on the fit of the data, the use of average flows, the use of more than one parameter, and the most conservative method (Natural Resources Canada & Public Safety Canada, 2019).

2.2.2 New Zealand Regulations

In NZ, the use of the Gumbel or GEV methods is recommended for FFA due to their linear structure allowing for easy estimation of return periods (Henderson & Collins, 2016). However, the Ministry for the Environment recommends the best method for a region depends entirely on the type of catchment being analysed, offering several potential methods that include Gumbel, GEV, peaks over thresholds, and LP3 (Ministry for the Environment, 2010). This results in local governments having their own FFA guidelines (Robson & Reed, 2008; Henderson & Collins, 2016).

The specific FFA methods used in NZ varies across the regions used in this research. In Northland, the Regional Council focuses their flood frequency methods on design rainfall and specific catchment models using LP3 and Gumbel (Inglis, 2021). The use of design rainfall reflects the unique climate of the area which is exposed to remnants of tropical cyclones that can lead to extreme precipitation events (as discussed in Section 2.3.4.2) (MacMurray & Henderson, 2008). ECAN recommends the use of LP3 and GEV due to the methods having a low error standard meaning they can be used in catchments with relatively short historical record lengths (less than 20 years) (Griffiths et al., 2011b). For the Wellington region, the GWRC also recommends the GEV method because it places more emphasis on larger rainfalls (Cardno, 2021). However, GWRC also recommends the use of more than one method for validation, for example the Regional Flood Frequency method (McKerchar and Pearson, 1989) which estimates peak flow using contours, which can increase the accuracy and reliability of results (Cardno, 2021).

The Bay of Plenty Regional Council recommends a range of methods based on the type of environment (Environmental Hazards Group, 2012). For example, they recommend the Regional Flood Frequency method (McKerchar and Pearson, 1989) is used for rural catchments while the LP3 method is used for urban catchments (Environmental Hazards Group, 2012). The GDC does not have any specific FFA guidelines, however, consultation with the GDC determined they use a range of methods and complete the Anderson-Darling (A-D)

and Kolmogorov-Smirnov (K-S) goodness-of-fit tests to find the best method that models their observed flow data (B. Bosworth, personal communication, May 31, 2022). The Marlborough District Council commonly uses and recommends Gumbel (Williman, 1995; Marlborough District Council, 2021).

With there not being a nationally accepted FFA method in NZ, this research will follow the methods recommended by the United States Water Resources Council (England et al., 2019) and by the NZ councils. Therefore, flood thresholds and the event datasets will be calculated using either the Gumbel, LP3, and GEV methods. These methods will be examined more closely in the following section.

2.2.3 Flood Frequency Analysis Methods

2.2.3.1 Gumbel

The Gumbel method is an extreme value distribution developed by Gumbel (1941). The method determines the return period of large floods by calculating a simple two-parameter (location and scale) probability distribution based on the annual maximum flow (Farooq et al., 2018). It involves creating a dataset of the annual maximum flows for the entire record period which are then ranked from largest to smallest, and the probability of that flow occurring is calculated using the following equation:

$$Q_T = \bar{Q} (1 + KC_v) \quad (2.1)$$

where Q_T is the probability of discharge with T return period, C_v is the coefficient of variation, \bar{Q} is the annual mean flood and K is the frequency factor which is calculated using the standard deviation and reduced extreme values from Gumbel's table (Al-Mashidani et al., 1978).

The method is applied to environments where the observed values are homogeneous, are made at constant time intervals, and are independent of one another. The homogeneous assumption is often difficult to meet as it assumes the catchment's land use, climate, and river channel has remained stationary throughout the entire record period (Stedinger & Griffis, 2011; Yu, 2017). This is a disadvantage of FFA methods because given the length of some records there will always be changes in both climatic variation and catchment land use. Flow will always reflect changes in the environment, but the methods will not be able to show

these in the probability distributions (Greis, 1983; Milly et al., 2008; Stedinger & Griffis, 2011; Yu, 2017). NZ rivers have undergone significant land use, climatic, and geomorphic changes throughout their record periods and are therefore unlikely to meet this assumption (Ministry for the Environment, 2010; Griffiths, 2013; Kingston & McMecking, 2015). However, despite NZ being unlikely to meet the homogeneous assumption, it has also been identified that Gumbel can satisfactorily estimate flood frequency in NZ catchments and it has been widely used in NZ as a result (Pearson, 1991; Henderson & Collins, 2016).

2.2.3.2 Generalised Extreme Values

The GEV method is a continuous probability distribution that combines the extreme value distributions: Gumbel, Weibull, and Fréchet, into one distribution (Morrison & Smith, 2002; Farooq et al., 2018). GEV is a three-parameter distribution (shape, location, and scale) and these parameters are estimated using either maximum likelihood estimation (MLE), L-moments (LMOM), or moments (MOM). The MLE method can produce large variances and errors in the estimation of flood quantiles when the shape parameter is negative, especially when the sample size of annual maximum events are small and has significant outliers (Martins & Stedinger, 2000; Morrison & Smith, 2002). LMOM and MOM are the preferred methods for parameter estimation because they produce smaller quantile estimate variances. However, LMOM is a better estimator for NZ environments when outliers are present in the data because it can more accurately estimate the FFA parameters, regions of homogeneity, and identify parent distributions (Pearson, 1991; Martins & Stedinger, 2000). The GEV method also uses the annual maximum values, and the return periods are calculated using the following equation:

$$G(x) \begin{cases} \exp\left\{-\left(1 - \frac{k(x-b)}{a}\right)^{1/k}\right\} \\ \exp\left\{-\left(e - \frac{(x-b)}{a}\right)\right\} \end{cases} \quad (2.2)$$

where a is the scale parameter, b is the location parameter and k is the shape parameter. If the shape parameter, k , equals zero the Gumbel distribution shape is favored, if k is greater

than zero the Weibull distribution is favored and if k is smaller than zero the Fréchet distribution is favored (Morrison & Smith, 2002).

The GEV method requires the data to be independent, normally distributed, and homogenous (Rust, 2009). As described in Section 2.2.3.1, NZ river flows are unlikely to be homogeneous due to variations in the climate and land use. The assumption of independence is also unlikely to be met because some maximum flow events will be influenced by the preceding state of the environment, i.e. the amount of water in a catchment and the amount of precipitation that occurred the day before, and some high flow events will be caused by the same weather event (Rust, 2009). Rust (2009) however suggests these assumptions of independence, normality, and homogeneity can be relaxed due to the use of annual maximums because the annual maximum is a collection of single events that often occur at different times of the year, so the events are most likely independent.

A significant advantage of the GEV method is that its combination of methods (i.e. Gumbel, Weibull, and Fréchet) allows for the use of location, shape, and scale parameters that increase the accuracy, reliability, and flexibility of the distributions fit to the observed data. However, Pearson (1991) states that three-parameter distributions like GEV and LP3 should not be used in catchments with a record length of less than 30 years because sampling errors can be significantly larger than those produced by two-parameter distributions like Gumbel. Fortunately, all 17 rivers in this study have record lengths larger than 30 years so the potential for large sampling errors is reduced.

2.2.3.3 Log Pearson Type 3

The LP3 method is another extreme value distribution. Like GEV, the method is a three-parameter distribution (shape, location, and scale) and the parameters are estimated using a logged LMOM (England et al., 2019). LP3 determines the logarithm of predicted discharge at specific return periods by calculating the standard deviation, skewness coefficient, mean, and variance of the observed annual maximum flow values using the following equation:

$$X_{LP,T} = \bar{x}_1 + K_{LP,T} S_1 \quad (2.3)$$

where $X_{LP,T}$ is the logarithm of predicted discharge at specific return periods, \bar{x}_1 is the mean of the logged annual maximum flows, $K_{LP,T}$ is the skew coefficient and S_1 is the standard deviation of the logged annual maximum flows (National Resources Conservation Service, 2007).

The LP3 distribution can be applied to many natural environments because its three-parameter distribution allows more flexibility (National Resources Conservation Service, 2007). The method has also been identified to more consistently fit the observed annual maximum data and produce more accurate flood frequency values compared to the Gumbel method, due to the LP3 accounting for skew (England et al., 2019). However, some disadvantages arise when fitting the logged probability distribution to catchments in arid and semiarid environments, environments that have a high interaction with groundwater systems that could lead to low flow, and when there are missing data due to measurement system error resulting in no flow recorded (Jennings & Bensen, 1969; National Resources Conservation Service, 2007). When zero and low flow values are logged, they can create negative values and negative skew which can lead to inaccurate probability distributions and non-normal flood-like distributions.

2.3 New Zealand's Climate

This next section reviews the key local and large-scale features of NZ's climate as well as the drivers of regional variation in precipitation. As discussed in Section 2.1.3, extreme rainfall from meteorological events is the main cause of flooding in NZ and therefore, these features will be investigated in this thesis as potential drivers of high flow events in NZ's eastern regions.

2.3.1 Geography

NZ is located between 34°S and 47°S in the southwest Pacific of the Southern Hemisphere. It is a narrow country comprising of two main islands, the North Island and the South Island, together extending about 1500 km in a north-south direction. NZ's widest point, extending 450 km, is near the centre of the North Island and its southernmost point, Stewart Island/Rakiura, is located 30km south of the South Island. NZ is surrounded by the Pacific Ocean to the east and the Tasman Sea to the west with the nearest continent, Australia,

residing about 2400 km west of NZ. As a result, NZ has primarily a maritime climate with minimal continental influence. However, NZ can be subject to a wide range of local climates as a result of its topography and interaction with prevailing maritime winds which can lead to regional differences in precipitation and flood-generating mechanisms (Tomlinson, 1992; Mosley, 2000).

Being located within the belt of the mid-latitude westerlies and associated storm track, NZ's climate is dominated by mid-latitude synoptic weather systems (i.e. extra-tropical cyclones and anticyclones). Oceanic moisture-laden air masses predominantly come from the west and northwest off the Tasman Sea, but also from the south from the Southern Ocean after cold frontal passages, and the north and northeast from the subtropical southwest Pacific Ocean (Mosley, 2000; Tomlinson, 1992; Purdy & Austin, 2003; Sturman & Tapper, 2006). The progression of weather in NZ is governed by eastward migrating anticyclones, fronts, and depressions that travel between 30°S and 50°S (Lorrey & Bostock, 2017). Frontal systems associated with eastward migrating troughs are the main drivers of precipitation in NZ, with precipitation commonly occurring through uplift mechanisms along fronts and their interaction with the steep topography (Tait & Fitzharris, 1998)

On average, the predominant wind direction in NZ is generally from a westerly direction, which becomes more prevalent moving southward toward the core of the westerlies over the Southern Ocean (Fig. 2.2). The North Island is located within the transitional sub-tropical ridge zone where the trade winds and westerlies converge. This results in the North Island having less directional consistency in the prevailing wind than the South Island (Salinger, 1980a). The South Island is embedded in the core of the mid-latitude westerly winds throughout the year, resulting in less variation in the predominant wind directions (Salinger, 1980a). As demonstrated in Fig. 2.2, during winter, the core of the westerly wind belt migrates northward to ~50°S resulting in a strengthening of the prevailing westerlies across the country (Fig. 2.2c). In summer, westerly winds remain dominant (Fig. 2.2b), but they weaken and become more variable, especially in the north, as the westerlies migrate south and NZ becomes more strongly influenced by the sub-tropical high-pressure belt (Tomlinson, 1992; Gibson et al., 2016). The North Island's variations in the predominant wind directions leads to moisture being transported from different sources significantly influencing the amount of precipitation a region may receive. Therefore, variations from the

climatological surface winds and moisture transport pathways are likely to be key features driving regional differences in the climatic conditions that cause flooding in NZ's eastern regions.

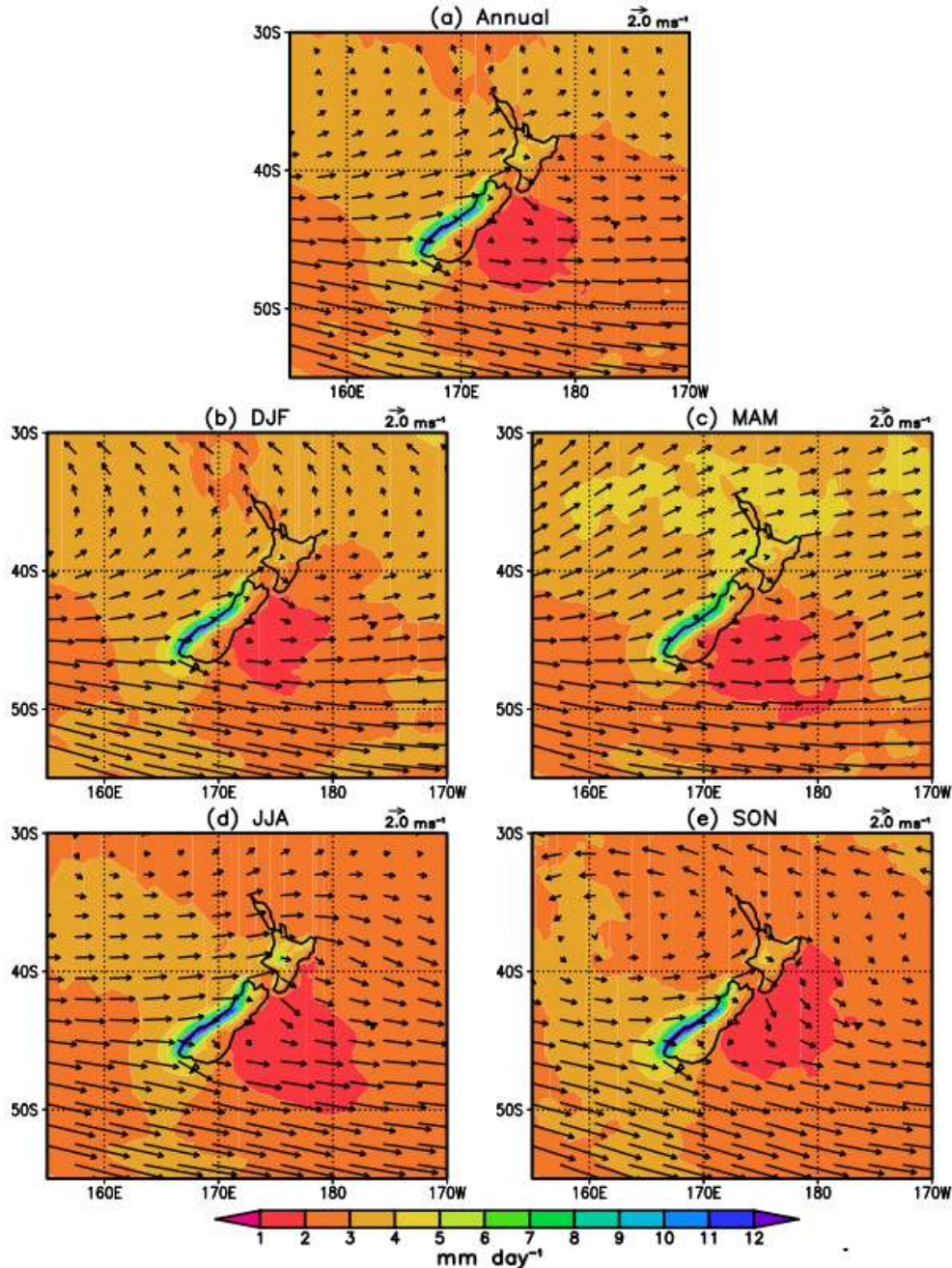


Figure 2.2: Average (a) annual and (b-e) seasonal climatological (1979-2020) precipitation (mm day^{-1}) and 10m wind (ms^{-1}) for the NZ region (source: ERA5). Seasons include (b) Summer (December, January, and February), (c) Autumn (March, April and May), (d) Winter (June, July and August), and (e) Spring (September, October and November).

The average climate zones in NZ are geographically varied as a result of the high elevation and narrow mountain range in the South Island (the Southern Alps) and the more complex, spatially varied topography of the North Island. The Southern Alps, with an approximate north-south orientation, lie perpendicular to the prevailing westerly winds and extend almost the entire length of the South Island, reaching elevations of 3724m (Salinger & Mullan, 1999; Kennett, 2021). This creates significant precipitation and (to a lesser degree) temperature gradients between the West and East Coast of the South Island due to orographic precipitation processes (Chater & Sturman, 1998; Sturman et al., 1999). As shown in Fig. 2.2, the windward West Coast has a significantly wetter climate (e.g., $>12\text{mm day}^{-1}$) compared to the leeward central regions and East Coast (e.g., $<5\text{mm day}^{-1}$) because the moist westerly air arriving from the Tasman Sea is forced upwards often resulting in precipitation in the west and thus reduced moisture on the leeward side east of the Main Divide. As a result, a climate “regime” (Figs. 2.3 and 2.4), the “Western South Island”, occurs on the windward side where annual precipitation exceeds $3,000\text{ mm yr}^{-1}$ in places near sea level, such as Hokitika ($\sim 42.5^\circ\text{S}$), with annual-mean precipitation increasing with increasing elevations (Macara, 2015). Weak seasonal variations in temperature and precipitation occur in the West Coast due to the persistent maritime westerly winds year-round.

Immediately downwind of the Southern Alps e.g. in the “Inland South Island” and “Eastern South Island”, a rain shadow effect occurs resulting in a much drier leeward climate and more continental-like seasonality in temperature (Figs. 2.3 and 2.4) (Macara, 2016). For example, Alexandra is within the Inland South Island and experiences semiarid summers and cold winters, and it is the most “continental” climate region in NZ, with precipitation averages rarely exceeding 300mm yr^{-1} due to the strong and persistent shadowing effect of the Southern Alps (F0 climate, Fig. 2.4) (Macara, 2016). Winds in the Eastern South Island climate zone, which includes the Canterbury region, are influenced by the deflection of westerly winds around the Southern Alps and the downward progression of dry foehn winds. Winds are more varied and most often come from a northeasterly direction, but at times from a southwesterly and northwesterly direction (Macara, 2016). Overall, the Eastern South Island region is sheltered from the southwest by the central high country and by the Southern Alps and North Island to the north and northwest, reducing precipitation in most westerly and

northerly airstreams, but on occasions where the flow is easterly, the region can experience orographically enhanced heavy precipitation (Kidson & Gordon, 1986; Macara, 2016). Thus, reversals of the mean westerly flow to an easterly flow is expected to be an important feature preceding river flooding in the Eastern South Island.

An east-west precipitation gradient is not as prevalent in the North Island, as a result of more variable wind directions and more spatially varied topography (Ummenhofer & England, 2007). Some mountainous features in the North Island reach elevations up to 2797m, such as the Central Plateau's Mt Ruapehu, the Raukūmara Ranges in the Bay of Plenty/Gisborne region, and the Tararua Ranges in the Wairarapa region, and create more localised east-west gradients in precipitation (Fig. 2.2) (Sturman et al., 1999; Ummenhofer & England, 2007; Kennett, 2021). Figure 2.2 shows higher amounts of precipitation occur around the mountainous topography of the Central North Island climate zone due to the orographic mechanisms of the volcanic plateau (Salinger, 1980a). New Plymouth is located at sea level west of the Central Plateau in the South-West North Island and receives on average 2400mm yr⁻¹ of precipitation due to the predominant maritime westerlies (A2 climate, Fig. 2.3 and 2.4).

Meanwhile, the Hawkes Bay and Wairarapa regions in the “Eastern North Island” are sheltered from the prevailing westerly winds by the Central Plateau and Tararua Ranges, leading to precipitation averages of only around 1000mm yr⁻¹ (Fig. 2.4). The Gisborne region (~38°S) however, is exposed to both westerly and easterly winds due to the southeast-northwest orientation of the Raukūmara Ranges and its exposure to sub-tropical and post-tropical cyclones to the north which can bring moist tropical airmasses and northeasterly winds, resulting in orographically enhanced precipitation in the region (C climate, Fig. 2.4) (Cullum et al., 2017). The “Northern New Zealand” climate zone is narrow with low topographic relief and less wind directional consistency, resulting in mostly uniform annual precipitation amounts (Chappell, 2013). Blocking anticyclones are also common east of NZ and can have a significant effect on these northern regions and will be discussed further in Section 2.3.3 (Salinger, 1980b; Lorrey & Bostock, 2017).

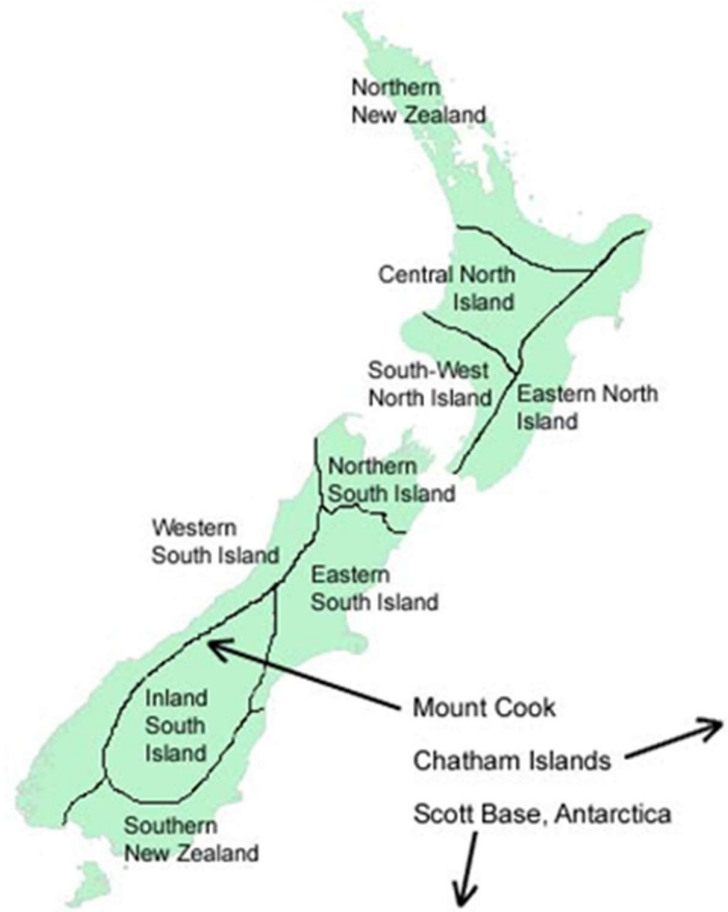


Figure 2.3: New Zealand climate zones (National Institute of Water and Atmospheric Research, 2022a).



A	Warm, humid summers, mild winters. Precipitation 1000–1500 mm year ⁻¹ , with winter maximum.
A2	As A, but with precipitation 1500–2400 mm year ⁻¹ .
B	Sunny, sheltered areas with very warm summers and mild winters. Precipitation 1000–1800 mm year ⁻¹ with winter maximum.
C	Very warm summers, with dry foehn wind from NW. Precipitation 1000–1500 mm year ⁻¹ , with low amount and reliability in spring and summer.
C0	As C, but with precipitation 600–1000 mm year ⁻¹ .
C2	Cooler and wetter hill climates. Precipitation 1500–2000 mm year ⁻¹ , with very heavy rains from S and SE.
D	Warm summers, mild winters, with prevailing W to NW winds. Precipitation 900–1300 mm year ⁻¹ , reliable and distributed throughout year.
E	Mild temperatures, with prevailing SW winds. High rainfall increases rapidly inland with elevation; winter minimum.
F	Warm summers with occasional hot NW foehn winds, and cool winters with frost. Precipitation 500–750 mm year ⁻¹ .
F2	Cooler and wetter hill climates, with prevailing NW winds. Precipitation 750–1500 mm year ⁻¹ , and snow lying for weeks in winter.
F0	Semiarid area with very warm dry summers and cold winters. Precipitation 300–500 mm year ⁻¹ .
G	Warm summers, cool winters. Precipitation 600–900 mm year ⁻¹ with slight reduction in winter.
G2	Wetter and slightly cooler than G, with cloudy, windy conditions and frequent showers. Precipitation 900–1300 mm year ⁻¹ .
M	Mountain climates; high precipitation up to 15 000 mm year ⁻¹ .

Figure 2.4: New Zealand's climate regions. Shaded areas depict mountainous features and lines with letters and numbers refer to that area's climate region description located in the below table. (From Fig. 1 of Mosley (2000)).

2.3.2 Large-scale Precipitation variability

NZ's location in the Southern Hemisphere middle latitudes results in several large-scale climate patterns influencing seasonal and interannual precipitation (Gordon, 1986; Mullan, 1995; Ummenhofer & England, 2007; Jiang, 2011; Harrington & Renwick, 2014).

Precipitation variability in NZ is primarily modulated by the El Niño-Southern Oscillation (ENSO) and the Southern Annular Mode (SAM) (Ummenhofer & England, 2007). These climate modes can influence the direction and strength of the prevailing winds and their associated interaction with the topography (Griffiths, 2011a; Harrington & Renwick, 2014). Therefore, variations in these large-scale patterns are likely important to understanding the preceding conditions that lead to river flooding in NZ.

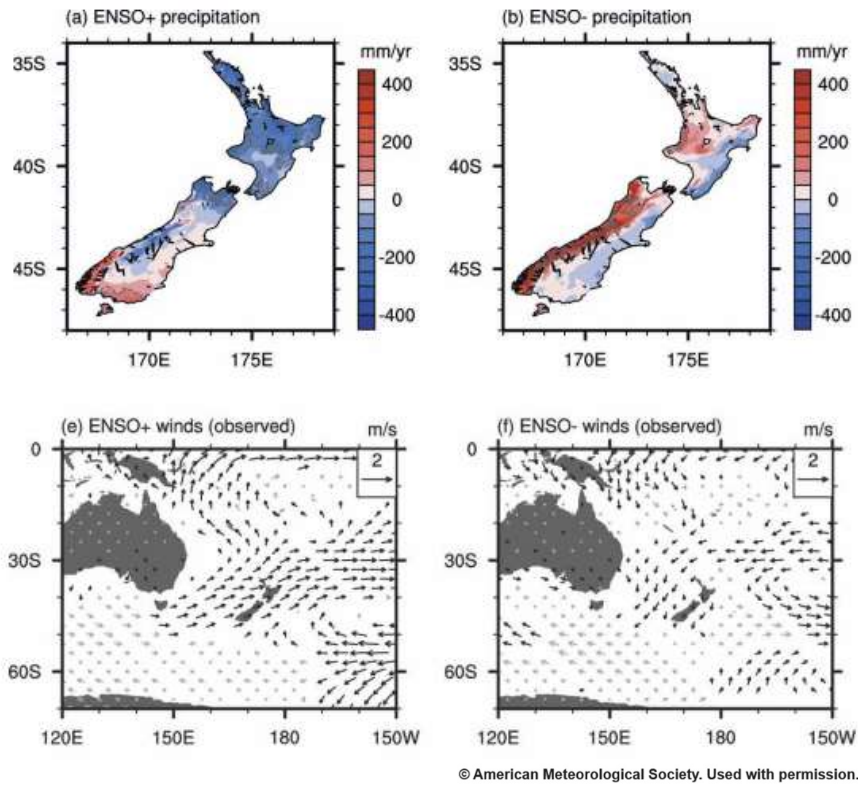
2.3.2.1 El Niño Southern Oscillation

The El Niño-Southern Oscillation (ENSO) is a mode of variability in the tropical Pacific that influences climatological precipitation in NZ on an interannual timescale and has been identified to influence flow in some NZ rivers (McKerchar & Pearson, 1994; McKerchar et al., 1996). There are two phases of ENSO, a cold phase (La Niña) and a warm phase (El Niño), that are defined by anomalies in sea surface temperature (SST) over the central and eastern tropical Pacific and associated changes in sea level pressure (Trenberth, 1997). During a La Niña, SSTs are colder than average in the central and eastern tropical Pacific accompanied by stronger than normal easterly trade winds while SSTs are above average in the western tropical Pacific (Hartmann, 2016). The strengthened trade winds and enhanced convection in the west leads to an enhancement of the zonal equatorial Walker Circulation (large-scale ascent in the western tropical Pacific and descent in the eastern tropical Pacific, as described by Bjerknes (1969)), leading to increased precipitation in the western Pacific and reduced precipitation in the east (Hartmann, 2016). An El Niño occurs when SSTs are above average in the central and eastern Pacific, weakening the easterly trade winds, shifting the deep convection into the central tropical Pacific, together leading to a breakdown of the Walker Circulation with a shift of the ascending branch to the central tropical Pacific (Hartmann, 2016).

The changes that occur to the Walker Circulation, along with the generation of poleward propagating planetary, or “Rossby”, waves forced from divergent flow out of the tropics near the tropopause associated with deep convection (described by Hoskins & Karoly (1981) and Trenberth et al. (1998)) during different ENSO phases can affect precipitation in NZ through altering regional circulation patterns and the strength/position of the westerly storm track (Salinger & Mullan, 1999; Griffiths, 2011a). On an annual-mean basis, winds

across NZ tend to be more northerly during a La Niña (Fig. 2.5f) which increases precipitation in the Central, North, and Eastern climate zones of the North Island and along much of the West Coast of the South Island (Fig. 2.5b; Ummenhofer & England, 2007; Griffiths, 2011a). These northerly winds are partly caused by increased cyclonic activity over the Tasman Sea and more stationary “blocking” anticyclones east of NZ (Fig. 2.5f; Mullan, 1989). The increased northerly flow transports moist sub-tropical airmasses southward onto the northern sections of the higher terrain of the North Island and the western sections of the Southern Alps, which enhances the orographic precipitation in these regions, potentially increasing their susceptibility to flooding (Tait & Fitzharris, 1998). Therefore, a La Niña may be an important driver of river flooding in eastern regions of NZ, especially in the North Island.

During an El Niño, on an annual-mean basis NZ experiences an increase in frequency and strength of colder southwesterly winds which leads to an increase in annual precipitation in the Southern New Zealand climate zone and the Fiordland region, while drier conditions generally occur for the rest of NZ especially in the north (Fig. 2.5a). The southwesterly flow illustrated in Fig. 2.5e is a result of a northward displacement of the climatological westerly winds and an increase in the frequency of cold frontal passages (Mullan, 1998; Kidson & Renwick, 2002). Despite the storm track (within the westerlies) shifting north over NZ, composite annual-mean anomalies of precipitation for El Niño, shown in Fig. 2.6a, indicate that the more southwesterly flow leads to an increase in precipitation only around areas most exposed to the moisture bearing winds in the south (Ummenhofer & England, 2007), and demonstrates that increased precipitation in the North Island is primarily tied to moist northerly flow more commonly seen during La Niña (Fig. 2.5a,b). However, below average precipitation in eastern NZ often leads to drought conditions, which provides favourable antecedent conditions for flooding, and thus both phases of ENSO will be examined in this thesis.



© American Meteorological Society. Used with permission.

Figure 2.5: Observed composites of annual (a-b) precipitation (mm/yr) and (e-f) wind anomalies (black vectors in 2m/s) in New Zealand during (a,e) El Niño and (b,f) La Niña between 1960 and 2004. (Modified from Fig. 13 of Ummenhofer & England (2007)).

There are important seasonal variations in the effects of El Niño and La Niña on NZ's precipitation which has been identified to also influence seasonal river flow. During summer, when the climatological westerlies shift south, El Niño strengthens the westerlies across much of the country (Griffiths, 2011a). This enhances the rain shadow effect for the East Coast regions of NZ, leading to locally dry summers and drought conditions (Kidson & Renwick, 2002; Griffiths, 2011a). In contrast, during an El Niño winter, the Eastern North Island and Southern New Zealand climate zones experience increased precipitation while the rest of NZ experiences drier conditions similar to those shown for the annual-mean in Fig. 2.5 (Gordon, 1986; Griffiths, 2011a). In a La Niña summer, an increase in northeasterly winds results in above average precipitation for the northern and eastern regions of NZ, such as the Bay of Plenty and Gisborne, and below average rainfall for the South Island's West Coast (Gordon, 1986; Griffiths, 2011a). During a La Niña winter, rainfall for most of NZ is above average (Griffiths, 2011a). During transitional seasons, in an autumn (spring) El Niño (La Niña), there is an increase in southwesterly (northeasterly) winds, which decreases (increases) extreme

precipitation events on the East Coast of the North Island (Gordon, 1986; Kidson & Renwick, 2002; Griffiths, 2011a).

Not surprisingly, ENSO has been identified to influence river flows in both the North and South Islands due to its influence on precipitation (McKerchar & Pearson, 1994; McKerchar et al., 1996). McKercher & Pearson (1994) identified higher winter and spring flows occur in the North Island's Whanganui River during a La Niña as a result of above average rainfall for the Central North Island. For the South Island's Clutha River, spring and summer flows during a La Niña were identified to be two times higher than flow during an El Niño due to the effect ENSO has on snow accumulation in the alpine regions and the associated summer snow melt period (McKerchar et al., 1996).

Variability in ENSO has also been shown to have an influence on rivers located in the northeastern regions of NZ. For example, in the Bay of Plenty and Gisborne regions, El Niño conditions lead to reduced river flow whereas La Niña conditions lead to higher river flow (Mosley, 2000). Mosley (2000) also identified that during an El Niño a significant reduction in river flows occurred in most rivers located in the North Island and Northern South Island, whereas during a La Niña, flood flows increased in these regions due to increased moisture bearing northerly and northeasterly winds. The largest ENSO-related impacts on river flow occurs in the Southern New Zealand climate zone (Mosley, 2000). In this zone, there is a strong tendency for increased flow during an El Niño and decreased flow during a La Niña (Mosley, 2000). Therefore, variability in ENSO and its effect on regional precipitation is an important yet highly variable (both seasonally and regionally) control on river flow in NZ that needs improved understanding to assess drivers of variability in (and vulnerability to) river flooding in NZ.

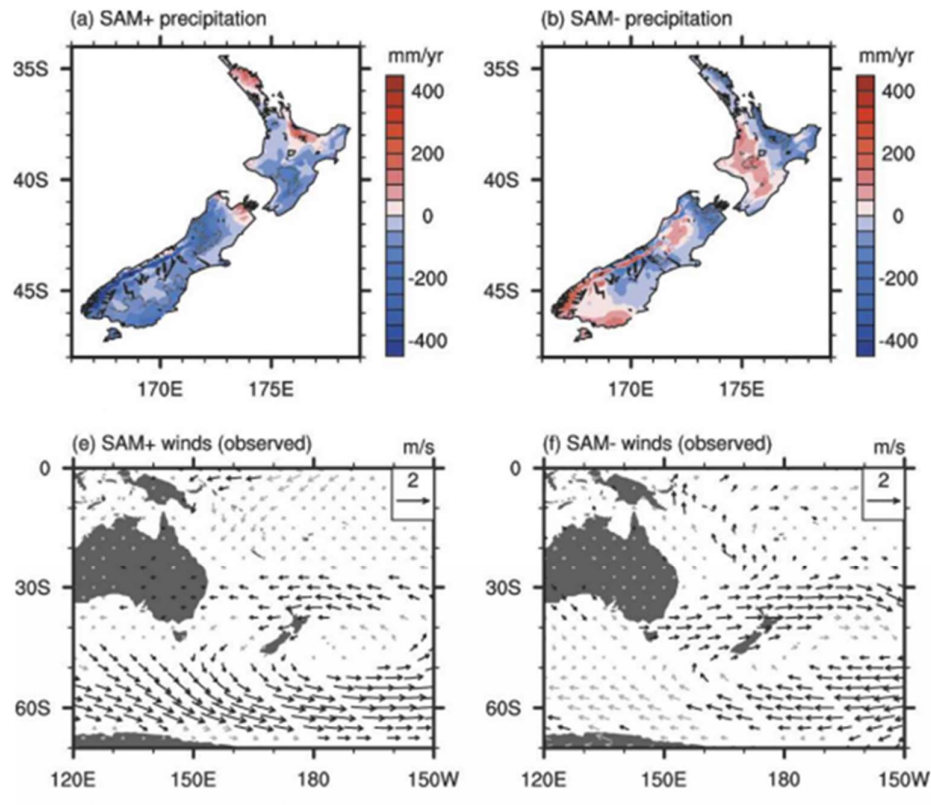
2.3.2.2 Southern Annular Mode

The SAM is the dominant mode of atmospheric circulation (pressure and wind) variability in the Southern Hemisphere and previous work has identified a strong link between precipitation anomalies in NZ and the phase of the SAM (Ummenhofer & England, 2007; Kidston et al., 2009; Fogt et al., 2012; Harrington & Renwick, 2014; Fogt & Marshall, 2020). Therefore, the SAM is potentially another important climate feature causing flood events in eastern NZ. The SAM is a zonally symmetric mode of Southern Hemisphere variability

characterised by meridional shifts about the climatological mean position of the mid-latitude westerlies (Kidston et al., 2009; Fogt et al., 2012). It has a ringlike structure of pressure and geopotential height anomalies that form over Antarctica ($60 - 90^{\circ}\text{S}$) and the middle latitudes between 35°S and 45°S (Kidston et al., 2009). The SAM has two phases, a positive phase and a negative phase, that relate to oscillations in the sign of geopotential height anomalies over the pole and middle latitudes (Gillett et al., 2006). The positive phase is associated with an increase in geopotential height over the middle latitudes, a decrease in geopotential height over the polar cap, and a poleward displacement and strengthening of the mid-latitude storm track over the Southern Ocean (Gillett et al., 2006; Renwick & Thompson, 2006). During a negative phase the opposite conditions occur, and the westerlies weaken and shift northward into middle latitudes along with the storm track. These fluctuations result in strong changes in storm activity and winds in the middle latitudes like NZ on a weekly to monthly/seasonal basis and thus have a strong influence on NZ's weather and climate (Gillett et al., 2006; Kidston et al., 2009).

As discussed in the previous sections, NZ precipitation is strongly influenced by the prevailing westerly winds and their interaction with topography. The SAM causes anomalous departures from the climatological westerly winds, which affects the mean climatological spatial distribution of precipitation described in Section 2.3.1 (Renwick & Thompson, 2006). Figure 2.6e illustrates that during a positive SAM, wind anomalies predominantly flow from the east, particularly in the North Island, while a reduction in westerly winds over the South Island occurs (Ummenhofer & England, 2007). Composite anomalies of annual precipitation during a positive SAM (Fig 2.6a) indicate that precipitation decreases over much of NZ except for East Coast regions, similar to a La Niña (Ummenhofer & England, 2007). This relates to anomalously dry conditions observed over the South Island due to the poleward shift of the westerlies/storm track and an increase in the frequency of blocking (persistent high-pressure) events (Gillett et al., 2006; Renwick, 2011). Meanwhile, precipitation increases in areas more exposed to the easterly winds, such as Northland, Bay of Plenty, and Marlborough regions, where an increase of up to 200mm yr^{-1} is observed (Fig. 2.6a; Ummenhofer & England, 2007). The reversal of the climatological precipitation observed in a positive SAM is largely explained by the topography, where the regions on the leeward side of main topographic features typically sheltered by the westerlies become exposed to orographic-enhanced precipitation

from easterly flow. Therefore, SAM may also be an important driver of river flooding in eastern regions of NZ, especially in the North Island.



© American Meteorological Society. Used with permission.

Figure 2.6: Same as Fig. 2.5 but for (a,e) positive SAM and (b,f) negative SAM. (Modified from Fig. 14 of Ummenhofer & England (2007)).

Meanwhile, westerly winds become stronger in a negative phase of the SAM, as seen in Fig. 2.6f. These westerly winds affect most of NZ and cause an enhancement of the mean climatological spatial distribution of precipitation (Fig. 2.2a). Composite anomalies of annual precipitation shown in Fig. 2.6b show an increase in precipitation in the Southern Alps and the West Coast of the North Island of up to 400mm yr^{-1} due to increased exposure to westerly winds and an increase in the frequency of trough types (low-pressure systems) passing over NZ (Ummenhofer & England, 2007; Renwick, 2011). An increase in precipitation is also observed in the southern South Island region around 45°S because of anomalously southwesterly flow over the region. Reduced northeasterly and easterly flow in NZ results in a decrease in precipitation for the eastern and northern regions of NZ that are more

orographically sheltered from the westerly winds therefore a negative phase of SAM may not be as important for river flooding in the regions of interest (Ummenhofer & England, 2007).

On a seasonal timescale, the ring like structure of the SAM becomes most zonally symmetric in summer and more zonally asymmetric in winter (Li & McGregor, 2017). In summer, a positive SAM leads to a reduction in precipitation over most of the western climate zones and an increase in precipitation in the eastern coastal regions of the North Island, such as Gisborne and Northland (Kidston et al., 2009; Griffiths, 2011a). However, the SAM has the greatest impact on wind and precipitation anomalies in NZ in winter. During a negative SAM, winter precipitation increases over both islands (Griffiths, 2011a). The Western and Southern South Island and South West North Island climate zones experience an increase in precipitation during a negative SAM winter (Kidston et al., 2009; Griffiths, 2011a; Li & McGregor, 2017). In contrast, when SAM is positive in winter, the anomalously strong north to northeast flow and increased blocking high-pressure systems around NZ result in the western regions being drier than average (Li & McGregor, 2017). For the Northern New Zealand and Eastern North Island climate zones the anomalous northeasterly flow increases precipitation, while the stronger westerlies in a negative phase enhance local rain shadow effect and reduce precipitation (Kidston et al., 2009; Griffiths, 2011a).

On shorter sub-seasonal (intraseasonal) time scales, variability in NZ river flow has also been linked with the week-to-week phase oscillations of the SAM (Li & McGregor, 2017). Li & McGregor (2017) identified statistically significant associations between river flow and the SAM in the Northern and Eastern South Island and Eastern North Island climate zones. High summer flows tended to occur during a negative phase of SAM (despite the general reduction in seasonal and annual-mean precipitation) in these regions due to an increase in synoptic storm systems crossing over NZ. High river flows in the South West North Island and Southern New Zealand climate zones were also identified to be strongly associated with the negative phase of the SAM in winter (Li & McGregor, 2017). The Canterbury region was the only region to have a strong relationship with both phases of the SAM, where a negative SAM resulted in low flows and a positive SAM led to high flows, perhaps due to it being located closer to the main core of the westerlies resulting in more coherent reversals in wind direction between the two SAM phases; indeed, the strongest association occurred during winter as a result of the more pronounced mid-latitude westerlies over the South Island (Li & McGregor, 2017).

While these findings are important for understanding how NZ river flow is influenced by the main modes of large-scale climate variability, less is known about their influence on occurrence of flooding (or more specifically, extreme high flow events) (Kingston et al., 2022). In particular, recently Kingston et al. (2022) identified flooding in inland South Island catchments did not show a clear association with SAM as it occurred during both positive and negative phases. Thus, further research is clearly needed to determine the SAM's influence on extreme river flow events across NZ.

2.3.3 Synoptic Precipitation Drivers

While fluctuations in modes of large-scale climate variability influence seasonal to annual precipitation across NZ, synoptic or “weather” events have a significant influence on local shorter-duration “events”. Unlike large-scale circulation features, synoptic weather features refer to regional variations in weather elements, such as day-to-day wind direction and strength, owing to individual passages of synoptic-scale high- and low-pressure systems (Kidson, 2000; Griffiths, 2011a). These features commonly set up the local weather conditions that cause precipitation and thus would be important features of river flooding. Pioneering research into this area by Kidson (2000) identified 12 main daily synoptic weather types over NZ through a cluster analysis based on 40 years of monthly 1000 hPa geopotential height (near-surface) data, as shown in Fig. 2.7. A comparison of these types and their frequencies and variations led to the identification of three main synoptic regimes: 1) Trough pattern, 2) Zonal pattern, and 3) Blocking pattern (Kidson, 2000). These regimes are defined, respectively, as: 1) primarily unsettled conditions with a high frequency of synoptic low-pressure systems affecting NZ, 2) high-pressure in the north and low-pressure to the south of NZ and zonal/westerly flow in the central and southern parts of NZ, and 3) anticyclonic conditions predominantly with highs in the south and east of NZ (Kidson, 2000; Renwick, 2011). The three regimes and their synoptic weather patterns are shown in Fig. 2.7. These weather types have strong but regionally varying effects on NZ’s precipitation which highlights the importance of examining weather conditions on shorter time scales in addition to ENSO and SAM phase.

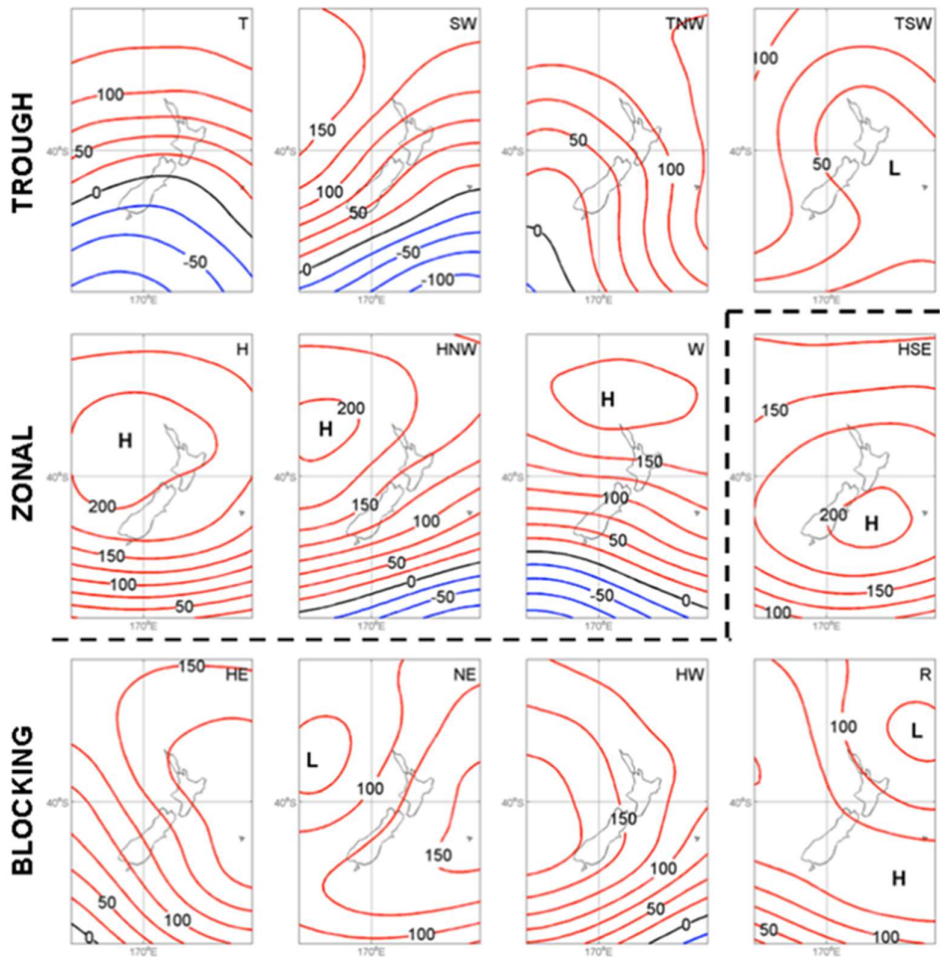


Figure 2.7: The 12 Kidson types and their associated regimes. Names of each synoptic type are denoted on the top right-hand corner, i.e. ‘T’ is Trough, ‘SW’ is Southwesterly flow, ‘TNW’ is Trough Northwesterly flow, and ‘TSW’ is Trough Southwesterly; for Zonal, ‘H’ is High over the country, ‘HNW’ is High to the Northwest, and ‘W’ is High to the North with Westerly flow; and for Blocking, ‘HSE’ is High to the Southeast, ‘HE’ is High to the East, ‘NE’ is Northeasterly flow, ‘HW’ is High to the West, and ‘R’ is Ridge. (From Fig. 1 of Griffiths (2011a), modified from Fig. 2 of Kidson (2000)).

The twelve “Kidson” synoptic types and their effect on average daily precipitation in NZ are shown in Fig. 2.8. Most of NZ experiences above average daily precipitation in a Trough regime (‘T’ and ‘TNW’) as a result of low-pressure/cyclonic systems dominating NZ (Kidson, 2000; Renwick, 2011; Pohl et al., 2022), similar to El Niño and negative SAM. The largest change in daily precipitation occurs in the Western South Island climate zone during a ‘T’ synoptic type where anomalies of +15mm per day occur because of the stronger westerly flow (Pohl et al., 2022). The increased storm activity also results in above average

precipitation in the South West and Central North Island climate zones during the ‘T’ and ‘TNW’ synoptic types in Fig. 2.8 (see caption in Fig. 2.7 for description of the individual regime types). However, the precipitation anomalies are generally weaker in the North Island due to the smaller topographic effects (Renwick, 2011; Pohl et al., 2022).

Blocking regimes result in above average precipitation in the North Island (Pohl et al., 2022), similar to La Niña conditions and positive SAM. During a Blocking regime, an increase in high-pressure anomalies to the east of NZ leads to anomalous northerly (‘HE’) and northeasterly (‘NE’) flow and a reduction in westerly winds. This results in above average precipitation in the climatologically drier “East Coast” regions of NZ and across the northern North Island, but below average on the West Coast (Griffiths, 2011a; Renwick, 2011). In a Zonal regime (‘H’ and ‘HNW’), high pressure generally dominates NZ, and the westerlies shift poleward to the most southern regions resulting in generally drier conditions across all of NZ (Renwick, 2011; Pohl et al., 2022). Therefore, Trough and Blocking regimes could be important for river flooding in the eastern regions of NZ.

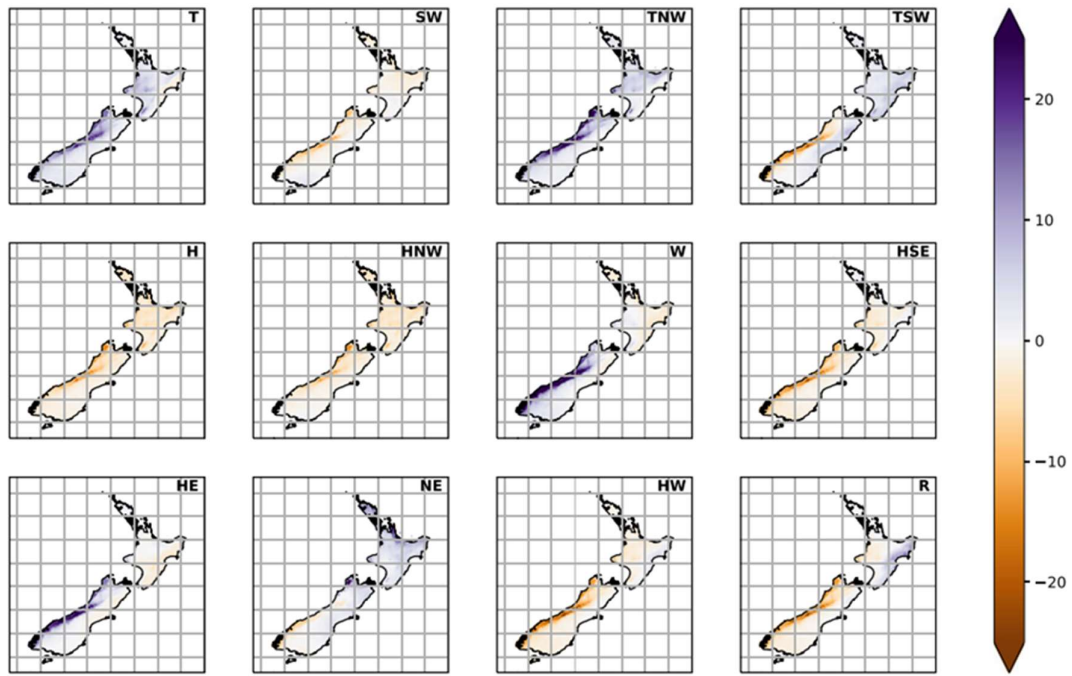


Figure 2.8: The 12 Kidson (2000) types and the associated daily precipitation anomalies in NZ between 1979 and 2019. The colour bar depicts precipitation anomalies in mm based on a 95% significance level, with blue indicating increased precipitation and orange indicating reduced precipitation. (From Fig. 10 of Pohl et al. (2022)).

The seasonality of precipitation anomalies in a Trough regime is invariant, with above average precipitation in all regions of NZ in every season. However, the 'T' synoptic type is most common to occur in spring resulting in particularly enhanced precipitation on the western side of the Southern Alps (Kidson, 2000; Renwick, 2011). The Blocking regime has the most seasonality with increased occurrence of 'HSE' and increased precipitation (and potentially increased flooding risk) on the East Coast of the North Island during summer and autumn (Griffiths, 2011a; Renwick, 2011; Kidson, 2000; Jiang, 2011). There is also an increase in the persistence of some synoptic types seasonally. During spring, the number of days a 'W' type is present increases, resulting in longer periods of above average precipitation on the West Coast of the South Island and an increase in the number of dry days for the East Coast of the North Island. Meanwhile Blocking regimes are not only more common but also more persistent in summer and autumn (Kidson, 2000; Renwick, 2011; Jiang, 2011), further increasing the likelihood that blocking is an important driver of river flooding in eastern regions.

More recently, variations in the Kidson synoptic types have also been linked to extreme precipitation events in NZ as shown in Fig. 2.9 and 2.10 (Griffiths, 2011a; Pohl et al., 2022). NIWA defines extreme or heavy precipitation events in NZ where more than 100mm of precipitation falls within 24 hours (NIWA, 2022b). Figures 2.9 and 2.10 illustrate that Trough synoptic types are the most common drivers of annual and seasonal extreme high precipitation events in NZ, except for the Northern and East Coast regions of the North Island and the Fiordland region where Blocking and Zonal synoptic types, respectively, more commonly lead to extreme precipitation in these regions. 'TSW' is the dominant Trough type that leads to extreme precipitation on the East Coast of the South Island whereas the 'T' and 'W' Trough and Zonal types are most common on the West Coast (Fig. 2.9). The Blocking types 'NE' and 'R' drive annual and seasonal extreme high precipitation in the Northern New Zealand and Eastern North Island climate zones for most of the year and are seven times more likely to cause extreme precipitation in these regions than any other synoptic type (Fig. 2.10; Griffiths, 2011a). In Northland, the Blocking type 'NE' produces extreme high precipitation as it can bring tropical moisture down from the north (Fig 2.9; Griffiths, 2011a; Pohl et al., 2022). The Blocking type 'NE' is also dominant in the Marlborough region with locally enhanced northeasterly flow (Fig 2.9). Therefore, with the Kidson types 'NE', 'TSW', and 'R' identified as

a drivers of extreme precipitation in the eastern regions of NZ, a trough to the southwest and a blocking high to the northeast are features of particular interest in this research.

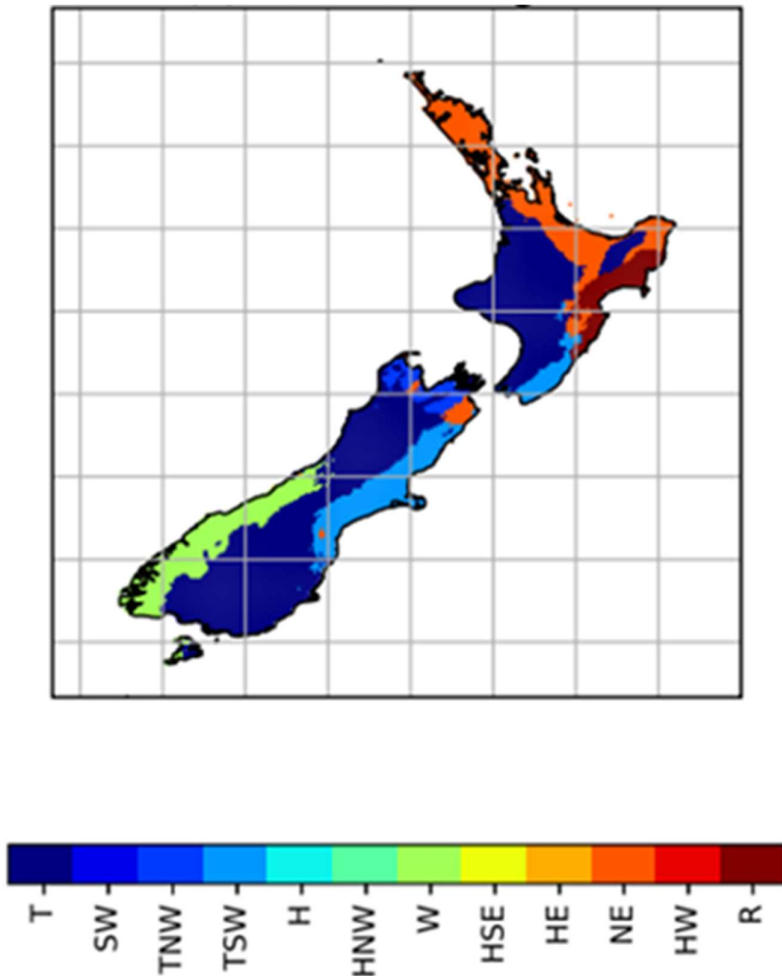


Figure 2.9: Dominant Kidson types that commonly lead to extreme precipitation (extreme precipitation is defined as daily anomalies above the 95% percentile by Pohl et al. (2022)). Colour shading relates to one of the 12 Kidson (2000) types. (From Fig. 15(b) of Pohl et al. (2022)).

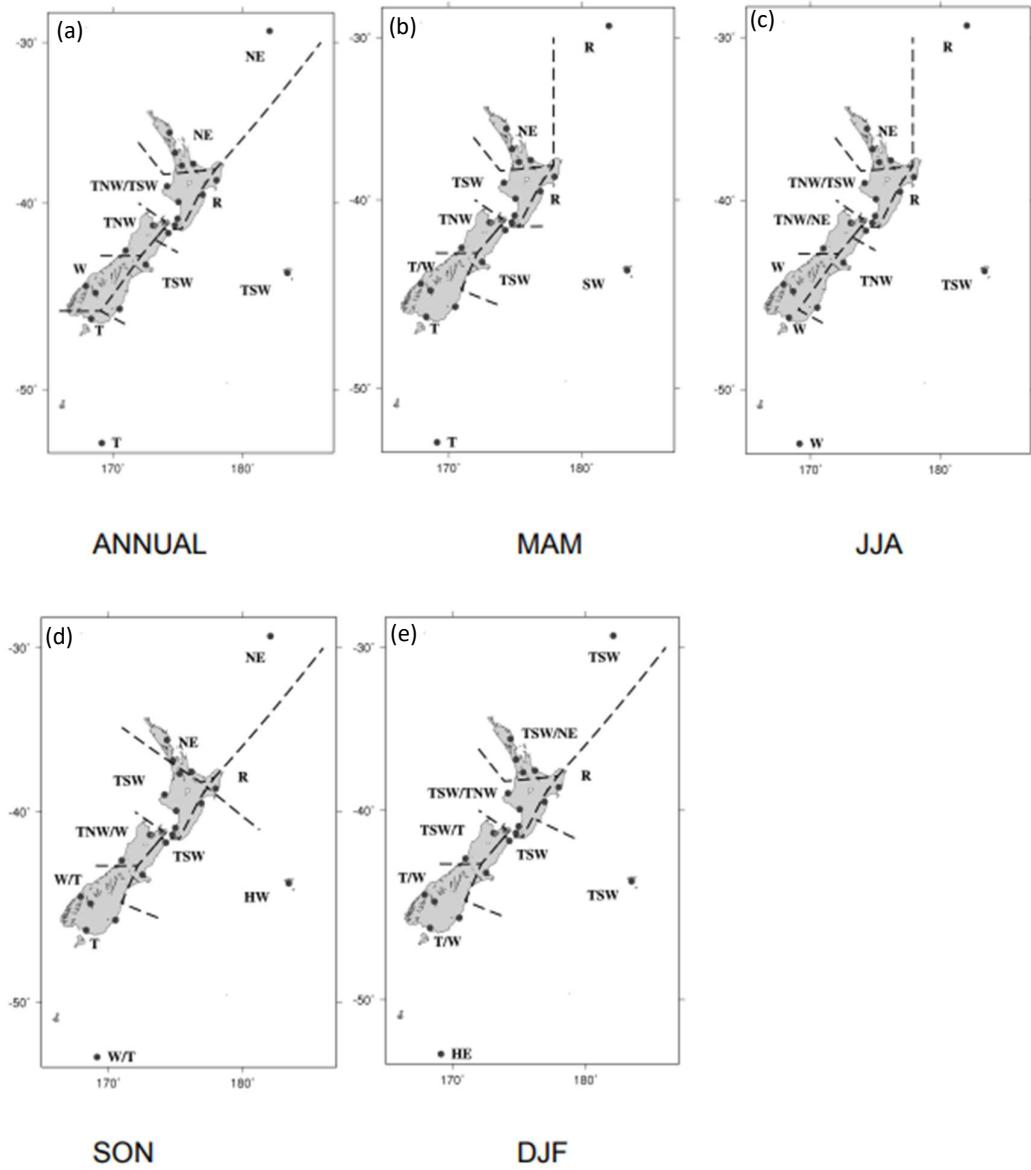


Figure 2.10: Dominant Kidson types with the highest percentage of occurrence during extreme (a) annual and (b-e) seasonal precipitation regionally within NZ. Seasons include (b) Autumn (March, April and May), (c) Winter (June, July and August), (d) Spring (September, October and November), and (e) Summer (December, January and February). (Modified from Fig. 3 of Griffiths (2011a)).

Kingston et al. (2022) identified that eight of the largest floods in five South Island river catchments, with headwaters located along the Main Divide of the Southern Alps, were most associated with the Trough Kidson regime. The Trough regime accounted for 57% of the

floods in the South Island's Rakaia and Pukaki Rivers due to the Trough regime's association with low-pressure systems south of NZ and the strong NW-W-SW flow which was found to complement the moisture transport pathway associated with high flow events (Kingston et al., 2022). Kingstons et al. (2022) supports the expectation that Kidson types that commonly lead to extreme precipitation will likely also lead to flooding, at least in NZ's South Island river catchments. However, this has not been investigated in North Island catchments.

2.3.4 Extreme Events

Extreme weather events, such as ARs, ex-tropical Cyclones, and thunderstorms, often bring large amounts of precipitation that can lead to devastating river flooding in many regions of NZ. To further understand the preceding circulation conditions of flooding in NZ, it is important to identify the drivers of NZ's worst historical weather and flooding events.

2.3.4.1 Atmospheric Rivers

In recent years it has been identified that ARs play a key role in NZ's hydrological cycle and the occurrence of extreme hydrometeorological events (Kingston et al., 2016; Griffin et al., 2020; Kennett, 2021; Kingston et al., 2022). ARs are narrow regions of enhanced poleward water vapour transport that span 2000km or more in length and most commonly occur in the middle latitudes (Shu et al., 2021). ARs can bring heavy precipitation when they make landfall, especially when they intercept regions of upslope topography (Kingston et al., 2022; Shu et al., 2021). Due to NZ's location in the middle latitudes and in a region of relatively high frequency in AR activity, ARs have been found to significantly contribute to both climatological (total annual) precipitation and the occurrence of extreme precipitation events, making NZ particularly susceptible to their impacts (Kingston et al., 2016; Kingston et al., 2022; Prince et al., 2021; Shu et al., 2021). In NZ, there are on average between 70 and 90 days annually where ARs influence precipitation (Shu et al., 2021). ARs are responsible for up to 50% of precipitation and 98% of extreme precipitation events (precipitation above the 99th percentile) in NZ, and they have also been attributed to nine of the ten most costly floods in NZ (Reid et al., 2021).

ARs most commonly occur on the West Coast, accounting for 80% of precipitation events (Shu et al., 2021). Regions east of the Southern Alps are not as often impacted by ARs arriving from the west because the moisture is typically depleted through precipitation on the western slopes. However, ARs have been identified as causing significant flooding events in eastern slopes of the Southern Alps when they arrive from the northeast and northwest (Reid et al., 2021; Shu et al., 2021). On the 30th of May 2021, Canterbury (Eastern South Island) was subject to an AR from the northeast direction that caused up to 238mm of rain to fall within 24 hours in Ashburton, double the average May monthly rainfall of Ashburton (Morton, 2021). The AR led to severe flooding in the Selwyn, Waimakariri, and Ashburton-Hakatere Rivers, which the Council described as a 1-in-200-year event (ECAN, 2021). ARs have also been identified as impacting the Northern South Island climate zone when arriving from a northwesterly direction (Horrell et al., 2012; Shu et al., 2021). Figure 2.11 illustrates an AR making landfall around the Marlborough region (Northern South Island) on the 29th of December 2010 (Shu et al., 2021). The AR brought moist air originating from the deep tropics which brought 230mm of precipitation within 24 hours and 1-in-100-year flooding occurred in the Wairau River (Stuff, 2010). In the North Island, ARs have also been linked to 70% and 80% of the most extreme precipitation events in the Bay of Plenty and Gisborne regions, respectively (Reid et al., 2021). Therefore, while ARs occur more frequently on the West Coast of the South Island, they can also have a significant impact in other regions of NZ and require investigation.

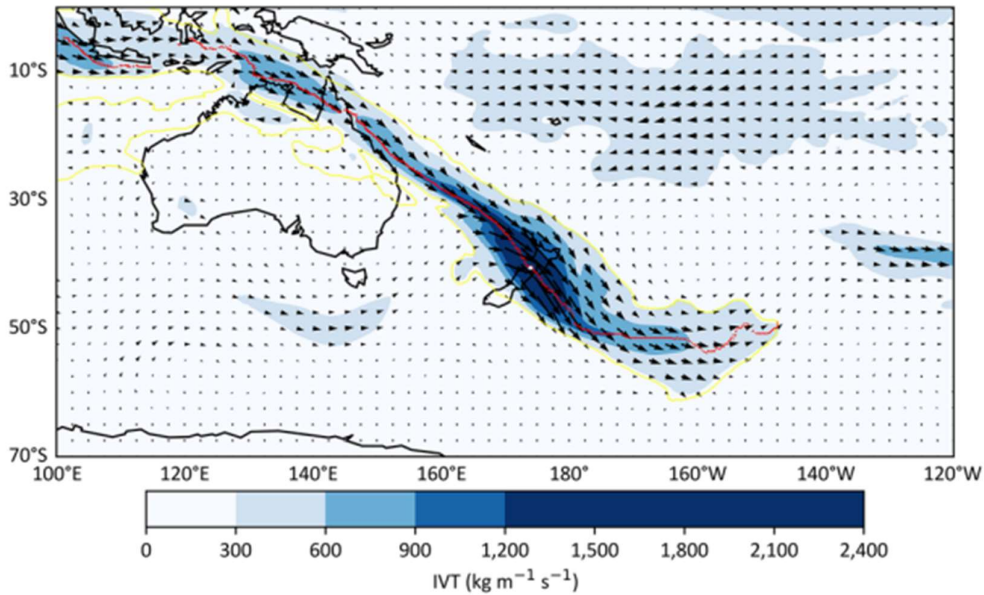


Figure 2.11: Atmospheric River (AR) originating in the subtropical regions north of Queensland, Australia on the 27th of December 2010 and making landfall around the Marlborough region. The yellow boundary depicts the shape of the AR, the white dot shows the approximate landfall location (174°E, 40.625°S) and the colour shading and vectors relate to measured integrated water vapour transport ($\text{kg m}^{-1} \text{s}^{-1}$) and direction of moisture flow respectfully. (From Fig. 6 of Shu et al. (2021)).

2.3.4.2 Ex-tropical Cyclones

Between November and April, NZ is subject to post-tropical cyclones from the north that can bring extreme wind and precipitation (Lorrey et al., 2014; MetService, 2015). Figure 2.12 shows tropical cyclones originating in the southwest tropical Pacific generally track westward toward Australia, but occasionally they track south towards NZ (Lorrey et al., 2014). Tropical cyclones typically weaken as they undergo extra-tropical transition, but they retain large amounts of tropical moisture that can produce heavy precipitation. On average NZ is exposed to one ex-tropical cyclone annually, with the northern and eastern regions of NZ being the most at risk (Bell, 1976; Lorrey et al., 2014).

Ex-tropical cyclones have caused some of NZ's most extreme and damaging weather events (Bell, 1976; Ulbrich et al., 2009; Eichler & Gottschalck, 2013; Lorrey et al., 2014). Ex-tropical Cyclone Bola was one of the most damaging cyclones to ever hit NZ. It occurred on the 4th of March 1988 and significantly impacted the Gisborne, Bay of Plenty, Northland, and

Hawkes Bay regions, causing extreme winds and heavy precipitation over a three-day period (NIWA, 2018a). Cyclone Bola originated near Fiji, where it tracked westward then turned poleward towards NZ. Gisborne was the worst affected region with over 900mm of rain falling within 72 hours, causing widespread erosion and flooding of rivers, especially the Hikuwai, and Waioeka Rivers, and it caused over \$189 million worth of damage (Chappell, 2016a; NIWA, 2018a). Recently, Gisborne has been subject to multiple ex-tropical cyclones such as Cyclone Cody and Cyclone Fili, both in 2022 (NZ Herald, 2022; Schwanecke & Sharpe, 2022). These events brought two 1-in-100-year rainfall events, with Cyclone Fili bringing 155.5mm of precipitation within 24 hours and causing significant flooding and disruption in the Tairāwhiti region (NZ Herald, 2022; Schwanecke & Sharpe, 2022).

Ex-tropical Cyclones can also cause extreme precipitation for the Lower North Island and South Island regions. Cyclone Giselle is NZ's worst recorded storm and had a significant impact on Wellington and Christchurch (Christchurch City Library, 2023a). The cyclone occurred on the 10th of April 1968 and caused 160km/hr winds, with some gusts reaching 275km/hr, as well as 14m seas, landslides, and torrential rain (Christchurch City Library, 2023a). Fifty-one people died when the Waihine, an inter-island ferry, crossing the Cook Strait was pushed off course, hit rocks and eventually sunk (Christchurch City Library, 2023a, 2023b). Cyclone Giselle also caused significant flooding in Christchurch's Avon and Heathcote Rivers as the cyclone moved south and floodwaters destroyed over 500 ha of land (Christchurch City Library, 2023a).

Thus, ex-tropical cyclones, although rare, are another important mechanism for extreme precipitation and flooding in NZ, particularly for the Northland, Bay of Plenty, and Gisborne regions, as these regions lie exposed to weather systems tracking southward out of the tropical Pacific (Fig. 2.12).

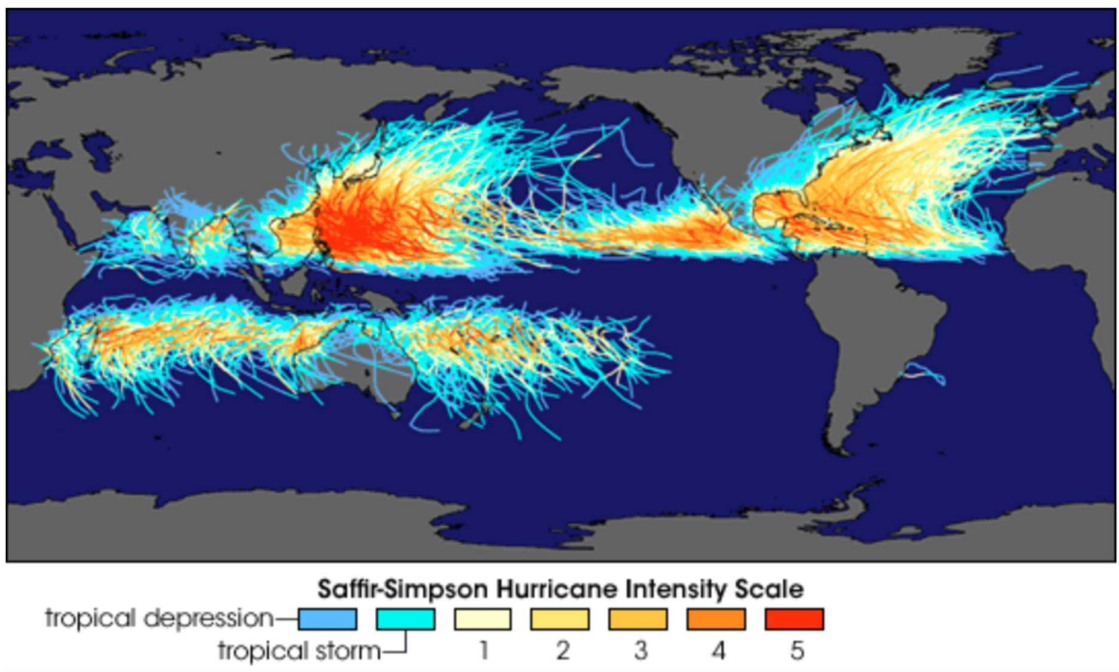


Figure 2.12: Tropical and ex-tropical cyclone storm tracks across the middle latitudes. The lines indicate the cyclone track, and the line colour refers to the intensity of the cyclone (From Rhode (2006)).

2.3.4.3 Thunderstorms

Finally, hazardous precipitation events can also occur through locally enhanced precipitation associated with convection (thunderstorms hereafter) (Tomlinson, 1992; Salinger et al., 2004). Thunderstorms can cause localised short-duration heavy precipitation events that often lead to flash flooding (Salinger et al., 2004). They typically occur in inland and northern regions of NZ during summer where there is moisture and strong diurnal surface heating that contributes to convective instability (Tomlinson, 1992).

On the west coast of NZ and in the Southern Alps, thunderstorms are commonly associated with fronts moving onto the country from the west and enhanced orographic uplift, while “southerly changes” (cold fronts) moving up eastern NZ can cause squall lines and thunderstorms on the East Coast (Chappell, 2013; Macara, 2013).

A recent example of the impact of thunderstorms was on the 21st of March 2022 when a large thunderstorm complex impacted much of the eastern North Island as it travelled southeast from Northland (Harris, 2022). Over 100mm of rain fell within 10 hours in Auckland,

significantly more than the monthly average, and led to severe flash flooding in Orewa and Auckland's North Shore (Harris, 2022). Even more recently, Auckland experienced its wettest day on record on 27 January 2023 due a complex of severe thunderstorms, with 258 mm of rainfall recorded at Auckland Airport in 24 hours causing severe flash flooding (Morton, 2023).

3. Data and Methods

The location, elevation, and characteristics of the 17 catchments used in this research will be outlined in the following chapter as well as the hydrological and climatological methods used to develop the event dataset and to investigate the regional and large-scale atmospheric conditions associated with high flow events.

3.1 Catchment Information

3.1.1 Catchment Selection

The catchments selected for this study are located on the eastern coasts of NZ's North and South Islands and are shown in Figs. 3.1 and 3.2. The regions were selected based on their location on the eastern coast of NZ, frequency of damaging floods and the proportion of the population residing on the flood plains of large rivers. Catchments within the regions were selected following consultation with the relevant councils and were required to be subject to high flow events and have available environmental monitoring that can be accessed via the councils. The catchments selected for this study were specifically mentioned by the councils as catchments that would benefit from additional research.

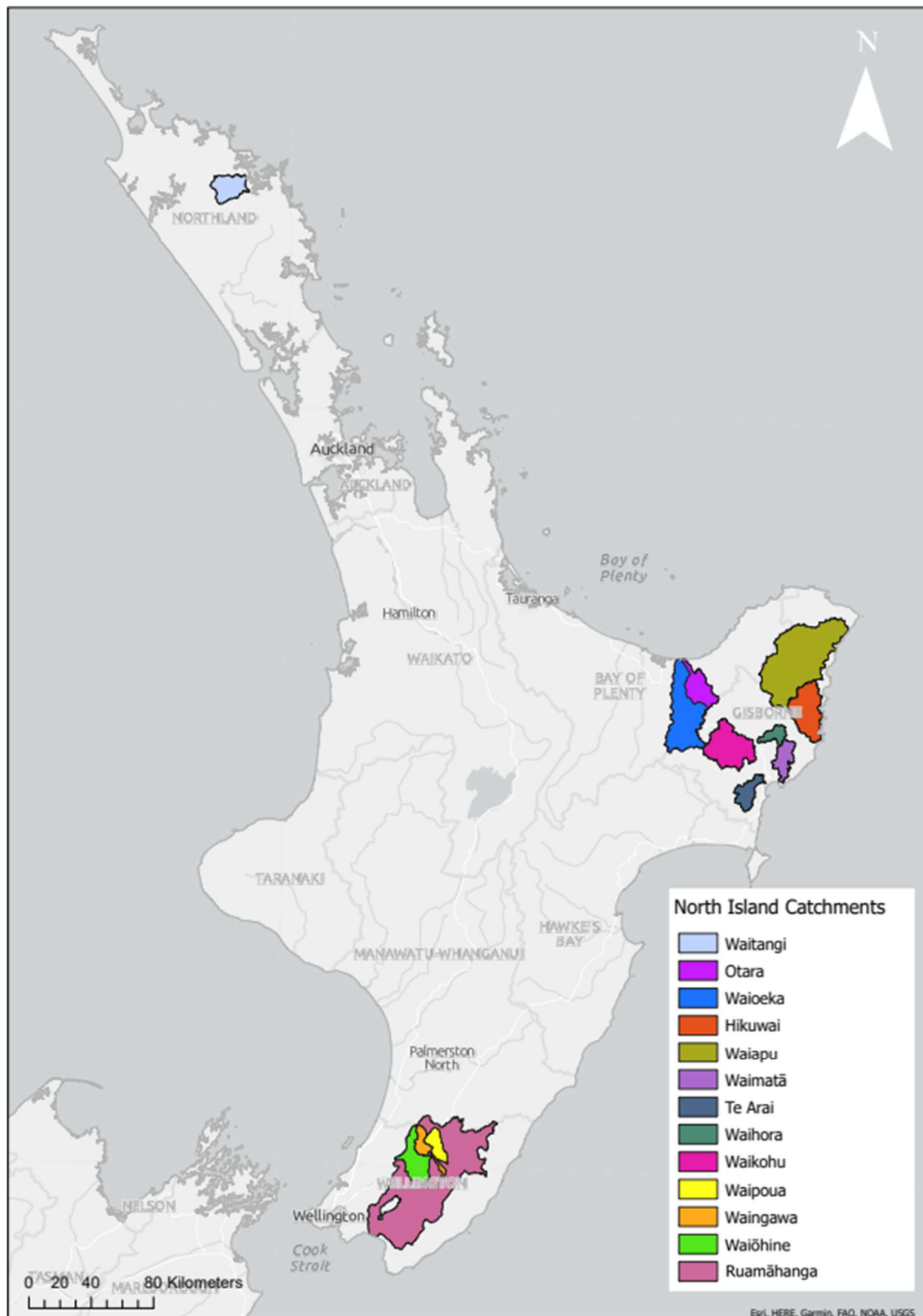


Figure 3.1: Locations of the selected 13 eastern North Island catchments examined in this thesis.

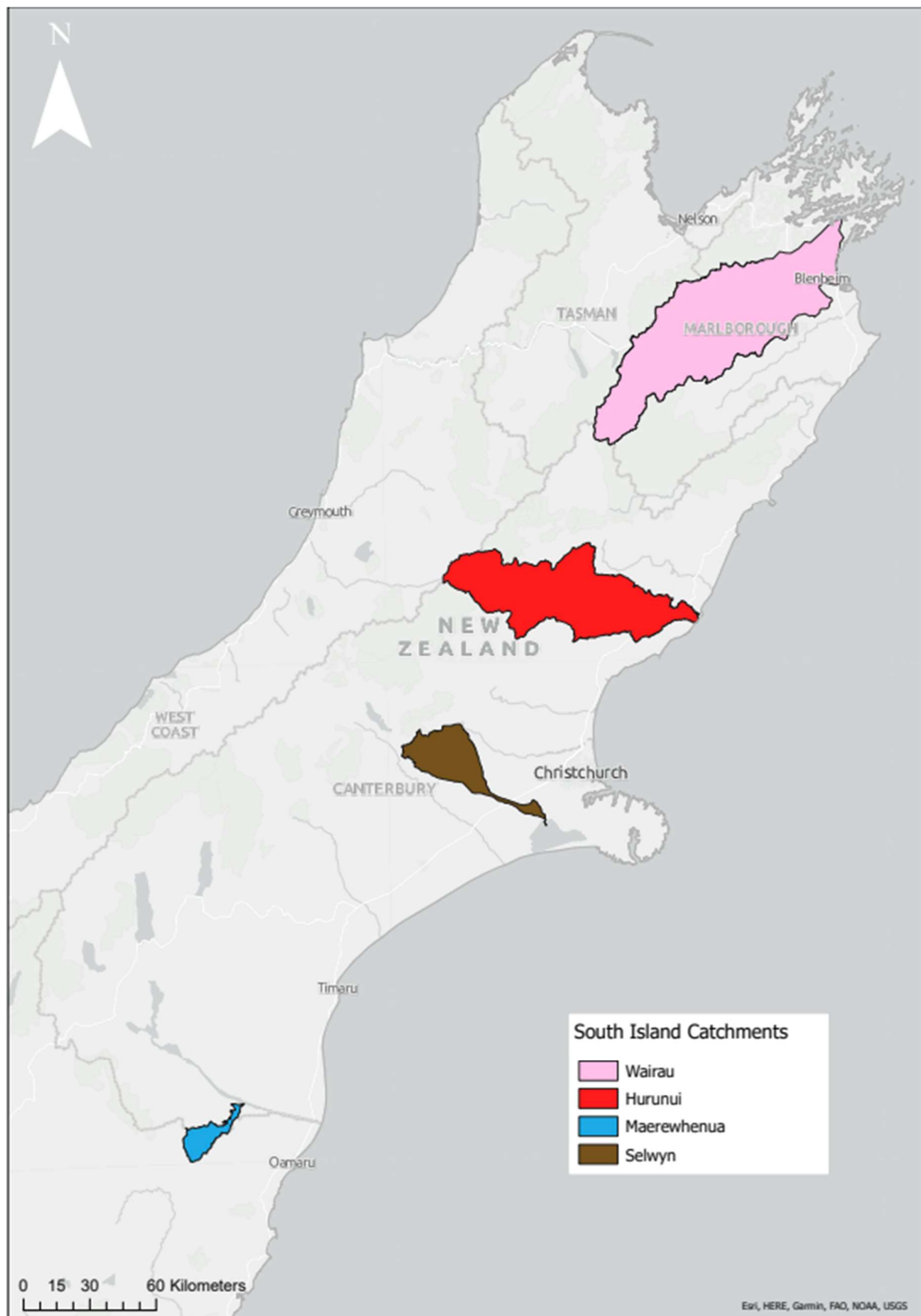


Figure 3.2: Locations of the selected four eastern South Island catchments examined in this thesis.

3.1.2 Upper North Island

The Upper North Island (UNI) region contains the Northland region's Waitangi River, and the Bay of Plenty region's Waioeka and Otara rivers. Both the Northland and Bay of Plenty regions fall within the Northern New Zealand climate zone as shown in Fig. 2.3 and were therefore grouped together in the UNI region for the hydrological and climate analysis. Thirty-three thousand five hundred people are exposed to flooding in this region (McDowall, 2019).

3.1.2.1 Waitangi River

The Waitangi River in Northland extends 37km and has a catchment area of 302km² (Land, Air, Water Aotearoa [LAWA], 2022k). Its headwaters are located east of Lake Āmāpere and the river flows east toward Haruru and the Waitangi Estuary before discharging out to the Bay of Islands. The catchment has a west-east orientation and the overall elevation in the catchment is low with Fig. 3.3b showing the highest elevation is 380m occurring in the west of the catchment. Figure 3.3a shows the catchment area includes State Highways 1, 10, and 11 which are important lifelines of the North Island, and it also includes the townships Ōkaihau, Moerewa, Kawakawa, and Kaikohe. The Waitangi River is fed by rainfall and runoff from the surrounding area and poor soil drainage results in an increased flood risk during high rainfall events, with Haruru being most at risk of severe flooding (Waitangi Catchment Group, 2017; McCarthy, 2021). A 1-in-100-year flood in this catchment is modelled to be 700m³/s (K. Walter, personal communication, February 7, 2023).

The Waitangi River flow data was collected from the NIWA monitoring site Waitangi @ Wakelins (Fig. 3.3a) and covers a period of 42 years. Figure 3.4 indicates low to moderate flow is common in the Waitangi River while high flows are relatively uncommon.

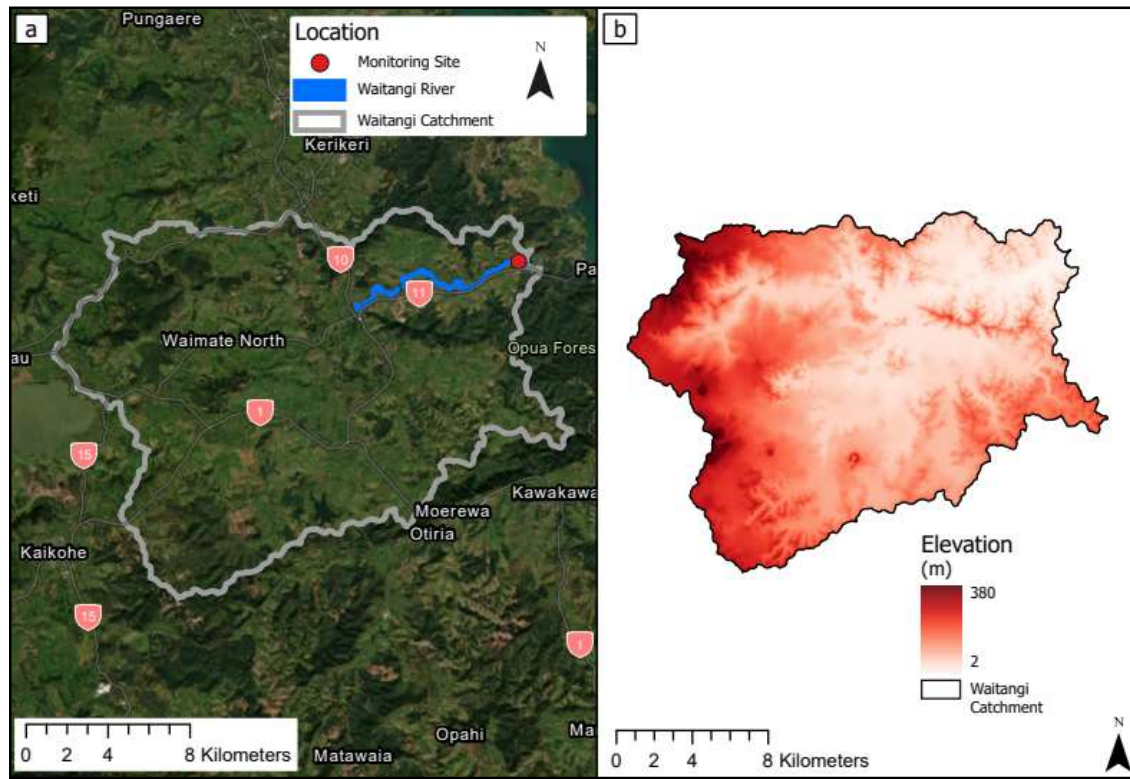


Figure 3.3: The Waitangi catchment (a) location and (b) elevation.

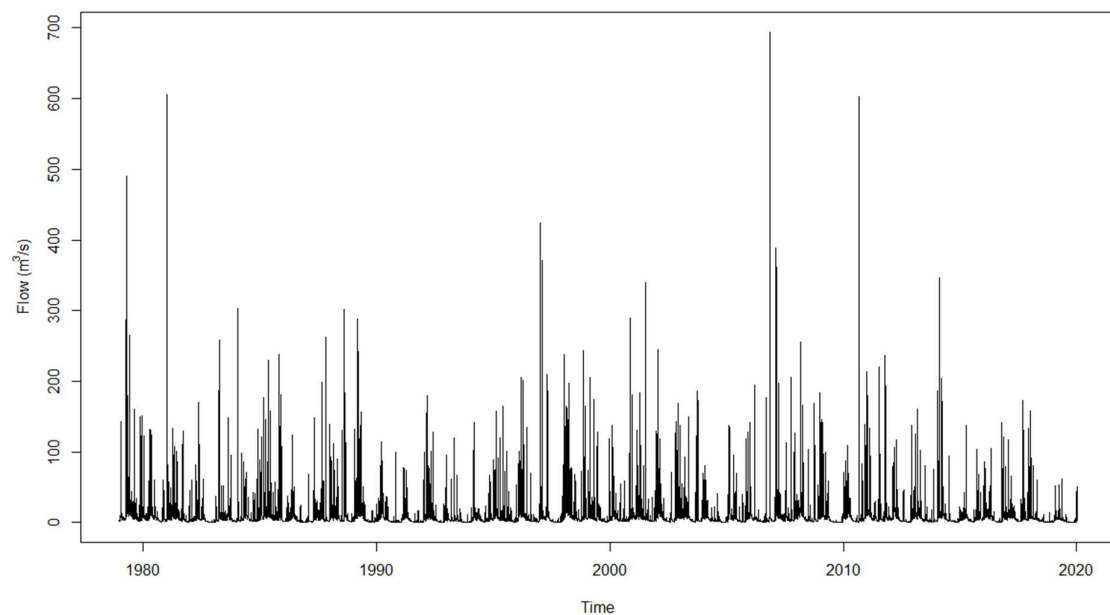


Figure 3.4: Waitangi River flow (m^3/s) timeseries (22/02/1979 – 14/11/2020).

3.1.2.2 Waioeka River

The Waioeka catchment covers an area of 825km², is 60km long, and is orientated in a north-south direction (LAWA, 2022h). Figure 3.5a shows the headwaters begin in the Raukūmara Ranges in the southern area of the catchment and flow through multiple townships before reaching the town of Ōpōtiki and discharging out from Waiotahē Beach. The river is primarily rain-fed and the catchment has good soil drainage (McCarthy, 2021). The steep ranges in which the headwaters are located form a suitable gradient to cause high energy and large flood events in the lower reaches of the catchment where the river mouth is influenced by tides and the Otara River (Freeman, 2008). The Bay of Plenty Regional Council (BOPRC) has calculated a 1-in-100-year flood event can exceed 1574m³/s and poses a significant risk to Ōpōtiki (Freeman, 2008).

Flow records for the Waioeka River were collected from the BOPRC Waioeka River at Cableway monitoring site (Fig. 3.5a) and covers a period of 49 years. The flow timeseries in Fig. 3.6 indicates periods of low to moderate flow are common in the Waioeka River, while high flow events are infrequent.

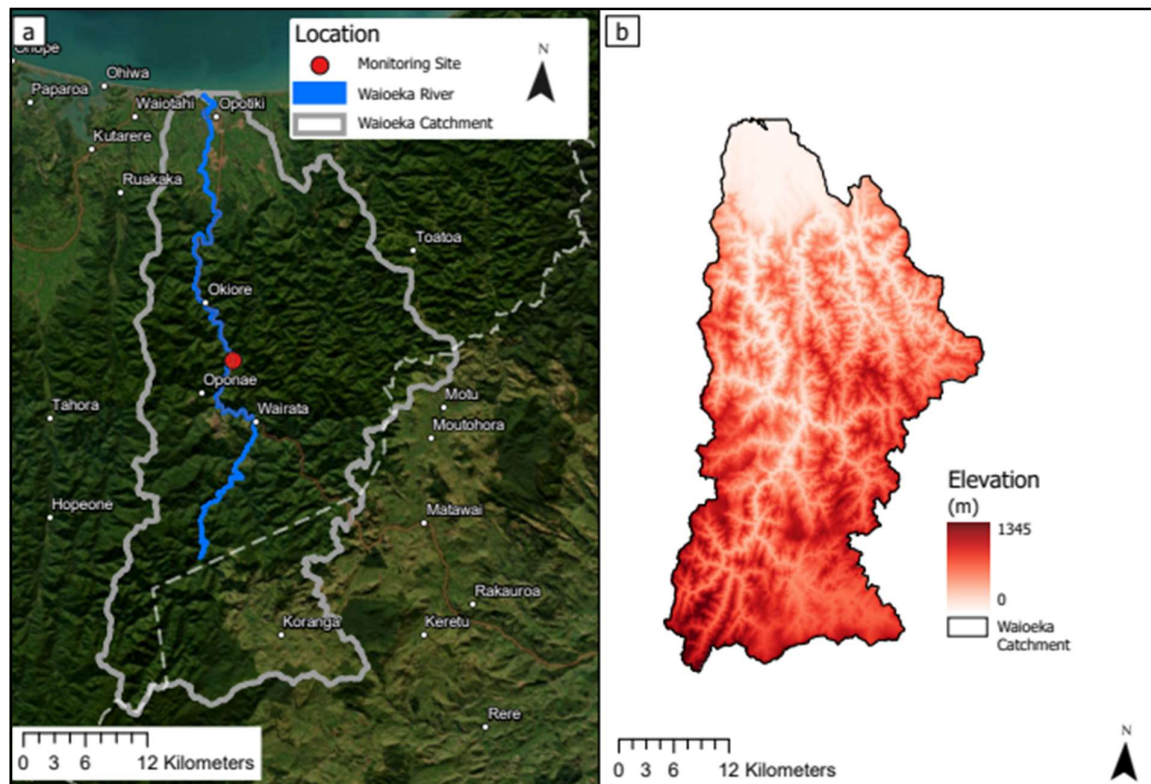


Figure 3.5: The Waioeka catchment (a) location and (b) elevation.

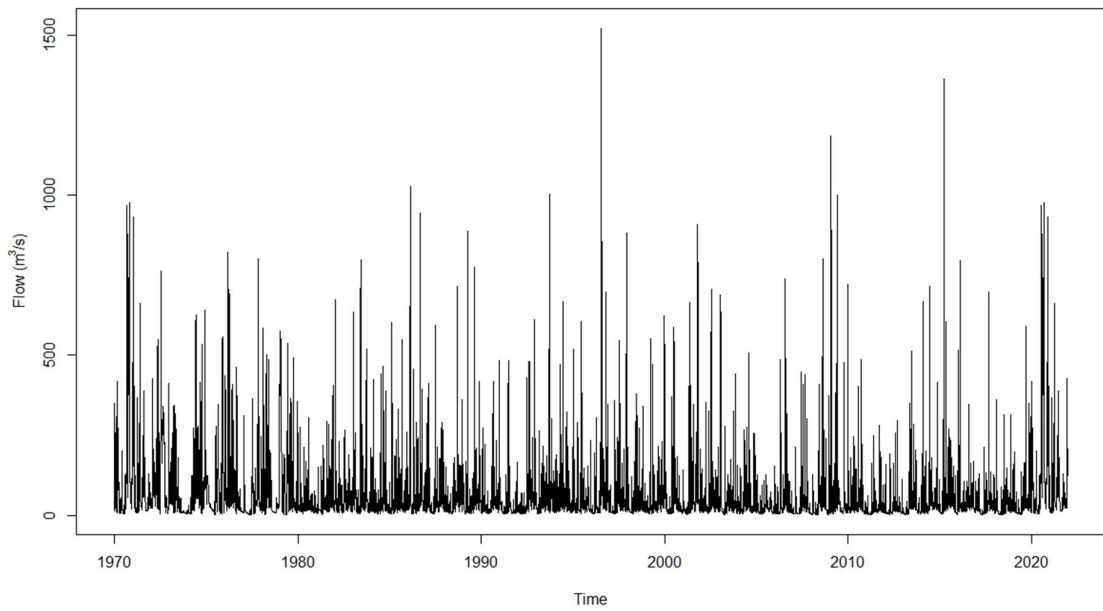


Figure 3.6: Waioeka River flow (m^3/s) data timeseries (01/01/70 – 24/03/2022).

3.1.2.3 Otara River

The Otara River has a catchment area of 350km^2 and the river extends 30km with the upper catchment located in the Raukūmara Ranges (Fig. 3.7a; LAWA, 2022d). Figure 3.7a shows the catchment has a northwest-southeast orientation and the river flows east of the Ōpōtiki township before joining the Waioeka River near Waiotahē Beach where it is discharged. The river is primarily rain-fed and has good soil drainage (McCarthy, 2021). Flooding from the Otara River has been a major issue for the Ōpōtiki township and led to the development of the Waioeka-Otara Rivers Scheme that encompasses substantial flood mitigation in the rural and urban areas of the two rivers. A 1-in-100-year flood event in this catchment has a flow magnitude of $928\text{m}^3/\text{s}$ (Freeman, 2008).

Flow records for the Otara River were taken from the BOPRC's Otara at Browns Bridge monitoring site (Fig. 3.7a) and covers a period of 44 years. Figure 3.8 indicates this river commonly experiences consistent moderate to high flows.

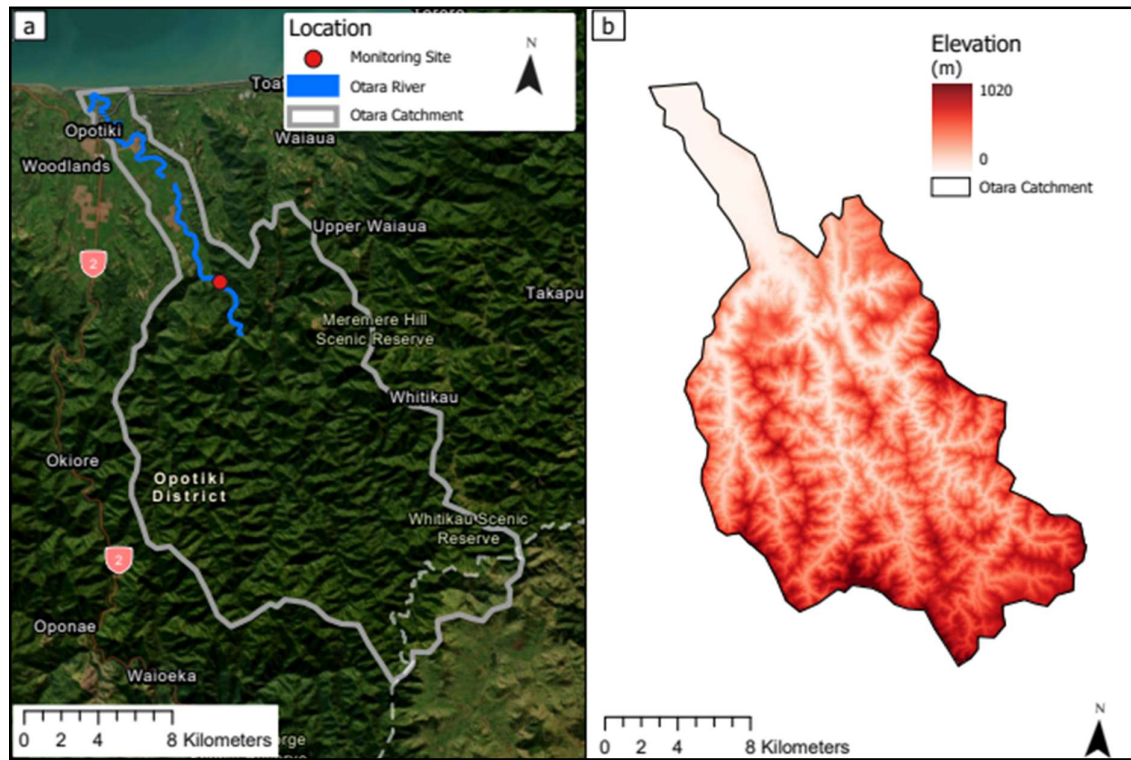


Figure 3.7: The Otara catchment (a) location and (b) elevation.

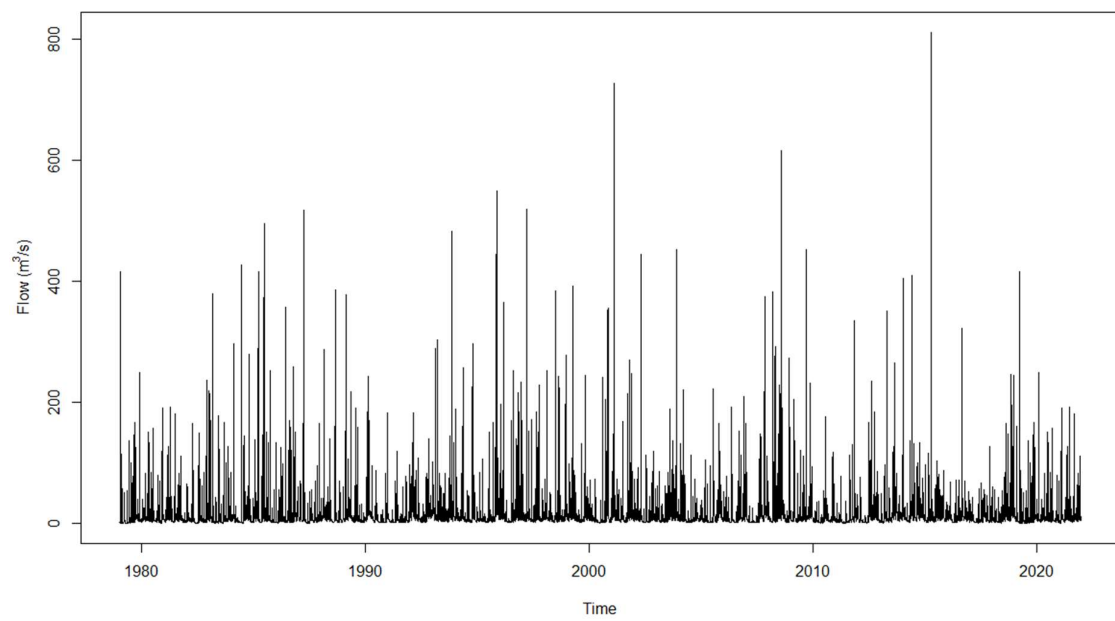


Figure 3.8: Otara River flow (m^3/s) timeseries (01/03/1979 – 14/01/2022).

3.1.3 East Coast North Island

The East Coast North Island (ECNI) region follows the Eastern North Island climate zone as shown in Fig. 2.3 and contains six Gisborne catchments: Hikuwai, Waimatā, Te Arai, Waikohu, Waihora, and Waiapu. There are 15,500 people exposed to flooding in this region (McDowall, 2019).

3.1.3.1 Hikuwai River

The Hikuwai River is a major tributary of the Ūawa River in the Gisborne region (LAWA, 2022a). Figure 3.9a shows the Hikuwai catchment has a north-southeast orientation, and the river flows southeast through step hill ridges parallel to the coast, following State Highway 35 before joining the Ūawa River near Tolaga Bay then discharging into the sea. Hill country and hilly steep lands make up the catchment land mass with the Raukūmara Ranges occurring to the west of the Hikuwai River (Fig. 3.9b; Rosser et al., 2019). The Hikuwai River is primarily fed by rainfall and runoff from the surrounding environment due to moderate soil drainage conditions which can lead to the water level rising quickly during extreme rainfall events (McCarthy, 2021). The risk to flooding for small settlements in the catchment is significant and during flood events large amounts of logging debris (also known as ‘slash’) can be transported downstream (Rosser et al., 2019). A 1-in-100-year flood in the Hikuwai has a modelled flow rate of 1454m³/s (B. Bosworth, personal communication, May 31, 2022).

The Hikuwai River data was collected from the Gisborne District Council’s (GDC) Hikuwai River at Willowflat site (Fig. 3.9a) which has a record length of 48 years. Figure 3.10 shows flow in the Hikuwai River undergoes a regular cycle where periods of moderate or high flows are followed by periods of low flows. The highest flow on record from Cyclone Bola in 1988 is a clear outlier.

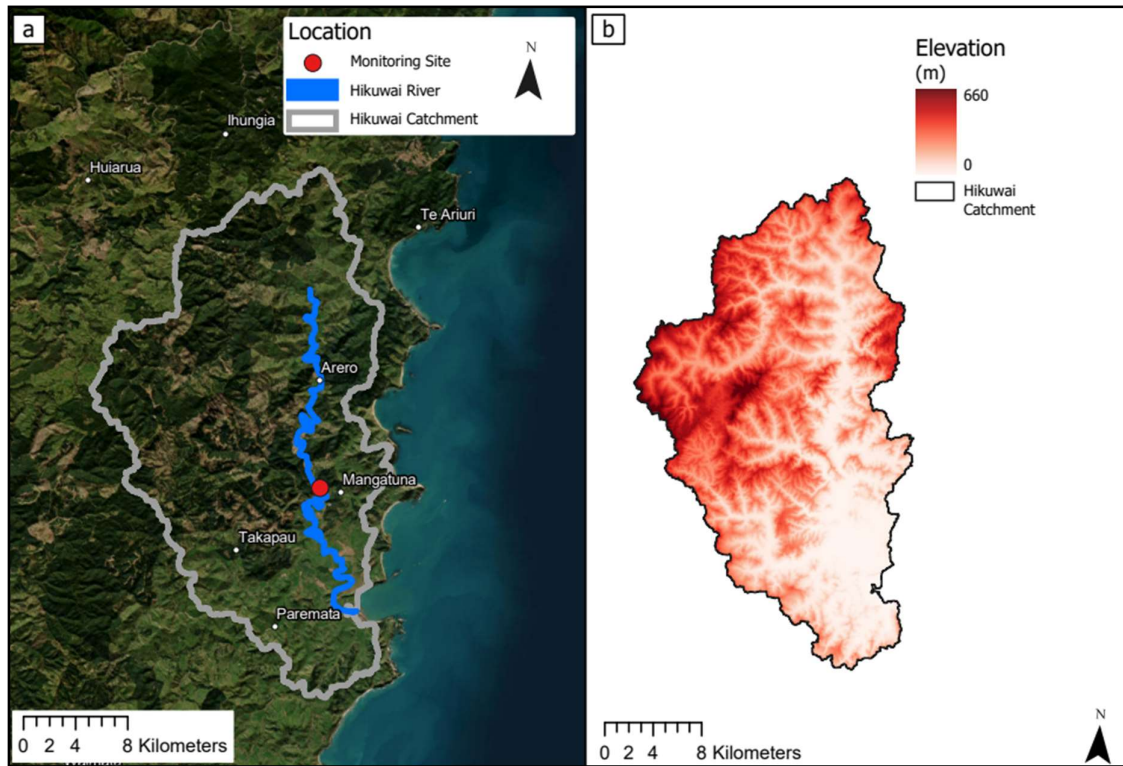


Figure 3.9: The Hikuwai catchment (a) location and (b) elevation.

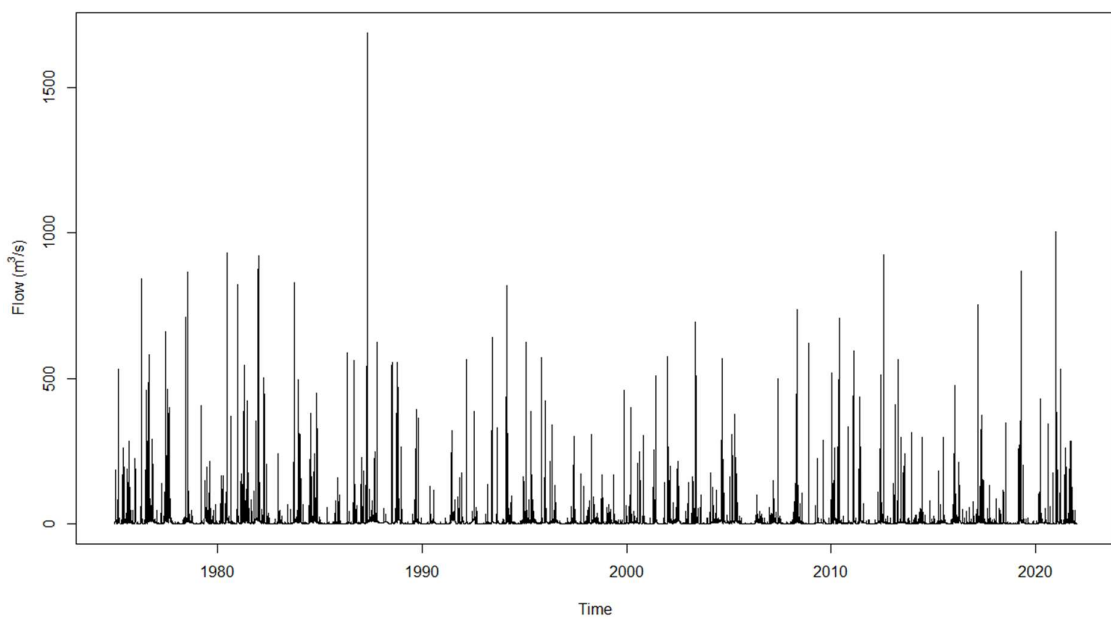


Figure 3.10: Hikuwai River flow (m^3/s) timeseries (01/01/1975 – 15/04/2022).

3.1.3.2 Waimatā River

The Waimatā River is one of the main rivers in the Gisborne region (LAWA, 2022g). The Waimatā catchment encompasses an area of 226km² and flows south through Gisborne City where it joins the Taruheru River before discharging into Poverty Bay (Fig. 3.11a; Cullum et al., 2017). Figure 3.11b shows the catchment has variable terrain where the northern part of the catchment is located in the steep V-shaped valleys of the Raukūmera Ranges while Gisborne is located on the flat land near the river south of the catchment (Cullum et.al, 2017). The Waimatā River is rain-fed, has moderate soil drainage and during high flow events it is common for transport infrastructure located on the Waimatā flood plain to be inundated with slash from forestry operations (McCarthy, 2021). The flow rate of a 1-in-100-year flood in the Waimatā River is modelled to be 1159m³/s (B. Bosworth, personal communication, May 31, 2022).

Data for the Waimatā River was collected from the GDC's Waimatā River Monowai Goodwins monitoring site (Fig. 3.11a) and has a record length of 45 years. Moderate to low flows are common in the Waimatā River while high flows are relatively rare, with the largest flow occurring during the 1985 Gisborne and Hawkes Bay floods and second largest occurring during Cyclone Bola in 1988 (Fig. 3.12; NIWA, 2018b).

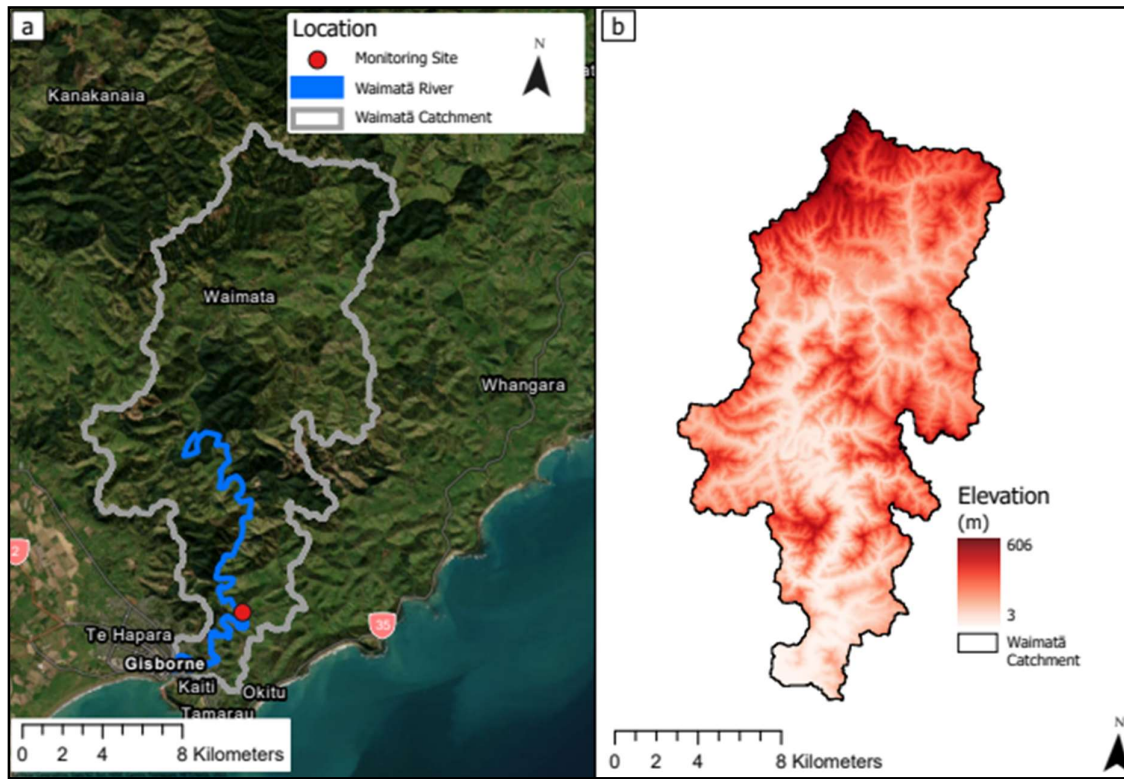


Figure 3.11: The Waimatā catchment (a) location and (b) elevation.

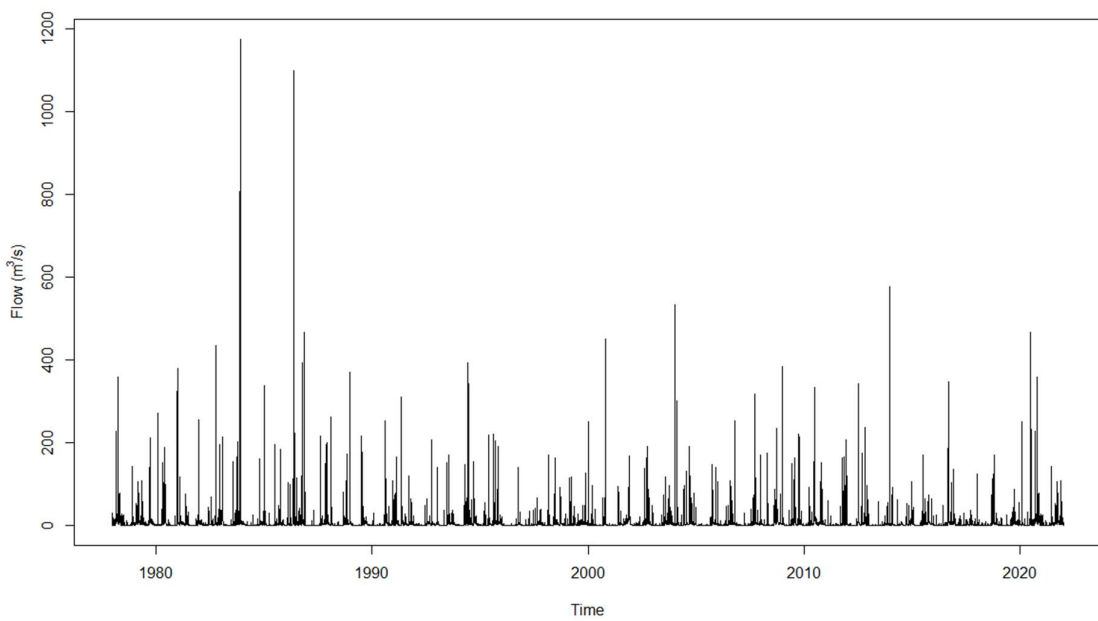


Figure 3.12: Waimatā River flow (m^3/s) timeseries (21/04/1978 – 15/04/2022).

3.1.3.3 Te Arai River

The Te Arai River is a major tributary of the Waipaoa River (Easton, 2015). It has a catchment size of 189km² and the river extends 32km, flowing north from its origins in Waingake before flowing northeast past Manutūkē to join the Waipaoa River at the confluence near the mouth of the Waipaoa where it discharges out to Poverty Bay (Fig. 3.13a; Easton, 2015). The catchment has a northeast-southwest orientation with the highest elevation areas occurring to the southwest of the catchment. The river is primarily rain-fed and is relatively natural despite the significant flood mitigation works, such as river straightening, in order to protect Manutūkē and State Highway 2 (Easton, 2015; Martindale & Van Der Raaij, 2018). Soils in this catchment have moderate drainage which increases the flood risk during extreme weather events (Easton, 2015; McCarthy, 2021). A 1-in-100-year flood in this catchment can exceed a flow rate of 427m³/s (B. Bosworth, personal communication, May 31, 2022).

The Te Arai River flow data was collected from the GDC's Te Arai River at Pykes Weir monitoring site (Fig. 3.13a) which has a total record length of 39 years. Figure 3.14 shows regular cycles of low, moderate, and high flows.

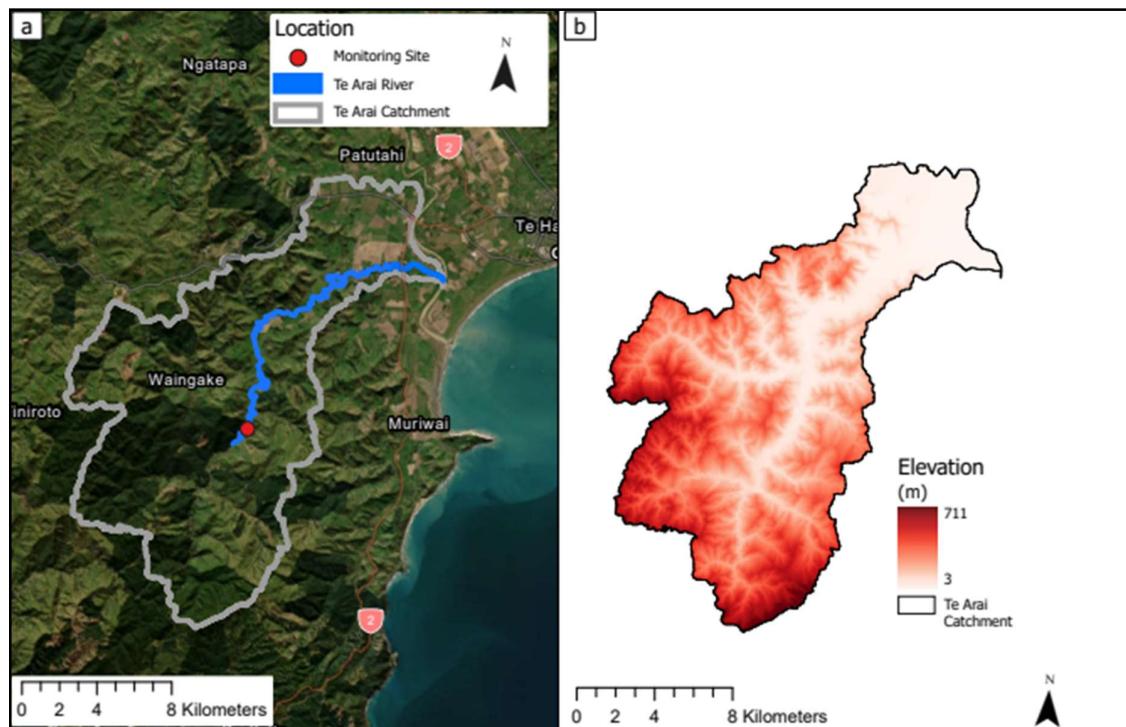


Figure 3.13: The Te Arai catchment (a) location and (b) elevation.

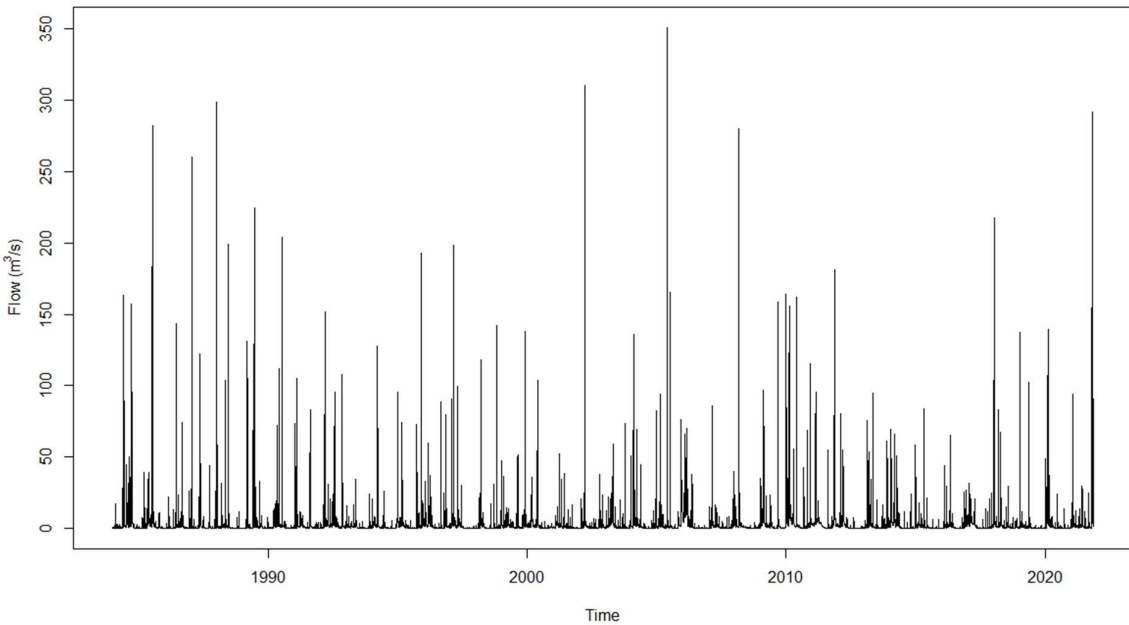


Figure 3.14: Te Arai River flow (m^3/s) timeseries (01/01/1984 – 14/04/2022).

3.1.3.4 Waikohu River

The Waikohu River is the northern tributary of the Waipaoa River. Figure 3.15a shows the Waikohu catchment is a meandering river that flows east towards Te Karaka where it joins with the Waipaoa River (GDC, 2021). The Waikohu catchment has an east-west orientation with the highest elevation areas located to the west and south of the catchment in the Huiarau Ranges where elevations can reach 1060m (Fig. 3.15b). The Waikohu River is primarily rain-fed however soil drainage is good, which reduces the flood risk during extreme rainfall (McCarthy, 2021). Te Karaka, a small settlement of importance to a number of iwi in the region, and State Highway 2 are both at risk of flooding from the Waikohu River. The 1-in-100-year flood has an estimated magnitude of $720\text{m}^3/\text{s}$ (B. Bosworth, personal communication, May 31, 2022).

The Waikohu River flow data was collected from the GDC's Waikohu River at Mahaki monitoring site (Fig. 3.15a) and has a record length of 44 years. The timeseries in Fig. 3.16 indicates regular cycles of low to moderate flow and high flows are rare.

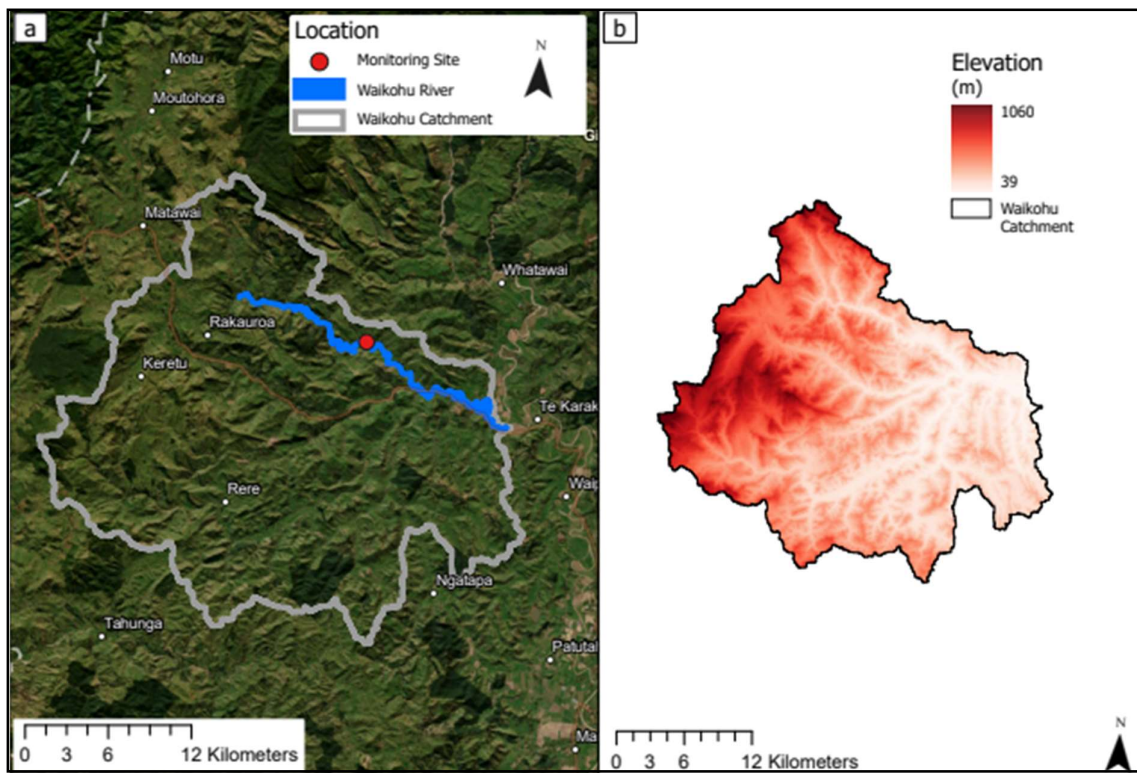


Figure 3.15: The Waikohu catchment (a) location and (b) elevation.

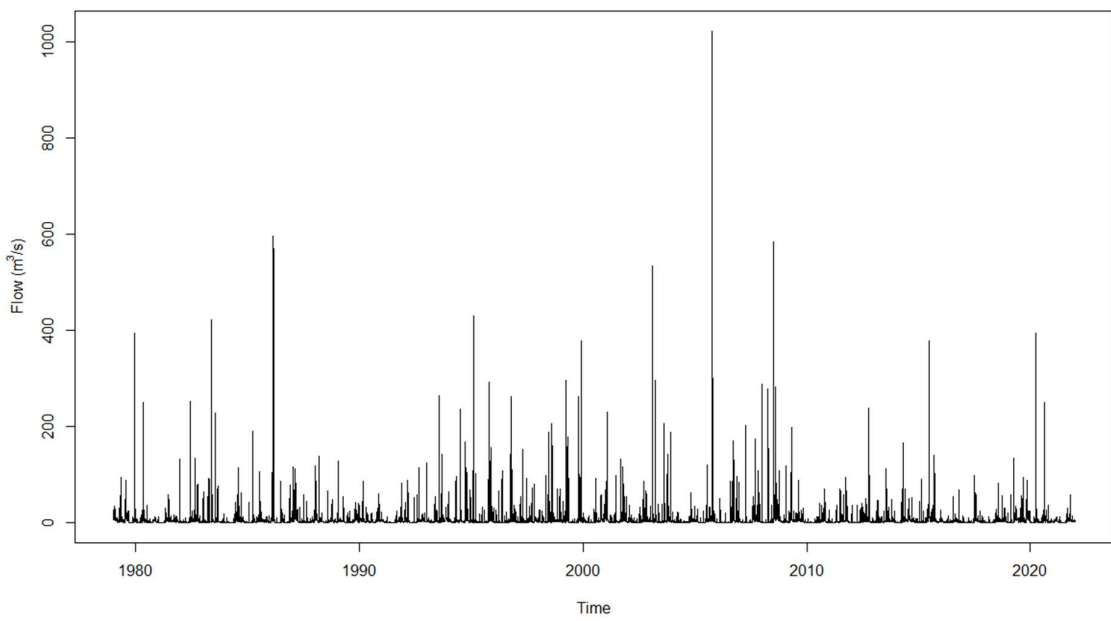


Figure 3.16: Waikohu River flow (m^3/s) timeseries (05/10/1979 – 14/04/2021).

3.1.3.5 Waihora River

Like the Te Arai and Waikohu Rivers, the Waihora River is a tributary of the Waipaoa River. The Waihora River is a smaller rain-fed river with moderate soil drainage and the catchment has a west-east orientation (McCarthy, 2021). Figure 3.17a shows the river flows west through dense hill country to the east with elevations reaching 622m (Fig. 3.17b), before joining the Waipaoa River at the confluence in Te Karaka. Flooding from the Waihora commonly impacts Te Karaka and a 1-in-100-year flood is modelled to have a flow rate of 873m³/s (B. Bosworth, personal communication, May 31, 2022).

Data for the Waihora River was collected from the GDC's Waihora River at No3 Bridge monitoring site (Fig. 3.17a) and has a record length of 37 years. Figure 3.18 shows that periods of low flow are very common while moderate to high flows are rare. The highest flow on record is seen for Cyclone Bola in 1988.

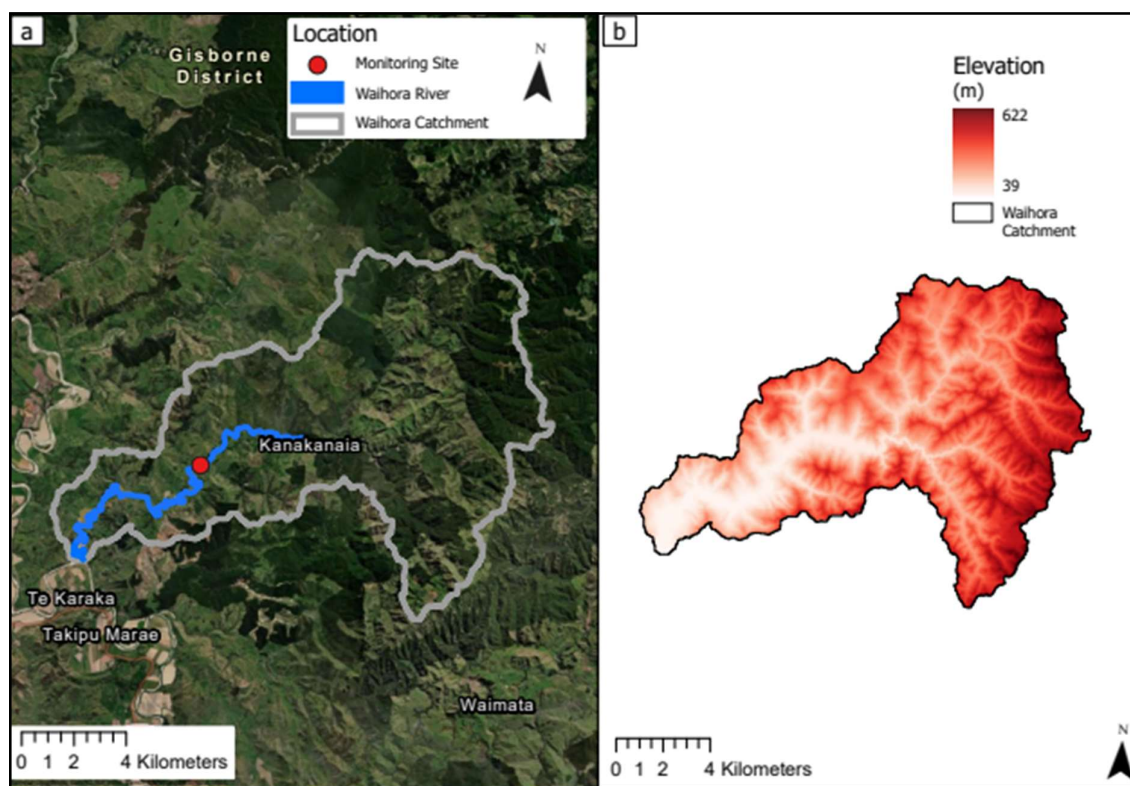


Figure 3.17: The Waihora catchment (a) location and (b) elevation.

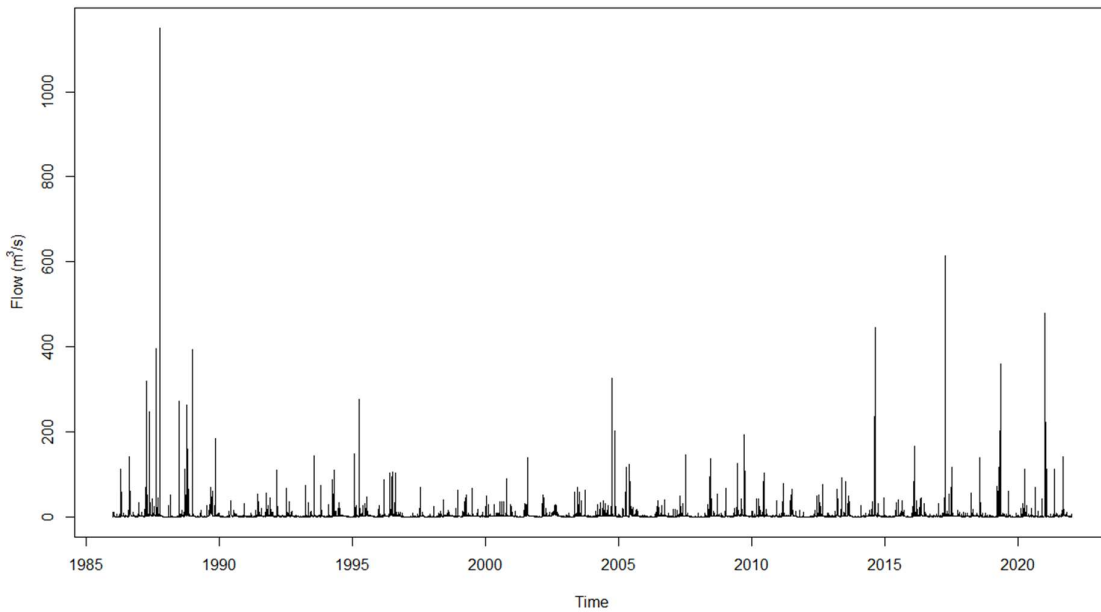


Figure 3.18: Waihora River flow (m^3/s) timeseries (04/12/1986 – 14/04/2022).

3.1.3.6 Waiapu River

The Waiapu River has a catchment area of 1734km^2 and extends 130km (Barnard et al., 2012). Figure 3.19a shows the Waiapu's upper reaches form in the Raukūmara Ranges and the river flows northeast towards Tikitiki where it discharges out to the coast (Fig. 3.19b). The catchment has a southwest-northeast orientation with the higher topography areas occurring to the southwest of the catchment. The Waiapu River is a rain-fed river that has moderate soil drainage, and past land use changes have resulted in an increase in flood risk to the surrounding rural areas, with a 1-in-100-year flood event exceeding $4721 \text{ m}^3/\text{s}$ (Barnard et al., 2012; McCarthy, 2021; B. Bosworth, personal communication, May 31, 2022).

The Waiapu River flow and stage data was collected from the GDC's Waiapu River at Rotokautuku Bridge monitoring site (Fig. 3.19a) and has a record length of 48 years. Figure 3.20 indicates periods of low flows are rare in this river, whereas moderate to high flows are common.

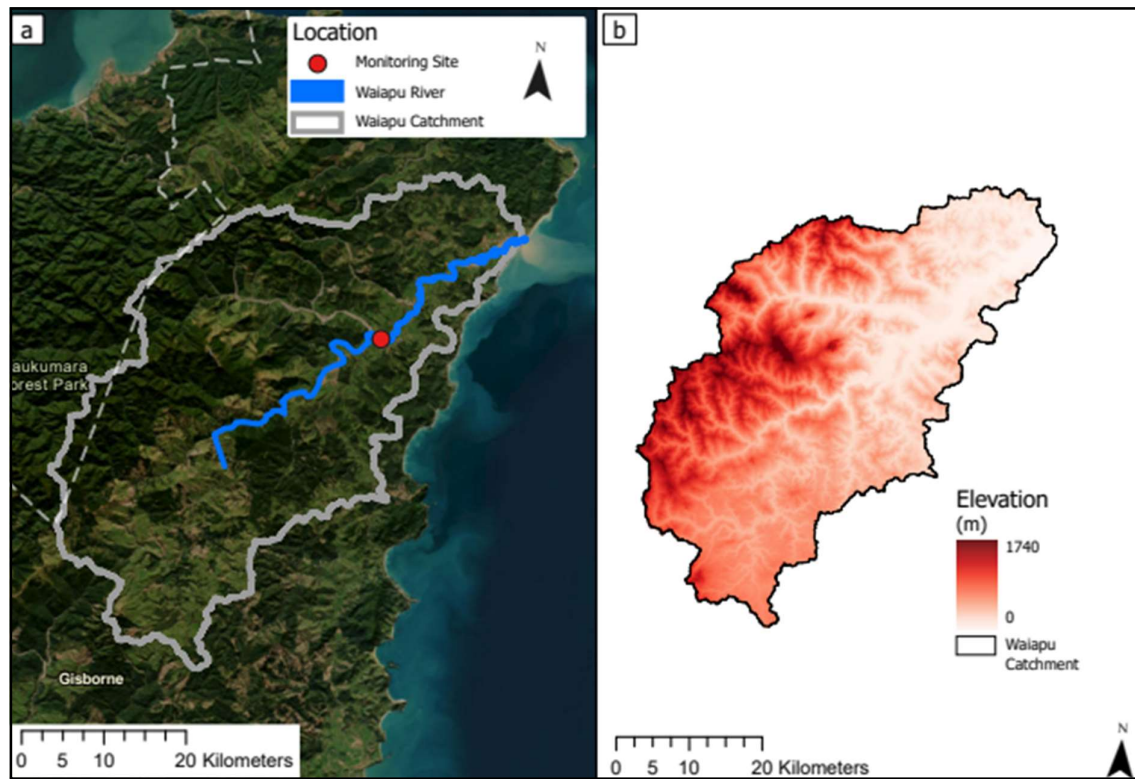


Figure 3.19: The Waipu catchment (a) location and (b) elevation.

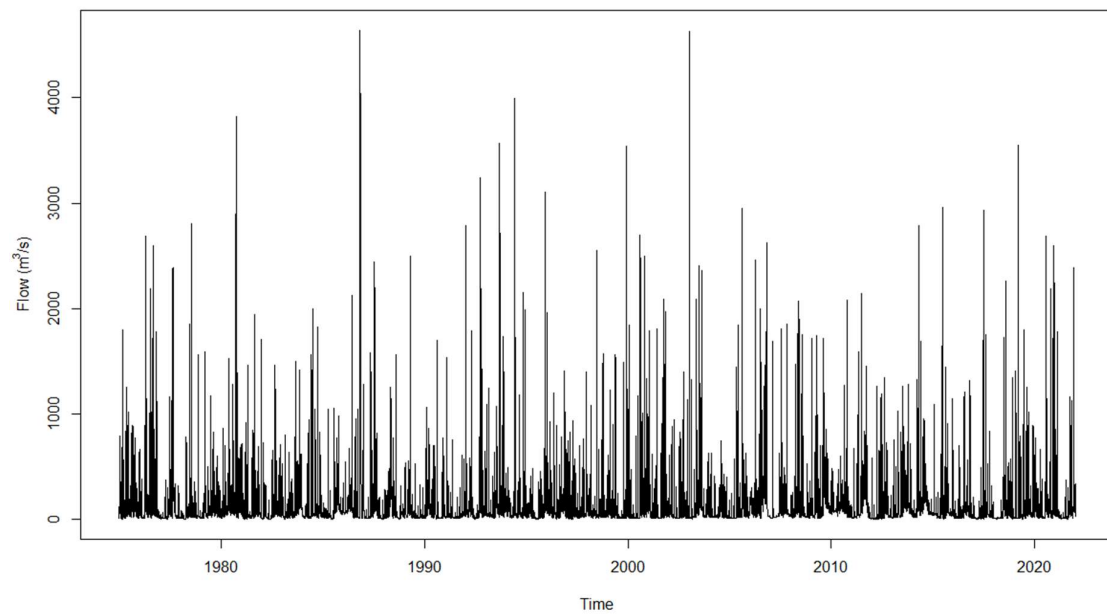


Figure 3.20: Waipu River flow (m^3/s) timeseries (01/01/1975 – 15/04/22).

3.1.4 Lower North Island

The Lower North Island (LNI) region includes the Wairarapa catchments: the Ruamāhanga, Waipoua, Waingawa, and Waiōhine. This region falls within the East Coast of the North Island climate zone as shown in Fig. 2.3. Given the distance from Gisborne, Gisborne's higher exposure to cyclones compared to the Wairarapa, and the location of the Wairarapa in the Greater Wellington region, it was decided a single region would be created for the Wairarapa catchments. There are 77,700 people at-risk of flooding in this region (McDowall, 2019).

3.1.4.1 Ruamāhanga River

Figure 3.21a shows the Ruamāhanga River has a northeast-southwest orientated catchment with an area of 3,555km² that occupies 44% of the total land area in the Wairarapa (LAWA, 2022e). The river extends 130km, with the upper reaches located in the Tararua Ranges which occur to the west of the catchment, where the river flows south along the ranges before turning southeast to flow over the Wairarapa Plains through Masterton and Martinborough and then discharging into Lake Onoke and Lake Ferry Beach (LAWA, 2022e; Watts & Perrie, 2007). It is a rain and snow fed river with good soil drainage and the Waipoua, Waingawa and Waiōhine rivers are significant tributaries which join the Ruamāhanga River in the Wairapapa Valley (McCarthy, 2021). The Ruamāhanga has a high base flow due to the amount of rainfall the Tararua Ranges receive and interaction with the groundwater aquifer system on the valley floor, resulting in an increased flood risk for Masterton and Martinborough during extreme rainfall (Fig. 3.21b; Watts & Perrie, 2007). Flooding is frequent and significant in this catchment and often causes damage to the surrounding rural communities (Greater Wellington Regional Council [GWRC], 2019). A 1-in-100-year flood magnitude for this catchment is 2108m³/s (GWRC, 2015).

The Ruamāhanga River data was collected from the Greater Wellington Regional Council's (GWRC) Ruamāhanga at Waihenga monitoring site (Fig. 3.21a) and has a record

length of 66 years. The time series of flow (Fig. 3.22) indicates this river rarely experiences periods of low flow, and moderate to high flows are relatively common.

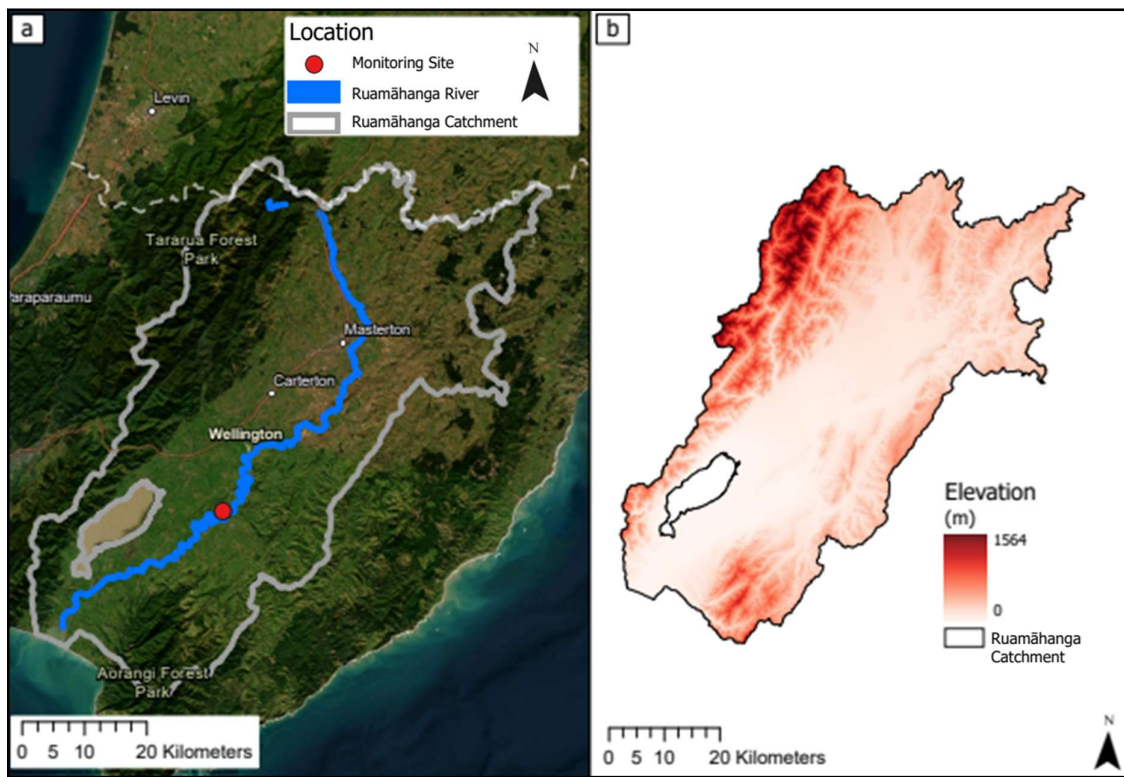


Figure 3.21: The Ruamāhanga catchment (a) location and (b) elevation.

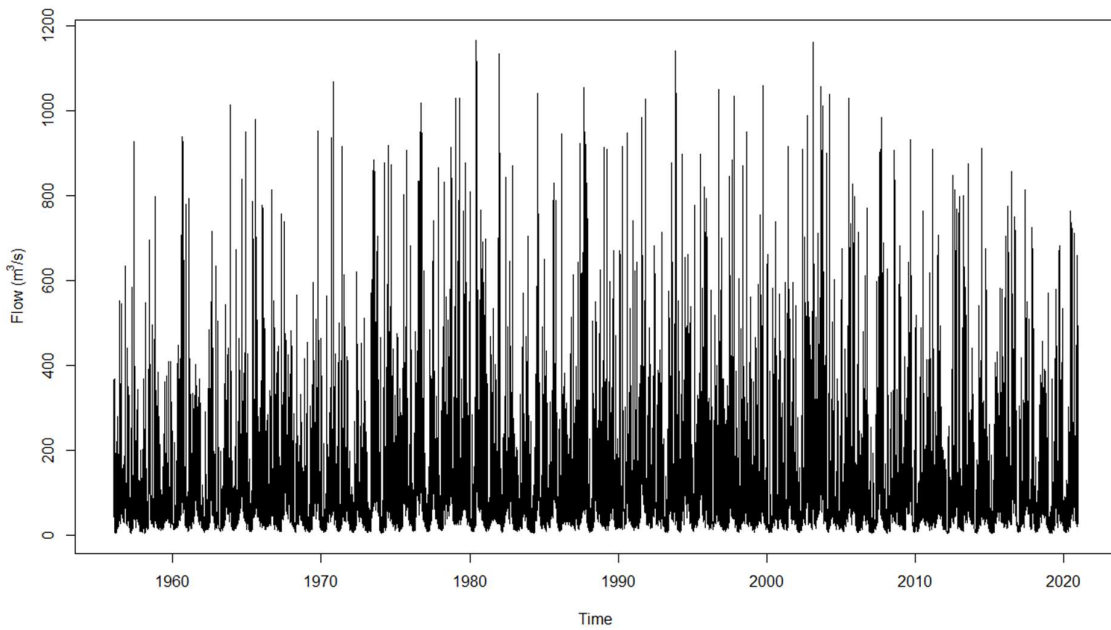


Figure 3.22: Ruamāhanga River flow (m³/s) timeseries (31/12/1956 – 31/12/2021).

3.1.4.2 Waipoua River

The Waipoua River is a tributary of the Ruamāhangā River and is located to the west of the Ruamāhangā (LAWA, 2022i). The catchment has a northwest-southeast orientation, encompasses an area of 149km², and the river extends 30km with its upper reaches located in the Blue Range of the Tararua Ranges (GWRC, 2019). Figure 3.23 shows the river flows southeast towards Masterton through steep-sided gorges and native forest before joining the Ruamāhangā on the Valley floor at Te Ore Ore east of Masterton. The Waipoua is largely fed by rainfall and runoff and has good to moderate soil drainage (McCarthy, 2021). Flooding in the Waipoua can be devastating because large flow events cannot be contained within the river channel (GWRC, 2019). Flooding in the Waipoua has the greatest potential of the Ruamāhangā's tributaries to affect the largest amount of people due to it flowing through Masterton (GWRC, 2019). A 1-in-100-year flood in this catchment exceeds 468m³/s (GWRC, 2015).

The Waipoua River data was collected from the GWRC's Waipoua at Mikimiki monitoring site (Fig. 3.23a) and has a data record that extends 31 years. This site had several problems with the monitoring instruments before the 2000s because of large flows washing out the riverbanks and destroying measurement instruments (GWRC, 2015). There have also been instances where flow was unable to accurately be recorded due to instruments being relocated to an unfavourable position on the river channel, resulting in some peak flow events not being reliable (potentially between 1985-1987 and 2014-2016 where the data does not start at zero). The GRWC has detailed records on these issues (GWRC, 2015). Figure 3.24 shows regular cycles of periods of low, moderate, and high flow.

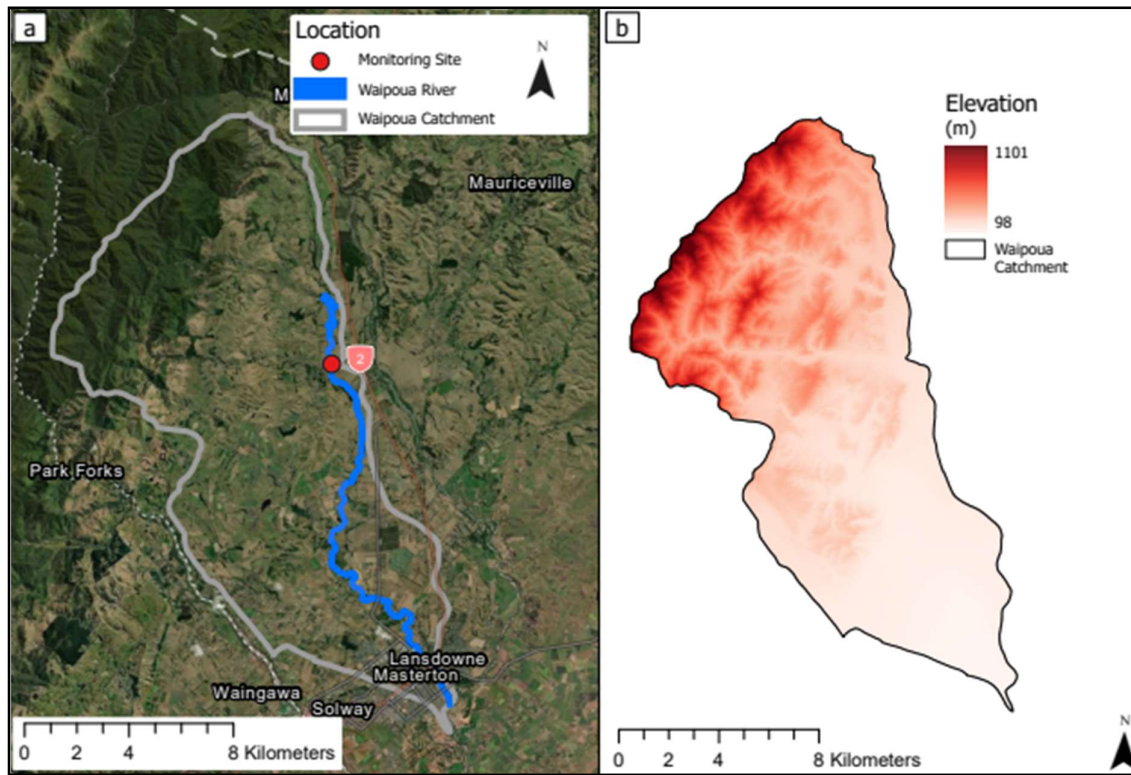


Figure 3.23: The Waipoua catchment (a) location and (b) elevation.

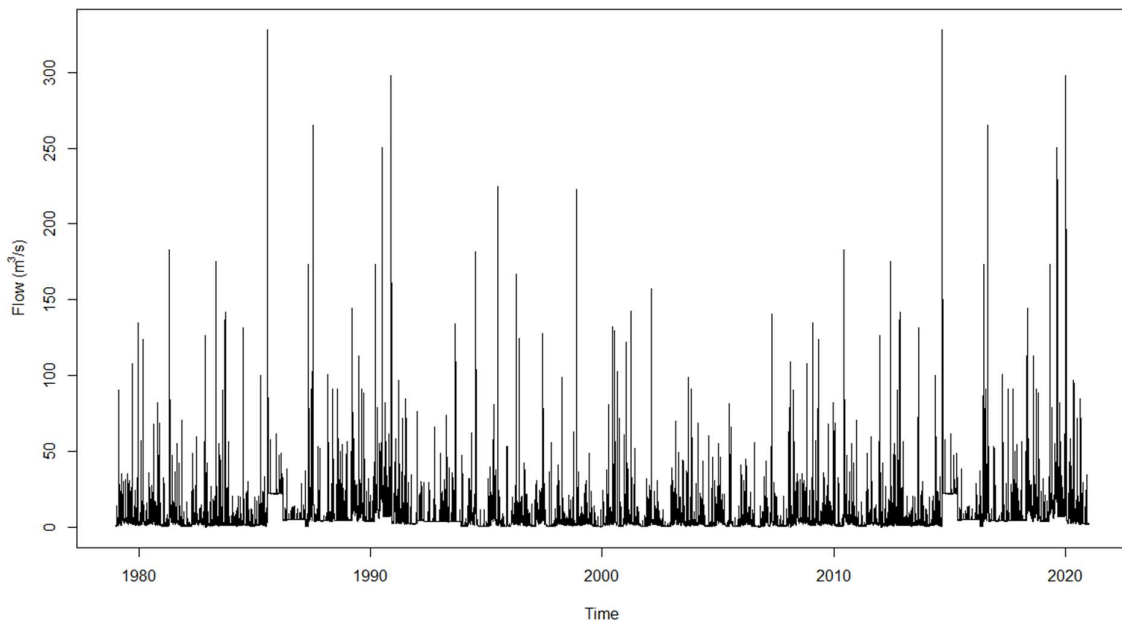


Figure 3.24: Waipoua River flow (m^3/s) timeseries (05/02/1979 – 20/07/2021).

3.1.4.3 Waingawa River

The Waingawa River has a catchment area of 79km² that has a northwest-southeast orientation (Fig. 3.25a). The river extends 48kms, with its upper reaches beginning in the Tararua Ranges, near the Tararua Forest Park, where it then flows through the Wairarapa Plains before joining with the Ruamāhangā River south of Masterton. The Waingawa River is primarily rain fed and has good soil drainage with some rural areas having poor drainage (McCarthy, 2021). The river has a natural highly constrained flood plain meaning that during high flow events it will likely be naturally contained by willows and some native forest. However, during floods the high energy flow often results in trees and vegetation being transported downstream from river bank erosion (GWRC, 2019). The Waingawa River is an important catchment for agriculture, transport infrastructure, and drinking water infrastructure for the Wairarapa region (GWRC, 2019). Flooding from the Waingawa River is common and poses a significant risk to Masterton and Carterton and a 1-in-100-year flood is modelled to be 510m³/s (GWRC, 2015).

The Waingawa River data was sourced from the GWRC's Waingawa at Kaituna monitoring site (Fig. 3.25a) and the record extends 47 years. Figure 3.26 shows periods of moderate to high flows are common while low flows are rare.

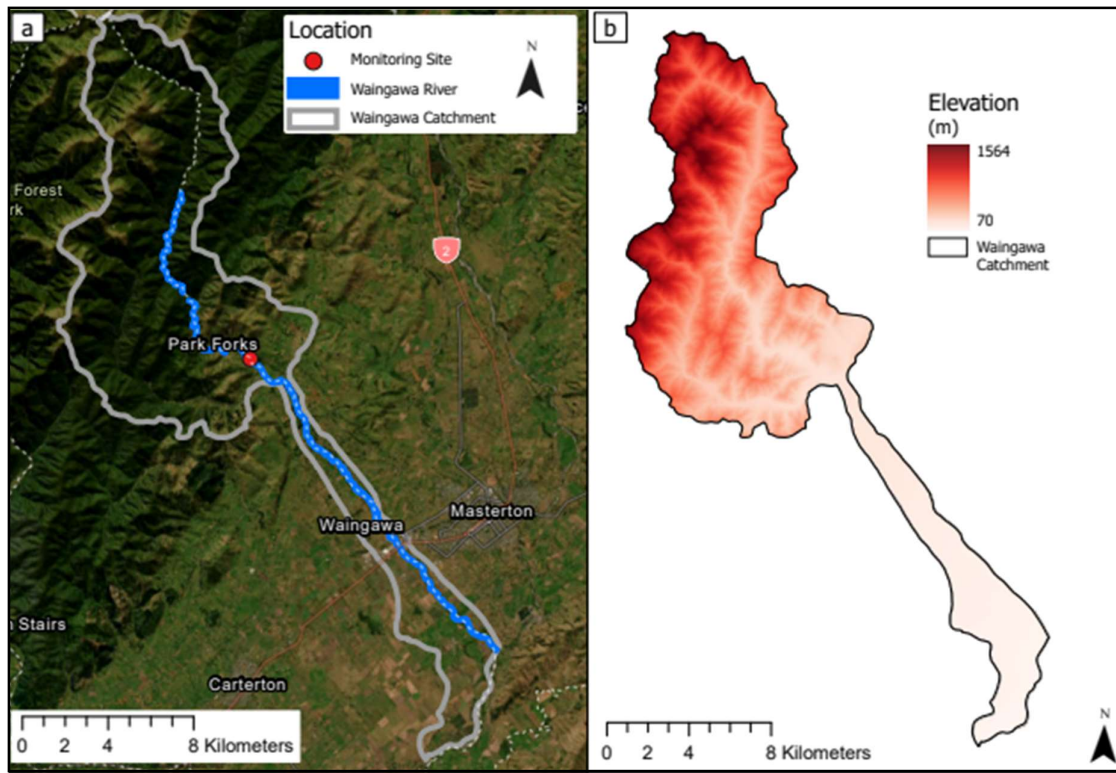


Figure 3.25: The Waingawa catchment (a) location and (b) elevation.

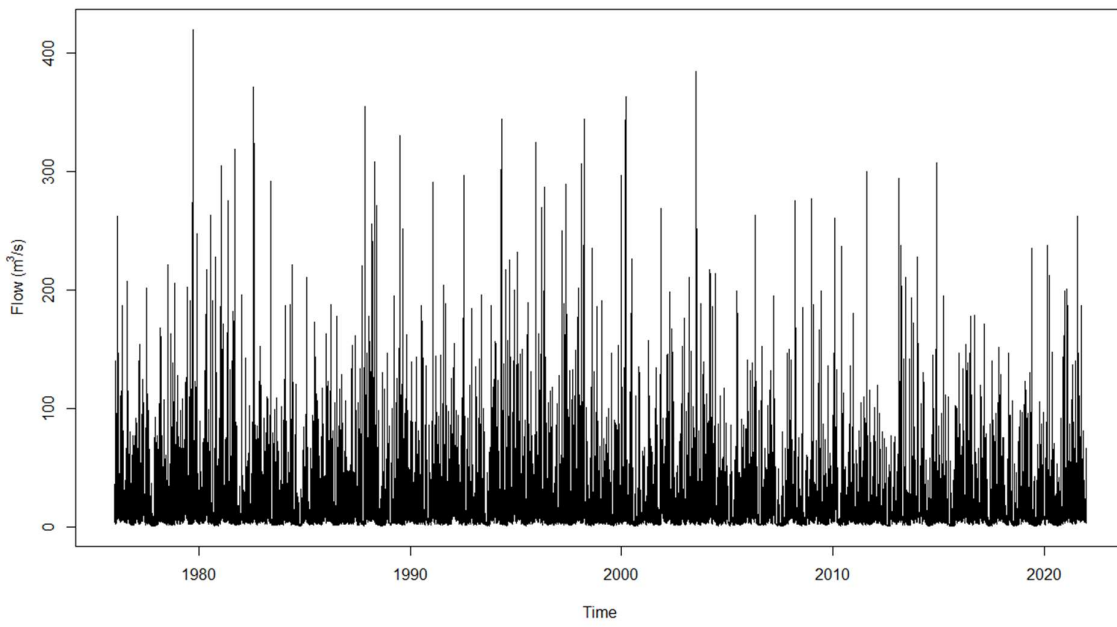


Figure 3.26: Waingawa River flow (m^3/s) timeseries (14/03/1976 – 01/01/2022).

3.1.4.4 Waiōhine River

Figure 3.27 shows the Waiōhine catchment has a catchment area of 378km² with a northwest-southeast orientation (GWRC, 2019). The river extends 60km over the Wairarapa Plains with the upper reaches located in the forested foothills of the Tararua Ranges. The river flows in a southeast direction towards Dalefield where it flows through Greytown and joins the Ruamāhangā River. In the last glacial maximum the Waiōhine River was a braided river, but has since evolved into a meandering river system as a result of changing land use, climate, and vegetation (Conn, 2019). The river is largely influenced by runoff from the surrounding environment especially from the Tararua Ranges as a result of moderate soil drainage (McCarthy, 2021). Flooding from the Waiōhine River occurs mostly around the meandering bends of the river, significantly impacting Greytown, and a 1-in-100-year flood exceeds 1700m³/s (GWRC, 2015, 2021).

The Waiōhine River data was collected from the GWRC's Waiōhine at Gorge monitoring site (Fig. 3.27a). Data from this catchment extends 69 years and is the longest record in this research. The timeseries in Fig. 3.28 indicates moderate and high flows are common in this river.

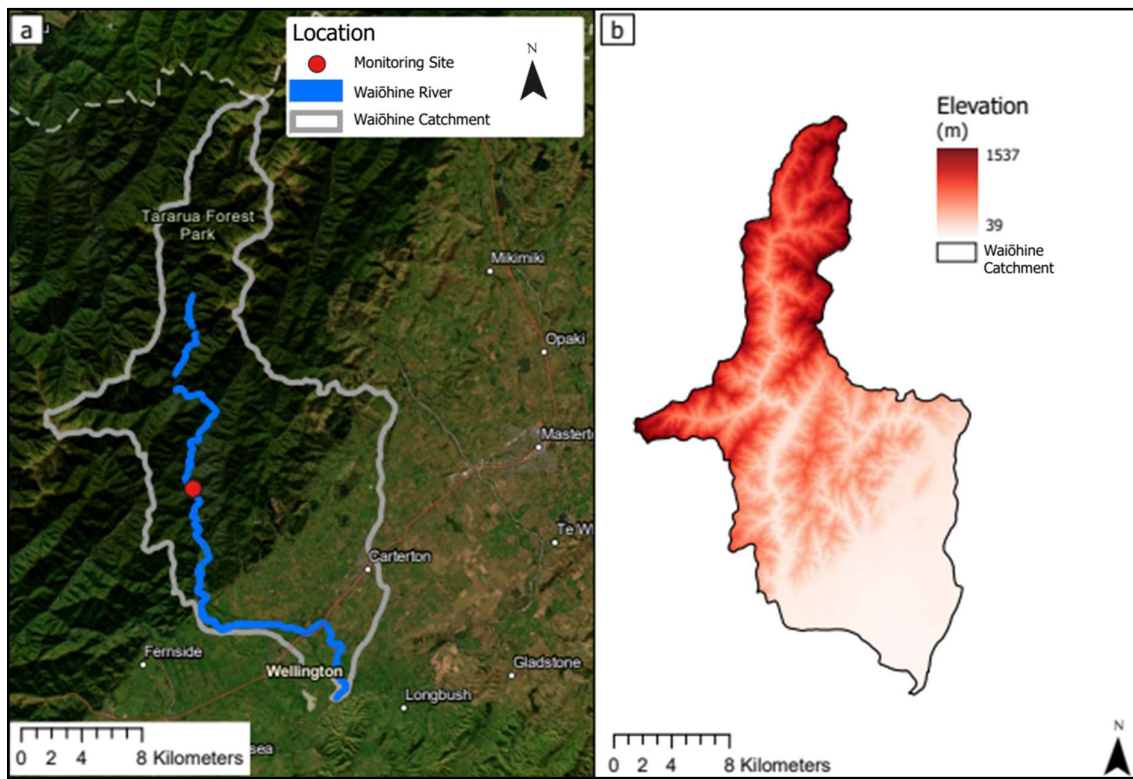


Figure 3.27: The Waiōhine catchment (a) location and (b) elevation.

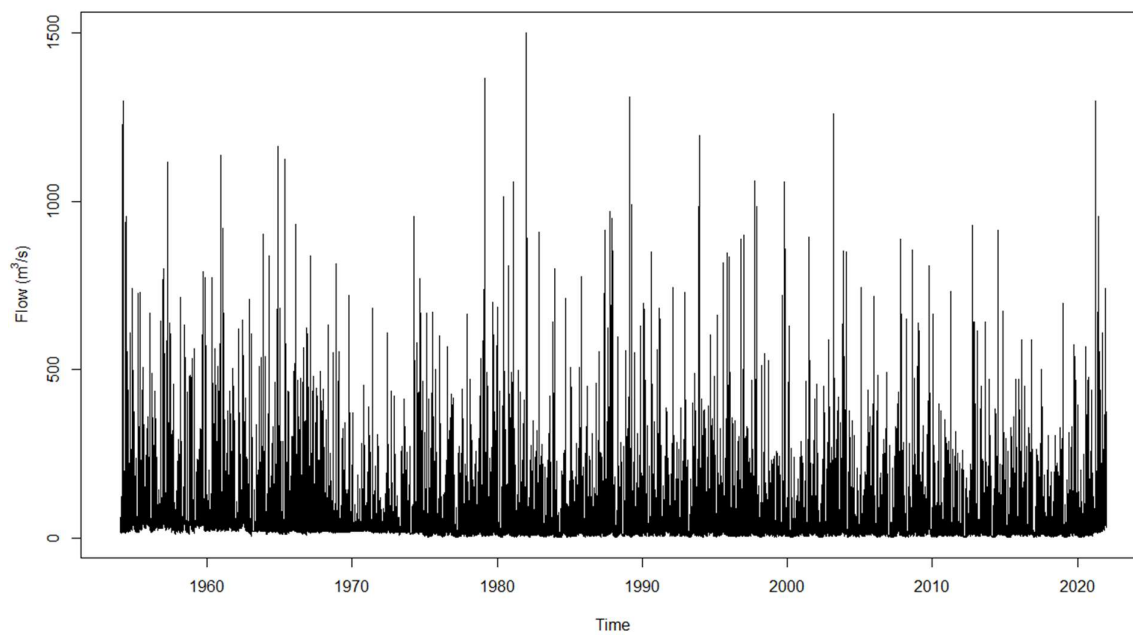


Figure 3.28: Waiōhine River flow (m^3/s) timeseries (27/12/1954 – 01/01/2022).

3.1.5 South Island

The South Island (SI) catchments include those from the Marlborough (Wairau River) and Canterbury (Hurunui, Selwyn, and Maerewhenua Rivers) regions. These regions are located in different climate zones as shown in Fig. 2.3, however, given there are only four catchments in the South Island compared to the 13 in the North Island, they were grouped together as one region. There are 189,000 and 4,700 people exposed to flooding in Canterbury and Marlborough respectively (McDowall, 2019).

3.1.5.1 Wairau River

The Wairau River catchment covers an area of 3430km² and extends 170km (Fig. 3.29a; LAWA, 2022j). It is a braided river that begins in the alpine environments of the Spenser Mountains and the Richmond and St Arnaud Ranges, reaching altitudes of more than 2200m (Fig. 3.29b), and flows to the west of Blenheim before discharging at the Wairau Bar located in Cloudy Bay near the Cook Strait (Christensen & Doscher, 2010). The catchment has a southwest to northeast orientation with high elevations occurring to the south of the catchment and is sheltered by Mount Richmond in the north (Fig. 3.29a). The catchment has good soil drainage and the river is primarily fed by rainfall and runoff but there are some groundwater interactions that sustain the flow (McCarthy, 2021). The Wairau River is a highly engineered river to reduce the flood risk to the lower reaches of the catchment and has a 1-in-100-year flow magnitude of 5500m³/s (Williman, 1995; Wilson & Wöhling, 2014).

Data for the Wairau River was collected from the Marlborough District Council's Wairau River at Tuamarina monitoring site (Fig. 3.29a) and has a total record period of 63 years. Figure 3.30 indicates this river experiences low to moderate flows, and high flows are less common.

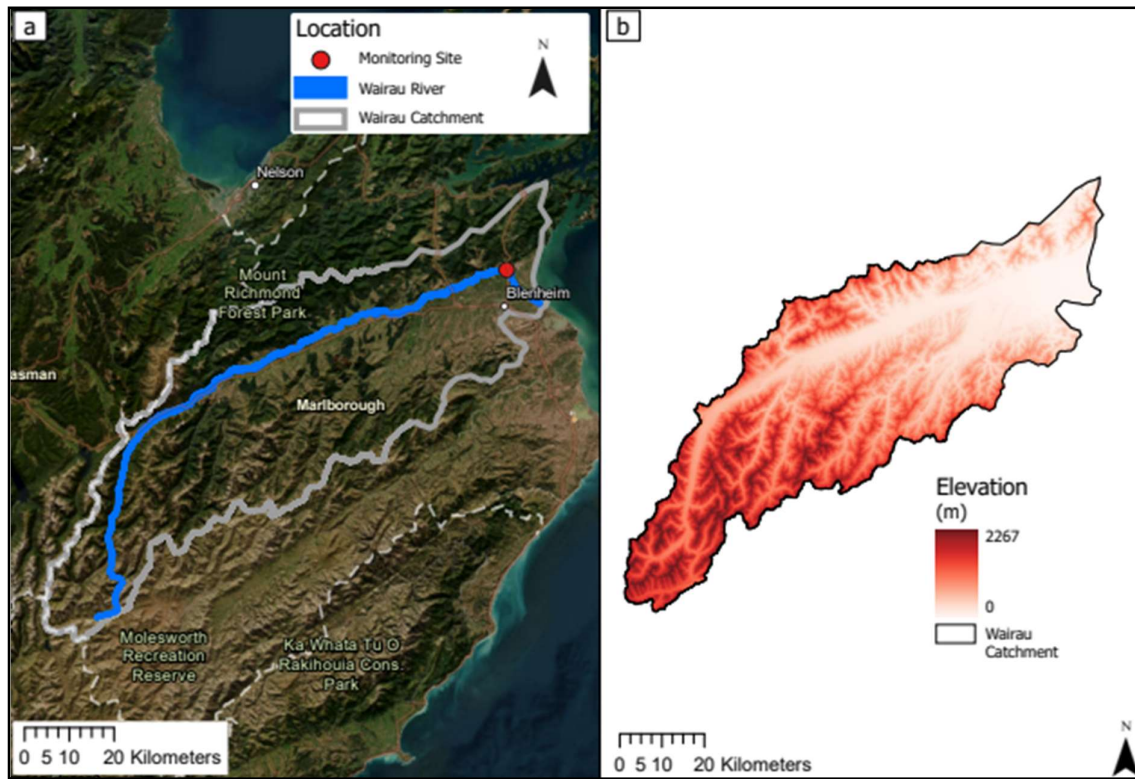


Figure 3.29: The Wairau catchment (a) location and (b) elevation.

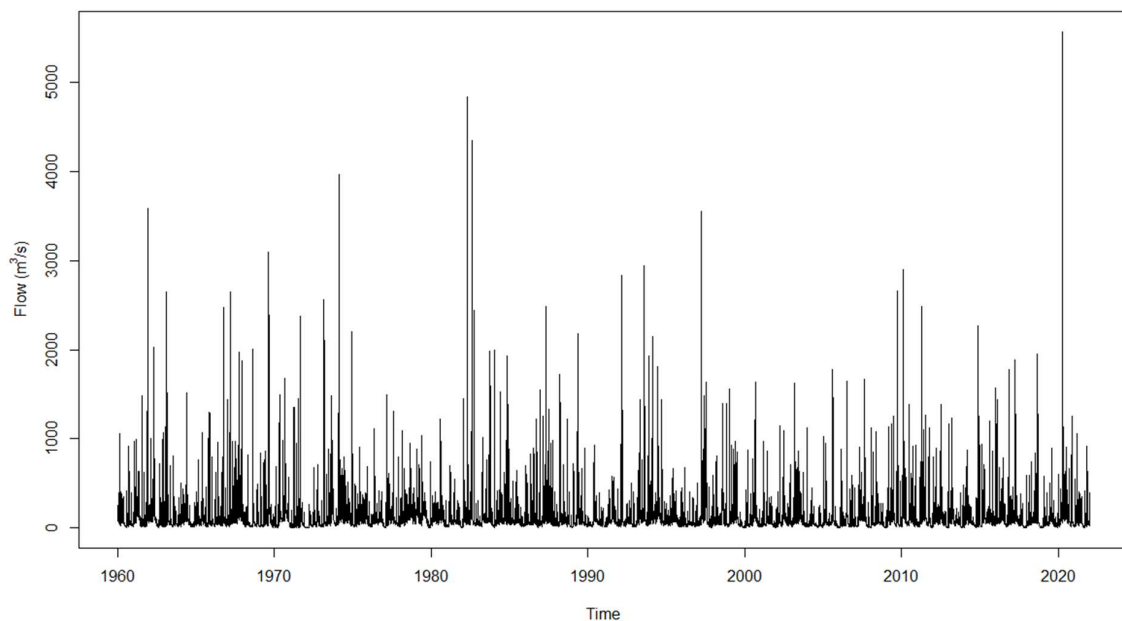


Figure 3.30: Wairau River flow (m^3/s) timeseries (05/07/1960- 23/05/2022).

3.1.5.2 Hurunui

The Hurunui River has a catchment area of 2671km² and west-east orientation (LAWA, 2022c). Figure 3.31 shows the Hurunui River extends 150km and flows east from the Southern Alps through a diverse range of terrain including alpine mountains, hill country, and the Canterbury Plains before discharging south of Port Robinson. The Hurunui River is rain fed and soil drainage moderate (McCarthy, 2021). There is some interaction between the river and groundwater which results in sustained flow during the year (LAWA, 2022c). Flooding is common after heavy rainfall due to the Hurunui's headwaters being located in the Southern Alps but the peak of the flood can be delayed due to dense forested areas (Hurunui District Council, 2022). The 1-in-100-year flood magnitude can exceed 2250 m³/s and flooding poses a significant risk to the Hurunui District and State Highways 1 and 7 (Tonkin & Taylor, 2017).

The Hurunui River flow data was collected from Environment Canterbury's (ECAN) Hurunui River at SH1 monitoring site (Fig. 3.31a) and has a record length of 49 years. The flow timeseries in Fig. 3.32 indicates the Hurunui River experiences regular cycles of low, moderate, and high flows throughout the whole record.

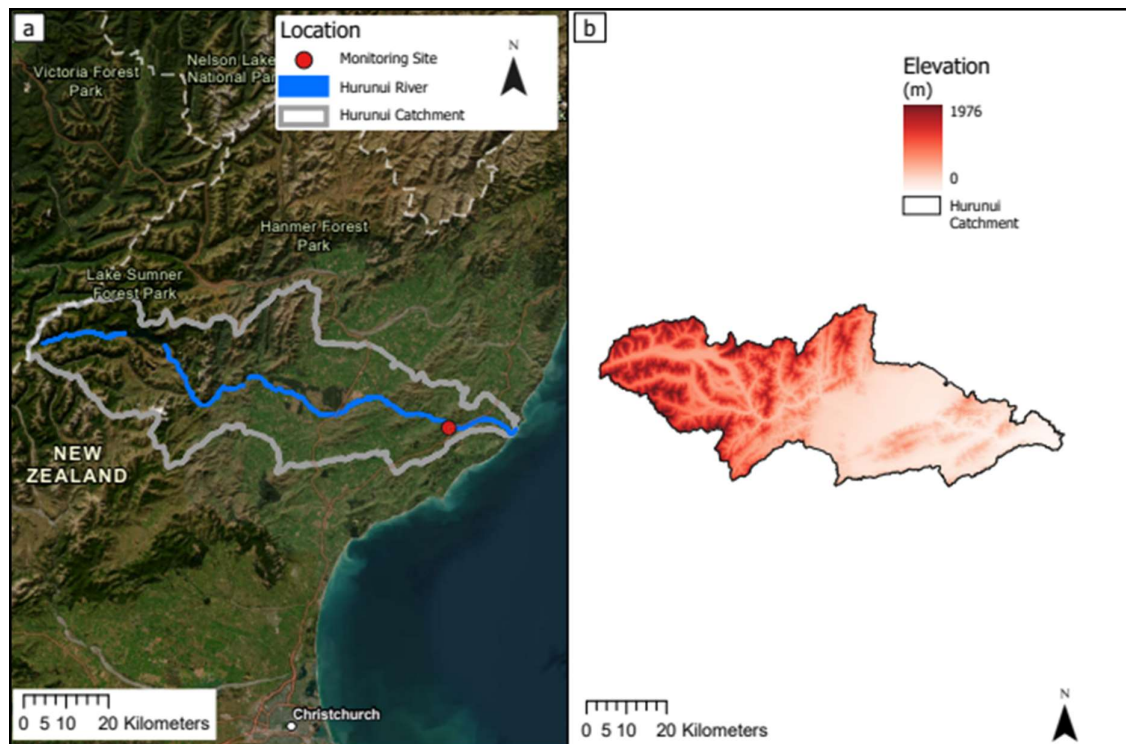


Figure 3.31: The Hurunui catchment (a) location and (b) elevation.

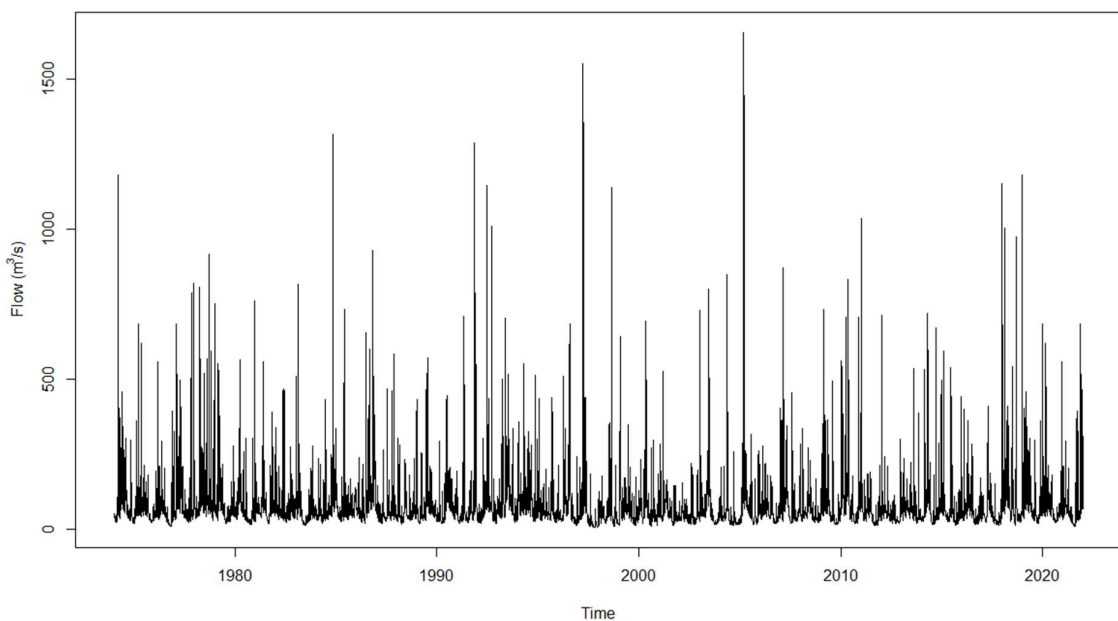


Figure 3.32: Hurunui River flow (m^3/s) timeseries (13/12/1974 – 31/03/2022).

3.1.5.3 Selwyn River

The Selwyn River has a catchment area of 770km^2 and northwest-southeast orientation (LAWA, 2022b). Figure 3.33 shows the Selwyn River extends 98Km and flows southeast through the Canterbury Foothills then east over the Canterbury Plains and it is bound by the Waikamariri River in the north, the Rakaia River in the south, the Southern Alps in the west, and Lake Ellsemere and the Pacific Ocean in the east (Larned et al., 2008). The river is primarily rain fed with moderate soil drainage and some interaction with the groundwater systems of the Canterbury plains (McCarthy, 2021). During periods of low rainfall, especially in summer, the Selwyn River dries up, and flow can be lost almost completely throughout the year in a central 43km segment of the river (Larned et.al, 2008). Flooding can impact the Selwyn District and State Highway 1 significantly and has a 1-in-100-year flow magnitude of $580\text{m}^3/\text{s}$ (Wild, 2019).

The Selwyn River data is from ECAN's Selwyn River at Coes Ford monitoring site (Fig. 3.33a) and has a record covering 31 years. The Selwyn River is known for drying out during summer with some areas of the river drying out completely during the year and this is

reflected in Fig. 3.34 where there are long periods of very low to no flow followed by brief high flow events.

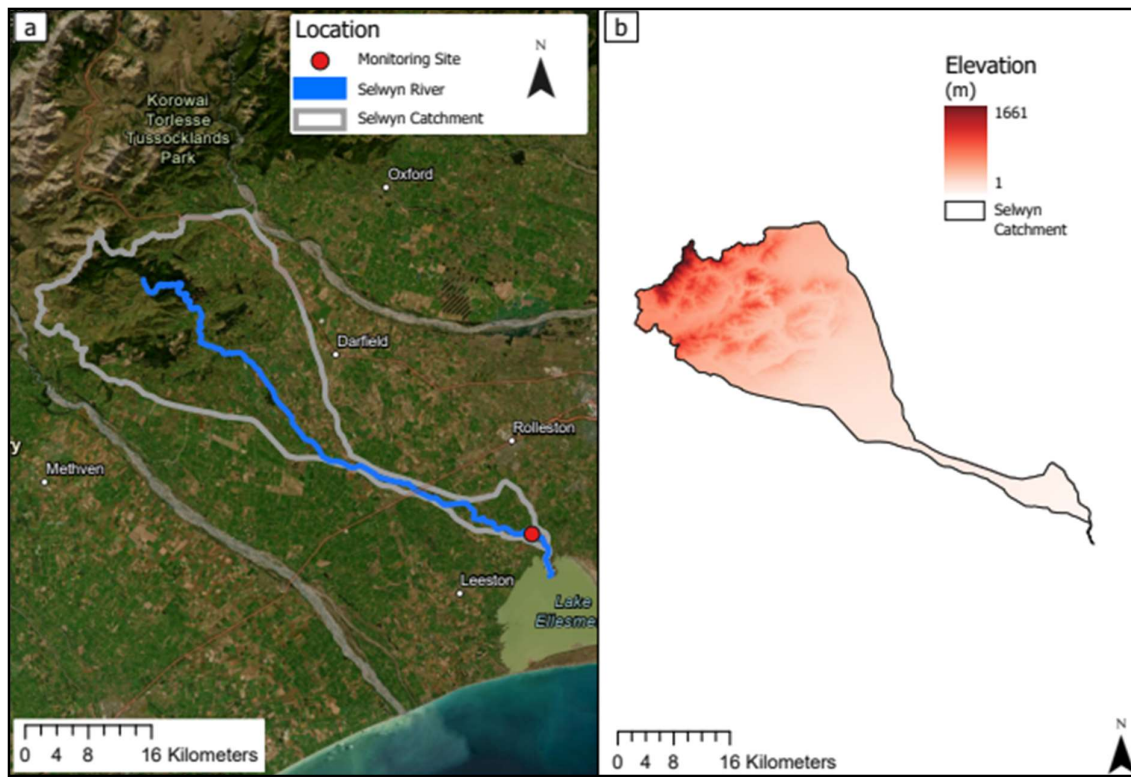


Figure 3.33: The Selwyn catchment (a) location and (b) elevation.

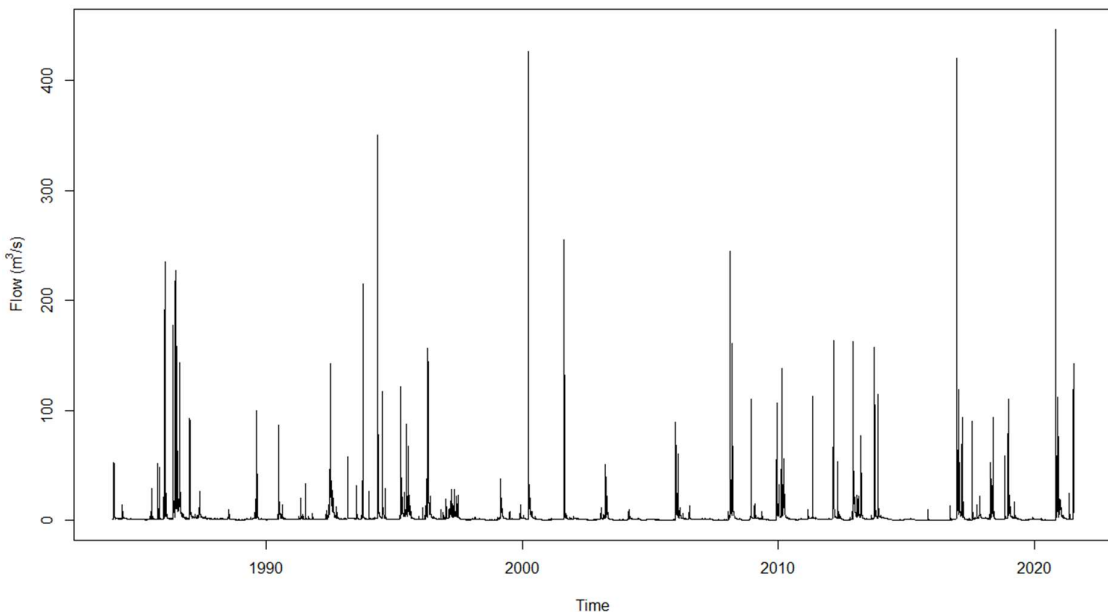


Figure 3.34: Selwyn River flow (m^3/s) timeseries (29/02/1984 – 22/02/2022).

3.1.5.4 Maerewhenua River

Located between Timaru and Oamaru, the Maerewhenua River has a southwest-northeast catchment orientation and an area of 290km² (LAWA, 2022f). It is a tributary of the Waitaki catchment and is the southernmost river in this research (Sutherland, 2006). Figure 3.35a shows the Maerewhenua River forms in the Kakanui Mountains then flows north-northeast towards Dunroon where it joins the Waitaki River. The river is primarily rain fed and has good soil drainage (LAWA, 2022f; McCarthy, 2021). Figure 3.35b shows most of the catchment is situated in high elevation areas due to its placement further south away from the Canterbury Plains, and it is sheltered in the west by the Southern Alps. State Highway 83 and Dunroon Domain are at risk of flooding from the Maerewhenua River and a 1-in-100-year flood can exceed 600m³/s (Steel et al., 2020).

The Maerewhenua River data was taken from ECAN's Maerewhenua River at Kellys Gully monitoring site, which has a record of 44 years (Fig. 3.35a). Figure 3.36 indicates this river experiences regular cycles of low, moderate, and high flows.

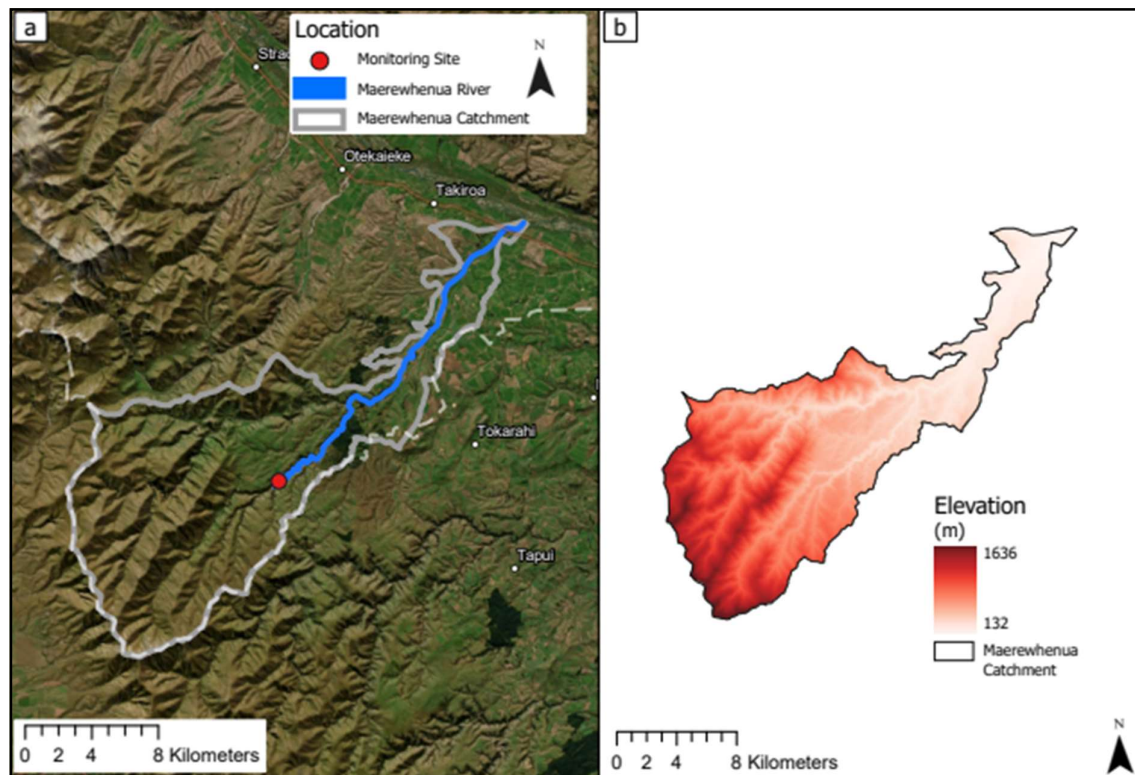


Figure 3.35: The Maerewhenua catchment (a) location and (b) elevation.

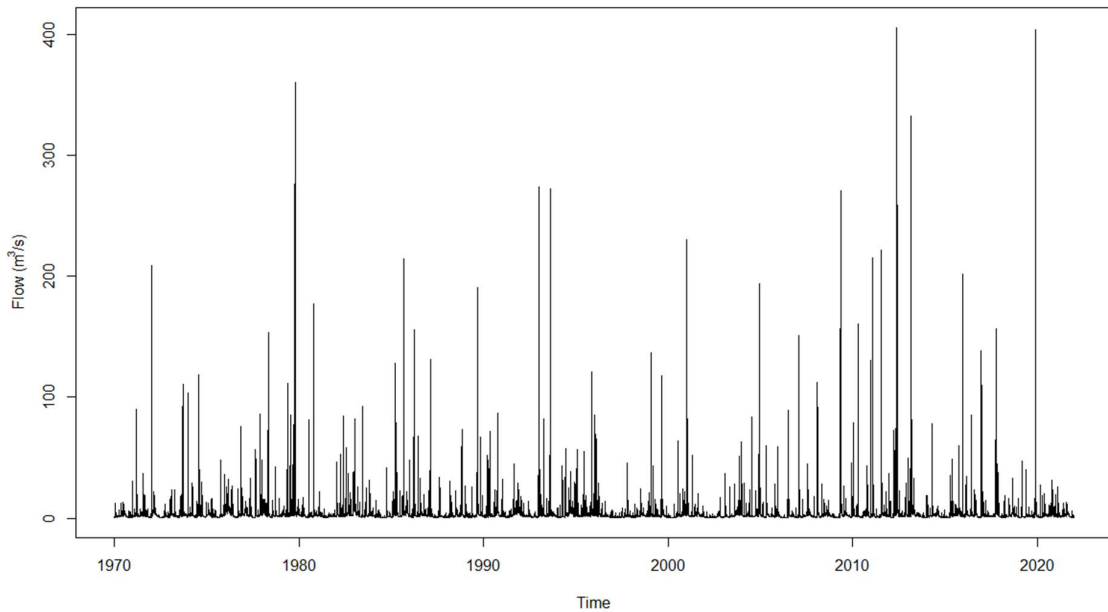


Figure 3.36: Maerewhenua River flow (m^3/s) timeseries (04/03/1970 – 23/03/2022).

3.2 Data and Methods

3.2.1 Data Collection

River flow data were provided by the relevant councils for the selected rivers. Data periods were to be at least 30 years and fall within 01/01/1979 to 31/03/2022 to correspond with the ERA-5 reanalysis data period for the climate analysis (see Section 3.3.1 for a description of ERA-5). For rivers with record periods longer than the period stated above, the records were to be trimmed and for rivers with records beginning after 1979 but with at least 30 years of data, the data would not be manipulated, to maintain the largest possible sample size.

3.2.2 Data Processing

Data collected from the councils were formatted in both 5-minute intervals and hourly means and for the purpose of the climate analysis, the flow data were processed into daily maximum flow. The peak flow of an event was of interest and therefore the daily maximum flow was chosen because it would retain this peak, while calculating the daily mean flow would lose it. The statistics program RStudio (R) was used to process the data into daily

maximum flow using the R package ‘data.table’ (Dowle et al., 2022) that would identify and extract the maximum value of a given day.

3.2.3 Generation of Flood Frequency Analysis and Threshold Identification

Annual maximum flow datasets were generated from the daily maximum datasets using Excel’s pivot table function for each catchment.

The Gumbel, LP3, and GEV methods were completed using the R package “lmom” (Hosking, 2010). The data were sorted from largest to smallest and the parameters were estimated using the LMOM method for Gumbel and GEV and log LMOM for LP3 (Pearson, 1991). The parameters were then used to generate a probability distribution using R for the relevant methods. The three probability distributions were plotted against each other on a single graph for each catchment with the observed values to visualize the fit of the modeled to the observed flows and allow comparison between each modelled distribution.

Flood magnitudes for the return periods were calculated using quantile and parameter functions for each method. The quantiles used for the return period calculations are shown in Table 4.1. These return period magnitudes were checked visually by estimating the return periods and the associated flow using the graphed probability distributions.

Table 3.1: Quantiles used for generating flow magnitudes for return periods.

Return Periods	Quantiles
1-in-5	0.77
1-in-10	0.88
1-in-50	0.97
1-in-100	0.99

To determine which FFA method is the best method for the observed annual maximum values for a catchment, a visual comparison, K-S, and Nash Sutcliffe Efficiency goodness-of-fit tests were completed.

A visual comparison, which compares the fit of the observed annual maximum flow values and the probability distributions, was completed on the FFA graphs produced. A ‘good fit’ was described as one where the modelled probability distributions followed the observed

value trend very well, with values being intercepted by the trendline. A ‘moderate fit’ was described as one where the probability distributions fit is average, where most observations were scattered around the trendline. A ‘poor fit’ was described as one where the probability distributions did not follow the observed values at all, with most values situated away from the trendline.

The K-S test is a non-parametric two-sided test that determines the difference between the observed distribution and the probability distribution by using random numbers based on the cumulative probability function of the flood frequency models when the flow data follows a continuous distribution (Rahman et al., 2013; Xiong et al., 2018). It will be used in this research to identify the FFA method that produces a modelled flow distribution most similar to the observed flow values for a catchment. An A-D test will not be completed despite it being more sensitive to the tails of the distribution and a better method for hydrological data on a global scale (Rahman et al., 2013). This is because internationally the K-S test is a common goodness-of-fit method and similar research has identified the method can accurately and efficiently be used to determine the best FFA method when working with 12 or more NZ catchments (Bonta & Shahalam, 2003; Mohssen, 2008; Xiong et al., 2018). Open-source code is also readily available for K-S and not for A-D, which further resulted in the decision to use the K-S test.

The K-S test was completed using the R package “dgof” (Shaonim, 2020; Arnold & Emerson, 2022). The code required the development of 4 variables, x, y, z, and w. The observed annual maximum flows for a catchment were variable x, while variables y, z, and w were a set of random variables that were calculated using the quantile and parameter functions of each probability distributions (Gumbel, GEV, and LP3 respectfully). The K-S test was then run using the observed values (x) and one of the distributions (either y, z, or w). The K-S test produces two values, a test statistic, and a p-value. The test statistic illustrates the maximum distance between the observed values and the probability distribution with the smaller the number indicating the modelled distribution accurately reflects the natural distribution of the observed values (Teegavarapu, 2019). The p-value further determines whether the modelled and observed distributions are similar (Teegavarapu, 2019). If the p-value was greater than 0.05, the null hypothesis cannot be rejected. The hypotheses for this research are as follows:

H_0 = The observed and probability distribution values are from the same continuous distribution.

H_a = The observed and probability distribution values are from different distributions.

The Nash Sutcliff Efficiency (NSE) calculates the residual variance of the probability distributions and compares it to the variance of the observed data (McCuen et al., 2006). The NSE statistic is primarily used for understanding the methods ability to predict, which is not a focus of this study, however, it can identify which methods have more uncertainty around modelling the higher flow values and return periods. Therefore, the NSE test is useful in this research to determine the reliability of the FFA flow magnitudes that will be used in the development of the event datasets (McCuen et al., 2006).

The R package “ie2misc” (Embry et al., 2022) was used to complete the NSE test on all 17 rivers. The open-source code examples from Willmott et al. (2012) were modified for this research and the same K-S test variables x, y, z, and w were used for the NSE test, for consistency. The NSE test produces a value between minus infinity and +1, with 0 indicating the mean of the observed values and the modeled values have the same accuracy at predicting, and 1 indicating the model is a perfect fit and can predict future events well. Negative values are common in flow data due to the uncertainty surrounding magnitude and frequency as well as bias around method used, sample size, and time dependence (McCuen et al., 2006). Negative values indicate the observed mean is more accurate at predicting flow. However, the closer the negative value is to 0 the more accurate the modeled distribution (Pushpalatha et al., 2012).

To determine whether Gumbel, GEV, or LP3 would be the best method for a specific catchment, the methods were required to have two out of three goodness-of-fit tests’ results indicating the FFA method was accurate at modelling the observed values. They therefore were required to either be identified as a ‘good fit’ from the visual comparison, have the lowest K-S test statistic, and/or have a NSE value close to zero.

3.2.4 Selection of Flood Events for Compositing

Thresholds were selected from each catchment based on the 1-in-5-year magnitudes, meaning that all values that were equal or greater than the 1-in-5-year magnitude would be used for the development of the event datasets and for compositing. The 1-in-5-year return period was used because it is not extrapolated, like the 1-in-100-year return period, would provide a larger sample size for the composite analysis, and is a direct reflection of the observed flow data. It was assumed that the best fit method would be reliable and provide accurate estimates for the catchments in this research.

An R code was developed using the R package “dplyr” (Wickham et al., 2022) which filtered all values from the daily maximum flow data (including the date and flow) that were equal or greater than the catchment-specific 1-in-5-year threshold within the selected time period of the 01/01/1979 to 31/03/2022. The filtered events were extracted from R to an Excel CSV file for the development of timesteps. For events that occurred within three days of each other, the date of the peak flow was selected and the other two flows were discarded to maintain independence between the high flow events as it was likely these high flow events occurred as a result of the same weather event.

3.2.5 Selection of Timesteps

Timesteps included the date of the high flow event and the prior two days. The first timestep started at 03/01/1979 as a result, and every timestep afterwards was a continuous addition. The dates and their timesteps were manually determined for all events identified and a catchment-specific code was developed to create river composites of all variables used for the climate analysis.

3.3 Climate Analysis Methods

3.3.1 Data Collection and Composite Development

To investigate the atmospheric conditions associated with high flow events, six-hourly atmospheric reanalysis data from The European Centre for Medium-range Weather Forecasts' (ECMWF) fifth generation atmospheric reanalysis (ERA-5) (Hersbach et al., 2020) for the period 01/01/1979 to 31/03/2022 were employed. These datasets are freely available

online and were downloaded from the Copernicus Climate Change Service (C3S) Climate Data Store (<https://cds.climate.copernicus.eu/#!/search?text=ERA5&type=dataset>). Because the focus of this research is on the synoptic to large-scale features, to save on storage space the data were first interpolated from their native grid of 0.5625° to a horizontal resolution of $1.5^{\circ} \times 1.5^{\circ}$. The ERA-5 dataset is the updated version of the ERA-interim reanalysis dataset developed by ECMWF that has been routinely used in atmospheric sciences, especially over the Southern Hemisphere (Hersbach et al., 2020). In particular, the ECMWF reanalysis has been shown to perform best over the data-sparse Southern Hemisphere compared to other modern reanalyses (Bracegirdle & Marshall, 2012; Marshall et al., 2022). The variables used in this research are shown in Table 3.2.

For this study, our interest is the anomalous synoptic and large-scale atmospheric circulation features during and preceding a high flow event. Thus, composite anomalies (mean of the anomalies for each group) for high flow events for each river were computed to examine the mean anomalous features during these events. To calculate the composites, daily means were computed from the six hourly data, and then daily anomalies based on the 1979-2021 climatology were calculated using the long-term mean of the 5-day pentad average centred on each day. From the daily anomalies, 3-day running means (of the anomalies) were calculated and used for compositing; the day of the high flow event and the two days prior were examined. In addition, to infer information on the development, movement, and/or persistence of cyclones and anticyclones, 3-day running standard deviations (square root of the variance) of the daily anomalies were also calculated for mean sea level pressure. The standard deviation (“MSL.var”, see Table 3.2) reflects areas of high and low variability or change during the 3-day period; areas with a high standard deviation are regions where pressure likely decreased or increased during the 3-day period, while areas with a low standard deviation reflect persistent pressure features.

The ERA5 skin temperature (or surface temperature), is equivalent to sea surface temperature over the ocean. Thus, we employed skin temperature to monitor anomalous SST features in regions around NZ and in the tropics outside of the ENSO region. Because skin temperature anomalies are significantly higher over land surfaces versus the ocean, for plotting purposes the 3-day running mean of standardised daily skin temperature anomalies (based on the 1979-2021 climatology of the 5-day centred running means/standard

deviations) were used to normalise the anomalies across the land and ocean. Lastly, to identify possible connections to tropical variability (i.e. circulation anomalies linked to forcing from deep tropical convection), daily-mean fields of satellite-derived outgoing longwave radiation (OLR) from the National Oceanic and Atmospheric Administration (NOAA) Interpolated OLR dataset (Liebmann & Smith, 1996) were employed, which has a $2.5^\circ \times 2.5^\circ$ horizontal grid spacing. As described in Table 3.2, OLR measures the cloud-top temperature or the surface of the earth in the absence of clouds. In the tropics, lower OLR values (colder temperatures) reflect areas of high and cold cloud tops associated with deep convection, while higher OLR values (warmer temperatures) reflect reductions in deep convection/clear skies. The 3-day OLR anomaly fields were calculated following the same procedure described above for ERA5 data.

Table 3.2: Data variables and their use in this research (with respect to the 3-day running mean anomaly).

Variable	Short Name	Long Name	Use	Units
1	MSL	Mean sea level pressure	Identifies areas of surface low and high-pressure.	hPa
2	MSL.var	Mean sea level pressure variance	Shows the change in surface pressure during the three days. Used to infer information on the development and/or movement of surface pressure systems.	Stdev
3	TCWV	Total column water vapour	Shows atmospheric moisture sources and transport.	mm
4	U10	Surface wind at 10m above ground level	The zonal (east-west) component of the near-surface wind. Used with V10 to create wind vectors to show transport pathways of moisture, the interaction with topography, and direction of near-surface flow intercepting the catchment.	ms^{-1}
5	V10	Wind velocity at 10m above ground level	The meridional (north-south) component of the near-surface wind.	Ms^{-1}
6	z500	Geopotential height at 500 hPa	Shows high (ridges) and low (troughs) pressure features in the mid-to-upper levels of the troposphere and is a useful field	m

			for investigating large-scale circulation patterns.	
7	SF200	Streamfunction at 200 hPa	A field of constant, non-divergent flow. This feature reflects geostrophic flow in the atmosphere and is particularly useful for identifying areas of high (anticyclonic flow) and low (cyclonic flow) pressure features, especially within the tropics where pressure changes are minimal. It is employed to identify planetary waves and their possible connection to tropical convection.	m^2s^{-1}
8	OLR	Outgoing longwave radiation	A measure of temperature at cloud-tops or surface in absence of clouds. Used to identify areas of deep convection in the troposphere, especially in the tropics (e.g. negative OLR anomalies reflect colder, higher, and deeper clouds; positive OLR anomalies reflect the absence of deep convection).	W m^{-2}
9	SKT	Skin temperature	Reflects seas surface temperatures over the ocean and has been standardised so anomalies over land and ocean could be examined equally.	Stdev

3.3.2 ENSO and SAM Conditions

Monthly-mean data for ENSO and SAM were examined to determine what large-scale Southern Hemispheric climate patterns were prevalent around the time of a high flow event. The Niño 3.4 SST anomaly and the Southern Oscillation Index (SOI) were used to determine the phase of ENSO (both accessed freely online from the NOAA Climate Prediction Center: <https://www.cpc.ncep.noaa.gov/data/indices/>), while the observation-based Southern Annular Mode index of Marshall (2003) was used to monitor the phase of the SAM (also accessed freely online: <https://climatedataguide.ucar.edu/climate-data/marshall-southern-annular-mode-sam-index-station-based>). The SAM Index is a station-based index which

measures the zonal pressure difference between mid-latitudes (around 40°S) and high-latitudes (65°S) (Marshall, 2003).

The Niño 3.4 measures the SST anomalies in the Central Tropical Pacific region between 5°N-5°S and 170°W-120°W, where negative values refer to the cold phase (La Niña) and positive values refer to a warm phase (El Niño) (Trenberth, 1997; National Oceanic and Atmospheric Administration, 2022). The SOI, which measures the difference in standardised MSLP anomalies between the Central Topical Pacific (Tahiti) and the Western Pacific Warm pool (Darwin) was also used, where negative values refer to a El Niño and positive values refer to a La Niña (Trenberth, 1997). Both indices were used to determine if a prominent ENSO phase/pattern (either oceanic or atmospheric) was occurring around the time of the high flow.

For both ENSO and SAM, the monthly values had to be greater than or equal to a critical value of ± 0.5 standard deviations (based on the monthly climatology over 1979-2021) to be considered an ENSO or SAM “event”. For ENSO, either the SOI or Niño 3.4 SST anomaly exceeding this threshold was considered an ENSO event. Values less than ± 0.5 standard deviations were considered “neutral” conditions. The phase of ENSO and SAM that was occurring during a high flow event was then identified using the month and year of each flow event generated in Section 3.2.4, and a percentage of events that occurred in a phase of ENSO or SAM was calculated. While the monthly-mean ENSO values are suitable for monitoring ENSO activity during the time of the high flow event (given ENSO operates on timescales of seasons to years), SAM variability is known to fluctuate on timescales of days to weeks (Fogt & Marshall, 2020). Therefore, it should be noted that the monthly-mean SAM conditions may not capture short-lived SAM events that may have contributed to a high flow. In an attempt to overcome this barrier, we analysed composite (3-day) anomalies for z500 over the full Southern Hemisphere to visually inspect potential SAM-like features.

4. Flood Frequency Analysis Results

In this chapter, the selection of the best FFA method and outcomes of the threshold generation for the event dataset will be discussed.

Table 4.1: Goodness-of-fit testing result

Region	River	Visual Comparison	Kolmogorov-Smirnov Two Sample Test*				Nash Sutcliffe Efficiency Test			
			Best fit method	Gumbel	GEV	LP3	Best Fit (lowest test statistic)	Gumbel	GEV	LP3
Upper North Island	Waitangi	LP3	0.190	0.167	0.167	GEV or LP3	-1.077	-1.656	-0.878	LP3
	Otara	GEV	0.227	0.136	0.136	GEV or LP3	-0.797	-0.954	-1.488	Gumbel
	Waioeka	Gumbel	0.187	0.167	0.146	LP3	-1.559	-1.664	-0.429	LP3
East Coast North Island	Hikuwai	Any	0.104	0.104	0.185	Gumbel or GEV	-1.059	-0.727	-0.653	LP3
	Waimatā	LP3 or GEV	0.2	0.156	0.111	LP3	-0.307	-2.233	-0.355	Gumbel
	Te Arai	Gumbel	0.102	0.128	0.154	Gumbel	-1.142	-0.805	-1.538	GEV
	Waikohu	LP3 or GEV	0.159	0.136	0.091	LP3	-0.864	-1.669	-1.917	Gumbel
	Waihora	LP3 or GEV	0.243	0.189	0.054	LP3	-0.303	-0.691	-0.361	Gumbel
	Waiapu	Any	0.083	0.083	0.125	Gumbel or GEV	-0.947	-0.911	-1.318	GEV
Lower North Island	Waipoua	GEV or Gumbel	0.129	0.129	0.290	Gumbel or GEV	-1.630	-1.148	-1.058	LP3
	Waingawa	GEV	0.217	0.109	0.174	GEV	-1.530	-0.978	-0.834	LP3
	Waiōhine	GEV or Gumbel	0.159	0.130	0.174	GEV	-0.549	0.976	-0.906	Gumbel
	Ruamāhangā	GEV	0.182	0.151	0.167	GEV	-0.948	-0.590	-1.575	GEV
South Island	Wairau	GEV	0.534	0.177	0.097	LP3	-0.659	-0.459	-1.344	GEV
	Hurunui	Gumbel or GEV	0.102	0.143	0.163	Gumbel	-1.601	-0.224	-1.551	GEV
	Selwyn	LP3	0.154	0.128	0.102	LP3	-1.168	-1.112	-0.898	LP3
	Maerewhenua	LP3	0.094	0.151	0.170	Gumbel	-1.879	-1.388	-0.739	LP3

*All K-S p-values were greater than 0.05 for all FFA method, so the H_0 hypothesis was accepted.

Table 4.2: Selected flood frequency method and threshold development results.

Region	River	Method used for thresholds	1-in-5-year (m ³ /s)	1-in-10-year (m ³ /s)	1-in-50-year (m ³ /s)	1-in-100-year (m ³ /s)	Number of events exceeding 1-in-5-year threshold (Continuous)	Number of events (Independent and within timeframe)
Upper North Island	Waitangi	LP3	307.50	408.74	682.61	976.52	11	8
	Otara	GEV - Weibull	447.48	535.27	696.47	808.64	11	10
	Waioeka	LP3	841.18	950.16	1112.36	1201.33	24	12
East Coast North Island	Hikuwai	GEV - Weibull	750.48	896.28	1163.06	1347.92	16	10
	Waimatā	LP3	373.18	492.60	822.60	1185.61	15	12
	Te Arai	Gumbel	206.67	253.86	348.50	421.19	11	9
	Waikohu	LP3	305.70	431.86	756.96	1080.23	14	11
	Waihora	LP3	232.50	357.88	752.83	1240.02	30	24
	Waiapu	GEV - Weibull	2899.75	3400.27	4352.93	5045.01	16	12
Lower North Island	Waipoua	GEV - Weibull	191.18	232.33	313.90	376.09	11	9
	Waingawa	GEV - Weibull	303.42	339.59	405.32	450.91	15	15
	Waiōhine	GEV - Weibull	983.29	1113.19	1324.42	1451.30	19	12
	Ruamāhangā	GEV - Weibull	1017.08	1062.12	1107.09	1121.58	32	19
South Island	Wairau	GEV - Fréchet	2316.60	2831.39	3915.29	4802.62	30	14
	Hurunui	Gumbel	932.12	1132.38	1534.02	1844.50	22	12
	Selwyn	LP3	212.28	295.45	404.62	446.99	14	9
	Maerewhenua	LP3	189.10	257.35	403.58	520.71	20	14

4.1 Upper North Island

A visual comparison of the three methods in Fig. 4.1a for the Waitangi catchment identified GEV and LP3 most accurately modelled the observed annual maximum flow distribution. A slight non-linear trend in the observed values, where some moderate and high flow values had similar flow rates but different return intervals, resulted in the linear distribution Gumbel being unable to accurately model the observed distribution while the more flexible three-parameter distributions were able to. All FFA methods appear to fit the observed flow well for the Waioeka catchment (Fig. 4.1b).

The LP3 distribution was identified through KS testing to be most like the observed values for both the Waitangi and Waioeka catchments (Table 4.1). NSE testing determined the mean of the observed values is a better predictor for both catchments due to the production of negative NSE values as shown in Table 4.1. The LP3 method for both catchments however had the closest value to zero (Table 4.1), suggesting that the LP3 method is more accurate at modelling the observed flows compared to GEV and Gumbel in the Waitangi and Waioeka catchments.

Therefore, the LP3 method was selected for threshold development for both the Waitangi and Waioeka catchments as two out of the three goodness-of-fit tests indicated it was the best fit method. Eight independent high flow events were identified to exceed the 1-in-5-year threshold of $307.50\text{m}^3/\text{s}$ calculated by the LP3 method for the Waitangi catchment. For the Waioeka catchment, a total of 24 events were identified to equal or exceed the $841.18\text{m}^3/\text{s}$ threshold, however upon further inspection of these events only 12 of them were independent, suggesting it is common for high flow events to occur over two days in this catchment.

Unlike the Waitangi and Waioeka catchments, Fig. 4.1c for the Otara catchment indicates the LP3 distribution does not fit the observed values well. The LP3 distribution appears to flatten once a 20-year return period is reached, suggesting the method may underestimate high flow events in the Otara catchment. Both the Gumbel and GEV distributions however have a good fit to the observed data especially towards the higher flow values. K-S testing identified that both the LP3 and GEV distributions had the same low test

statistic (Table 4.1) indicating both distributions fit the observed values well despite the visual comparison implying the LP3 distribution did not fit. This may reflect the use of random values for K-S testing and the flexibility of LP3 as discussed in Section 2.2.3.3. The Gumbel method was identified as being a more accurate method compared to GEV and LP3 through NSE testing, however the GEV method was selected for threshold development because the visual comparison and K-S testing identified it as the best fit method. The k shape parameter value for GEV was also identified to be greater than zero and the GEV method was determined to favour the Weibull distribution (Table 4.2). The 1-in-5-year threshold generated for the Otara catchment was $447.48\text{m}^3/\text{s}$ and 10 independent high flow events were identified (Table 4.2). The specific events extracted from the daily maximum flow data for each catchment in the UNI are shown in Table A of the Appendix.

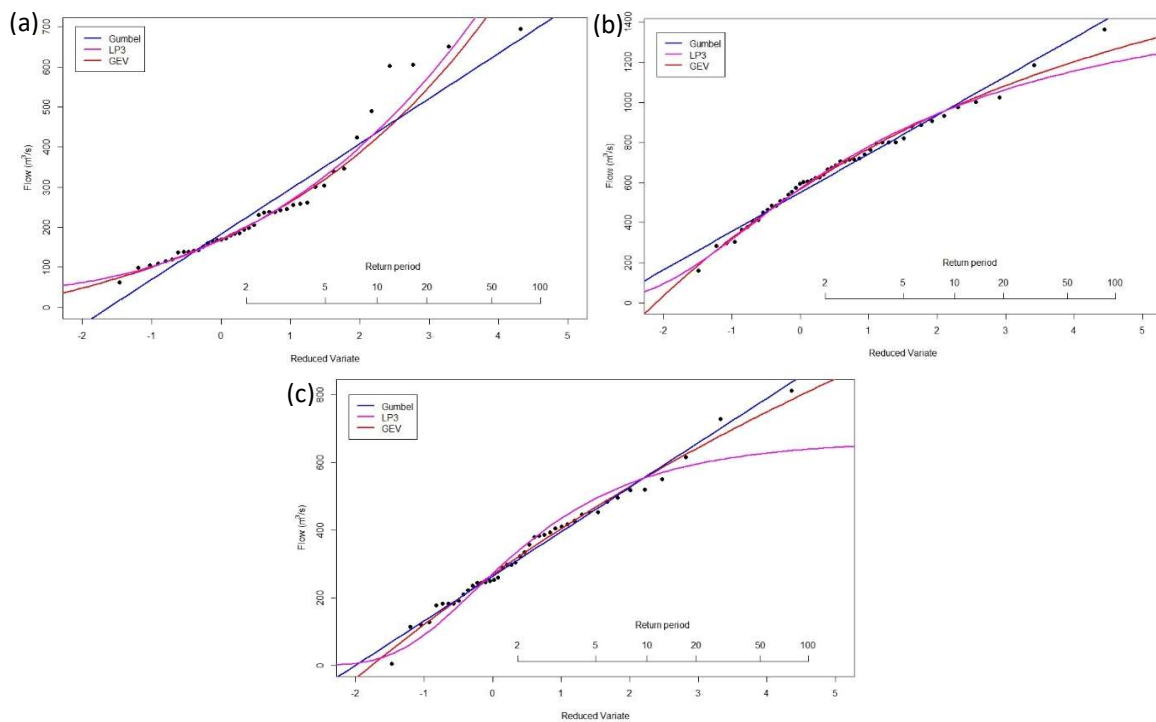


Figure 4.1: Flood frequency analysis results for the UNI catchments: (a) Waitangi, (b) Waioeka, and (c) Otara catchment. Flow (m^3/s) is on the y axis and the return period (years) and reduced variate are on the x axis, with the Gumbel distribution in blue, LP3 in pink and GEV in purple.

4.2 East Coast North Island

A visual comparison of the results in Fig. 4.2 for the ECNI catchments show that all three modelled distributions for the Hikuwai (Fig. 4.2a), Te Arai (Fig. 4.2c), and Waiapu (4.2e) catchments fit the observed data well. However, a significant outlier in the Hikuwai catchment around $1500\text{m}^3/\text{s}$ (Fig. 4.2a), which is most likely Cyclone Bola (see Section 3.1.3.1), results in less accurate distributions for the LP3 compared to Gumbel and GEV, leading to an underestimation of the higher return periods. The Gumbel and GEV methods appear to produce distributions that can more accurately estimate outliers in the Hikuwai River. GEVs consideration of the extreme values around $1000\text{m}^3/\text{s}$ as well as the outlier above $1500\text{m}^3/\text{s}$, results in the GEV method being the most accurate method for the Hikuwai catchment visually.

K-S testing identified the Gumbel and GEV distributions had the same low test statistic values for the Hikuwai and Waiapu catchments while Gumbel had the lowest value for the Te Arai catchment (Table 4.1). NSE testing identified the mean of the observed values is a better predictor of flow in all catchments due to the presence of negative values, but it was identified that GEV is a more accurate method for the Te Arai and Waiapu catchments. The LP3 method was identified to be the more accurate method for predicting flow for the Hikuwai catchment despite the potential underestimation of the larger return period floods.

The GEV method was therefore selected for threshold generation in the Hikuwai and Waiapu catchments because the visual comparison and K-S testing indicated it was the most accurate method for modelling flow in these catchments. The k shape parameter values for both the Hikuwai and Waiapu catchments were greater than zero and the Weibull distribution shape was favoured (Table 4.2). A 1-in-5-year threshold of $750.48\text{m}^3/\text{s}$ was calculated for the Hikuwai catchment, and 10 independent high flow events were identified to exceed/equal this threshold. The 1-in-5-year threshold for the Waiapu catchment was the largest in this study with a flow rate of $2899.75\text{m}^3/\text{s}$ (Table 4.2). Twelve independent high flow events were extracted from the daily maximum dataset for this catchment. The goodness-of-fit testing identified the Gumbel method was more accurate for the Te Arai catchment and nine events were identified to exceed or equal the 1-in-5-year threshold of $206.67\text{m}^3/\text{s}$.

Figure 4.2 shows the LP3 and GEV methods fit the observed data well for the Wamatā (Fig. 4.2b), Waikohu (Fig. 4.2d), and Waihora (Fig. 4.2f) catchments due to the flexibility of both methods to account for non-linear distributions in observed flow data (England et al., 2019). Unlike the Hikuwai catchment (Fig. 4.2a), the outliers in the Wamatā, Waikohu, and Waihora catchments, which are most likely from Cyclone Bola (see Section 3.1.3), result in an observed non-linear trend which the linear Gumbel method fails to accurately model in these catchments.

K-S testing for the Waimatā, Waikohu, and Waihora (Table 4.1) catchments identified the LP3 method had the lowest test statistic for the three catchments, suggesting this method best fits the observed value distributions. NSE testing identified the Gumbel distribution is the more accurate method for predictions in all three catchments despite the Gumbel not visually fitting the data well. These results suggest that for more efficient prediction capability it would be best to remove outliers from the data, because the Gumbel method would then be able to more accurately fit the observed distribution. However, given the accuracy of the LP3 and GEV methods at modelling the observed flow data with these outliers, the outliers will not be removed.

The visual comparison and K-S testing indicated the LP3 method was most accurate at modelling the observed flow for the Waimatā, Waikohu, and Waihora catchments and was selected for threshold generation (Table 4.1). Twelve independent events were identified to exceed or equal a threshold of $373.18\text{m}^3/\text{s}$ for the Waimatā catchment, whereas 11 events were identified to exceed or equal Waikohu catchments threshold of $305.70\text{m}^3/\text{s}$ (Table 4.2). For the last catchment, the Waihora, the threshold was $232.50\text{m}^3/\text{s}$ and 24 independent events were identified to exceed or equal this threshold. The Waihora catchment had the most events in this study. The induvial high flow events identified for the ECNI region are shown in Table A in the Appendix.

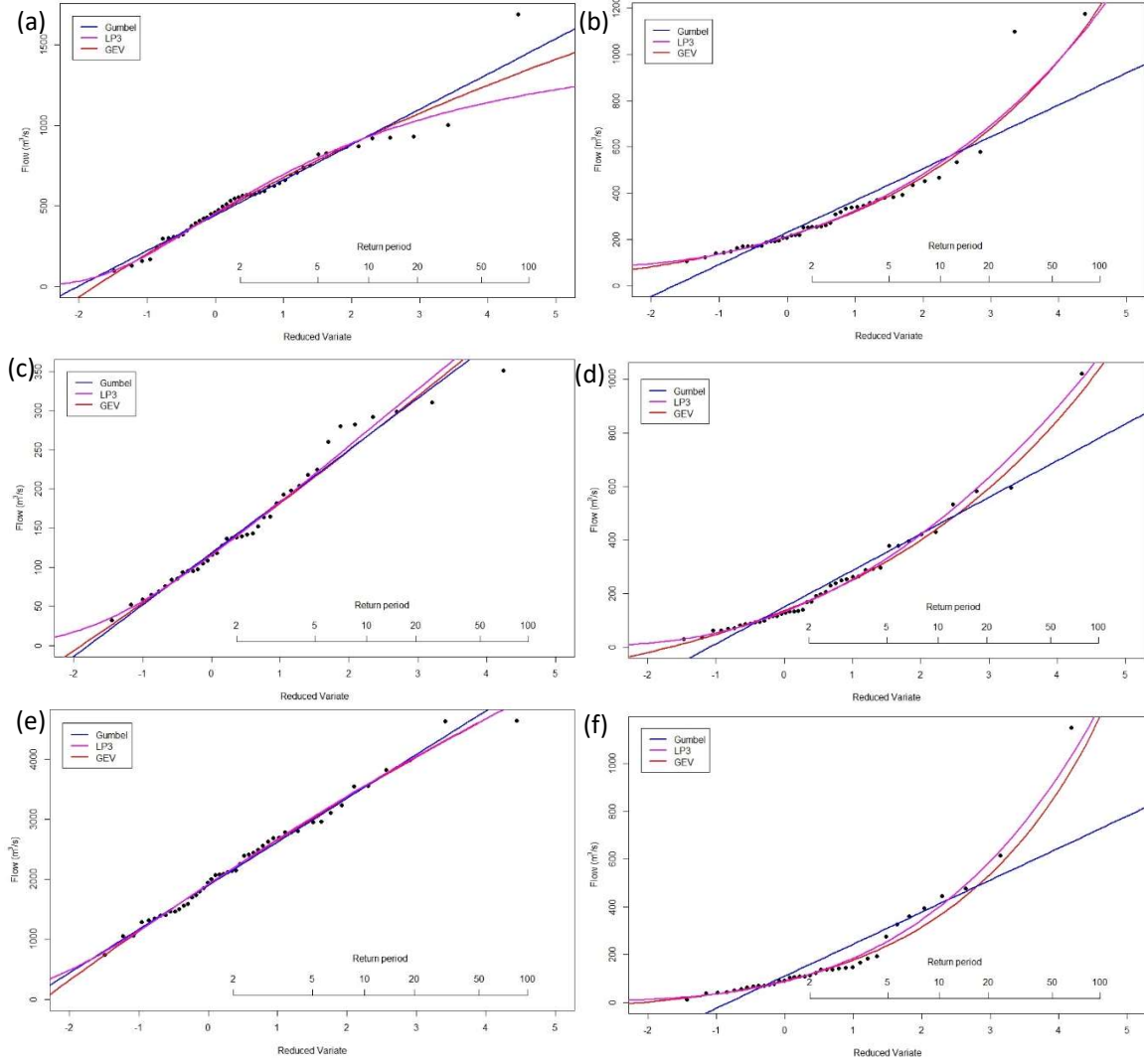


Figure 4.2: Same as Fig. 4.1 but for the ECNI catchments: (a) Hikuwai, (b) Waimatā, (c) Te Arai, (d) Waikohu, (e) Waipoua, and (f) Waihora.

4.3 Lower North Island

A visual comparison of the FFA methods for the Waipoua catchment (Fig. 4.3a) identified the GEV and Gumbel modelled distributions fit the linear distribution of the observed values well. The LP3 distribution appears to be non-linear which has a moderate fit to the observed data and may potentially result in an underestimation of the higher flow values above $250\text{m}^3/\text{s}$ (Fig. 4.3a) where the line curves downwards.

K-S testing for the Waipoua catchment identified the Gumbel and GEV distributions were most similar to the observed values while NSE testing identified the LP3 method was more

accurate for predicting in this catchment. The GEV method (favouring the Weibull distribution) was therefore chosen for threshold generation due to the visual comparison and K-S testing identifying it as most accurate in this catchment. The 1-in-5-year threshold for the Waipoua catchment was $191.18\text{m}^3/\text{s}$ and 11 events were identified to exceed this threshold, nine of which were independent.

For the Waingawa catchment, a visual comparison of Fig. 4.3b indicates all FFA methods have a good fit to the observed data, suggesting all methods are accurate for this catchment. K-S testing results shown in Table 4.1 identified the GEV was most like the observed values, and NSE testing suggested the Gumbel method was more accurate. Given both GEV and Gumbel were identified as accurate methods for the Waingawa catchment through goodness-of-fit testing, either method could be selected for threshold generation. Based on the FFA method results in Table 4.2 of the other catchments in the LNI, the GEV – Weibull method was selected for consistency. Therefore, the 1-in-5-year threshold for the Waingawa catchment was $303.42\text{m}^3/\text{s}$ and all 15 events identified to be equal or exceed this threshold were independent.

For the larger catchments in the Lower North Island, the Waiōhine (Fig. 4.3c) and Ruamāhangā (Fig. 4.3d), the observed values follow a slight non-linear distribution unlike the Waipoua and Waingawa catchments (Figs. 4.3a,b). A visual comparison of Fig. 4.3c shows the Gumbel and GEV distributions fit the observed data better than the LP3 distribution for the Waiōhine catchment. Figure 4.3d shows the Ruamāhangā catchment's observed flow values flatten once a flow of $1000\text{m}^3/\text{s}$ is reached and most flow occurs between 600 - $1000\text{m}^3/\text{s}$. The Gumbel method has a linear distribution which appears to put more emphasis on these values between 600 - $1000\text{m}^3/\text{s}$ and is unable to accurately model the low and high flow values as a result, leading to a very poor fit between the modelled and observed distribution. The LP3 and GEV methods produced a non-linear distributions and therefore fit the observed data well.

K-S testing results in Table 4.1 identified the GEV - Weibull method produced values most similar to the observed distribution for both the Waiōhine and Ruamāhangā. NSE testing identified the Gumbel method as being more accurate for the Waiōhine catchment while the GEV method was identified for the Ruamāhangā.

The GEV method was therefore selected for threshold generation for the Waiōhine catchment because the visual and K-S test identified it as the most accurate method and Table 4. 2 shows 12 independent high flow events were identified above its 1-in-5-year threshold of $983.29\text{m}^3/\text{s}$. All three goodness-of-fit tests identified the GEV method was best for the Ruamāhangā and it was therefore selected for threshold generation. The Ruamāhangā catchments 1-in-5-year threshold was $1017.08\text{m}^3/\text{s}$ and 19 independent events were identified to exceed or equal this threshold (Table 4.2). The specific events identified for all catchments are shown in Table A of the Appendix.

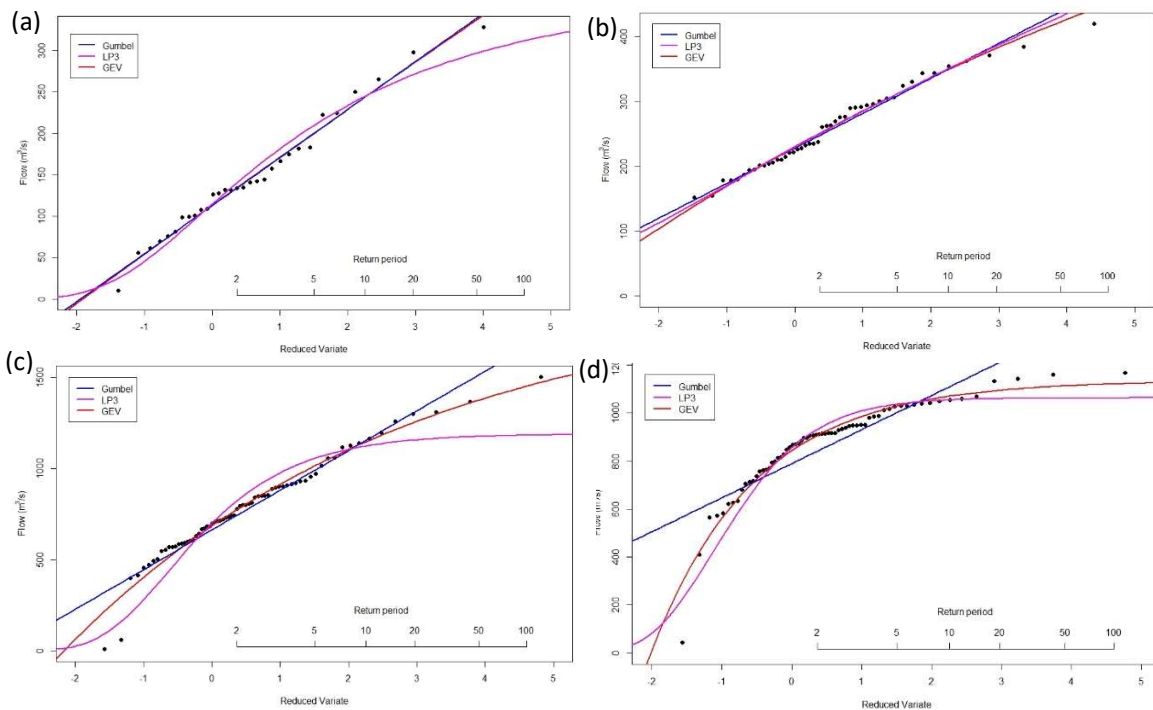


Figure 4.3: Same as Fig. 4.1 but for the LNI catchments: (a) Waipoua, (b) Waingawa, (c) Waiōhine, and (d) Ruamāhangā.

4.4 South Island

A visual comparison of the FFA method accuracy for the Wairau catchment in Fig. 4.4a identified that all distributions have a good fit to the observed data with GEV and LP3 distributions fitting the low flow values better. The LP3 distribution was determined to be most similar to the observed values through K-S testing and NSE testing identified the GEV method is a more accurate method at predicting flow compared to the other methods. With

the visual comparison and NSE testing indicating the GEV method was an accurate method for the Wairau catchment, it was selected for threshold generation. The k shape parameter value was determined to be smaller than zero and thus the Fréchet distribution was favoured. Thirty events were identified to equal or exceed the 1-in-5-year threshold of $2316.60\text{m}^3/\text{s}$ for the Wairau catchment. Of these 30 events, 16 occurred within two days of the peak flow, leaving a total of 14 independent events (Table 4.2).

GEV and Gumbel fit the observed data best for the Hurunui catchment as shown in Fig. 4.4b, while the LP3 distribution has a poor fit as it does not accurately model the high and low flows of the observed data. K-S testing identified the Gumbel distribution was most similar to the observed values whereas NSE testing suggested GEV was a more accurate method for prediction. Therefore, with two goodness-of-fit tests suggesting the Gumbel method is an accurate method for the Hurunui catchment, it was selected for threshold development and 12 independent events were identified to equal or exceed the 1-in-5-year threshold of $932.12\text{m}^3/\text{s}$ (Table 4.2).

Figure 4.4c shows all distributions fit the observed flow data in the Selwyn catchment well. The LP3 distribution follows the curvature of the observed values the best, especially the lower values, and fits the higher flow values more accurately compared to the other distributions. The Gumbel and GEV distributions only appear to fit the middle flow values accurately (Fig. 4.4c). K-S and NSE testing identified the LP3 distribution was most similar to the observed data and the more accurate method for prediction (Table 4.1). Therefore, the LP3 method was selected for threshold development and Table 4.2 shows 14 events were equalled or exceeded the 1-in-5-year threshold of $212.28\text{m}^3/\text{s}$, nine of which were independent.

Similar to the Selwyn catchment, all three FFA methods fit the observed Maerewhenua flow data well, however the LP3 distribution fits the data better than the other two methods as it follows the trend of the low and high values more accurately (Fig. 4.4d). K-S testing identified the Gumbel method produces a distribution most similar to the observed values while NSE testing identified the LP3 method was better for prediction in this catchment. As the visual comparison and NSE testing identified the LP3 was more accurate in the Maerewhenua catchment it was selected for threshold development. The 1-in-5-year

threshold for this catchment is $189.10\text{m}^3/\text{s}$ and 14 independent events were identified to exceed/equal this threshold (Table 4.2). The individual events extracted from the daily maximum flow data are shown in Table A of the Appendix.

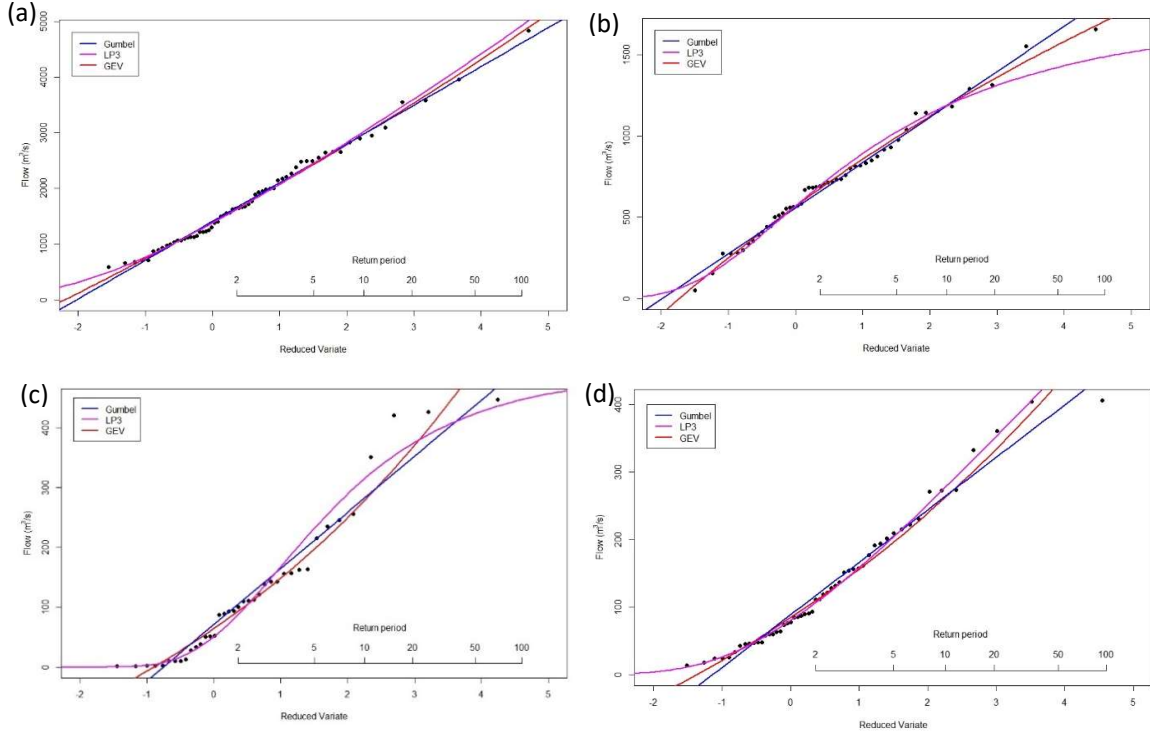


Figure 4.4: Same as Fig. 4.1 but for the SI catchments: (a) Wairau, (b) Hurunui, (c) Selwyn, and (d) Maerewhenua.

5. Climate Results

In this chapter, composite anomalies of the large-scale and regional atmospheric circulation for the three days during and preceding high river flow in the four eastern regions of NZ are presented, along with the SAM and ENSO conditions.

5.1 Upper North Island

The local synoptic situation in Fig. 5.1 indicates high flow events occurred in the Otara catchment, located in the UNI, when there was a deep low-pressure system to the west of NZ combined with a strong high-pressure system to the east and southeast of the country, taking the formation of the Kidson ‘TNW’ (Trough) and ‘NE’ (Blocking) synoptic types (Kidson, 2000). The MSLP variance in Fig. 5.1c suggests these features were part of an east to southeastward propagating pattern, with the largest change in MSLP occurring to the southeast and west of the low-pressure system (e.g. low-pressure moving/developing southeastward) and increasing in pressure to the west (e.g. moving in behind the low). Of potential importance, the lowest variance occurred in the northern portion of the high to the east near 40°S, 165°W in Fig 5.1c, suggesting that while high-pressure built southward favouring strong northerly flow, the northern portion would have remained stationary allowing for a persistent low-latitude moisture source. An associated surface boundary/cold front was oriented in a near north-south direction to the west of the North Island over the Tasman Sea with a warm front to the south of the catchment, thus the flooding occurred while the catchment was in a broad and moist warm sector of the cyclone rather than along a front (Fig. 5.1d). The Waioeka (Fig. 5.1e) and Waitangi (Fig. 5.1a) catchments showed a similar pattern and were also located within the middle of a warm sector ahead of an approaching cold front from the west. The Waitangi catchment (in Northland), however, had a warm front present around 40°S, orientated east-west around the Wellington region as seen in Fig. 5.1b.

Strong and unobstructed poleward transport of moisture out of the tropics through northerly winds can be seen within the warm sector covering the North Island and maximising over the eastern North Island, intersecting the UNI with nearly due north winds for all three catchments in the UNI (Figs. 5.1b, d, f). The low to the west and high to the east, shown in Fig 5.1c, play a key role in this moisture transport to the Otara catchment. The northeasterly

winds on the western side of the anticyclone and north-westerly winds occurring to the northwest of NZ in the warm sector of the cyclone, converge over the UNI and likely aid in low-level convergence within a highly moist environment that would promote heavy precipitation across the catchments. The location of the high and low centres differs slightly for the Waitangi and Waioeka catchments. The Waitangi catchment has a low centre situated further north above the UNI regions and a high-pressure centre south that covers NZ (Fig. 5.1a), whereas the centre of the low is located northwest of NZ with a high-pressure centre east of central NZ for the Waioeka catchment (Fig. 5.1e). Despite these differences in the location of the high and low centres, the direction of moisture transport and the moisture source region is similar for all three catchments.

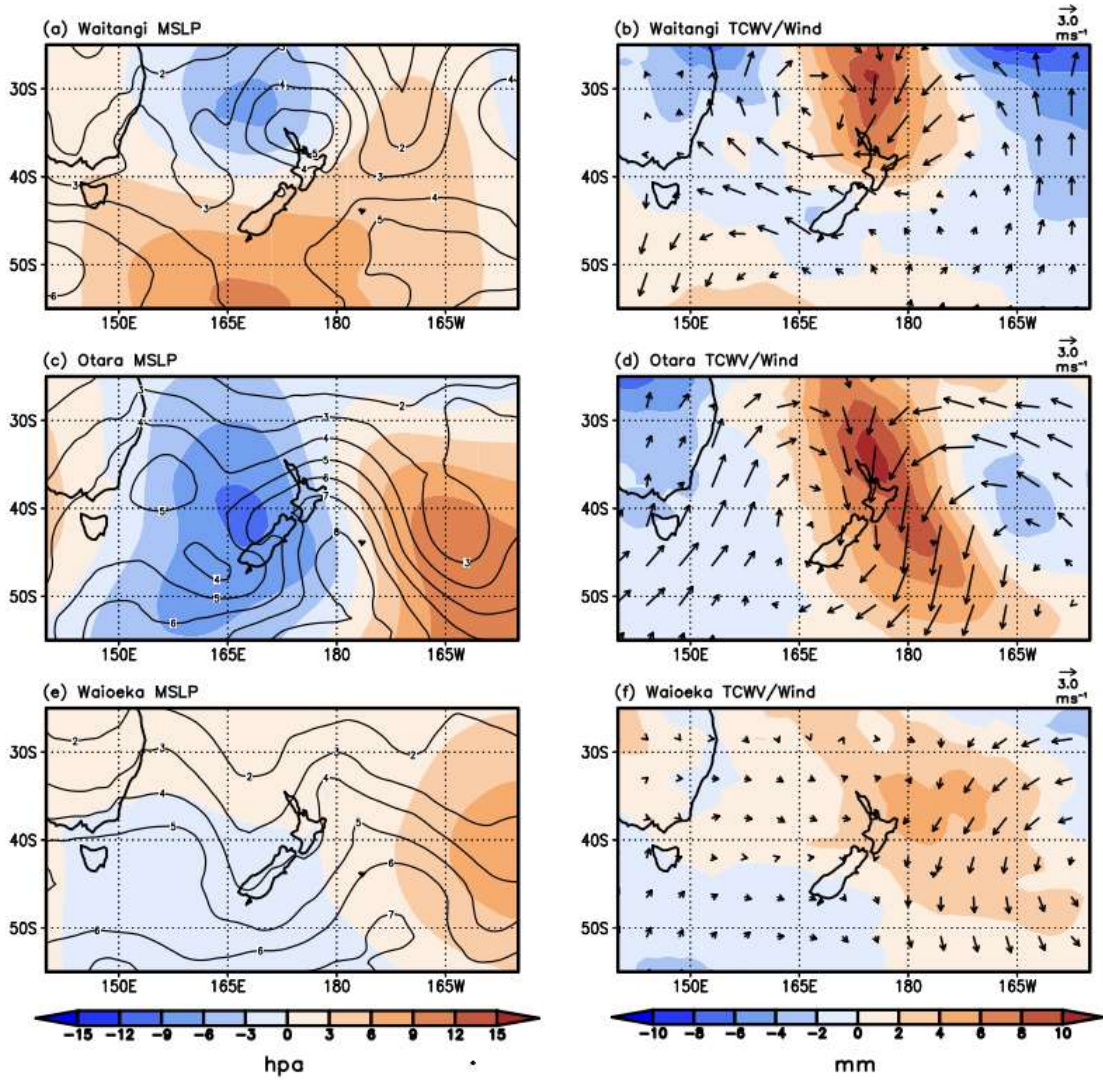


Figure 5.1: Local circulation features that occurred during high flow events in the UNI catchments. The left column shows composite anomalies of mean sea level pressure (MSLP) (shaded) and MSLP variance (contours) for (a) Waitangi, (c) Otara, and (e) Waioeka catchments. The right column shows composite of total column water vapour (TCWV) anomalies (shaded) and 10-m wind (vectors) for (b) Waitangi, (d) Otara, and (f) Waioeka catchments.

The large-scale circulation pattern (Figs. 5.2b-c) indicated by the Z500 and SF200 anomalies clearly show a zonally-oriented wave train (zonal wave 4; four high-low-pressure pairs) across the middle latitudes with no clear zonally-symmetric SAM pattern. In the tropics, the sf200 and sea surface temperature (SST) anomalies show a La Niña-like pattern for Otara (Figs. 5.2d and 5.3c) and Waioeka (Figs. 5.2f and 5.3e), with cold SST anomalies and suppressed convection in the central equatorial Pacific and warm SST anomalies/enhanced convection in the western tropical Pacific, but an El Niño pattern is seen for Waitangi (Figs.

5.2b and 5.3a). High flow events are more likely to occur during a La Niña phase of ENSO with high flow events in the Otara and Waioeka catchments occurring with a La Niña 70% (Fig. 5.4c) and 67% (Fig. 5.4e) of the time, respectively. However, the Waitangi catchment shows no preference to ENSO with high flow events occurring 38% (Fig. 5.4a) of the time during both a La Niña and El Niño. While La Niña is associated with higher pressure to the east and northeast of NZ (Ummenhofer & England, 2007), the lack of a coherent/consistent ENSO/SAM signal suggests an amplified mid-latitude zonal wave pattern is likely the primary large-scale pattern that leads to high flow events (i.e. the pattern can occur independent of ENSO), while La Niña would help to place the high-pressure to the east thus likely playing a complimentary role. Similarly, there is no consistent SAM pattern in Fig. 5.2 for all UNI catchments. Figures 5.4b and 5.4d show that high flow events in the Waitangi and Otara catchments occur 50% of the time during a negative and positive SAM respectively, while the Waioeka catchment shows a slight preference to negative SAM or SAM neutral conditions (Fig. 5.4f). Again, the asymmetric zonal wave 4 seen in all catchments indicates an amplified mid-latitude wave train (rather than a zonally symmetric SAM pattern) is key to setting up the conditions that lead to high flow events in the UNI.

Lastly, one potentially important feature is that locally warm SST anomalies to the north of NZ are seen for all three catchments (Fig. 5.3). Figure 5.3 shows that the warm SST temperature anomalies generally correspond to the region where the poleward stream of moisture is located to the north of NZ (Figs. 5.1b,d,f and Figs. 5.3a,c,d). For the Waitangi catchment, cold SST anomalies dominate the eastern regions of the UNI except for the very top of the North Island where the Waitangi catchment is located in Fig. 5.3a. This area of warm SST anomalies, though small, corresponds to strong moisture transport from the tropics that is seen intercepting the catchment in Fig. 5.1a. A much larger area of warm SST anomalies is seen dominating NZ in Fig. 5.3c for the Otara catchment and corresponds to a much deeper and longer moisture stream in Fig. 5.1d, following similar characteristics to the Waitangi moisture and SST anomalies. In contrast, the Waioeka catchment is surrounded by much stronger and warmer SST anomalies seen in Fig. 5.3e, so it would be expected the moisture transported poleward would be similar to that seen in Figs. 5.1b and d, however, moisture is instead weaker, much wider, and covers the entire North Island and much of the surrounding ocean (Fig. 5.1f). These local positive SST anomalies for all UNI catchments would aid in

enhancing local atmospheric moisture thus increasing the chances for heavier rainfall that could cause high flow events. Both Otara and Waioeka show these warm SSTs were likely part of the broader La Niña SST pattern, and this suggests that this may be another supporting role of La Niña.

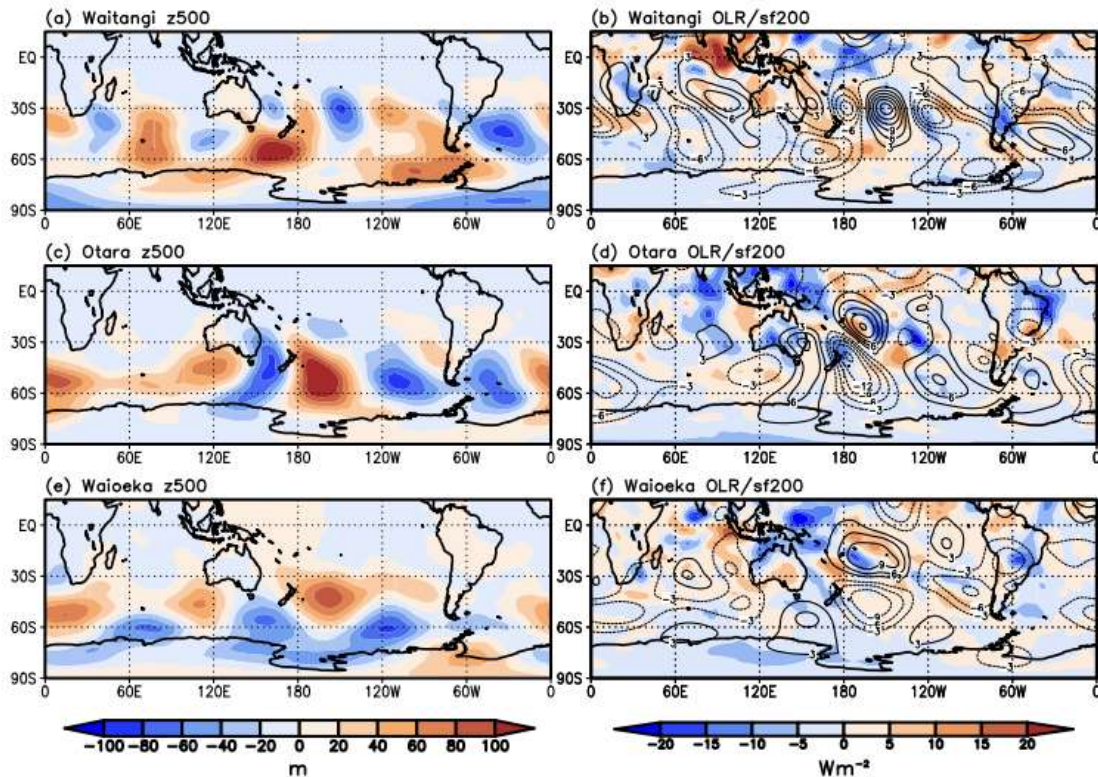


Figure 5.2: Large-scale Southern Hemispheric circulation features occurring during high flow events in the UNI catchments. The left column shows 500 hPa geopotential height (z500) anomalies (shaded) for the (a) Waitangi, (c) Otara, and (e) Waioeka catchments. The right column shows outgoing longwave radiation (OLR) anomalies (shaded) and 200 hPa streamfunction (sf200) anomalies for the (b) Waitangi, (d) Otara, and (f) Waioeka catchments.

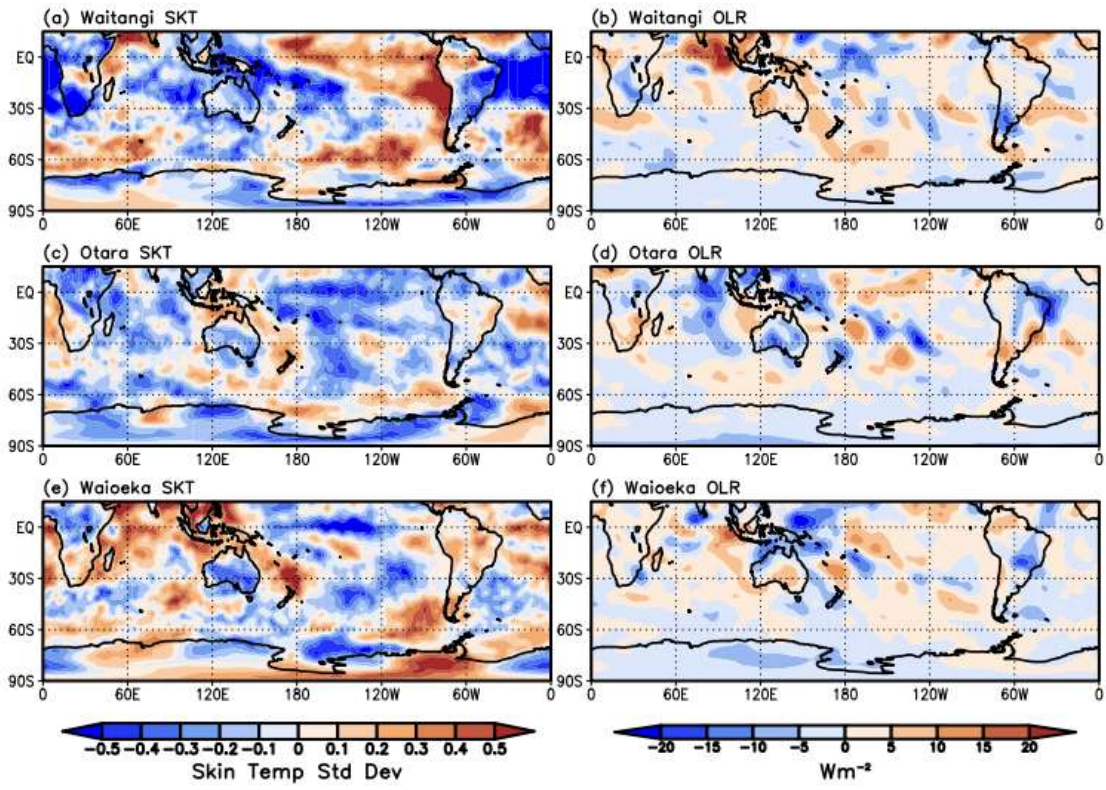


Figure 5.3: Large-scale Southern Hemispheric variability occurring during high flow events in the UNI catchments. The left column shows skin temperature (SKT/SST) anomalies (shaded) for the (a) Waitangi, (c) Otara, and (e) Waioeka catchments. The right column shows outgoing longwave radiation (OLR) anomalies (shaded) for the (b) Waitangi, (d) Otara, and (f) Waioeka catchments.

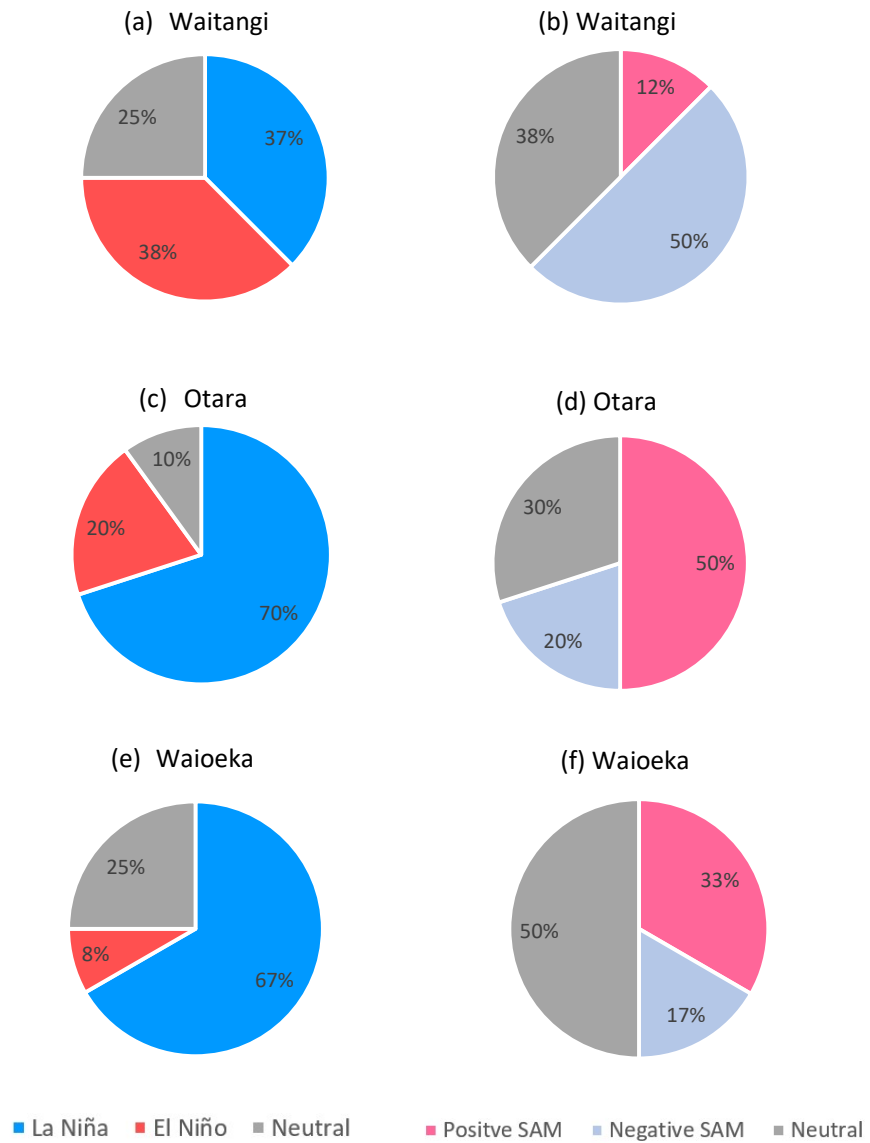


Figure 5.4: Pie charts showing the percentage of ENSO and SAM phases for the high flow events in the UNI catchments used for compositing based on the monthly-mean phases of ENSO (left column) and SAM (right column). (a-b) Waitangi, (c-d) Otara, and (e-f) Waioeka catchments.

5.2 East Coast North Island

Focusing on the Te Arai River catchment in the ECNI, the local synoptic situation (Fig. 5.5e), which is broadly similar for all four ECNI catchments shown in Fig. 5.5 (as well as the Waiapu and Waihora not shown), indicates high flow events in the Te Arai catchment occurred when there was a deep low-pressure over the northern half of the North Island centred along the east coast of Northland combined with a high-pressure system to the south/southeast of

the South Island, taking the formation of the Kidson 'NE' (Blocking) synoptic type (Kidson, 2000). The MSLP variance in Fig. 5.5e clearly shows that for all four catchments the low-pressure system tracked/deepened southeastward along the Bay of Plenty where the largest change in pressure occurred. All four catchments also show a warm front/surface convergence zone present orientated east-west across central NZ (Figs. 5.5 right column). The only differences across the catchments are the precise location and overall extent of the high-pressure to the south of the country. Regardless, the high-pressure system to the south/southeast of the low-pressure system tracking southeastward from Northland to the Bay of Plenty is clearly a prominent feature seen for all ECNI catchments (Fig. 5.5).

In all ECNI catchments, strong poleward transport of moisture out of the tropics through northeasterly winds (compared to northerly winds for the UNI) within the warm sector of the cyclone is seen (Fig. 5.5). Figure 5.5 shows this stream of moisture is located northeast of the East Coast with local easterly winds intercepting each catchment guided along the northern edge of the high-pressure to the south. Similar to the UNI, the coupling of the low and high-pressure system in Fig. 5.5 plays a key role in drawing the moisture down from the tropics and steering it along a path that intercepts the coast at a near perpendicular angle that would enhance low level convergence and promote heavy precipitation.

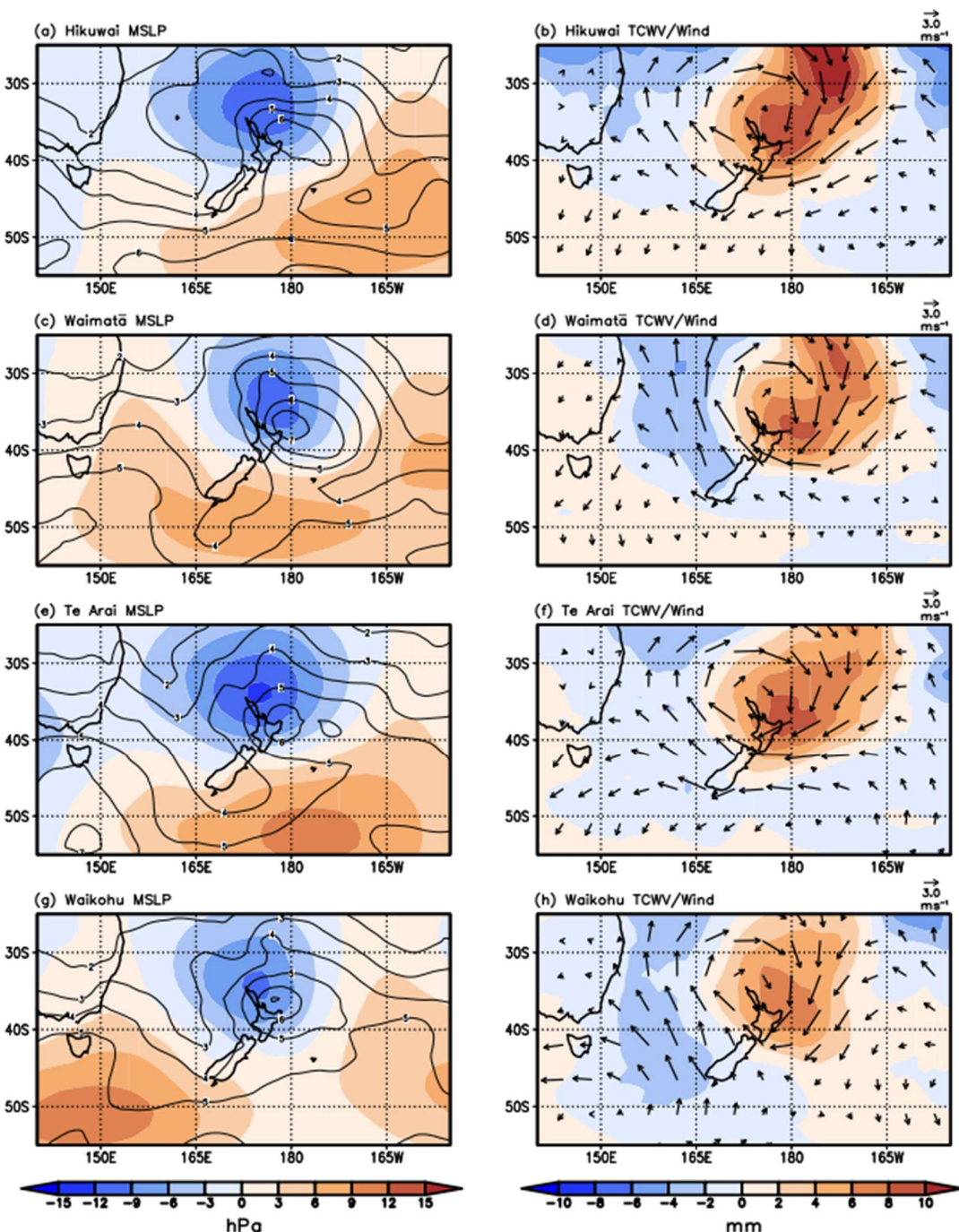


Figure 5.5: Local circulation features that occurred during high flow events in the ECNI catchments. The left column shows composite anomalies of mean sea level pressure (MSLP) (shaded) and MSLP variance (contours) for (a) Hikuwai, (c) Waimatā, (e) Te Arai, and (g) Waikohu catchments. The right column shows composites of total column water vapour (TCWV) anomalies (shaded) and wind (vectors) for (b) Hikuwai, (d) Waimatā, (f) Te Arai, and (h) Waikohu catchments.

The large-scale circulation patterns (Fig. 5.6) are slightly more zonally symmetrical than the UNI, particularly over the south Pacific region, with low-pressure anomalies over Antarctica and high-pressure anomalies in mid-latitudes resembling the positive phase of the SAM. Additionally, embedded within this pattern is a northwest-southeast oriented wave train extending from the southwest tropical Pacific across NZ southeastward to Antarctica, resembling a La Niña-forced pattern which can also be clearly seen in the sf200 and SST anomalies (Figs. 5.6f and 5.7). Indeed, La Niña conditions are preferred for Waimatā, Te Arai, and Waikohu (Figs. 5.8c, e, and f, respectively). Waimatā also shows a strong preference for positive SAM (Fig. 5.8d), while the SAM preference is more varied for the other three catchments. This suggests La Niña and a northwest-southeast oriented wave train across NZ may be the main large-scale pattern that results in these local synoptic conditions. However, looking more closely at the SST and convective anomalies (Fig. 5.7), the most pronounced feature is enhanced convection to the north of NZ in the South Pacific Convergence Zone (SPCZ) rather than a robust La Niña signal (i.e., the highly variable tropical Pacific SSTs). Thus, this convection may be an important mechanism triggering the wave train, while La Niña, being a lower-frequency pattern (i.e. timescale of months), may provide favourable background conditions for enhanced convection in the poleward edge of the SPCZ as has been shown in previous studies (Clem et al. 2019).

Unlike the UNI catchments, Fig. 5.7 shows generally cold SST anomalies around the North Island of NZ for the Hikuwai, Te Arai and Waikohu catchments, suggesting local SST may not play a determining role in producing high moisture content for these catchments. The exception is the Waimatā catchment (Fig. 5.7c) where the northeasterly stream of moisture is seen in Fig. 5.5d. Therefore, a moist northeasterly flow between high-pressure to the southeast of NZ and an approaching low from the northwest, favoured during La Niña and potentially triggered by deep convection in the SPCZ, appears key to ECNI high flow events.

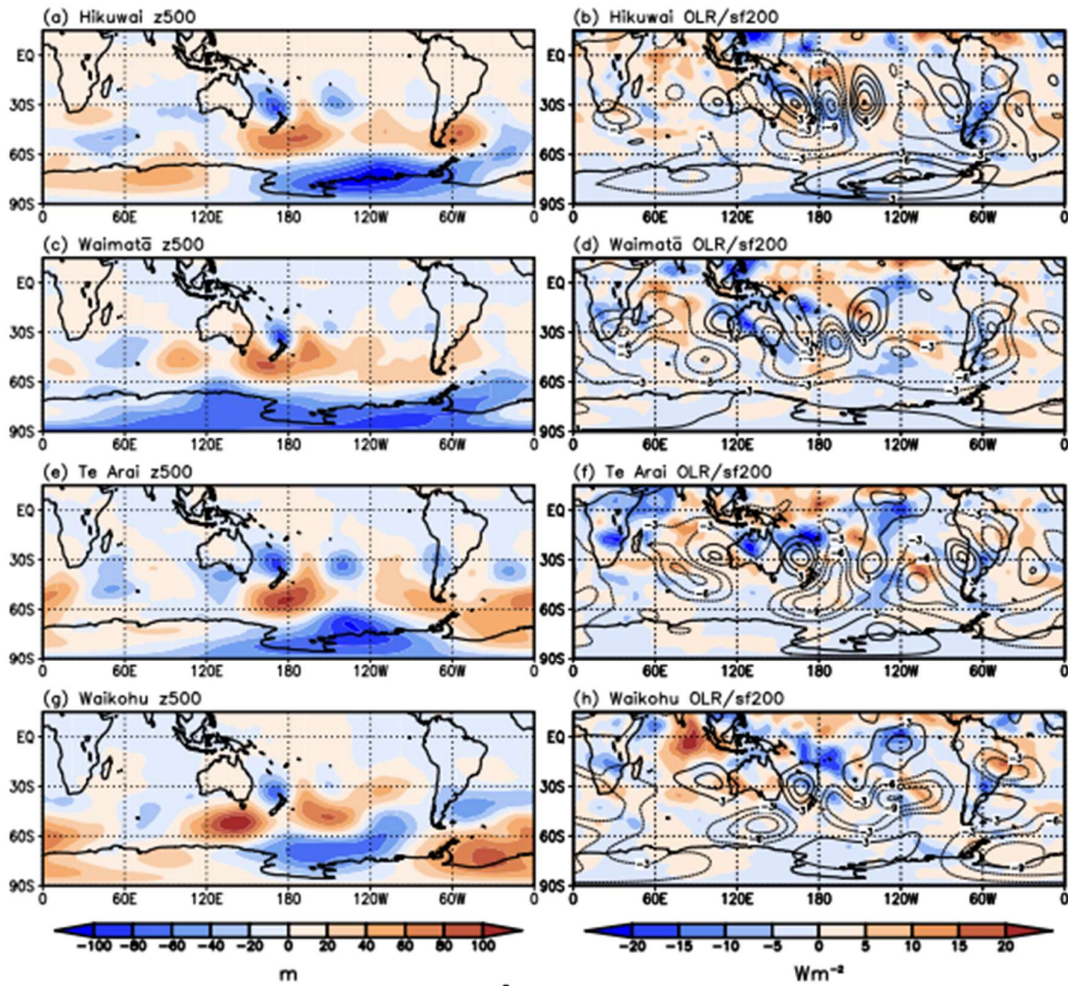


Figure 5.6: Large-scale Southern Hemispheric circulation features occurring during high flow events in the ECNI catchments. The left column shows 500 hPa geopotential heights (z500) anomalies (shaded) for (a) Hikuwai, (c) Waimatā, (e) Te Arai, and (g) Waikohu catchments. The right column shows outgoing longwave radiation (OLR) anomalies (shaded) and 200 hPa streamfunction (sf200) anomalies for the (b) Hikuwai, (d) Waimatā, (f) Te Arai, and (h) Waikohu catchments.

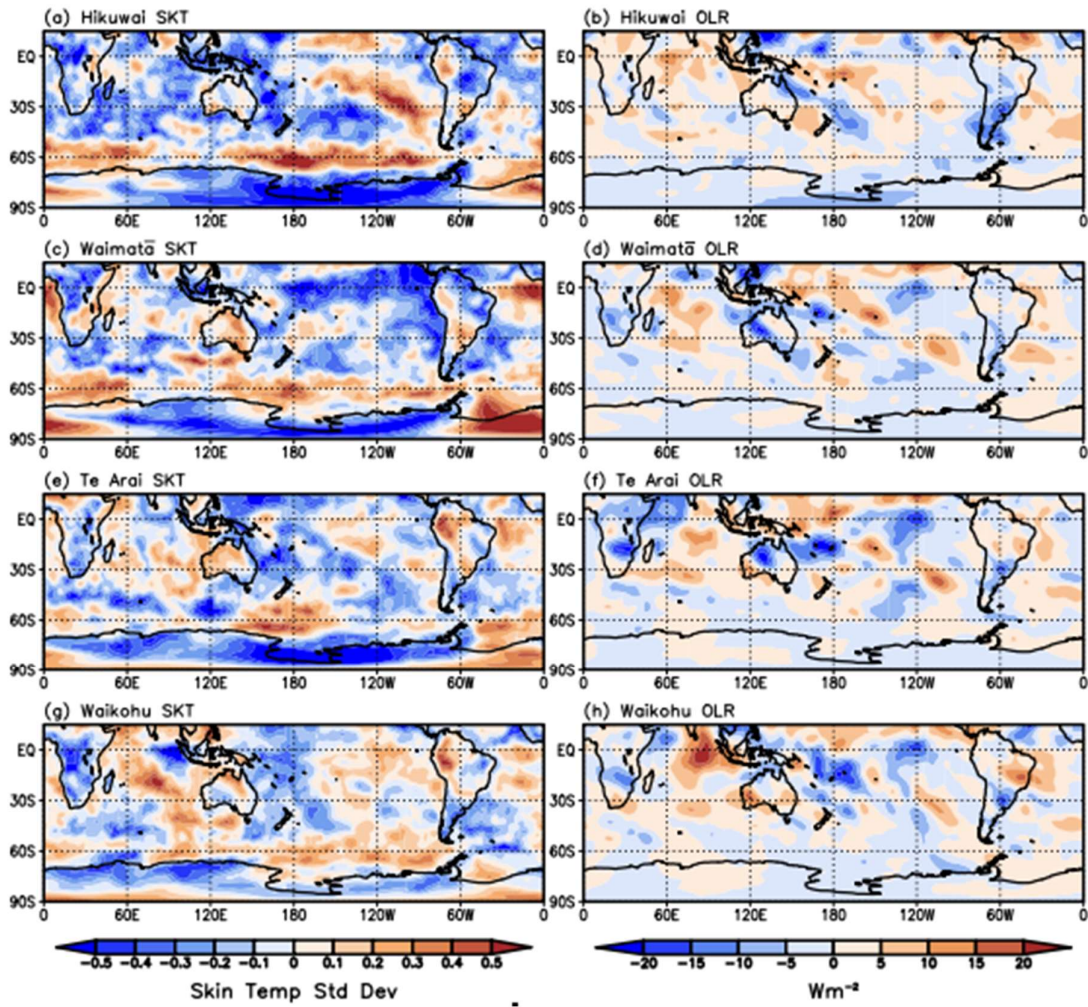


Figure 5.7: Large-scale Southern Hemispheric variability occurring during high flow events in the ECNI catchments. The left column shows skin temperature (SKT/SST) anomalies (shaded) for the (a) Hikuwai, (c) Waimatā, (e) Te Arai, and (g) Waikohu catchments. The right column shows OLR (shaded) anomalies for the (b) Hikuwai, (d) Waimatā, (f) Te Arai, and (h) Waikohu catchments.

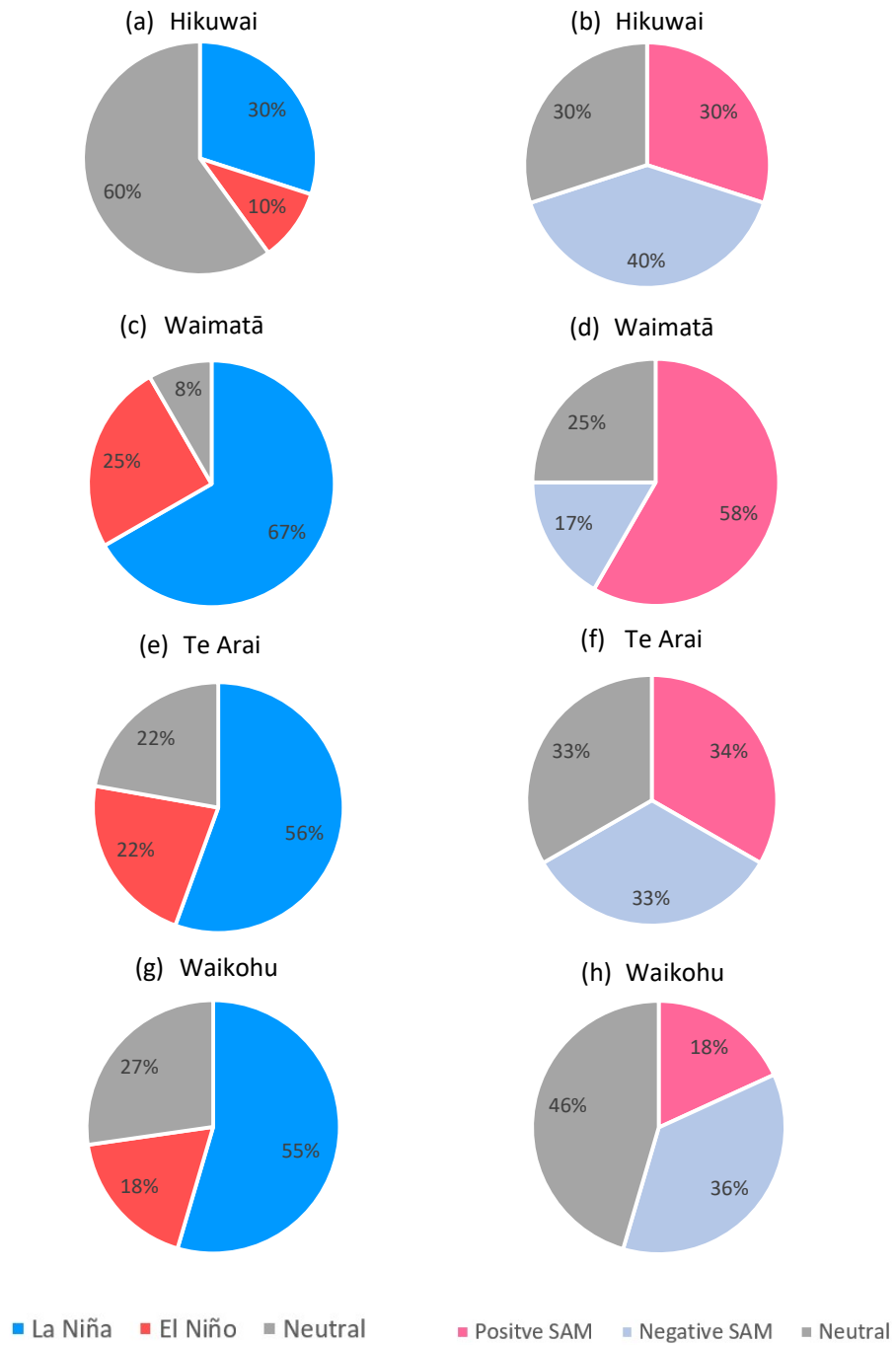


Figure 5.8: Pie charts showing the percentage of ENSO and SAM phases for the high flow events in the ECNI catchments used for compositing based on the monthly-mean phase of ENSO (left column) and SAM (right column). (a-b) Hikuwai, (c-d) Waimatā, (e-f) Te Arai, and (g-h) Waikohu catchments.

5.3 Lower North Island

Shifting south to the LNI in the Wairarapa region, and in sharp contrast to the UNI and ECNI, the local synoptic situation in Fig. 5.9e shows high flow events in the Waiōhine catchment occurred when there was a deep and broad low-pressure system to the south of NZ combined with a broad high-pressure anomaly to the northeast of the North Island, taking the formation of the Kidson ‘W’ (Zonal) synoptic type (Kidson, 2000; Pohl et al. 2022). The MSLP variance in Fig. 5.9e suggests the high to the northeast remained relatively persistent while the low significantly deepened/moved southeast off the east coast of the South Island. Figure 5.9f shows a clear northwest-southeast oriented cold front located across central NZ centred over Cook Strait. The cold front was located at the boundary between the low and high-pressure in a northwest-southeast orientation in the broad warm sector of the cyclone and moved northeast intercepting the Waiōhine catchment. Similar patterns and progression of the high- and low-pressure occur in the Waipoua (Fig. 5.9a) and Waingawa (Fig. 5.9c) catchments, however, the centre of the low-pressure system is east of the South Island for the Waipoua and further south for the Waingawa compared to the Waiōhine.

In the Ruamāhangā catchment, in Fig. 5.9g, high flow events occurred when there was a low-pressure system centred over the middle of NZ taking the formation of a Kidson ‘T’ synoptic type (Kidson, 2000). It is unclear from the MSLP variance in Fig. 5.9g how exactly this system propagated/developed, but the largest change in pressure occurred over the South Island.

The LNI catchments in this study are all located on the leeward side of the Tararua Ranges and are generally dry in westerly flow due to the orographic mechanisms of the ranges (Chappell, 2017). Therefore, it was expected that moisture would be transported through easterly winds, as seen in the ECNI catchments. However, as shown in Fig. 5.9, for three of the four catchments (Waipoua, Waingawa and Waiōhine catchments; Figs. 5.9b,d,f) moisture is being transported through northwesterly flow along the cold front to the south of the LNI. Unlike the northerly origin of moisture in the UNI (Fig. 5.1 right column) and ECNI (Fig. 5.5 right column), moisture is being transported from the west and northwest from the Tasman Sea towards the three catchments and ahead of the cold front (Fig. 5.9, right column). Thus, cold-frontal precipitation is likely the key feature leading to high flow events in the three

LNI/Wairarapa catchments. It is also likely the ‘W’ Zonal positioning of the low- and high-pressure and primarily westerly flow from the Tasman Sea with a northerly component is crucial for driving moisture into the LNI catchments. In sharp contrast, during flood events in the Ruamāhangā catchment, where a low-pressure is centred over NZ (Fig. 5.9g), winds are weaker and more easterly, resembling a warm front draped across the LNI (Fig. 5.9h), and the moisture transport originates from the east. The southeasterly flow would intercept the Tararua Ranges leading to orographically-enhanced rainfall in the Ruamāhangā catchment, which would be further intensified by the warm front.

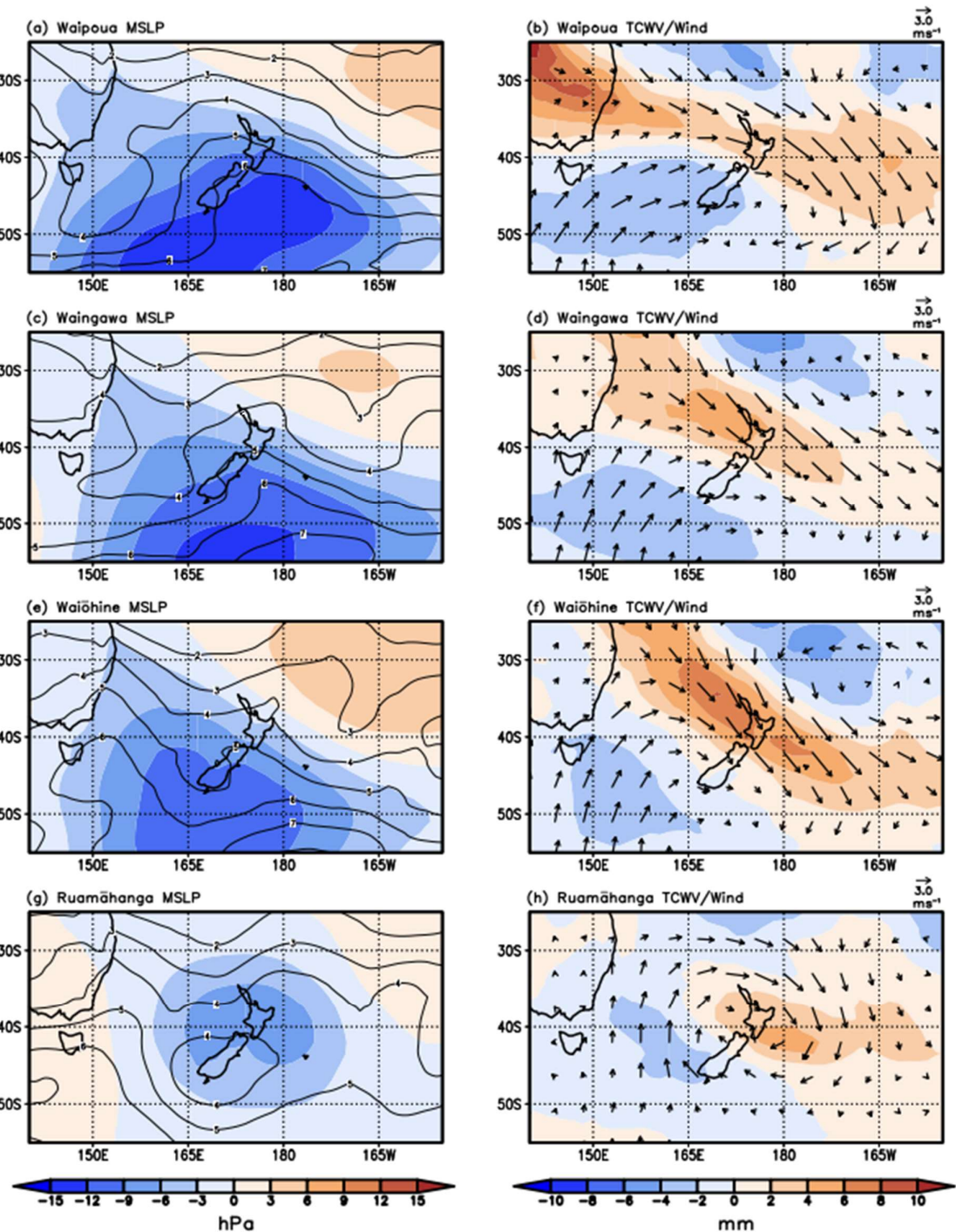


Figure 5.9: Local circulation features that occurred during high flow events in the LNI catchments. The left column shows composite anomalies of mean sea level pressure (MSLP) (shaded) and MSLP variance (contours) for (a) Waipoua, (c) Waingawa, (e) Waiōhine, and (g) Ruamāhanga catchments. The right column shows composites of total column water vapour (TCWV) anomalies (shaded) and wind (vectors) for (b) Waipoua, (d) Waingawa, (f) Waiōhine, and (h) Ruamāhanga catchments.

There appears to be a southeastward-oriented wave train that originates in the western tropical Pacific (Fig. 5.10a-f) with La Niña-like SST and OLR anomalies (Fig. 5.11a-f) showing suppressed convection across the central tropical Pacific and enhanced convection in the western tropical Pacific. During a La Niña, higher than normal pressure commonly occurs to the east and northeast of NZ (Ummenhofer & England, 2007) which is also seen occurring in Fig. 5.9 (right column). Indeed, Fig. 12 shows most events occur during a La Niña phase, especially for the Waipoua (89%; Fig. 12a) and Waingawa catchments (67%; Fig. 5.12c). The large-scale circulation patterns shown in Fig. 5.10 are nearly the opposite of the zonally symmetric pattern seen across the ECNI (Fig. 5.7). For Waipoua, Waingawa and Waiōhine catchments (Figs. 5.10a,c,e), high-pressure anomalies over Antarctica generally resemble a negative phase of the SAM, however there is no clear symmetrical pressure anomaly in middle latitudes as seen in Fig. 5.10 (left column), and indeed there is no preference for any phase of the SAM (Fig. 5.12) implying a specific SAM phase does not have a determining role in producing floods for these catchments.

Furthermore, for the Waipoua, Waingawa, and Waiōhine catchments, where northwesterly flow from the Tasman Sea is key, positive SST anomalies across the Tasman Sea also appear to play a contributing role in the anomalously high moisture content (Figs. 5.9b,d,f and Figs. 5.11a,c,f). The positive SST anomalies correspond to the moisture transport pathway, as was also seen for the UNI. A similar but weaker SST pattern is seen for the Ruamāhangā catchment (Fig. 5.12g), suggesting a similar broad pattern, but they do not correspond to the immediate moisture flow from the southeast seen in Fig. 5.9h. However, it is possible the moisture being transported to the Ruamāhangā catchment originated from the Tasman Sea and was then later transported to the catchment on the southeasterly flow.

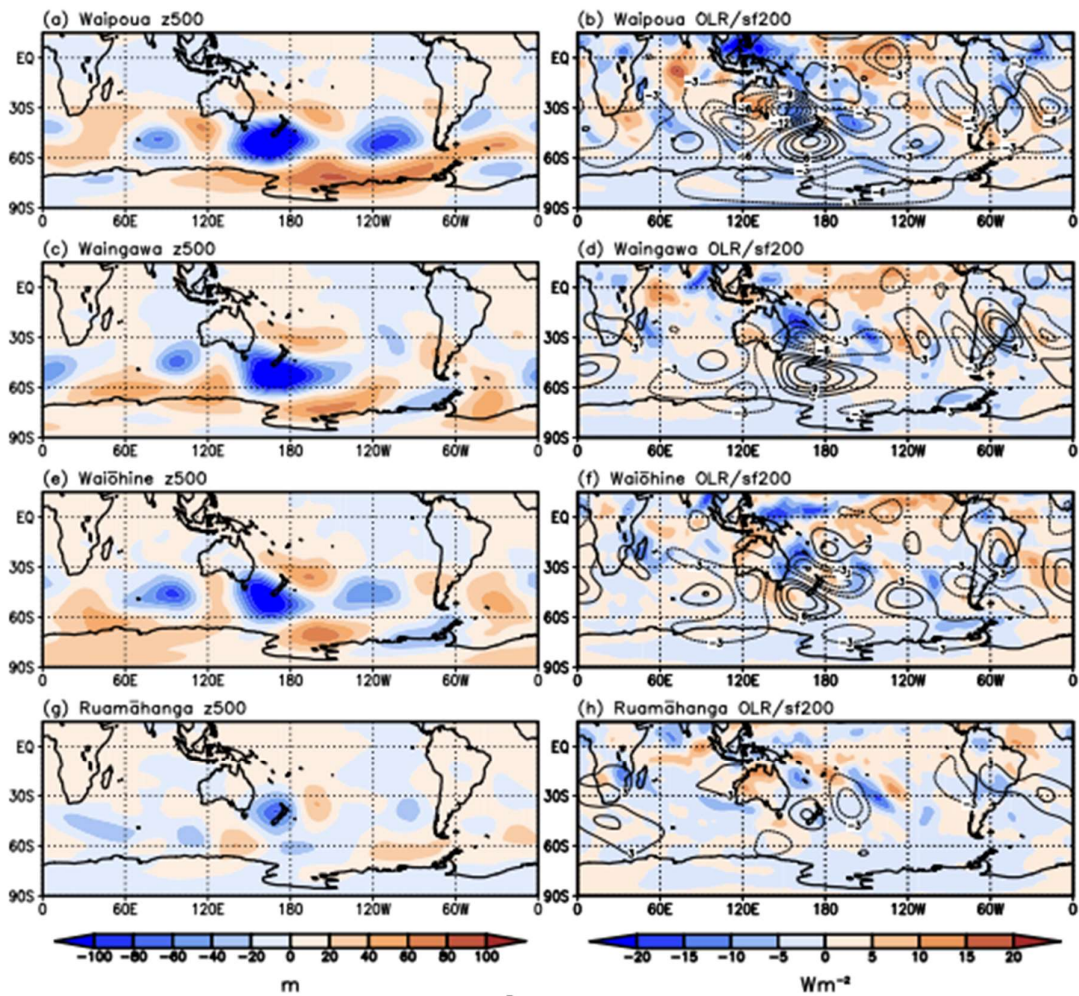


Figure 5.10: Large-scale Southern Hemispheric circulation features occurring during high flow events in the LNI catchments. The left column shows 500 hPa geopotential heights (z500) anomalies (shaded) for (a) Waipoua, (c) Waingawa, (e) Waiōhine, and (g) Ruamāhanga catchments. The right column shows outgoing longwave radiation (OLR) anomalies (shaded) and sf200 anomalies for the (b) Waipoua, (d) Waingawa, (f) Waiōhine, and (h) Ruamāhanga catchments.

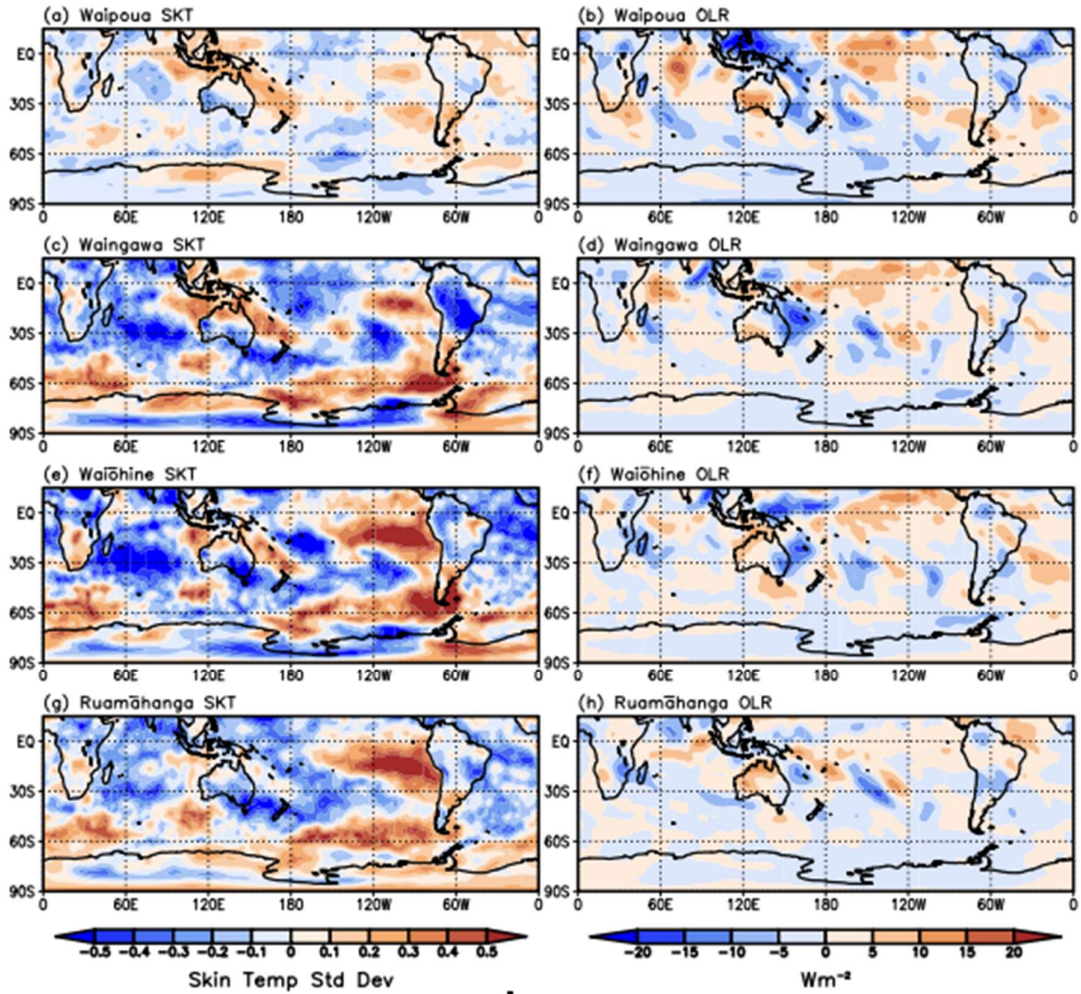


Figure 5.11: Large-scale Southern Hemispheric variability occurring during high flow events in the LNI catchments. The left column shows skin temperature (SKT/SST) anomalies (shaded) for the (a) Waipoua, (c) Waingawa, (e) Waiōhine, and (g) Ruamāhangā catchments. The right column shows OLR (shaded) anomalies for the (b) Waipoua, (d) Waingawa, (f) Waiōhine, and (h) Ruamāhangā catchments.

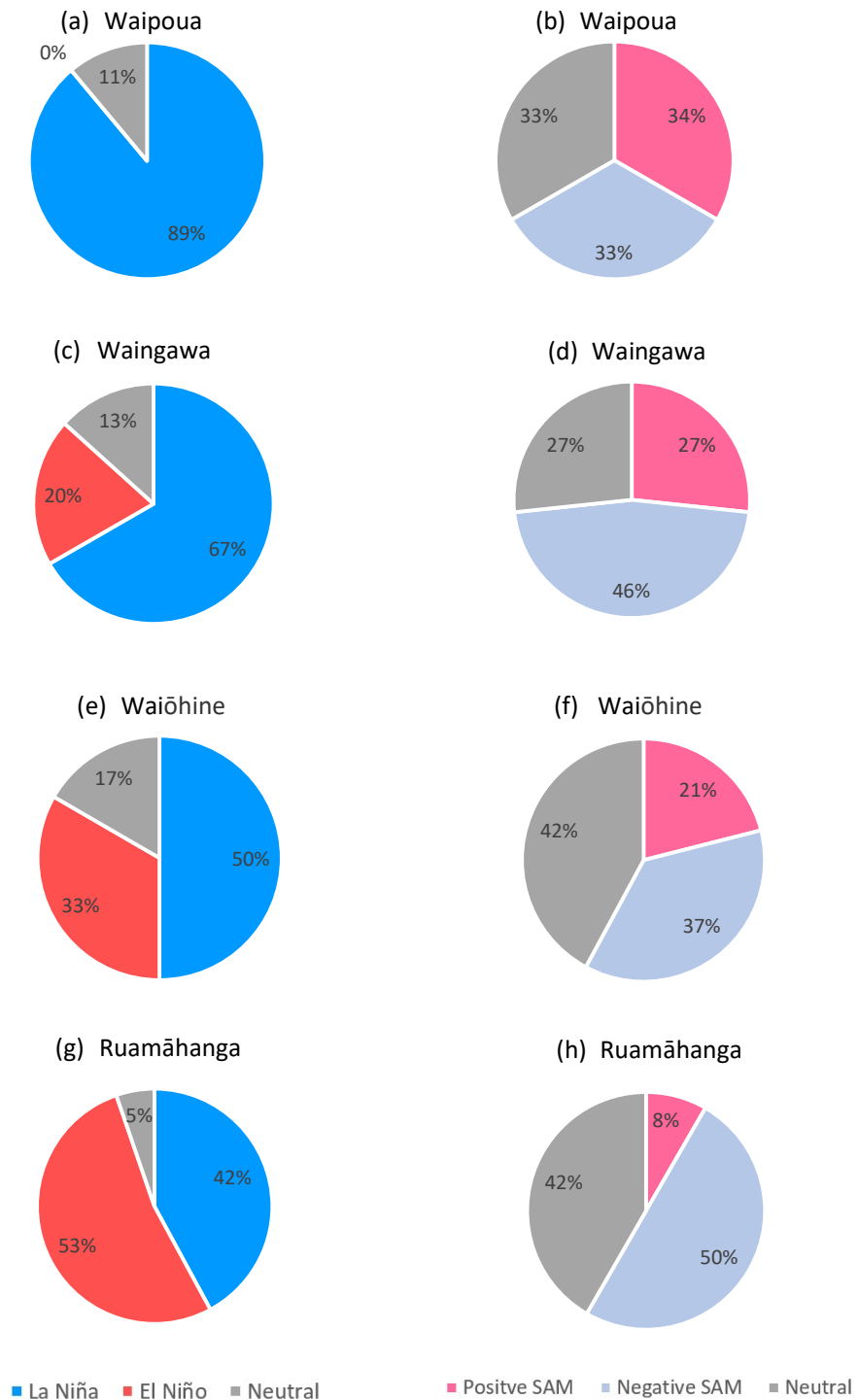


Figure 5.12: Pie charts showing the percentage of ENSO and SAM phases for the high flow events in the LNI catchments used for compositing based on the monthly-mean phase of ENSO (left column) and SAM (right column). (a-b) Waipoua, (c-d) Waingawa, (e-f) Waiōhine, and (g-h) Ruamāhangā catchments.

5.4 South Island

The local synoptic situation in eastern regions of the SI is shown in Fig. 5.13. The Wairau is located in the northeast South Island in the Marlborough region, while the Hurunui, Selwyn, and Maerewhenua catchments are located in the Canterbury region of the east-central portion of the South Island. Starting with the Canterbury catchments, Figs. 5.13c,e,g indicates that historical high flow events were very similar for the three catchments and occurred with a deep low-pressure system over NZ combined with a high-pressure system to the south, taking the formation of the Kidson ‘HE’ and ‘R’ (Blocking) synoptic types (Kidson, 2000). The MSLP variance in Figs. 5.13c,e,g suggests a southeastward moving low with the largest variance occurring to the southeast of the low-pressure centre. Interestingly, similar locations and southeastward propagation of the low-pressure are seen in the ECNI catchments (Figs. 5.5 left column), except for these Canterbury catchments where the high-pressure is located to the south of NZ rather than the northeast. Together, these produce moist easterly flow into the Canterbury region (Figs. 5.13d,f,h). In contrast, the other South Island catchment, the Wairau, has a similar positioning and movement of the low, but Fig. 5.13a shows the high-pressure is located to the east of NZ and produces moist northerly flow to this catchment, resembling the ‘TNW’ and ‘HE’ Kidson synoptic types (Fig. 5.13b). Also of potential importance, MSLP variance for Wairau (Fig. 5.13a) shows the lowest variance occurred over the northern edge of the high-pressure system, which would again suggest the northern portion of the high remained stationary while the high also developed/built southward ahead of the approaching low allowing for a persistent moisture source rooted in lower tropical latitudes.

For the Wairau catchment farther north (Figs. 5.13a-b), strong poleward moisture transport occurs through due north winds out of the deep tropics which intercept the Marlborough region (Fig. 5.13b). The other three Canterbury catchments also source moisture out of the tropics ahead of the low, but this pathway is farther east toward 180° longitude, and with locally higher moisture anomalies off the east coast of the South Island (Figs. 5.13d,f,h). Altogether, high flow events in the Wairau catchments are comprised of a moist north/northwesterly flow similar to that in many of the other NZ catchments already discussed, while for Canterbury the circulation anomalies reveal a reversal of the average

westerly flow over the South Island (as discussed in Section 2.3.1) which would also allow for orographically-enhanced precipitation on the eastern side of the Southern Alps.

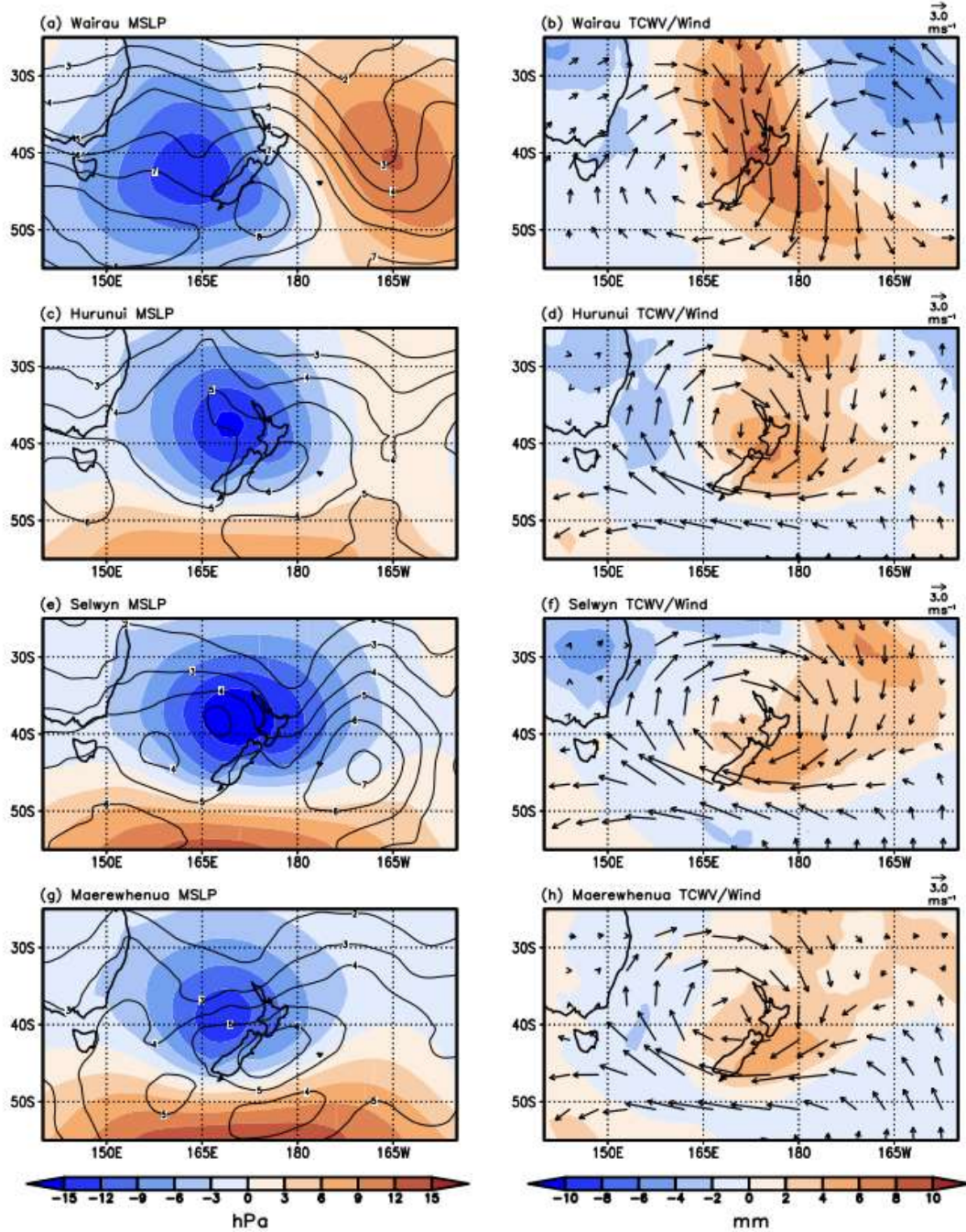


Figure 5.13: Local circulation features that occurred during high flow events in the SI catchments. The left column shows composite anomalies of mean sea level pressure (MSLP) (shaded) and MSLP variance (contours) for (a) Wairau, (c) Hurunui, (e) Selwyn, and (g) Maerewhenua catchments. The right column shows composite of total column water vapour (TCWV) anomalies (shaded) and wind (vectors) for (b) Wairau, (d) Hurunui, (f) Selwyn, and (h) Maerewhenua catchments.

The large-scale circulation patterns (Figs. 5.14c,e,g) for the Canterbury catchments show the presence of a zonally-orientated wave train in middle latitudes resembling a zonal wave 4 pattern (four high-low-pressure pairs) and with no clear symmetrical SAM pattern. In contrast, the Wairau catchment (Figs. 5.14a-b) resembles a positive SAM pattern with low-pressure anomalies over Antarctica, but more relevant to the local NZ circulation anomalies is a wave packet extending eastward from the Indian Ocean into the Tasman Sea and northeastward across NZ seen in Fig. 5.14b. The OLR and sf200 anomalies (Fig. 5.14b) show enhanced convection over the tropical Indian Ocean, suggesting this circulation pattern may be comprised of a wave train propagating along a great circle path southeastward over the Indian Ocean and northeastward across NZ. As for the SST anomalies (Fig. 5.15 left column), all catchments show an El Niño-like pattern, with positive SST anomalies in the central and eastern tropical Pacific and negative SST anomalies in the western tropical Pacific. However, there is no clear ENSO-like convection pattern, and there is no preference for flooding during El Niño events for any catchments (Fig. 5.16) indicating this connection is not clear. On the other hand, Fig. 5.16b shows the Wairau catchment has a preference for positive SAM conditions, which is consistent with the negative pressure anomalies over Antarctica (Fig. 5.14a). Thus, the wave propagation out of the Indian Ocean may be further promoted by positive SAM conditions, while high flow events in the Canterbury catchments appears to occur with an amplified mid-latitude wave number 4 pattern and high to the south which produces the easterly flow into the region. The lack of a clear/consistent ENSO pattern in these catchments suggests that these conditions may act as complimentary drivers in high flow events, especially for the Wairau catchment.

With regards to moisture enhancement from local SST anomalies around NZ, for Wairau there are locally positive SST anomalies to the north of the North Island corresponding to the area of moisture transport (Figs. 5.13b and 5.15a). For the Canterbury catchments in Figs. 5.15c,e,g, there are positive SST anomalies to the southeast of NZ that slightly correspond to the easterly moisture transport, especially for the Selwyn catchment (Fig. 5.15e), but overall negative SST anomalies are seen around most of NZ, which may just reflect the broader El Niño-like SST pattern over the Pacific. Thus, making it unclear whether they play a determining role in the occurrence of high flow events.

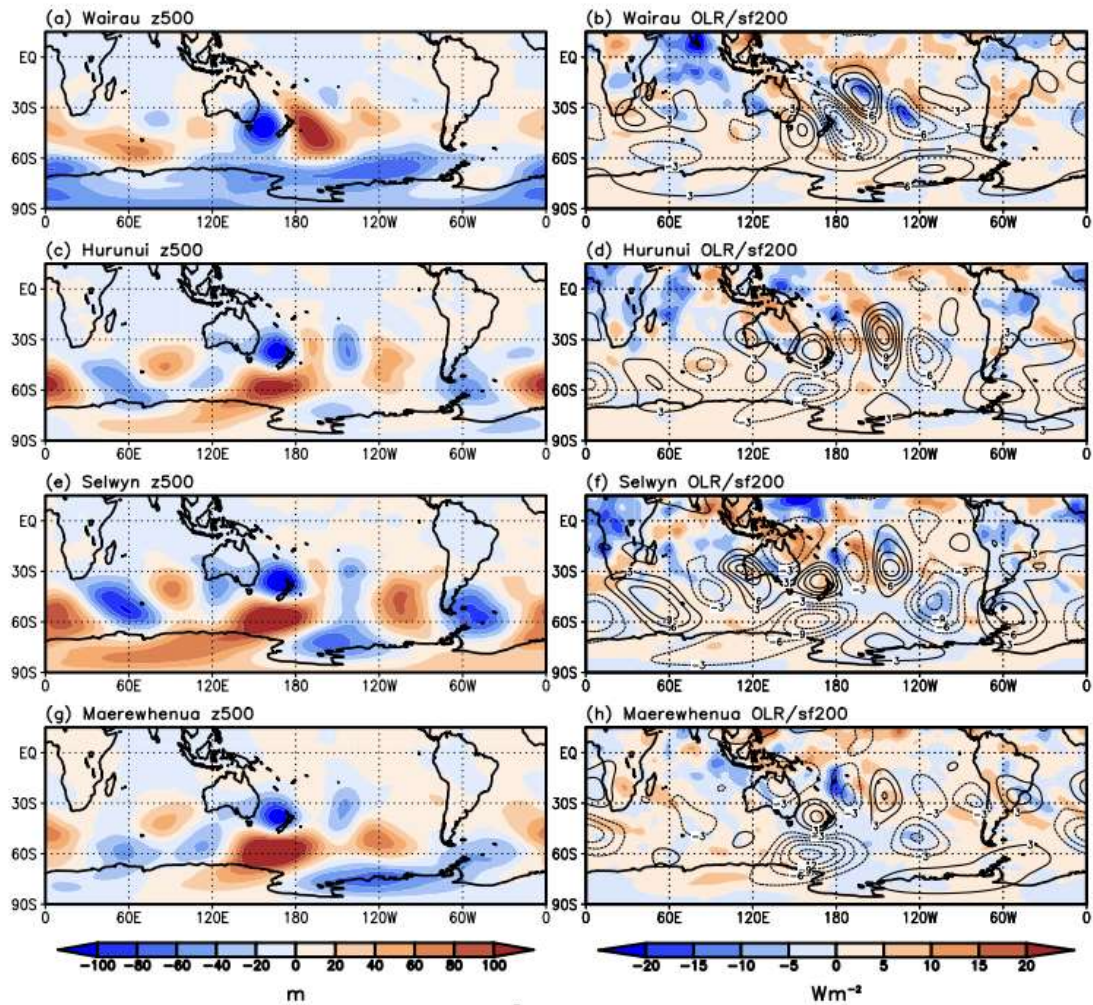


Figure 5.14: Large-scale Southern Hemispheric circulation features occurring during high flow events in the SI catchments. The left column shows 500 hPa geopotential heights (z500) anomalies (shaded) for the (a) Wairau, (c) Hurunui, (e) Selwyn, and (g) Maerewhenua catchments. The right column shows outgoing longwave radiation (OLR) anomalies (shaded) and sf200 anomalies for the (b) Wairau, (d) Hurunui, (f) Selwyn, and (h) Maerewhenua catchments.

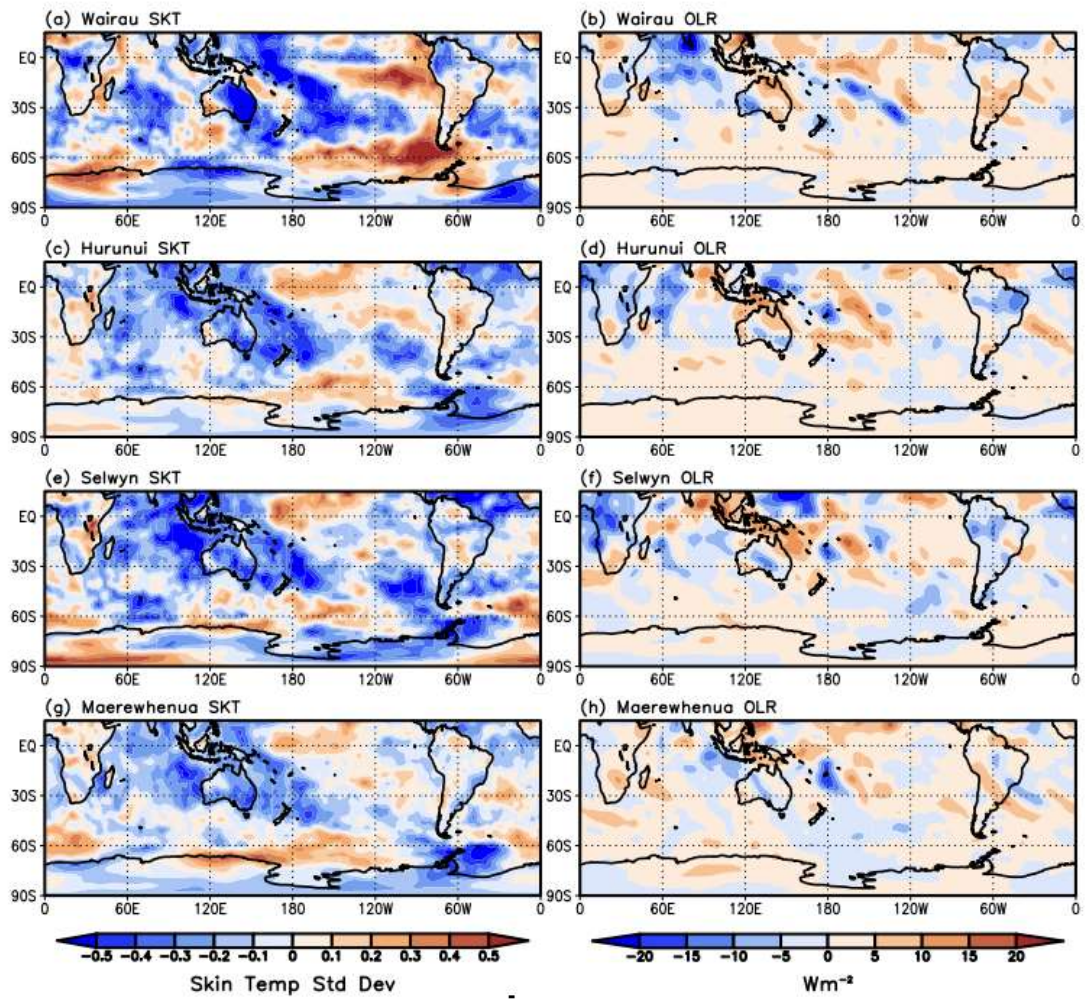


Figure 5.15: Large-scale Southern Hemispheric variability occurring during high flow events in the SI catchments. The left column shows skin temperature (SKT/SST) anomalies (shaded) for the ((a) Wairau, (c) Hurunui, (e) Selwyn, and (g) Maerewhenua catchments. The right column shows outgoing longwave radiation (OLR) anomalies (shaded) for the (b) Wairau, (d) Hurunui, (f) Selwyn, and (h) Maerewhenua catchments.

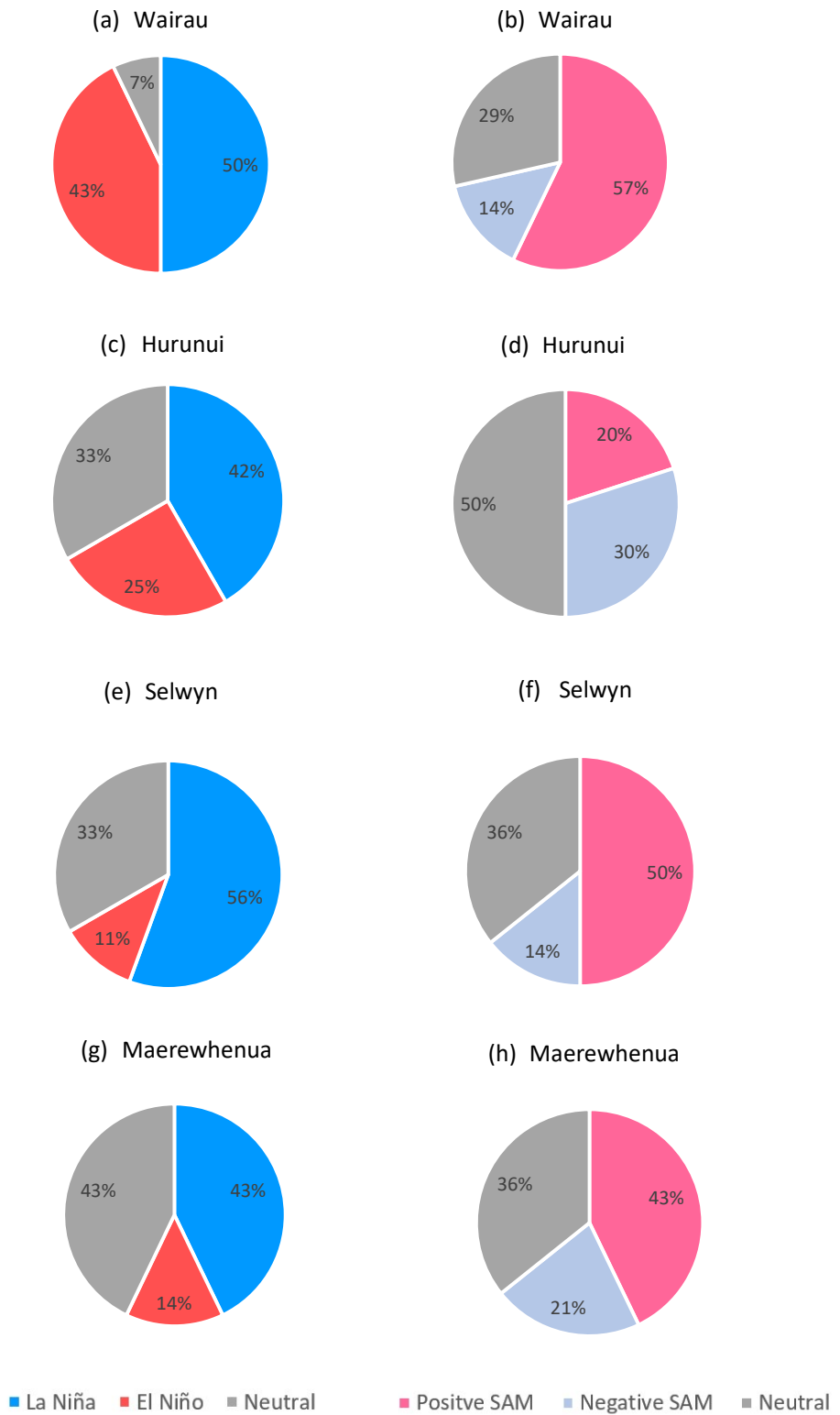


Figure 5.16: Pie charts showing the percentage of ENSO and SAM phases for the high flow events in the SI catchments used for compositing based on the monthly-mean phase of ENSO (left column) and SAM (right column). (a-b) Wairau, (c-d) Hurunui, (e-f) Selwyn, and (g-h) Maerewhenua catchments.

5.5 Seasonality

Turning to the seasonality of the high flow events (Fig. 5.17), there is a preference for flow events above the 1-in-5-year threshold to occur in winter for the SI (51%; Fig. 5.17). Figure 5.17 also shows high flow events in the UNI commonly occurred in winter (43%), however the percentage difference between the other seasons is minimal suggesting a weak seasonal preference. For the LNI catchments there is a strong preference for spring (44%) and summer (29%; Fig. 5.17). The ECNI catchments have no clear seasonal preference, with the identified flood events occurring ~30% of the time in spring, autumn, and winter, and are therefore vulnerable to flooding all year round. The specific season each high flow event occurred during is shown in Table A of the Appendix.

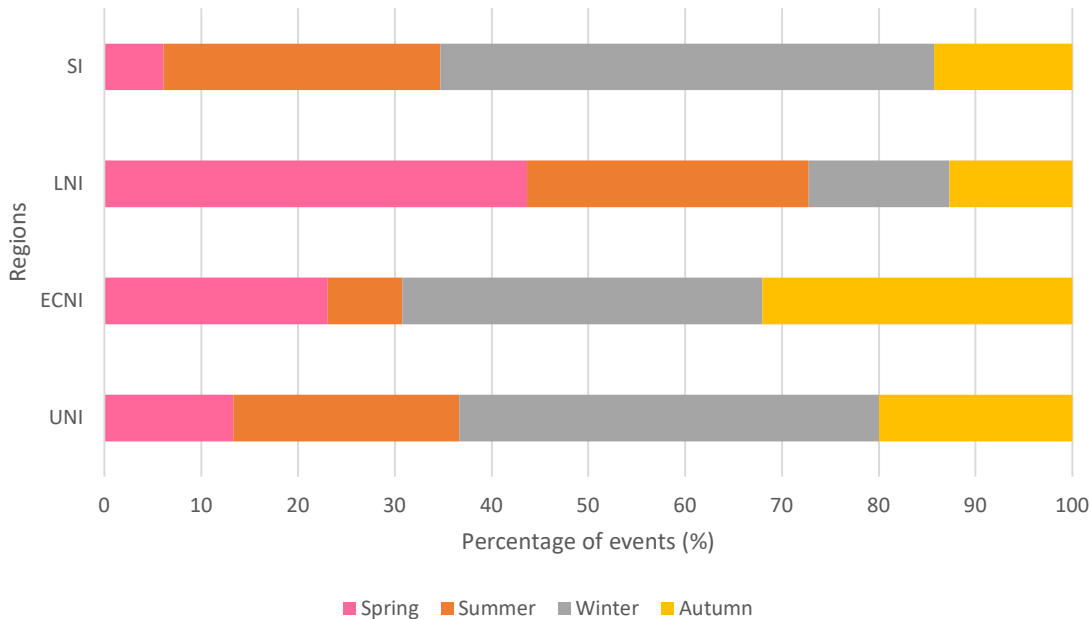


Figure 5.17: Percentage bar chart showing the percentage of high flow events (identified to equal or exceed a catchment-specific 1-in-5-year threshold) that occurred in spring, summer, winter, and autumn.

6. Discussion and Conclusion

This thesis has advanced knowledge on high impact hydrological and meteorological hazards in eastern regions of NZ. This final chapter summarises the key findings and implications, how these fit into the current state of knowledge, and suggestions for future work.

6.1 Flood Frequency Analysis

FFA was carried out in 17 catchments in four of NZ's eastern regions to understand high flow events in these catchments, and to develop catchment-specific event datasets for the climate analysis. The results show the most suitable FFA method varied across different regions and even for individual catchments within regions. The LNI was the only region to have a single method, GEV, identified as the most accurate method for all four catchments within that region. The exact reason for this is unknown but it may be due to the Waipoua, Waiōhine, and Waingawa Rivers being tributaries of the Ruamāhangā River, their catchments being located within the Ruamāhangā catchment, and the monitoring sites being located within 20km above the confluence of the Ruamāhangā (Fig. 2.13; GWRC, 2015). This would likely mean the topography, land use, and soil does not change significantly between the rivers, leading to similar flow characteristics and high flow events, and therefore the same FFA method was most accurate for all catchments. Figure 6.1 illustrates that overall GEV was the most preferred method (47% of cases) followed by LP3 (43%) and the Gumbel method (12%). This implies the GEV and LP3 methods tend to be the most accurate for NZ's eastern environments, but it also highlights the need for individual analyses of catchments when deciding which method is most suitable. All catchments that GEV was identified to most accurately model favoured the Weibull distribution except for the Wairau which favoured the Fréchet distribution (Table Table 4.2).

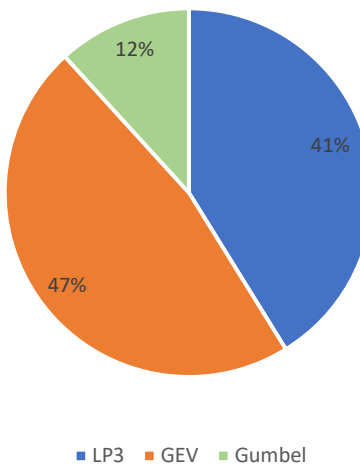


Figure 6.1: The percentage of Log Pearson Type III, Gumbel and Generalised Extreme Value flood frequency methods selected as the best fit model for the 17 eastern catchments in this research.

The methods selected for the threshold development generally align with the methods recommended by each council regulation as described in Section 2.2.2. The only exception to this is for the Wairau catchment where this research identified the GEV method was the most accurate at modelling flow, whereas the Gumbel method has been exclusively used to model flow in this catchment by the Marlborough District Council since 1995 (Williman, 1995). The 1-in-100-year magnitudes identified in this research (as shown in Table 4.2) were similar to values found in available literature for each catchment described in Section 3.1. This study found that the 1-in-100-year thresholds for some catchments were lower than those calculated by councils, which may be due to a number of reasons such as the record periods used, changes in the parameters and/or parameter estimation methods, or the use of different FFA methods by the councils. Some councils also undertake extensive data analysis and discount years with potentially erroneous data (B. Bosworth, personal communication, May 31, 2022). However, based on the rigorous goodness-of-fit testing completed and visual accuracy of the methods, the FFA results presented in this research provide a reliable source of recommendations for councils.

Gumbel was unexpectedly the least accurate option, only being identified as the best model for the Te Arai and Hurunui Rivers, yet previous studies and councils have suggested it has been widely used in NZ, sometimes performing better than LP3 and GEV (Pearson, 1991;

Williman, 1995; Ministry for the Environment, 2010). Due to the presence of significant outliers in the flow data from extreme events such as Cyclone Bola and non-linear trends, such as for the Ruamāhangā River, which most likely exists because of extensive changes to the river due to flood mitigation (GWRC, 2019), the Gumbel method was unable to accurately model the distribution of observed values. This is likely a result of the method only using two parameters (location and scale), excluding the shape parameter, which does not allow the modelled linear distribution flexibility to account for these changes in the observed flow data (Al-Mashidani et al., 1978). It appears the three-parameter distributions of LP3 and GEV are better suited for eastern NZ environments because including the extra parameter shape allows more flexibility to account for extreme events and changes in the physical environment that may affect flow (Jennings & Bensen, 1969; Stedinger & Griffis, 2011).

By isolating individual events rather than using the full dataset, this research found it was common in the Ruamāhangā, Waiōhine, Wairau, Hurunui, Maerewhenua, Waihora, and Waioeka catchments for high flow events above the 1-in-5-year threshold to occur over the course of three days. This may be a result of a significant rainfall event causing high river flows to occur over more than one day as the river takes longer to recover to base flow, or because high flow events require preconditioning of the catchment (e.g., the soil) that produces favourable conditions for longer periods of high flow (Frei et al., 2000; Patel et al., 2021). More research is needed to determine the true nature of this finding.

Both the K-S and NSE tests performed well for goodness-of-fit testing together with the visual comparison testing. However, there are some limitations around the use of NSE for these catchments based on the negative NSE results. As discussed, the NSE test can be difficult and subjective because the test is sensitive to several factors like sample size, size of the variance, and presence of outliers, which can increase the uncertainty around results (McCuen et al., 2006). Negative values were expected using flow data due to the uncertainties surrounding flow data measurements and the presence of outliers. High flow events are often difficult to measure due to field measurements being unsafe to undertake, floodwaters breaching their banks which underestimates peak flow rate, and instruments potentially getting damaged from debris flow (NIWA, 2010). The models could be improved for prediction by changing the parameter values to get better NSE results, and this should be done for prediction purposes but was not a focus of this thesis (McCuen et al., 2006). However,

improving the NSE and completing the A-D goodness-of-fit test alongside the K-S test would be beneficial for future research.

Lastly, this thesis clearly highlights the importance of good quality and accessible flow data. Accurate flow records and documentation on any changes to monitoring instruments are required to fully understand how a river responds to a precipitation event and to model how a river may respond to increasing severity of heavy precipitation events with climate change. Fortunately, accurate flow data were made accessible from the relevant councils and only the Waipoua River had noticeable issues with the data. As discussed previously, detailed records of measurement issues were kept for the Waipoua River, which allowed for a better understanding of the uncertainties and how the river changes during a high flow event (GWRC, 2015). Therefore, it is important, to enable research like that undertaken in this thesis to occur, that reliable flow monitoring of NZ rivers, and detailed record keeping of any issues or changes in monitoring devices, continues, and is made accessible to researchers. This will be especially important in the future when flow is expected to be more variable and potentially more uncertain, including an increased risk of damage to measurement instruments (Ministry for the Environment, 2010; Kundzewicz et al., 2019; Collins, 2021).

Future research could include the following:

1. Investigating why FFA methods vary between and within regions in NZ and whether similar results are identified for catchments in western NZ. Potential reasons may include the influence of tributaries, land use, climate variation, or monitoring site location. These could be targeted areas of research.
2. Determining what causes high river flow to occur over a period of three days for some catchments in eastern NZ but not all of them. Understanding whether the antecedent conditions (soil type) or other factors such as the size of the catchment, length of record, or type of monitoring, play a role and could be investigated further.
3. Mckerchar and Pearsons (1989) Regional Flood Frequency method was not completed in this research, but the GWRC and BOPRC suggested this was a good method to use alongside LP3 and GEV, therefore, future research could determine

whether this method is better suited for some environments in NZ, especially the rural environments as recommended by BOPRC (Environmental Hazards Group, 2012; Cardno, 2021).

4. Comparing the use of A-D compared to K-S for goodness-of-fit testing for NZ catchments, because A-D has been globally acclaimed to be a stronger goodness-of-fit test (Rahman et al., 2013).

Altogether, the FFA component of this research has achieved three main objectives: (1) an analysis of current flood frequency methods used in NZ and identifying their suitability for eastern regions of NZ; (2) developing a set of flooding thresholds using catchment-specific and the most robust flood frequency methods and flood magnitudes; and (3) developing a robust dataset of high flow events that have the potential to damage life and property. These results can serve as a foundation for the councils involved in this research when planning and preparing for further flood events and associated mitigation.

6.2 climate Analysis

This research identified the anomalous synoptic and large-scale circulation conditions associated with high flow events (above 1-in-5-year threshold) in eastern catchments of NZ. Generally, the coupling of a low- and high-pressure system was identified to be crucial for setting up the orientation and strength of moisture transport and its local interception of the catchment to enhance low level convergence that likely promotes heavy precipitation. Some differences in the location of these systems were identified in the Wairau, Waimatā, and Ruamāhanga catchments compared to the other catchments in their respective regions. This likely reflects the importance of local topographic differences, such as orientation or topographic features and its associated interception of the local synoptic flow which could affect the intensity and location of the heaviest precipitation, as well as the size of the catchment, because a larger sized catchment would have more variety in the weather events that can lead to flooding (Kingston et al., 2022).

High flow events in the UNI catchments generally consisted of a low-pressure anomaly to the west of NZ and a high-pressure anomaly to the east and southeast, resembling the Kidson types ‘TNW’ and ‘NE’ (Fig. 5.1). These synoptic features transport moisture to the UNI from

the north out of the central sub-tropical Pacific region and locally intercept the UNI catchments at a north to northeasterly angle. Anomalously warm SSTs were located to the north of the North Island for all catchments and these anomalies corresponded to the poleward stream of tropical moisture, likely enhancing the atmospheric moisture content (Fig. 5.3). Local frontal forcing did not appear to play a role in high flow events for this region. The high to the southeast and the coupling of the high- and low-pressure with northerly flow are therefore the key components of high flow events in the Waitangi, Waioeka, and Otara catchments.

High flow events in the ECNI occurred when there was a low-pressure anomaly to the north of the North Island and a high-pressure anomaly to the south and southeast of the South Island, resembling the Kisdon type ‘NE’ (Fig. 5.5). Similar to the UNI, these synoptic features transport moisture towards the ECNI from the central sub-tropical Pacific, but at a northeasterly angle with easterly winds that directly intercept the catchments. Anomalously cold SSTs dominated the areas around NZ and did not appear to play a determining role in flows above the 1-in-5-year threshold, with the exception of the Waimatā catchment where warm SSTs located to the northeast corresponded to the stream of tropical moisture (Fig. 5.7). Fronts did not appear to play a role in the high flow events in the ECNI either and therefore, the presence of the strong easterly flow towards the catchments driven by the blocking high to the southeast is a key component preceding high flow events in the ECNI.

For the LNI, high flow events in the Waiōhine, Waipoua, and Waingawa catchments generally consisted of a low-pressure anomaly to the south of NZ and a high-pressure anomaly to the northeast of the North Island, resembling the Kidson type ‘W’, and an advancing cold front into the region from the south (Fig. 5.9). Conversely, high flow events in the Ruamāhangā consisted of a low-pressure anomaly over central NZ, resembling a Kidson type ‘T’, with a warm front located over the region. For the former, the synoptic features transported moisture from the west/northwest off the Tasman Sea ahead of the cold front. For the Ruamāhangā catchment, moisture transport occurred from the northeast and east and intercepts at a southeasterly angle. Anomalously warm SSTs were located to the northwest of the North Island, aligning with the transport of moisture from the Tasman Sea in all LNI catchments (Fig. 5.11). These findings suggest cold-frontal precipitation as well as the strong low-pressure system to the south favours strong westerly flow (with a northerly

component) towards the catchments is key for high flow events in the Waiōhine, Waipoua, and Waingawa catchments while orographically enhanced precipitation along a warm front is key for the Ruamāhangā catchment.

High flow events in the SI's Hurunui, Selwyn, and Maerewhenua catchments occurred when there was a low-pressure anomaly over NZ with a high-pressure anomaly to the south, resembling the Kidson types 'HE' and 'R' (Fig. 5.13). These synoptic features transport moisture poleward from the central sub-tropical Pacific and then westward (through easterly winds) toward the catchment showing a complete reversal of the average westerly winds. Anomalously cold SSTs were seen around most of NZ and did not appear to play a role in enhancing the moisture (Fig. 5.15). Local frontal forcing also did not appear to play a contributing role, and therefore, the moist easterly flow was more important for high flow events in the Hurunui, Selwyn, and Maerewhenua catchments by creating orographically enhanced precipitation. For the Wairau catchment, high flow events generally consisted of a low-pressure anomaly over NZ and a high-pressure anomaly to the east of the country, resembling the Kidson types 'TNW' and 'HE' (Fig. 5.13a). Moisture transport also occurred from the central sub-tropical Pacific but due to the easterly placement of the high, the moisture transport intercepted the Wairau catchment at a northerly angle. Anomalously warm SSTs occurred to the north of the North Island during flood events in the Wairau and correspond to the tropical transport of moisture (Fig. 5.15a). Fronts were not identified to play a direct role and thus the positioning of the low- and high-pressure are key components of high flow events in the Wairau catchment.

Zonal wave 4 (ZW4) was identified to occur during high flow events in the UNI (Fig. 5.2) and SI (Figs. 5.14c-h) (except for the Wairau) catchments when SAM was not present, suggesting an amplified mid-latitude wave train is key to setting up conditions that lead to high flow events in these regions. ZW4 is a lesser-studied wave pattern in the Southern Hemisphere than zonal waves 1 and 3 (Senapati et al., 2021) but is more likely to occur in mid-to-sub-tropical latitudes like NZ due to the larger circumference of the Earth. It is a pattern of four anomalous highs-lows pressure pairs that occurs across the middle latitudes and is thought to be generated by Rossby Waves in the southern Indo-Atlantic Ocean Basin (Senapati et al., 2021). Zonal wave 3 (ZW3) and its effects on NZ have been widely studied, including its influence on flooding in the South Island (Kingston et al. 2022), whereas less is

known about ZW4 and its effects on the Southern Hemisphere's climate (Irving & Simmonds, 2015; Senapati et al., 2021). ZW4 has however been identified to play a key role in flooding in south eastern Australia (Senapati et al., 2021). Because of the inherent high amplitude nature of zonal wave patterns, including strong north-south flow, future research should examine what drives variability in ZW4 across NZ latitudes, and how that variability influences the formation of the local synoptic patterns identified here as leading to flooding.

Flood events in the LNI (Fig. 5.11), UNI (Fig. 5.3), and Waimatā (Fig. 5.7c) (ECNI) catchments were also found to occur when local positive SST anomalies dominated NZ and corresponded to the region of high moisture transported from the Tropics (UNI and Waimatā) and Tasman Sea (LNI). In these catchments there was also a strong La Niña signal that this research showed the SSTs were likely playing a supporting role in the broader La Niña pattern. These findings are supported by Evans & Boyer-Souchet (2012) who identified the atmospheric circulation changes associated with a La Niña event were not sufficient by itself to produce the extreme rainfall and flooding observed in Queensland, Australia, in December 2010, finding that positive SST anomalies around northern Australia added 25% more rainfall to the La Niña. Therefore, positive SST anomalies likely play a significant role in high flow events in these eastern catchments of NZ by increasing the amount of water the catchments receive during a La Niña. With SSTs expected to increase in temperature and frequency in the future with a warming climate, these results suggest the LNI, UNI, and Waimatā catchments are at an increased risk of more severe flooding in the future, especially alongside the favourable positioning of the low- and high-pressure systems and La Niña conditions (Evans & Boyer-Souchet, 2012).

A clear connection between SAM and high flow events was not identified in this thesis. Most catchments in the UNI, ECNI, and LNI had a preference towards a negative SAM which generally results in a reduction in precipitation to these eastern regions, whereas the SI and Waitangi (UNI) catchments had a preference for a positive phase of the SAM which increases precipitation to these regions (Ummenhofer & England, 2007). This research found that other large-scale features of the circulation (such as a La Niña, positive SST anomalies, and ZW4) had a stronger role in producing the atmospheric conditions that preceded flood events in these catchments. Li & McGregor (2017) and Kingston et al. (2022) were also unable to find a clear association between SAM and extreme high flow events. A potential explanation for the

weak SAM connection is the SAM reflects a zonally symmetric, hemispheric scale pattern that describes fluctuations in zonal flow rather than meridional flow, the latter being crucial for moisture transport from the tropics to middle latitudes. On the other hand, circulation anomalies forced by ENSO variability take the form of alternating high- and low-pressure anomalies that are more likely to induce poleward moisture transport. However, a closer analysis of the seasonal relationships between SAM and flood events on NZ's eastern regions should also be completed as SAM was identified to influence flow in NZ on a sub-seasonal timescale.

A limitation of this study, but also a benefit, is that we did not quantitatively assign the composites as Kidson types. There were many similarities to several Kidson types that match with the results from Pohl et al. (2022) work on the synoptic drivers of extreme precipitation. However, our results highlight that limiting to these 12 types can miss important features that are relevant to individual catchments. For most of the catchments in this study, more than one Kidson type, usually a combination of a Blocking and Trough type, was identified to be key components driving flow and moisture to intercept the catchment. Therefore, this research has provided insight into catchment-specific synoptic patterns that can lead to high flow events. Future research could determine the trends and future projections of Kidson types and based on the findings of Pohl et al. (2022) combined with the results presented in this thesis, identify which eastern catchments may be most at risk of flooding in the future.

The results of this research provide important new insight into the key regional and large-scale features that are associated with heavy rainfall that leads to potentially damaging high river flow in eastern regions of NZ. This knowledge is useful for operational personnel making real-time forecasts of potential river flooding because it provides guidance on the key features to look for when considering flood risk. In particular, the precise locations of the high- and low-pressure systems, resultant large-scale moisture transport and source, and local interception of the flow with the NZ mainland are key features to take into consideration. For example, on the 10th of January 2023, post tropical Cyclone Hale brought heavy precipitation and severe flooding to the Gisborne region, and flow in the Hikuwai River broke the previous long standing record set by the infamous Cyclone Bola (Gisborne District Council, 2023). Low lying residents of Tolaga Bay had to evacuate and many farms

surrounding the river were inundated with damaging floodwaters for the fourth time in a year (RNZ, 2023b). Figure 6.2 shows the location of Cyclone Hale moving towards the ECNI. On a visual comparison of Fig. 6.2 to Fig. 5.5a for the Hikuwai catchment, the locations of the low-pressure systems are very similar and the location of precipitation in Fig. 6.2 corresponds to the moisture transport in Fig. 5.5b. This suggests that the results of this research could have aided in local preparation for this event, as the synoptic pattern associated with Cyclone Hale's approach, as well as the moisture transport from the northeast, align with Fig. 5.5a, indicating that this event would likely have high flood potential specifically in the Hikuwai catchment.

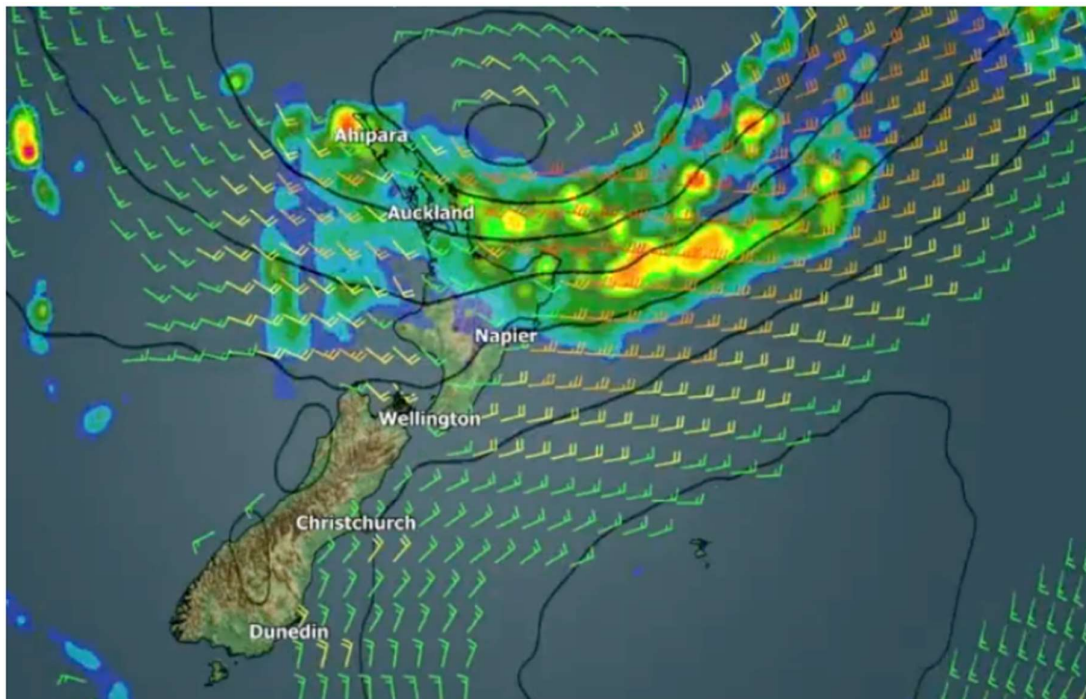


Figure 6.2: Mean sea level pressure (contours), precipitation (shaded), and wind (arrows) map of the atmospheric conditions preceding post tropical Cyclone Hale on the 10th of January 2023 at 3pm (Weather Watch, 2023).

The results of this research are also useful for seasonal to longer-term risk assessment/projections, as seasonal and long-term risk forecasters can examine how the frequency and/or intensity of these key atmospheric circulation patterns and regional SSTs may change in the future, shedding light on the most at-risk regions. For example, if certain patterns are expected to increase in occurrence in the future, vulnerable regions can be identified. This is especially relevant with the current La Niña conditions and warm SSTs

around NZ which has led to a very wet and flood ridden summer for many eastern regions of NZ (Morton, 2023).

Future research topics could include the following:

1. A more comprehensive diagnosis of the dynamic and thermodynamic conditions associated with these synoptic patterns, such as if cold conditions aloft (increasing instability) or upper-level dynamic forcing (such a divergence and/or vorticity) is a determining factor.
2. Investigation into how the identified circulation patterns may change with climate change, and how this may affect flooding in the eastern regions of NZ.
3. A more comprehensive study of the role of SST and ZW4, and further understand why ZW4 was found to influence flooding in both the UNI and SI catchments when both regions had different characteristics in SST, SAM, and ENSO and are located on different islands of NZ.
4. Using a daily SAM index instead of a monthly index may provide a clearer indication of the role of hemispheric patterns in high flow events.
5. While there was a winter seasonal preference in the SI and UNI, and spring and summer for LNI, the signals were not clear and it would be beneficial for more research to be undertaken to determine if there are any seasonal trends or preferences in flooding.
6. Limitations of this research include the role of preceding conditions, such as whether soils in the catchment need to be saturated or dry prior to the event for the river to exceed a 1-in-5-year flow threshold. Therefore, investigation could be done into the role antecedent conditions play in increasing a region's flood risk to specific weather events, using land use and flood prone soil maps (Paulik et al., 2019) and historical environmental observations and measurements from NIWA's freely accessible National Climate Data Base (<https://cliflo.niwa.co.nz/>).
7. ARs were identified in Section 2.3.4.1 to drive many historical river flooding events in NZ, and this research would benefit by examining if AR frequency and/or intensity played a

role in producing these high-flow events. This would also shed light on the large-scale and synoptic weather patterns governing ARs in eastern regions of NZ.

8. The Hawke's Bay region was originally left out of the analysis due to time limitations. However, based on the findings of this thesis and recent events, it is recommended that the future analysis should be extended to include the Hawke's Bay region.

9. References

- 1News. (2022, March 23). Gisborne hit by 3 months worth of rain in 24 hours. *1News*.
<https://www.1news.co.nz/2022/03/23/live-gisborne-hit-by-3-months-worth-of-rain-in-24-hours/>
- Alfieri, L., Bisselink, B., Dottori, F., Naumann, G., de Roo, A., Salamon, P., Wyser, K., & Feyen, L. (2017). Global projections of river flood risk in a warmer world: River flood risk in a warmer world. *Earth's Future*, 5(2), 171–182.
<https://doi.org/10.1002/2016EF000485>
- Al-Mashidani, G., Lal, P., & Mujda, F. (1978). A simple version of Gumbel's method for flood estimation. *Hydrological Sciences Bulletin*, 23(3), 373–380.
<https://doi.org/10.1080/02626667809491810>
- Arnold, T., & Emerson, J. (2022). *dgof: Discrete Goodness-of-Fit Tests*. Comprehensive R Archive Network (CRAN). <https://CRAN.R-project.org/package=dgof>
- Ball, J., Babister, M., Nathan, R., Weeks, W., Weinmann, E., Retallick, M., & Testoni, I. (2019). *Australian Rainfall and Runoff: A Guide to Flood Estimation*. Geoscience Australia.
https://www.arr-software.org/pdfs/ARR_190514_Book3.pdf
- Barnard, T., Barry, L., Garrett, D., Harrison, H., Jones, D., & Moore, D. (2012). *Waiapu River Catchment Study – Final Report* (No. 15201). Scion.
<https://ref.coastalrestorationtrust.org.nz/site/assets/files/6859/waiapu-river-catchment-study-scion-2012.pdf>
- Basheer, G., Mulholland, M., & Giberson, C. (2013). *Stopbanks renewal prioritisation manual* (No. 2013/57). Waikato Regional Council.
<https://www.waikatoregion.govt.nz/assets/PageFiles/Templates/Stopbanks-Renewal-prioritisation-manual.pdf>
- Bell, D. (1976). High intensity rainstorms and geological hazards: Cyclone Alison, March 1975, Kaikoura, New Zealand. *Bulletin of the International Association of Engineering Geology*, 13(1), 189–200. <https://doi.org/10.1007/BF02634795>

- Berghuijs, W., Woods, R., Hutton, C., & Sivapalan, M. (2016). Dominant flood generating mechanisms across the United States: Flood Mechanisms Across the U.S. *Geophysical Research Letters*, 43(9), 4382–4390.
<https://doi.org/10.1002/2016GL068070>
- Bhagat, N. (2017). Flood Frequency Analysis Using Gumbel's Distribution Method: A Case Study of Lower Mahi Basin, India. *Journal of Water Resources and Ocean Science*, 6(4), 51. <https://doi.org/10.11648/j.wros.20170604.11>
- Bischiniotis, K., van den Hurk, B., Jongman, B., Coughlan de Perez, E., Veldkamp, T., de Moel, H., & Aerts, J. (2018). The influence of antecedent conditions on flood risk in sub-Saharan Africa. *Natural Hazards and Earth System Sciences*, 18(1), 271–285.
<https://doi.org/10.5194/nhess-18-271-2018>
- Bjerknes, J. (1969). Atmospheric Teleconnections from the Equatorial Pacific. *Monthly Weather Review*, 97, 163–172.
- Blöschl, G., Gaál, L., Hall, J., Kiss, A., Komma, J., Nester, T., Parajka, J., Perdigão, R. A. P., Plavcová, L., Rogger, M., Salinas, J. L., & Viglione, A. (2015). Increasing river floods: Fiction or reality? *Wiley Interdisciplinary Review Water*, 2(4), 329–344.
<https://doi.org/10.1002/wat2.1079>
- Bonta, J., & Shahalam, A. (2003). Cumulative storm rainfall distributions: Comparison of Huff curves. *Journal of Hydrology (New Zealand)*, 42(1), 65–74. JSTOR.
- Boothway, D. (2014). *Stopbank Design and Construction Guidelines* (No. 1179–9609). Bay of Plenty Regional Council. <https://www.boprc.govt.nz/media/395649/stopbank-design-and-construction-guidelines.pdf>
- Bracegirdle, T., & Marshall, G. (2012). The Reliability of Antarctic Tropospheric Pressure and Temperature in the Latest Global Reanalyses. *Journal of Climate*, 25(20), 7138–7146.
<https://doi.org/10.1175/JCLI-D-11-00685.1>
- Bosworth, B. (2022, May 31). *Gisborne Rivers Flood Frequency* [Personal communication].

- Cardno. (2021). *Flood Hazard Modelling Standard* (p. 92). Greater Wellington Regional Council. <https://archive.gw.govt.nz/assets/floodprotection/GWRC-Flood-Hazard-Modelling-Standard-R1-May-2021.pdf>
- Cardwell, H. (2022, August 17). Insurance costs could increase massively as climate risk rises—Modeller. *RNZ*. <https://www.rnz.co.nz/news/national/473005/insurance-costs-could-increase-massively-as-climate-risk-rises-modeller#:~:text=Claims%20for%20extreme%20weather%20events,to%20extreme%20sea%2Dlevel%20rise>.
- Cave, M. (2021). *Waimata River in Flood*. [Photograph]. Personal Communication.
- Chappell, P. (2013). *The Climate and Weather of Northland* (No. 59; NIWA Science and Technology Series). <https://niwa.co.nz/static/Northland%20ClimateWEB.pdf>
- Chappell, P. (2016). *The Climate and Weather of Gisborne* (No. 70; NIWA Science and Technology Series). NIWA.
<https://niwa.co.nz/sites/niwa.co.nz/files/WEB%20Gisborne%20Climate%20book2019.pdf>
- Chappell, P. (2017). *The Climate and Weather of Wellington* (No. 65; NIWA Science and Technology Series). <https://niwa.co.nz/node/110337>
- Chater, A., & Sturman, A. (1998). Atmospheric conditions influencing the spillover of rainfall to lee of the Southern Alps, New Zealand. *International Journal of Climatology*, 18(1), 77–92. [https://doi.org/10.1002/\(SICI\)1097-0088\(199801\)18:1<77::AID-JOC218>3.0.CO;2-M](https://doi.org/10.1002/(SICI)1097-0088(199801)18:1<77::AID-JOC218>3.0.CO;2-M)
- Christchurch City Library. (2023a). *Cyclone Giselle*.
<https://my.christchurchcitylibraries.com/cyclone-giselle>
- Christchurch City Library. (2023b). *Wahine shipwreck*.
<https://my.christchurchcitylibraries.com/wahine>
- Christensen, K., & Doscher, C. (2010). The interaction of river engineering and geomorphology in the Lower Wairau River, Marlborough, New Zealand. *Journal of Hydrology (New Zealand)*, 49(2), 79–98. JSTOR.

- Collins, D. (2021). Hydrological sentinels and the relative emergence of climate change signals in New Zealand river flows. *Hydrological Sciences Journal*, 66(15), 2146–2154. <https://doi.org/10.1080/02626667.2021.1987439>
- Conn, S. (2019). *Waiohine River—Geomorphic Trends Assessment and its Application to River Management*. 11. https://www.waternz.org.nz/Attachment?Action=Download&Attachment_id=4102
- Crawford-Flett, K., Blake, D., Pascoal, E., Wilson, M., & Wotherspoon, L. (2022). A standardised inventory for New Zealand's stopbank (levee) network and its application for natural hazard exposure assessments. *Journal of Flood Risk Management*, 15(2). <https://doi.org/10.1111/jfr3.12777>
- Cuff, T. (2022). *Whangamoa River flooding in the Whangamoa River Valley*. [Photograph]. NZHerald. <https://www.nzherald.co.nz/nz/weather-nelson-flooding-households-communities-stunned-by-damage/ZLUTHPTKHCZHMG2OYRVMZ4KSXE/>
- Cullum, C., Brierley, G., & Marden, M. (2017). *Landscapes and Rivers of the Waimatā and Taruheru* (No. 1; Te Awaroa, p. 97). Auckland University.
- Davies, T., & McSaveney, M. (2011). Bedload sediment flux and flood risk management in New Zealand. *Journal of Hydrology New Zealand*, 50.
- Dowle, M., Srinivasan, A., Gorecki, J., Chirico, M., & Stetsenko, P. (2022). *data.table: Extension of “data.frame.”* R Studio. <https://cran.r-project.org/web/packages/data.table/index.html>
- Easton, L. (2015). *Te Arai River – Assessment of Ecological Impact of Proposed Managed Aquifer Recharge Trial* (No. 2/2015; p. 13). Gisborne District Council.
- Eichler, T. P., & Gottschalck, J. (2013). A Comparison of Southern Hemisphere Cyclone Track Climatology and Interannual Variability in Coarse-Gridded Reanalysis Datasets. *Advances in Meteorology*, 2013, 1–16. <https://doi.org/10.1155/2013/891260>
- Embry, I., Hoos, A., & Diehl, T. (2022). *ie2misc: Irucka Embry's Miscellaneous USGS Functions*. Comprehensive R Archive Network (CRAN). <https://CRAN.R-project.org/package=ie2misc>

- England, J., Cohn, T., Faber, B., Stedinger, J., Thomas, W., Veilleux, A., Kiang, J., & Mason, R. (2019). *Guidelines for Determining Flood Flow Frequency Bulletin 17C* (1.1, Vol. 17c). United States Geological Society.
- Environment Canterbury. (2021). *Canterbury floods May/June 2021*. Environment Canterbury. <https://www.ecan.govt.nz/your-region/your-environment/river-and-drain-management/canterbury-flood-recovery/flooding-events/>
- Environment Canterbury. (2022). *Flood probabilities*. Environment Canterbury. <https://www.ecan.govt.nz/your-region/your-environment/natural-hazards/floods/flood-probabilities/>
- Environmental Hazards Group. (2012). *Hydrological and Hydraulic Guidelines* (1179 9609; p. 74). Bay of Plenty Regional Council. boprc.govt.nz/media/373948/hydrological-and-hydraulic-guidelines.pdf
- Ettrick, T., Mawdsey, J., & Metcalfe, A. (1987). The influence of antecedent catchment conditions on seasonal flood risk. *Water Resources Research*, 23(3), 481–488. <https://doi.org/10.1029/WR023i003p00481>
- Evans, J., & Boyer-Souchet, I. (2012). Local sea surface temperatures add to extreme precipitation in northeast Australia during La Niña. *Geophysical Research Letters*, 39(10), n/a-n/a. <https://doi.org/10.1029/2012GL052014>
- Farooq, M., Shafique, M., & Khattak, M. S. (2018). Flood frequency analysis of river swat using Log Pearson type 3, Generalized Extreme Value, Normal, and Gumbel Max distribution methods. *Arabian Journal of Geosciences*, 11(9), 216. <https://doi.org/10.1007/s12517-018-3553-z>
- Fogt, R., Jones, J., & Renwick, J. (2012). Seasonal Zonal Asymmetries in the Southern Annular Mode and Their Impact on Regional Temperature Anomalies. *Journal of Climate*, 25(18), 6253–6270. <https://doi.org/10.1175/JCLI-D-11-00474.1>
- Fogt, R., & Marshall, G. (2020). The Southern Annular Mode: Variability, trends, and climate impacts across the Southern Hemisphere. *Wiley Interdisciplinary Review Climate Change*, 11(4). <https://doi.org/10.1002/wcc.652>

- Forestieri, A., Lo Conti, F., Blenkinsop, S., Cannarozzo, M., Fowler, H., & Noto, L. (2018). Regional frequency analysis of extreme rainfall in Sicily (Italy). *International Journal of Climatology*, 38, e698–e716. <https://doi.org/10.1002/joc.5400>
- Freeman, J. (2008). *Waioeka-Otara Rivers: Provisional Flood Frequency Analyses* (Local Government No. 2008/02). Environment Bay of Plenty.
<https://www.boprc.govt.nz/media/33379/Report-081000-WaioekaOtaraRiversProvisionalFloodFrequencyAnalysesOctober2008.pdf>
- Frei, C., Davies, H., Gutz, J., & Schär, C. (2000). Climate dynamics and extreme precipitation and flood events in Central Europe. *Integrated Assessment*, 1(4), 281–300.
<https://doi.org/10.1023/A:1018983226334>
- Galuszka, J. (2022, April 6). Flood protection short by \$150m per year as councils grapple with climate change impact. *Stuff*. <https://www.stuff.co.nz/environment/climate-news/300559806/flood-protection-short-by-150m-per-year-as-councils-grapple-with-climate-change-impact>
- Gibson, P., Perkins-Kirkpatrick, S., & Renwick, J. (2016). Projected changes in synoptic weather patterns over New Zealand examined through self-organizing maps. *International Journal of Climatology*, 36(12), 3934–3948.
<https://doi.org/10.1002/joc.4604>
- Gillett, N., Kell, T., & Jones, P. (2006). Regional climate impacts of the Southern Annular Mode. *Geophysical Research Letters*, 33(23), L23704.
<https://doi.org/10.1029/2006GL027721>
- Gisborne District Council. (2021, March 18). *About our rivers*. Gisborne District Council.
<https://www.gdc.govt.nz/environment/our-rivers/rivers>
- Gisborne District Council. (2023, October 1). *Cyclone Hale Hitting East Coast Now / Scoop News*. <https://www.scoop.co.nz/stories/AK2301/S00108/cyclone-hale-hitting-east-coast-now.htm>

- Gordon, N. D. (1986). The Southern Oscillation and New Zealand Weather. *Monthly Weather Review*, 114(2), 371–387. [https://doi.org/10.1175/1520-0493\(1986\)114<0371:TSOANZ>2.0.CO;2](https://doi.org/10.1175/1520-0493(1986)114<0371:TSOANZ>2.0.CO;2)
- Greater Wellington Regional Council. (2015). *Hydro Stats Draft* (p. 287). Greater Wellington Regional Council.
- Greater Wellington Regional Council. (2019). *Te Kāuru Upper Ruamāhanga floodplain management plan* (No. 978-0-473-54532-1; p. 224). Greater Wellington Regional Council. <https://archive.gw.govt.nz/assets/Uploads/FINALTe-Kauru-Final-incl-dust-cover.pdf>
- Greater Wellington Regional Council. (2021). *Waiohine River*.
<https://archive.gw.govt.nz/waiohineriver/>
- Greis, N. (1983). Flood frequency analysis: A review of 1979–1982. *Reviews of Geophysics*, 21(3), 699. <https://doi.org/10.1029/RG021i003p00699>
- Griffin, J., Wade, A. J., Lavers, D. A., & Watts, G. (2020). Atmospheric river orientation determines flood occurrence. *Hydrological Processes*, 34(23), 4547–4555.
<https://doi.org/10.1002/hyp.13905>
- Griffiths, G. (2011a). Drivers of extreme daily rainfalls in New Zealand. *Weather and Climate*, 31, 24. <https://doi.org/10.2307/26169716>
- Griffiths, G., Alistair, M., & Pearson, C. (2011b). *Review of flood frequency in the Canterbury region* (No. 978-7-927161-80-7; p. 26). NIWA.
file:///C:/Users/ajbri/Downloads/ReviewoffloodfrequencyintheCanterburyRegion%20(2).PDF
- Griffiths, G. (2013). New Zealand six main centre extreme rainfall trends 1962–2011. *Weather and Climate*, 33, 76. <https://doi.org/10.2307/26169738>
- Guan, B., & Waliser, D. (2015). Detection of atmospheric rivers: Evaluation and application of an algorithm for global studies: Detection of Atmospheric Rivers. *Journal of Geophysical Research: Atmospheres*, 120(24), 12514–12535.
<https://doi.org/10.1002/2015JD024257>

- Gulap, S., & Gitika, T. (2019). Flood frequency analysis using Gumbel's distribution method: A lower downstream of the Lohit River (Dangori River), Assam (India). *International Journal of Civil Engineering and Technology*, 10(11), 229–234.
- Gumbel, E. (1941). Probability-interpretation of the observed return-periods of floods. *Transactions, American Geophysical Union*, 22(3), 836.
<https://doi.org/10.1029/TR022i003p00836>
- Heard, G. (2021). *The extent of the flooding is clear from a helicopter. [Photograph]*. NZHerald. <https://www.nzherald.co.nz/nz/wild-weather-extent-of-flooding-revealed-in-aerial-photos-of-stricken-westport/U4MCAIC63PNYQTL4AHHTVCN7WQ/>
- Harrington, L., & Renwick, J. (2014). Secular changes in New Zealand rainfall characteristics 1950–2009. *Weather and Climate*, 34, 50–59. JSTOR.
<https://doi.org/10.2307/26169744>
- Harris, S. (2022, March 21). In pictures: Flooding, and severe thunderstorms hit Auckland and Northland. Stuff. <https://www.stuff.co.nz/national/weather-news/300546021/in-pictures-flooding-and-severe-thunderstorms-hit-auckland-and-northland>
- Hartmann, D. (2016). *Global Physical Climatology* (Second). Elsevier.
- Henderson, R., & Collins, D. (2016). *Regional Flood Estimation Tool for New Zealand* (No. 2016049CH; p. 38). NIWA. <http://tools.envirolink.govt.nz/assets/Uploads/Regional-flood-estimation-tool-for-New-Zealand.pdf>
- Hersbach, H., Bell, B., Berrisford, P., Hirahara, S., Horányi, A., Muñoz-Sabater, J., Nicolas, J., Peubey, C., Radu, R., Schepers, D., Simmons, A., Soci, C., Abdalla, S., Abellan, X., Balsamo, G., Bechtold, P., Biavati, G., Bidlot, J., Bonavita, M., ... Thépaut, J. (2020). The ERA5 global reanalysis. *Quarterly Journal of the Royal Meteorological Society*, 146(730), 1999–2049. <https://doi.org/10.1002/qj.3803>
- Horrell, G., McKerchar, A., Griffiths, G., & Griffiths, G. (2012). South Island storms and floods of December 2010. *Journal of Hydrology (New Zealand)*, 51(1), 63–81. JSTOR.

- Hoskins, B., & Karoly, D. (1981). The Steady Linear Response of a Spherical Atmosphere to Thermal and Orographic Forcing. *Journal of the Atmospheric Sciences*, 38(6), 1179–1196. [https://doi.org/10.1175/1520-0469\(1981\)038<1179:TSLROA>2.0.CO;2](https://doi.org/10.1175/1520-0469(1981)038<1179:TSLROA>2.0.CO;2)
- Hunter, R. (2022). *Floodwater scouring on Devenish Place, Atawhai*. [Photograph]. Stuff. <https://www.stuff.co.nz/national/weather-news/300665061/in-pictures-dangerous-slips-flooding-as-extreme-rain-wreaks-havoc>
- Hurunui District Council. (2022). *Hazards in your District—Hurunui District Council*. <https://www.hurunui.govt.nz/community/cd/hazards-in-your-district>
- Inglis, L. (2021). *Design Modelling Whangarei Catchment (M01)* (M01_20010434_R02V01a_Validation_Report.docx; p. 41). Water Technology. <https://www.nrc.govt.nz/media/iz3nk4ry/whangarei-catchment.pdf>
- Insurance Council of New Zealand. (2022). *Cost of natural disasters*. <https://www.icnz.org.nz/industry/cost-of-natural-disasters/>
- Irving, D., & Simmonds, I. (2015). A Novel Approach to Diagnosing Southern Hemisphere Planetary Wave Activity and Its Influence on Regional Climate Variability. *Journal of Climate*, 28(23), 9041–9057. <https://doi.org/10.1175/JCLI-D-15-0287.1>
- Jennings, M., & Bensen, M. (1969). Frequency Curves for Annual Flood Series with Some Zero Events of Incomplete Data. *Water Resources Research*, 5(1), 276–280.
- Jiang, N. (2011). A new objective procedure for classifying New Zealand synoptic weather types during 1958–2008. *International Journal of Climatology*, 31(6), 863–879. <https://doi.org/10.1002/joc.2126>
- Kennett, D. (2021). *Drivers and Impacts of Atmospheric Rivers in New Zealand* [Open Access Victoria University of Wellington | Te Herenga Waka]. <https://doi.org/10.26686/wgtn.16583864.v1>
- Kidson, J. (2000). An analysis of New Zealand synoptic types and their use in defining weather regimes. *International Journal of Climatology*, 20(3), 299–316. [https://doi.org/10.1002/\(SICI\)1097-0088\(20000315\)20:3<299::AID-JOC474>3.0.CO;2-B](https://doi.org/10.1002/(SICI)1097-0088(20000315)20:3<299::AID-JOC474>3.0.CO;2-B)

- Kidson, J., & Gordon, N. (1986). Interannual variations in New Zealand temperature and precipitation patterns. *New Zealand Journal of Geology and Geophysics*, 29(3), 363–375. <https://doi.org/10.1080/00288306.1986.10422159>
- Kidson, J., & Renwick, J. (2002). Patterns of convection in the tropical pacific and their influence on New Zealand weather. *International Journal of Climatology*, 22(2), 151–174. <https://doi.org/10.1002/joc.737>
- Kidston, J., Renwick, J., & McGregor, J. (2009). Hemispheric-Scale Seasonality of the Southern Annular Mode and Impacts on the Climate of New Zealand. *Journal of Climate*, 22(18), 4759–4770. <https://doi.org/10.1175/2009JCLI2640.1>
- King, A., Klingaman, N., Alexander, L., Donat, M., Jourdain, N., & Maher, P. (2014). Extreme Rainfall Variability in Australia: Patterns, Drivers, and Predictability*. *Journal of Climate*, 27(15), 6035–6050. <https://doi.org/10.1175/JCLI-D-13-00715.1>
- Kingston, D., Webster, C., & Sirguey, P. (2016). Atmospheric circulation drivers of lake inflow for the Waitaki River, New Zealand. *International Journal of Climatology*, 36(3), 1102–1113. <https://doi.org/10.1002/joc.4405>
- Kingston, D., Lavers, D., & Hannah, D. (2022). Characteristics and large-scale drivers of atmospheric rivers associated with extreme floods in New Zealand. *International Journal of Climatology*, 42(5), 3208–3224. <https://doi.org/10.1002/joc.7415>
- Kingston, D., & McMecking, J. (2015). Precipitation delivery trajectories associated with extreme river flow for the Waitaki River, New Zealand. *Proceedings of the International Association of Hydrological Sciences*, 369, 19–24. <https://doi.org/10.5194/piahs-369-19-2015>
- Kingston, D., Lavers, D., & Hannah, D. (2016). Floods in the Southern Alps of New Zealand: The importance of atmospheric rivers: Atmospheric Rivers and Floods in New Zealand. *Hydrological Processes*, 30(26), 5063–5070. <https://doi.org/10.1002/hyp.10982>

- Kumar, R. (2019). Flood Frequency Analysis of the Rapti River Basin using Log Pearson Type-III and Gumbel Extreme Value-1 Methods. *Journal of the Geological Society of India*, 94(5), 480–484. <https://doi.org/10.1007/s12594-019-1344-0>
- Kundzewicz, Z., Szwed, M., & Pińskwar, I. (2019). Climate Variability and Floods—A global Review. *Water*, 11(7), 1399. <https://doi.org/10.3390/w11071399>
- Land, Air, Water Aotearoa. (2022a). *Ellesmere / Waihora Catchment*.
<https://www.lawa.org.nz/explore-data/canterbury-region/river-quality/ellesmere-waihora-catchment/>
- Land, Air, Water Aotearoa. (2022b). *Environmental monitoring data for Uawa River*. Land, Air, Water Aotearoa (LAWA). <https://www.lawa.org.nz/explore-data/gisborne-region/river-quality/uawa-river/>
- Land, Air, Water Aotearoa. (2022c). *Hurunui River Catchment*.
<https://www.lawa.org.nz/explore-data/canterbury-region/river-quality/hurunui-river-catchment/>
- Land, Air, Water Aotearoa. (2022d). *Otara*. <https://www.lawa.org.nz/explore-data/bay-of-plenty-region/river-quality/otara/>
- Land, Air, Water Aotearoa. (2022e). *Ruamahanga*. <https://www.lawa.org.nz/explore-data/wellington-region/water-quantity/surface-water-zones/ruamahanga/>
- Land, Air, Water Aotearoa. (2022f). *Upper and Lower Waitaki Catchment*.
<https://www.lawa.org.nz/explore-data/canterbury-region/river-quality/upper-and-lower-waitaki-catchment/>
- Land, Air, Water Aotearoa. (2022g). *Waimata River*. <https://www.lawa.org.nz/explore-data/gisborne-region/river-quality/waimata-river/>
- Land, Air, Water Aotearoa. (2022h). *Waioeka*. <https://www.lawa.org.nz/explore-data/bay-of-plenty-region/river-quality/waioeka/>
- Land, Air, Water Aotearoa. (2022i). *Waipoua River at Colombo Road Bridge*.
<https://www.lawa.org.nz/explore-data/wellington-region/river-quality/ruam%C4%81hangwaipoua-river-at-colombo-rd-bridge/>

- Land, Air, Water Aotearoa. (2022j). *Wairau River*. <https://www.lawa.org.nz/explore-data/marlborough-region/water-quantity/surface-water-zones/wairau-river/>
- Land, Air, Water Aotearoa. (2022k). *Waitangi River*. <https://www.lawa.org.nz/explore-data/northland-region/river-quality/waitangi-river/>
- Larned, S., Hicks, D. M., Schmidt, J., Davey, A., Dey, K., Scarsbrook, M., Arscott, D., & Woods, R. (2008). The Selwyn River of New Zealand: A benchmark system for alluvial plain rivers. *River Research and Applications*, 24(1), 1–21.
<https://doi.org/10.1002/rra.1054>
- Leask, A., & Heard, G. (2021, July 18). Wild weather: Extent of flooding revealed in aerial photos of stricken Westport. *NZ Herald*. <https://www.nzherald.co.nz/nz/wild-weather-extent-of-flooding-revealed-in-aerial-photos-of-stricken-westport/U4MCAIC63PNYQTL4AHHTVCN7WQ/>
- Li, N., & McGregor, G. (2017). Linking interannual river flow river variability across New Zealand to the Southern Annular Mode, 1979–2011. *Hydrological Processes*, 31(12), 2261–2276. <https://doi.org/10.1002/hyp.11184>
- Liebmann, B., & Smith, C. (1996). Description of a Complete (Interpolated) Outgoing Longwave Radiation Dataset. *Bulletin of the American Meteorological Society*, 77, 1275–1277.
- Lorrey, A., & Bostock, H. (2017). The Climate of New Zealand Through the Quaternary. In J. Shulmeister (Ed.), *Landscape and Quaternary Environmental Change in New Zealand* (pp. 67–139). Atlantis Press. https://doi.org/10.2991/978-94-6239-237-3_3
- Lorrey, A., Griffiths, G., Fauchereau, N., Diamond, H., Chappell, P., & Renwick, J. (2014). An ex-tropical cyclone climatology for Auckland, New Zealand: AN EX-TROPICAL CYCLONE CLIMATOLOGY FOR AUCKLAND, NEW ZEALAND. *International Journal of Climatology*, 34(4), 1157–1168. <https://doi.org/10.1002/joc.3753>
- Macara, G. (2013). *The Climate and Weather in Southland* (No. 63; NIWA Science and Technology Series). <https://niwa.co.nz/static/Southland%20ClimateWEB.pdf>

- Macara, G. (2015). *The Climate and Weather of Otago* (No. 67; NIWA Science and Technology Series). NIWA. <https://docs.niwa.co.nz/library/public/NIWAssts67.pdf>
- Macara, G. (2016). *The Climate and Weather of Canterbury* (No. 68; NIWA Science and Technology Series). <https://niwa.co.nz/our-science/climate/publications/regional-climatologies/canterbury>
- MacManus, J. (2021, November 5). Gisborne floods: State of emergency lifted as water levels recede. *Stuff*. <https://www.stuff.co.nz/national/weather-news/126897175/gisborne-floods-state-of-emergency-lifted-as-water-levels-recede>
- MacMurray, A., & Henderson, R. (2008). *Kaihu Flood Control Scheme Investigation Report on Stages 1 and 2* (BM 1-238; p. 26). Barnett & MacMurray Limited. <https://www.nrc.govt.nz/media/sp0m4hqb/kaihustage1and2report.pdf>
- Marlborough District Council. (2021). *Discussion of Flood Sizes*. <https://www.marlborough.govt.nz/services/river-management/flood-information/discussion-of-flood-sizes>
- Marshall, G. (2003). Trends in the Southern Annular Mode from Observations and Reanalyses. *Journal of Climate*, 16(24), 4134–4143. [https://doi.org/10.1175/1520-0442\(2003\)016<4134:TITSAM>2.0.CO;2](https://doi.org/10.1175/1520-0442(2003)016<4134:TITSAM>2.0.CO;2)
- Marshall, G., Fogt, R., Turner, J., & Clem, K. (2022). Can current reanalyses accurately portray changes in Southern Annular Mode structure prior to 1979? *Climate Dynamics*, 59(11–12), 3717–3740. <https://doi.org/10.1007/s00382-022-06292-3>
- Martindale, H., & Van Der Raaij, R. (2018). *Investigation of groundwater-surface water interaction in the Te Arai River, Gisborne, using radon-222 and concurrent stream flow gauging*. <https://doi.org/10.21420/G2SD24>
- Martins, E., & Stedinger, J. (2000). Generalized maximum-likelihood generalized extreme-value quantile estimators for hydrologic data. *Water Resources Research*, 36(3), 737–744. <https://doi.org/10.1029/1999WR900330>

- Mathewson, N., Dalley, J., & Conway, G. (2014, April 30). Heavy rain, flooding again in Christchurch. *Stuff*. <https://www.stuff.co.nz/the-press/news/your-weather/9987870/Heavy-rain-flooding-again-in-Christchurch>
- McCarthy, J. (2021). *New Zealand Environmental Data Stack (NZEnvDS)* [Data set]. Manaaki Whenua Landcare Research. <https://doi.org/10.7931/M6RM-VZ40>
- McCuen, R., Knight, Z., & Cutter, A. G. (2006). Evaluation of the Nash–Sutcliffe Efficiency Index. *Journal of Hydrologic Engineering*, 11(6), 597–602.
[https://doi.org/10.1061/\(ASCE\)1084-0699\(2006\)11:6\(597\)](https://doi.org/10.1061/(ASCE)1084-0699(2006)11:6(597))
- McDowall, C. (2019). Where are people and land at risk from flooding? *The Spinoff*.
<https://thespinoff.co.nz/climate/floods/>
- McKerchar, A., & Henderson, R. (2003). Shifts in flood and low-flow regimes in New Zealand due to interdecadal climate variations. *Hydrological Sciences Journal*, 48(4), 637–654.
- McKerchar, A., & Pearson, C. (1989). *Flood Frequency in New Zealand*. Hydrology Centre Publication.
- McKerchar, A., & Pearson, C. (1994). Forecasts of seasonal rivers flows using Southern Oscillation Index. *Journal of Hydrology (New Zealand)*, 32(2), 16–29. JSTOR.
- McKerchar, A., Pearson, C., & Moss, M. (1996). Prediction of summer inflows to lakes in the Southern Alps, New Zealand, using the spring Southern Oscillation Index. *Journal of Hydrology*, 184(3–4), 175–187. [https://doi.org/10.1016/0022-1694\(95\)02994-X](https://doi.org/10.1016/0022-1694(95)02994-X)
- McKerchar, A., & Pearson, C. P. (2001). Factors causing flooding to be New Zealand's number one hazard. *Tephra*, 18, 9–15.
- Merz, B., Blöschl, G., Vorogushyn, S., Dottori, F., Aerts, P., Bertola, M., Kemter, M., Kreibich, H., Lall, U., & Macdonald, E. (2021). Causes, impacts and patterns of disastrous river floods. *Nature Reviews Earth & Environment*, 2(9), 592–609.
<https://doi.org/10.1038/s43017-021-00195-3>
- Merz, R., & Blöschl, G. (2003). A process typology of regional floods. *Water Resources Research*, 39(12). <https://doi.org/10.1029/2002WR001952>

- MetService. (2015). *Tropical Cyclone Monitoring*. <https://about.metservice.com/our-company/national-weather-services/tropical-cyclones/>
- Milly, P., Betancourt, J., Falkenmark, M., Hirsch, R., Kundzewicz, Z., Lettenmaier, D., & Stouffer, R. (2008). Stationarity Is Dead: Whither Water Management? *Science*, 319(5863), 573–574. <https://doi.org/10.1126/science.1151915>
- Ministry for the Environment. (2010). *Preparing for future flooding: A guide for local government in New Zealand*. Ministry for the Environment.
- Ministry for the Environment. (2022, August 18). *Adapting to flood risk in Westport*. Ministry for the Environment. <https://environment.govt.nz/what-you-can-do/stories/adapting-to-flood-risk-in-westport/>
- Mohssen, M. (2008). An insight into flood frequency for design floods. *Flood Recovery, Innovation and Response I, I*, 155–164. <https://doi.org/10.2495/FRIAR080161>
- Morrison, J., & Smith, J. (2002). Stochastic modeling of flood peaks using the generalized extreme value distribution: Flood peak modeling using GEV. *Water Resources Research*, 38(12), 41-1-41-12. <https://doi.org/10.1029/2001WR000502>
- Morton, J. (2020, September 28). \$160m a year: Sweeping new assessment of NZ's big flood threat. *NZ Herald*. <https://www.nzherald.co.nz/nz/160m-a-year-sweeping-new-assessment-of-nzs-big-flood-threat/XJGW7ZNXDYMKGROHRRZ2Q6I5QU/>
- Morton, J. (2021, June 1). What caused the Canterbury flood? Three questions answered. *NZ Herald*. <https://www.nzherald.co.nz/nz/weather-what-caused-the-canterbury-flood-three-questions-answered/BY2TK23FSO4LON5ZCMBJFSRKFQ/>
- Morton, J. (2023, January 28). Explained: What caused Auckland's wettest day—And where climate change fits in. *NZ Herald*. <https://www.nzherald.co.nz/nz/explained-what-caused-aucklands-wettest-day-and-where-climate-change-fits-in/M7A456YCAJGJ3GEGZ7HUMOFJRU/>
- Mosely, P. (1992). *Waters of New Zealand*. New Zealand Hydrological Society.

- Mosley, M. (2000). Regional differences in the effects of El Niño and La Niña on low flows and floods. *Hydrological Sciences Journal*, 45(2), 249–267.
<https://doi.org/10.1080/02626660009492323>
- Mullan, A. (1995). On the linearity and stability of Southern Oscillation-climate relationships for New Zealand. *International Journal of Climatology*, 15(12), 1365–1386.
<https://doi.org/10.1002/joc.3370151205>
- Mullan, A. (1998). Southern hemisphere sea-surface temperatures and their contemporary and lag association with New Zealand temperature and precipitation. *International Journal of Climatology*, 18(8), 817–840. [https://doi.org/10.1002/\(SICI\)1097-0088\(19980630\)18:8<817::AID-JOC261>3.0.CO;2-E](https://doi.org/10.1002/(SICI)1097-0088(19980630)18:8<817::AID-JOC261>3.0.CO;2-E)
- Naish, J. (2021, August 12). Climate change made the May flooding in Canterbury more severe—Researchers. *Stuff*. <https://www.stuff.co.nz/environment/climate-news/127210511/climate-change-made-the-may-flooding-in-canterbury-more-severe--researchers>
- <https://earthobservatory.nasa.gov/images/7079/historic-tropical-cyclone-tracks>
- National Institute of Water and Atmospheric Research. (2010). *High flow current meter—NIWA POEM*. NIWA. <https://niwa.co.nz/our-services/instruments/instrumentsystems/products/water-flow-instruments/poem>
- National Institute of Water and Atmospheric Research. (2011). *Floods*.
<https://niwa.co.nz/natural-hazards/hazards/floods>
- National Institute of Water and Atmospheric Research. (2018a). *March 1988 North Island Ex-tropical Cyclone Bola (1988-03-06)*.
https://hwe.niwa.co.nz/event/March_1988_North_Island_Ex-tropical_Cyclone_Bola
- National Institute of Water and Atmospheric Research. (2018b). *July 1985 Gisborne and Hawke's Bay Flooding (1985-07-26)*.
https://hwe.niwa.co.nz/event/July_1985_Gisborne_and_Hawkes_Bay_Flooding

National Institute of Water and Atmospheric Research. (2019). *March 2019 South Island Flooding (2019-03-24).*

https://hwe.niwa.co.nz/event/March_2019_South_Island_Flooding

National Institute of Water and Atmospheric Research. (2021). *July 2021 South Island Flooding (2021-07-16).*

https://hwe.niwa.co.nz/event/July_2021_South_Island_Flooding

National Institute of Water and Atmospheric Research. (2022a). *Climate—NZ climate zones.*

NIWA. <https://niwa.co.nz/media-gallery/detail/109725/24940>

National Institute of Water and Atmospheric Research. (2022b). *Extreme weather—Heavy rainfall.* <https://niwa.co.nz/natural-hazards/extreme-weather-heavy-rainfall>

National Institute of Water and Atmospheric Research. (2022c, August 25). “*Exceptional” August atmospheric river sets record.* NIWA. <https://niwa.co.nz/news/exceptional-august-atmospheric-river-sets-record>

National Oceanic and Atmospheric Administration. (2022). *Climate Prediction Center—Monitoring & Data: Current Monthly Atmospheric and Sea Surface Temperatures Index Values.* <https://www.cpc.ncep.noaa.gov/data/indices/>

National Resources Conservation Service. (2007). *Stream Hydrology.* United States Department of Agriculture.

<https://directives.sc.egov.usda.gov/OpenNonWebContent.aspx?content=17781.wba>

Natural Resources Canada & Public Safety Canada. (2019). *Federal hydrologic and hydraulic procedures for floodplain delineation* (No. 113e; version 1.0, p. 113e).

<https://doi.org/10.4095/299808>

New Zealand Media and Entertainment. (2017, August 29). Farmers still recovering from deluge wrought by Cyclone Debbie. *NZ Herald.* <https://www.nzherald.co.nz/the-country/news/farmers-still-recovering-from-deluge-wrought-by-cyclone-debbie/6LU6L5D47X34ZQRSRMQ7YZ34VY/>

Patel, K., Fansler, S., Campbell, T., Bond-Lamberty, B., Smith, A. P., RoyChowdhury, T., McCue, L. A., Varga, T., & Bailey, V. (2021). Soil texture and environmental conditions

- influence the biogeochemical responses of soils to drought and flooding.
- Communications Earth & Environment*, 2(1), 127. <https://doi.org/10.1038/s43247-021-00198-4>
- Paulik, R., Craig, H., & Collins, D. (2019). *New Zealand Fluvial and Pluvial Flood Exposure—The Deep South Challenge* (No. 2019118WN). NIWA.
<https://deepsouthchallenge.co.nz/wp-content/uploads/2021/01/Exposure-to-River-Flooding-Final-Report.pdf>
- Paulik, R., Crowley, K., Cradock-Henry, N. A., Wilson, T., & McSporran, A. (2021). Flood Impacts on Dairy Farms in the Bay of Plenty Region, New Zealand. *Climate*, 9(2), 30. <https://doi.org/10.3390/cli9020030>
- Pearson, C. (1991). New Zealand regional flood frequency analysis using L-moments. *Journal of Hydrology (New Zealand)*, 30(2), 53–64. JSTOR.
- Pohl, B., Sturman, A., Renwick, J., Quénol, H., Fauchereau, N., Lorrey, A., & Pergaud, J. (2022). Precipitation and temperature anomalies over Aotearoa New Zealand analysed by weather types and descriptors of atmospheric centres of action. *International Journal of Climatology*, 43(1), 331–353. <https://doi.org/10.1002/joc.7762>
- Prince, H., Cullen, N., Gibson, P., Conway, J., & Kingston, D. (2021). A Climatology of Atmospheric Rivers in New Zealand. *Journal of Climate*, 34(11), 1–56. <https://doi.org/10.1175/JCLI-D-20-0664.1>
- Purdy, J., & Austin, G. (2003). The role of synoptic cloud in orographic rainfall in the Southern Alps of New Zealand: Role of synoptic cloud in orographic rainfall. *Meteorological Applications*, 10(4), 355–365. <https://doi.org/10.1017/S1350482703001087>
- Pushpalatha, R., Perrin, C., Moine, N. L., & Andréassian, V. (2012). A review of efficiency criteria suitable for evaluating low-flow simulations. *Journal of Hydrology*, 420–421, 171–182. <https://doi.org/10.1016/j.jhydrol.2011.11.055>

Radio New Zealand. (2022a, February 2). Westport and Buller prepare for heavy rain, locals warned to avoid non-essential travel. *Radio New Zealand*.

<https://www.rnz.co.nz/news/national/460704/westport-and-buller-prepare-for-heavy-rain-locals-warned-to-avoid-non-essential-travel>

Radio New Zealand. (2023a, August 1). Coromandel residents warned to prepare for “hard hitting” Cyclone Hale. *RNZ*.

<https://www.rnz.co.nz/news/national/482076/coromandel-residents-warned-to-prepare-for-hard-hitting-cyclone-hale>

Rahman, A., Rahman, A., Zaman, M., Haddad, K., Ahsan, A., & Imteaz, M. (2013). A study on selection of probability distributions for at-site flood frequency analysis in Australia.

Natural Hazards, 69(3), 1803–1813. <https://doi.org/10.1007/s11069-013-0775-y>

Reid, K., Rosier, S., Harrington, L., King, A., & Lane, T. (2021). Extreme rainfall in New Zealand and its association with Atmospheric Rivers. *Environmental Research Letters*, 16(4), 044012. <https://doi.org/10.1088/1748-9326/abeae0>

Renwick, J. (2011). Kidson’s Synoptic Weather Types and Surface Climate Variability over New Zealand. *Weather and Climate*, 31, 3. <https://doi.org/10.2307/26169715>

Renwick, J., & Thompson, D. (2006). The Southern Annular Mode and New Zealand climate. *Water & Atmosphere*, 14(2), 24–25.

Rhode, R. (2006). *Historic Tropical Cyclone Tracks*.

<https://earthobservatory.nasa.gov/images/7079/historic-tropical-cyclone-tracks>

Robson, A., & Reed, D. (2008). *Statistical procedures for flood frequency estimation* (Vol. 3). NERC. https://www.ceh.ac.uk/sites/default/files/2021-11/Flood-Estimation-Handbook-3-Statistical-Procedures-For-Flood-Frequency-Estimation_Alice-Robson_Duncan-Reed.pdf

Rosser, B., Dellow, S., & Ashraf, S. (2019). *Assessment of the use of differencing satellite imagery as a tool for quantifying landslide impacts from significant storms – a case study in the Uawa catchment, Tolaga Bay* (No. 2019/93; p. 60). GNS.

<https://www.envirolink.govt.nz/assets/1916-GSDC154-Uawa-Catchment-Tolaga>

- Bay-landslides.pdf
- Rust, H. (2009). The effect of long-range dependence on modelling extremes with the generalised extreme value distribution. *The European Physical Journal Special Topics*, 174(1), 91–97. <https://doi.org/10.1140/epjst/e2009-01092-8>
- Salinger, J. (1980a). New Zealand Climate: I. Precipitation Patterns. *Monthly Weather Review*, 108(11), 1892–1904. [https://doi.org/10.1175/1520-0493\(1980\)108<1892:NZCIPP>2.0.CO;2](https://doi.org/10.1175/1520-0493(1980)108<1892:NZCIPP>2.0.CO;2)
- Salinger, J. (1980b). New Zealand Climate: II. Temperature Patterns. *Monthly Weather Review*, 108(11), 1905–1912. [https://doi.org/10.1175/1520-0493\(1980\)108<1905:NZCITP>2.0.CO;2](https://doi.org/10.1175/1520-0493(1980)108<1905:NZCITP>2.0.CO;2)
- Salinger, J., Gray, W., Mullan, B., & Wratt, W. (2004). Atmospheric circulation and precipitation. In *Freshwaters of New Zealand*. New Zealand Hydrological Society.
- Salinger, J., & Mullan, B. (1999). New Zealand climate: Temperature and precipitation variations and their links with atmospheric circulation 1930–1994. *International Journal of Climatology*, 19(10), 1049–1071. [https://doi.org/10.1002/\(SICI\)1097-0088\(199908\)19:10<1049::AID-JOC417>3.0.CO;2-Z](https://doi.org/10.1002/(SICI)1097-0088(199908)19:10<1049::AID-JOC417>3.0.CO;2-Z)
- Senapati, B., Dash, M., & Behera, S. (2021). Global wave number-4 pattern in the southern subtropical sea surface temperature. *Scientific Reports*, 11(1), 142. <https://doi.org/10.1038/s41598-020-80492-x>
- Shaonim. (2020, July 20). Kolmogorov-Smirnov Test in R Programming. *GeeksforGeeks*. <https://www.geeksforgeeks.org/kolmogorov-smirnov-test-in-r-programming/>
- Shu, J., Shamseldin, A., & Weller, E. (2021). The impact of atmospheric rivers on rainfall in New Zealand. *Scientific Reports*, 11(1), 5869. <https://doi.org/10.1038/s41598-021-85297-0>
- Smart, G., & McKerchar, A. (2010). More flood disasters in New Zealand. *Journal of Hydrology (New Zealand)*, 49(2), 69–78. JSTOR.

- Stedinger, J., & Griffis, V. (2011). Getting From Here to Where? Flood Frequency Analysis and Climate1: Getting From Here to Where? Flood Frequency Analysis and Climate. *Journal of the American Water Resources Association*, 47(3), 506–513.
<https://doi.org/10.1111/j.1752-1688.2011.00545.x>
- Steel, K., Martin, A., & Lintott, C. (2020). *Flood frequency analysis for Canterbury rivers Part 2* (No. 978-1-99-002718-5).
file:///E:/PU1C%208742%20%20Flood%20frequency%20analysis%20for%20Canterbury%20rivers%20Part%202.pdf
- Stein, L., Clark, M., Knoben, W., Pianosi, F., & Woods, R. (2021). How Do Climate and Catchment Attributes Influence Flood Generating Processes? A Large-Sample Study for 671 Catchments Across the Contiguous USA. *Water Resources Research*, 57(4).
<https://doi.org/10.1029/2020WR028300>
- Stuff. (2022, July 15). More than 400 homes still not repaired one year on from Westport floods. *Stuff*. <https://www.stuff.co.nz/the-press/news/west-coast/300636197/more-than-400-homes-still-not-repaired-one-year-on-from-westport-floods>
- Sturman, A., McGowan, H., & Spronken-Smith, R. (1999). Mesoscale and local climates in New Zealand. *Progress in Physical Geography: Earth and Environment*, 23(4), 611–635. <https://doi.org/10.1177/03091339902300407>
- Sturman, A., & Tapper, N. (2006). *The Weather and Climate of Australia and New Zealand* (Second). Oxford University Press.
- Sutherland, N. (2006). *Priority 2 rivers report: Status of gravel resources and management implications*. Environment Canterbury.
- Tait, A., & Fitzharris, B. (1998). Relationships between New Zealand rainfall and south-west Pacific pressure patterns. *International Journal of Climatology*, 18(4), 407–424.
[https://doi.org/10.1002/\(SICI\)1097-0088\(19980330\)18:4<407::AID-JOC256>3.0.CO;2-S](https://doi.org/10.1002/(SICI)1097-0088(19980330)18:4<407::AID-JOC256>3.0.CO;2-S)

- Teegavarapu, R. (2019). Methods for Analysis of Trends and Changes in Hydroclimatological Time-Series. In *Trends and Changes in Hydroclimatic Variables* (pp. 1–89). Elsevier.
<https://doi.org/10.1016/B978-0-12-810985-4.00001-3>
- Tomlinson, A. (1992). Precipitation and the Atmosphere. In *Waters of New Zealand*. New Zealand Hydrological Society.
- Tonkin & Taylor. (2017). *Flood frequency analysis for Canterbury Rivers* (31371.001.v2; p. 414). file:///E:/C17C%20109083%20%20484-15%2016,%20Flood%20frequency%20analysis%20for%20Canterbury%20Report%20Issue%201,%20Tonkin%20&%20Taylor.pdf
- Trenberth, K. (1997). The Definition of El Niño. *Bulletin of the American Meteorological Society*, 78(12), 2771–2777. [https://doi.org/10.1175/1520-0477\(1997\)078<2771:TDOENO>2.0.CO;2](https://doi.org/10.1175/1520-0477(1997)078<2771:TDOENO>2.0.CO;2)
- Trenberth, K., Branstator, G., Karoly, D., Kumar, A., Lau, N.-C., & Ropelewski, C. (1998). Progress during TOGA in understanding and modeling global teleconnections associated with tropical sea surface temperatures. *Journal of Geophysical Research: Oceans*, 103(C7), 14291–14324. <https://doi.org/10.1029/97JC01444>
- Trotter, C. (1988). Cyclone Bola: The inevitable disaster. *New Zealand Engineering*, July(1), 13–16.
- Ulbrich, U., Leckebusch, G., & Pinto, J. (2009). Extra-tropical cyclones in the present and future climate: A review. *Theoretical and Applied Climatology*, 96(1–2), 117–131. <https://doi.org/10.1007/s00704-008-0083-8>
- Ummenhofer, C., & England, M. (2007). Interannual Extremes in New Zealand Precipitation Linked to Modes of Southern Hemisphere Climate Variability. *Journal of Climate*, 20(21), 5418–5440. [https://doi.org/10.1175/2007JCLI1430.1 © American Meteorological Society. Used with permission.](https://doi.org/10.1175/2007JCLI1430.1)
- Waitangi Catchment Group. (2017). *Waitangi Catchment Management Plan* (p. 38). Northland Regional Council.
<https://www.nrc.govt.nz/media/xavlx1m/waitangicatchmentplanaugust2017.pdf>

- Waka Kotahi. (2022). *Damage to a section of State Highway 6 between Nelson and Blenheim*. [Photograph]. NZHerald. <https://www.nzherald.co.nz/nz/weather-nelson-flooding-households-communities-stunned-by-damage/ZLUTHPTKHCZHMG2OYRVMZ4KSXE/>
- Walter, K. (2023, February 7). *Waitangi River 1-in-100 year flood* [Personal communication].
- Watts, L., & Perrie, A. (2007). *Lower Ruamahanga River instream flow assessment: Stage 1: Instream flow issues report* (GW/EMI-G-07/135; p. 59). Greater Wellington Regional Council. <https://www.gw.govt.nz/assets/Documents/2007/06/Lower-Ruamahanga-River-instream-flow-assessment-report-screen-version.pdf>
- Weather Watch. (2023, January 10). Tuesday's national forecast: Ex-Cyclone Hale moves closer. *Weather Watch*. <https://www.weatherwatch.co.nz/content/tuesdays-national-forecast-low-moves-in>
- Wickham, H., Francois, R., Henry, L., & Muller, K. (2022, September 1). *A Grammar of Data Manipulation [R package dplyr version 1.0.10]*. Comprehensive R Archive Network (CRAN). <https://CRAN.R-project.org/package=dplyr>
- Wild, M. (2019). *Selwyn River/ Waikirikiri floodplain investigation* (No. 978-1-98-859330-2; p. 99). Environment Canterbury. <https://www.ecan.govt.nz/data/document-library/?Search=PU1C%2F8608>
- Williman, E. (1995). Flood frequency analysis for the Wairau River, Marlborough. *Journal of Hydrology (New Zealand)*, 33(2), 71–93. JSTOR.
- Willmott, C., Robeson, S., & Matsuura, K. (2012). A refined index of model performance. *International Journal of Climatology*, 32(13), 2088–2094. <https://doi.org/10.1002/joc.2419>
- Wilson, S., & Wöhling, T. (2014). *Wairau River-Wairau Aquifer Interaction* (No. 1003-5-R1; p. 49). Lincoln Agritech.

- Xiong, F., Guo, S., Chen, L., Yin, J., & Liu, P. (2018). Flood Frequency Analysis Using Halphen Distribution and Maximum Entropy. *Journal of Hydrologic Engineering*, 23(5), 04018012. [https://doi.org/10.1061/\(ASCE\)HE.1943-5584.0001637](https://doi.org/10.1061/(ASCE)HE.1943-5584.0001637)
- Yu, X. (2017). *Flood Frequency Analysis in Context of Climate Change or with Mixed Populations* [Cornell University]. <http://hdl.handle.net/1813/51597>
- Zhou, X., Bai, Z., & Yang, Y. (2017). Linking trends in urban extreme rainfall to urban flooding in China. *International Journal of Climatology*, 37(13), 4586–4593. <https://doi.org/10.1002/joc.5107>

8. Appendix

Table A: Event data set containing the date and flow of the all flow events that equaled or exceeded the catchment-specific 1-in-5-year threshold (thresholds found in Table 4.2), the timestep of the event, the phase of the ENSO ('LN' = *La Niña*, 'EN' = *El Niño* and 'N' = *Neutral phase*) and the phase of the SAM ('+' = *Positive SAM*, '-' = *Negative SAM*, and '0' = *Natural phase*) that corresponds to the month and year of the flood occurrence, and the season the flood occurred in.

Region	Catchment	Event	Flow	Timestep	ENSO Phase	SAM Phase	Season
Upper North Island	Waitangi	13/06/1979	489.7628	162	LN	+	Winter
		20/03/1981	605.1817	808	EN	-	Autumn
		2/06/1997	424.0037	6726	EN	0	Winter
		30/06/1997	371.1632	6754	EN	0	Winter
		29/03/2007	694.319	10313	N	-	Autumn
		10/07/2007	388.813	10416	LN	-	Winter
		29/01/2011	603	11715	LN	0	Summer
		17/07/2020	650.0578	15172	N	-	Winter
	Otara	11/06/1986	495.5545	2717	LN	-	Winter
		22/01/1989	517.0497	3673	LN	0	Summer
		22/05/1996	483.1562	6350	LN	+	Autumn
		10/07/1998	549.7791	7129	LN	+	Winter
		11/11/1999	519.3483	7618	LN	+	Spring
		4/10/2003	727.4551	9041	N	0	Spring
		7/08/2006	451.8592	10079	EN	-	Winter
		26/05/2011	615.6678	11832	LN	+	Autumn
		16/07/2012	452.1597	12249	EN	+	Winter
		12/02/2018	811.3689	14286	LN	0	Summer
	Waioeka	17/02/1988	1025.887	3333	N	0	Summer
		30/08/1988	943.1856	3528	LN	-	Winter

		5/04/1991	887.2002	4476	EN	-	Autumn
		3/10/1995	1001.91	6118	LN	0	Spring
		19/07/1998	1520.535	7138	LN	+	Winter
		30/07/1998	853.053	7149	LN	+	Winter
		5/12/1999	882.2707	7642	LN	+	Summer
		24/10/2003	906.9405	9061	N	0	Spring
		4/02/2011	1051.028	11721	LN	0	Summer
		9/02/2011	1185.07	11726	LN	0	Summer
		7/06/2011	998.4613	11844	LN	0	Winter
		9/04/2017	1362.971	13977	N	+	Autumn
East Coast North Island	Hikuwai	22/06/1980	931.214	537	N	+	Winter
		27/12/1980	823.896	725	N	0	Summer
		10/04/1982	921.978	1194	N	+	Autumn
		7/06/1984	827.43	1983	LN	0	Winter
		7/03/1988	1688.282	3352	LN	-	Autumn
		8/04/1995	819.559	5940	EN	0	Autumn
		25/09/2013	924.039	12685	N	-	Spring
		4/06/2018	753.341	14398	N	-	Winter
		18/07/2020	868.875	15173	N	-	Winter
		23/03/2022	1002.327	15786	LN	+	Autumn
	Waimatā	10/04/1982	379.532	1194	N	+	Autumn
		7/06/1984	434.499	1983	EN	0	Winter
		26/07/1985	1174.812	2397	LN	+	Winter
		8/03/1988	1097.784	3353	LN	-	Autumn
		18/07/1988	393.476	3485	LN	0	Winter
		1/09/1988	466.532	3530	LN	-	Spring
		31/03/1996	393.37	6298	LN	+	Autumn
		6/08/2002	451.1	8617	EN	+	Winter
		21/10/2005	533.101	9789	LN	0	Spring

		13/10/2010	384.009	11607	LN	+	Spring
		21/09/2015	577.388	13411	EN	+	Spring
		24/03/2022	466.997	15787	LN	+	Autumn
Te Arai		26/07/1985	282.609	2397	LN	+	Winter
		21/03/1987	260.024	3000	EN	-	Autumn
		8/03/1988	299.027	3353	LN	-	Autumn
		10/09/1989	224.524	3904	LN	0	Spring
		6/08/2002	310.614	8617	EN	+	Winter
		21/10/2005	351.173	9789	LN	0	Spring
		30/07/2008	280.345	10802	N	0	Winter
		12/06/2018	217.987	14406	N	-	Winter
		24/03/2022	291.98	15787	LN	+	Autumn
		27/12/1980	394.572	725	N	0	Summer
Waikohu		23/05/1985	422.26	2333	LN	0	Autumn
		7/03/1988	595.162	3352	LN	-	Autumn
		1/09/1988	570.562	3530	LN	-	Spring
		19/10/1997	429.788	6865	EN	-	Spring
		6/08/2002	377.599	8617	EN	+	Winter
		21/10/2005	533.507	9789	LN	0	Spring
		30/07/2008	1022.124	10802	N	0	Winter
		3/08/2008	549.225	10806	LN	0	Winter
		26/04/2011	583.249	11802	LN	+	Autumn
		12/06/2018	377.742	14406	N	-	Winter
Waiapu		27/12/1980	3824.189	725	N	0	Summer
		8/03/1988	4641.586	3353	LN	-	Autumn
		8/04/1995	3237.006	5940	EN	0	Autumn
		31/03/1996	3564.012	6298	LN	+	Autumn
		30/12/1996	3992.204	6572	LN	-	Summer
		2/07/1998	3106.323	7121	LN	+	Winter

		21/06/2002	3543.425	8571	EN	-	Winter
		22/10/2005	4629.924	9790	LN	0	Spring
		30/07/2008	2953.756	10802	N	0	Winter
		12/06/2018	2956.279	14406	N	+	Winter
		26/06/2020	2928.192	15151	EN	0	Winter
		23/03/2022	3553.783	15786	LN	+	Autumn
Waihora		27/12/1980	394.572	725	N	0	Summer
		10/04/1982	249.389	1194	N	+	Autumn
		7/06/1984	252.93	1983	EN	0	Winter
		23/05/1985	422.26	2333	LN	0	Autumn
		7/03/1988	595.162	3352	LN	-	Autumn
		1/09/1988	570.562	3530	LN	-	Spring
		31/03/1996	264.356	6298	LN	+	Autumn
		12/03/1997	236.543	6644	EN	+	Autumn
		19/10/1997	429.788	6865	EN	-	Spring
		2/07/1998	292.434	7121	LN	+	Winter
		16/06/1999	262.323	7470	LN	-	Winter
		9/12/2001	296.663	8377	EN	0	Summer
		21/06/2002	262.668	8571	EN	-	Winter
		6/08/2002	377.599	8617	EN	+	Winter
		21/10/2005	533.507	9789	LN	0	Spring
		28/11/2005	295.898	9827	N	0	Spring
		30/07/2008	1022.124	10802	N	0	Winter
		3/08/2008	549.225	10806	LN	0	Winter
		14/10/2010	287.961	11608	LN	+	Spring
		29/01/2011	277.417	11715	LN	0	Summer
		26/04/2011	583.249	11802	LN	+	Autumn
		27/05/2011	282.895	11833	LN	+	Autumn
		21/09/2015	238.953	13411	EN	+	Spring

		12/06/2018	377.742	14406	N	-	Winter
Waipoua	Waipoua	20/10/1998	328.27	7231	LN	0	Spring
		2/10/2000	244.797	7944	LN	+	Spring
		9/10/2000	265.21	7951	LN	+	Spring
		3/10/2003	250.457	9040	N	0	Spring
		12/02/2004	297.648	9172	LN	-	Summer
		16/02/2004	230.818	9176	LN	-	Summer
		19/02/2004	196.33	9179	LN	-	Summer
		7/10/2008	224.628	10871	LN	+	Spring
		3/03/2012	222.865	12114	LN	0	Autumn
		20/01/1980	419.725	383	N	0	Summer
Waingawa	Waingawa	21/05/1981	305	870	LN	0	Autumn
		23/01/1982	318.468	1117	LN	-	Summer
		11/12/1982	370.9	1439	EN	-	Summer
		19/05/1988	354.739	3425	LN	-	Autumn
		6/11/1988	308.41	3596	LN	+	Spring
		17/01/1990	330.229	4033	N	-	Summer
		22/11/1994	343.677	5803	EN	-	Spring
		30/06/1996	324.564	6389	LN	-	Winter
		6/09/1998	306.627	7187	LN	0	Spring
		20/10/1998	343.841	7231	LN	0	Spring
		2/10/2000	343.32	7944	LN	+	Spring
		9/10/2000	362.548	7951	LN	+	Spring
		12/02/2004	384.184	9172	LN	-	Summer
		20/06/2015	307.07	13318	EN	+	Winter
Waiōhine	Waiōhine	20/01/1980	1365.166	383	N	0	Summer
		21/05/1981	1014.025	870	LN	0	Autumn
		23/01/1982	1056.882	1117	LN	-	Summer
		11/12/1982	1501.667	1439	EN	-	Summer

		17/01/1990	1308.988	4033	N	-	Summer
		13/03/1990	991.8	4088	EN	0	Autumn
		8/11/1994	985.712	5789	EN	-	Spring
		22/11/1994	1196.142	5803	EN	-	Spring
		6/09/1998	1059.638	7187	LN	0	Spring
		28/10/1998	985.324	7239	LN	0	Spring
		2/10/2000	1056.85	7944	LN	+	Spring
		12/02/2004	1259.275	9172	LN	-	Summer
Ruamāhangā		20/01/1980	1031.038	383	N	0	Summer
		11/04/1980	1030.416	465	EN	-	Autumn
		21/05/1981	1167.533	870	LN	0	Autumn
		8/06/1981	1116.824	888	LN	0	Winter
		12/12/1982	1134.337	1440	EN	-	Summer
		28/07/1985	1042.02	2399	LN	+	Winter
		3/09/1988	1055.372	3532	LN	-	Spring
		16/10/1992	1028.152	5036	EN	0	Spring
		8/11/1994	1142.188	5789	EN	-	Spring
		22/11/1994	1041.653	5803	EN	-	Spring
		5/10/1997	1050.675	6851	EN	-	Spring
		21/10/1998	1035.044	7232	LN	0	Spring
		28/10/1998	1024.842	7239	LN	0	Spring
		1/10/2000	1059.372	7943	LN	+	Spring
		16/02/2004	1161.344	9176	LN	-	Summer
		19/08/2004	1056.592	9361	EN	0	Autumn
		31/03/2005	1039.569	9585	EN	0	Autumn
		5/07/2006	1030.835	10046	EN	+	Winter
		21/07/2006	1026.079	10062	EN	+	Winter
South Island	Wairau	10/07/1983	4833.654	1650	EN	+	Winter
		22/10/1983	4344.204	1754	LN	+	Spring

		10/12/1983	2443.778	1803	LN	+	Summer
		24/07/1988	2488.405	3491	LN	0	Winter
		12/08/1990	2180.265	4240	N	0	Winter
		13/06/1993	2827.902	5276	EN	0	Winter
		8/11/1994	2945.912	5789	EN	-	Spring
		28/05/1995	2143.346	5990	EN	+	Autumn
		2/07/1998	3552.244	7121	LN	+	Winter
		28/12/2010	2657.936	11683	LN	0	Summer
		26/05/2011	2900.726	11832	LN	+	Autumn
		15/07/2012	2489.223	12248	EN	+	Winter
		18/02/2016	2266.491	13561	EN	+	Summer
		17/07/2021	5565.93	15537	LN	-	Winter
Hurunui		11/08/1986	1316.978	2778	N	+	Winter
		23/12/1993	1289.609	5469	N	+	Summer
		27/07/1994	1145.822	5685	EN	0	Winter
		8/11/1994	1011.927	5789	EN	-	Spring
		19/08/2000	1551.285	7900	LN	-	Winter
		13/01/2002	1139.233	8412	N	+	Summer
		31/07/2008	1656.998	10803	N	0	Winter
		25/08/2008	1447.108	10828	LN	0	Winter
		11/06/2014	1038.196	12944	EN	0	Winter
		31/05/2021	1153.289	15490	LN	0	Autumn
		17/07/2021	1003.735	15537	LN	-	Winter
		13/02/2022	975.257	15748	LN	+	Summer
Selwyn		14/03/1986	235.12	2628	LN	-	Autumn
		12/08/1986	226.993	2779	N	+	Winter
		24/12/1993	215.142	5470	N	0	Summer
		27/07/1994	350.684	5685	EN	0	Winter
		20/08/2000	426.81	7901	LN	-	Winter

		14/01/2002	255.499	8413	N	+	Summer
		1/08/2008	245.069	10804	LN	0	Winter
		22/07/2017	420.454	14081	LN	0	Winter
		31/05/2021	446.966	15490	LN	0	Autumn
Maerewhenua		5/06/1980	359.951	520	N	+	Winter
		11/08/1986	214.663	2778	N	+	Winter
		24/08/1990	190.771	4252	N	0	Winter
		23/12/1993	273.347	5469	N	0	Summer
		27/07/1994	271.907	5685	EN	0	Winter
		12/01/2002	229.75	8411	N	+	Summer
		23/12/2005	193.941	9852	LN	-	Summer
		25/05/2010	270.169	11466	LN	+	Autumn
		23/02/2012	214.983	12105	LN	-	Summer
		15/08/2012	221.766	12279	EN	+	Winter
		17/06/2013	405.457	12585	LN	0	Winter
		18/04/2014	332.219	12890	LN	0	Autumn
		22/01/2017	201.55	13900	N	-	Summer
		2/01/2021	403.863	15341	LN	+	Summer